STUDIES ON SOME CHEMICAL SENSORS FOR BIOMOLECULES AND TOXIC METALS

Ph.D. THESIS

by

SUDHIR KUMAR SHOORA

**DEPARTMENT OF CHEMISTRY
INDIAN INSTITUTE OF TECHNOLOGY ROORKEE
ROORKEE - 247 667 (INDIA)
DECEMBER, 2015**

STUDIES ON SOME CHEMICAL SENSORS FOR BIOMOLECULES AND TOXIC METALS

A THESIS

*Submitted in partial fulfilment of the
requirements for the award of the degree*

of
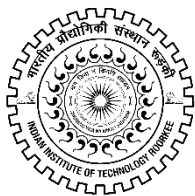
DOCTOR OF PHILOSOPHY

in

CHEMISTRY

by

SUDHIR KUMAR SHOORA

**DEPARTMENT OF CHEMISTRY
INDIAN INSTITUTE OF TECHNOLOGY ROORKEE
ROORKEE-247 667 (INDIA)
DECEMBER, 2015**

INDIAN INSTITUTE OF TECHNOLOGY ROORKEE
ROORKEE

CANDIDATE'S DECLARATION

I hereby certify that the work which is being presented in this thesis entitled **"STUDIES ON SOME CHEMICAL SENSORS FOR BIOMOLECULES AND TOXIC METALS"** in partial fulfilment of the requirements for the award of the Degree of Doctor of Philosophy and submitted in the Department of Chemistry of the Indian Institute of Technology Roorkee, Roorkee is an authentic record of my own work carried out during a period from December, 2010 to December, 2015 under the supervision of Dr. V. K. Gupta, Professor and Dr. A. K. Jain, (Retd.) Professor, Department of Chemistry, Indian Institute of Technology Roorkee, Roorkee.

The matter presented in this thesis has not been submitted by me for the award of any other degree of this or any other Institute.

(SUDHIR KUMAR SHOORA)

This is to certify that the above statement made by the candidate is correct to the best of our knowledge.

(V. K. Gupta)   (A. K. Jain)
 Supervisor   Supervisor

Date: …………

      The Ph.D. Viva-Voce Examination of **Mr. Sudhir Kumar Shoora**, Research Scholar, has been held on ....

Chairman, SRC   Signature of External Examiner

      This is to certify that the student has made all the corrections in the thesis.

Signature of Supervisors   Head of the Department

Abstract

Analytical chemistry has developed tools and methods for qualitative and quantitative analysis of species in a various variety of samples. In these days, growing industrialization has exerted substantial pressure on the environment. The global emission of raw materials, intermediates and final products from industries have become a severe problem to living organisms. Because of the negative influences of these contaminants, a number of analytical methods have been applied for their removal from water and soil samples. However, many of those methods are expensive as they require specialized reagents and apparatus, and they may also produce a large quantity of waste.

Currently an overview of analytical chemistry expansion reveals that amongst the wide variety of sensors, spectrophotometric and electrochemical sensors are preferred choice of analytical chemists as they provide convenient, fast and low cost analysis over a wide measuring concentration range. However, sometimes the application of sensors is limited by poor selectivity and sensitivity. Thus, there is a need for preparing sensors of higher sensitivity and selectivity with wide working concentration range. Keeping this in view, a number of sensors have been prepared and investigated for the determination of some metals and biomolecules. The work carried out is incorporated in the present thesis which consists of five chapters. A brief abstract of the subject matter presented in various chapters is discussed here.

The **First Chapter** is a general introduction about the subject and summarizes important literature on sensors dealing with determination of biomolecules, metals and anions. The chapter ends up with an outline of the objective of the present work.

The first chapter is followed by the **Second Chapter** which mainly deals with principles, theory and practice of voltammetric, ion selective electrodes and spectrophotometric sensors. Furthermore, the methodology and experimentation has also been detailed in this chapter.

The **Third Chapter** deals with the simultaneous determination of ascorbic acid (AA) and caffeine (CAF) by a voltammetric sensor using a glassy carbon electrode (GCE). The glassy carbon electrode was further modified with a multiwall carbon nanotube (MWCNT) to improve the performance of the electrode. It was found that the oxidation of AA and CAF

occurred at 202 mV and 1402 mV with bare GCE whereas the same process occurred at −10 mV and 1103 mV respectively for MGCE, a much lower oxidation potential. Further mechanistic investigation of the oxidation process has shown that the equal number of electrons and protons are involved in the oxidation of both the drugs. The peak current was found to be proportional to concentration of drugs and could therefore be used for their determination. The electrodes could thus be used for the determination of AA and CAF in a wide working concentration range 10–500 µM, with a detection limit of 1.0×10^{-2} µM and 3.52×10^{-3} µM for MWCNT modified GCE, whereas for bare GCE are 5.29×10^{-1} µM and 9.41×10^{-2} µM respectively. The lower value shows that the modified glassy carbon electrode is superior to bare glassy carbon electrode. Further, the alternative approach of determining AA and CAF by square wave voltammetry is convenient, faster and accurate. In view of high sensitivity for the detection of the drugs, the technique has been used for the reliable determination of AA and CAF in tea leaves, coffee, cold drink (mountain dew), pharmaceutical preparations and urine samples. Thus, it can be said that this biosensor is a useful addition in the field of analytical chemistry for the determination of biomolecules in environmental as well as medicinal samples.

The **Fourth Chapter** deals with the preparation and investigation of a cadamium selective sensor. The sensor makes use of poly(vinyl chloride) (PVC) based membranes of p-*tert*-butylcalix[6]arene as an ionophore (I). The preliminary investigations revealed that these PVC membranes developed shows potential response to Cd^{2+} ions, hence can be used for its determination. The performance of the membrane was improved by the addition of plasticizer and anion excluder sodium tetraphenylborate (NaTPB). The plasticizer di-octyl phthalate (DOP) was found to improve the performance to the maximum extent. By varying the amounts of various ingredients of the membrane, the composition of the membranes was optimized. It was found that the best performance of the membrane is obtained when its composition is I-PVC-NaTPB-DOP in the ratio 1:33:1:65 (w/w). The electrode gives linear potential response to Cd^{2+} ions over the concentration range 9.7×10^{-5} to 1.0×10^{-1} mol dm^{-3} with a Nernstian slope of 29.0 ± 1 mV decade^{-1} of activity. Hence, it could be used for Cd^{2+} determination in this concentration range. The sensor was found to be work satisfactorily in non-aqueous medium (water-ethanol (20%) and water-methanol (20%) mixtures). Further, the response of the electrode is fast with a response time of 35 seconds. The sensor exhibited a

shelf life time of about 4 months. The selectivity studies show that the electrode is selective to Cd^{2+} over many alkali, alkaline earth and heavy metals. Thus, the Cd^{2+} selective electrode developed is sufficiently selective and sensitive and can be considered a good addition to the family reported of Cd^{2+} selective sensors.

The **Fifth Chapter** deals with determination of aluminum by fluorescent sensors based on Schiff bases and an azo compound. A new azo compound, 1-(2-pyridylazo)-2-naphthol (**R1**) has been prepared and characterized by various analytical techniques such as elemental analysis, FT–IR, ^{1}H–NMR, ^{13}C–NMR and HRMS. Preliminary studies revealed that this azo compound shows strong interaction with Al^{3+} metal ions with the emission of fluorescence. The fluorescence developed is proportional to concentration of Al^{3+} and can be used for its determination. Further, this azo compound shows less fluorescence emission with other metal ions (Ba^{2+}, Cs^+, Ca^{2+}, Cr^{3+}, Fe^{2+}, Fe^{3+}, Gd^{3+}, Hg^{2+}, Li^+, Na^+, K^+, Mg^{2+}, Mn^{2+}, Nd^{3+}, Pb^{2+}, Co^{2+}, Cd^{2+}, Cu^{2+}, Zn^{2+}, Ni^{2+} and Sr^{2+}) indicating that the fluorescence response of the azo compound is selective to Al^{3+} ions with high sensitivity (detection limit 1.81×10^{-8} M). Thus, this fluorescence chemosensor could be used for the determination of Al^{3+} and may be a useful tool for quantification of Al^{3+} in various environmental and biological samples.

Two new Schiff bases *N,N'*-bis(salicylidene)-m-phenylenediamine (**R2**) and *N,N'*-bis(salicylidene)-o-phenylenediamine (**R3**) have been synthesized and characterized by HRMS, FT–IR, ^{1}H–NMR and ^{13}C–NMR spectroscopic techniques. The Schiff bases were found to strongly interact with Al^{3+} causing emission of sharp bright blue fluorescence on exposure to UV light owing to chelation enhanced fluorescence (CHEF) effect. Thus, the Schiff bases formed complexes with Al^{3+} and act as receptors for it. The fluorescence intensity was found to be proportional to concentration of Al^{3+} and can be used for its determination. The stability constants of Al^{3+} and receptor complexes were determined to be 1.41×10^4 M^{-1} and 1.59×10^4 M^{-1}, respectively. Both the receptors were used to determine Al^{3+} with the detection limit of 4.79×10^{-8} M and 8.28×10^{-8} M for receptors **R2** and **R3**, respectively. Moreover, the reported receptors work glowing in the physiological pH spectrum. The spectroscopic studies showed that the response of receptors to Al^{3+} is selective over a number of metals (Ba^{2+}, Ca^{2+}, Co^{2+}, Cd^{2+}, Cs^+, Cr^{3+}, Cu^{2+}, Fe^{2+}, Fe^{3+}, Hg^{2+}, K^+, Li^+, Na^+, Mg^{2+}, Mn^{2+}, Gd^{3+}, Nd^{3+}, Pb^{2+}, Sr^{2+}, Zn^{2+} and Ni^{2+}). Finally, the voltammetric studies (decrease in HOMO–LUMO band gap energy) coupled with spectroscopic studies showed the higher binding ability

of receptors to Al^{3+}. Hence, the fluorescence sensors developed using **R2** and **R3** can be used for quantification of Al^{3+} in various samples.

In addition to the above reported Schiff bases, two more Schiff bases *N,N'*-bis(o-hydroxyacetophenone)-m-phenylenediamine (**R4**) and *N*-(o-hydroxyacetophenone)-o-phenylenediamine (**R5**) were synthesized and characterized by a number of analytical techniques viz. elemental analysis, FT–IR, HRMS, ^{1}H–NMR and ^{13}C–NMR. Both the Schiff bases act as receptors for Al^{3+} due to complex formation. The complex formed emits strong bright blue fluorescence on exposure to the UV radiation. The intensity of fluorescence was found to be directly proportional to Al^{3+} concentration, hence could be used for its determination. Studies revealed that the stability constant of the complexes were found to be $6.64 \times 10^3 \ M^{-1}$ and $7.29 \times 10^3 \ M^{-1}$ for receptors **R4** and **R5**, respectively. These receptors do not show significant fluorescence emission on the addition of other metal ions. Hence, the response is selective and the fluorescence sensor developed can be used for Al^{3+} determination in various samples.

ACKNOWLEDGEMENTS

brother in law *Dr. Sumit Chaudhary*, who directly or indirectly, has lent their hand in this venture and encouragement extended to me.

Last but surely not least, I am very thankful to God. It is only through his sympathetic love that I found the strength and perseverance within myself to carry on with my studies. His love and joy in my life are obviously evident in the number of truthfully gifted and marvelous people. I would again like to thank Almighty who instilled in me the courage, confidence and patience to fulfill my task. It is only his will that I am able to complete my research on "*Studies on some chemical sensors for biomolecules and toxic metals*".

Dated: **(SUDHIR KUMAR SHOORA)**

Table of Contents

Chapter 3   Simultaneous Determination of Ascorbic Acid and Caffeine by a Voltammetric Sensor

List of Figures

xviii

List of Tables

List of Schemes

List of Publications

1. V.K. Gupta, A.K. Jain, **S.K. Shoora**, Multiwall carbon nanotube modified glassy carbon electrode as voltammetric sensor for the simultaneous determination of ascorbic acid and caffeine, *Electrochim. Acta* **93** (2013) 248–253.

2. V.K. Gupta, S. Kumar, R. Singh, L.P. Singh, **S.K. Shoora**, B. Sethi, Cadmium (II) ion sensing through p-tert-butyl calix[6]arene based potentiometric sensor, *J. Mol. Liq.* **195** (2014) 65–68.

3. V.K. Gupta, **S.K. Shoora**, L.K. Kumawat, A.K. Jain, A highly selective colorimetric and turn-on fluorescent chemosensor based on 1-(2-pyridylazo)-2-naphthol for the detection of aluminium(III) ions, *Sens. Actuators B* **209** (2015) 15–24.

4. **S.K. Shoora**, A.K. Jain, V.K. Gupta, A simple Schiff base based novel optical probe for aluminium(III) ions, *Sens. Actuators B* **216** (2015) 86–104.

5. V.K. Gupta, A.K. Jain, **S.K. Shoora**, New "on–off" optical probe based on Schiff base responding to Al^{3+} ions: Logic gate application, *Sens. Actuators B* **219** (2015) 218–231.

CHAPTER 1
General Introduction

1.1. Introduction

Analytical chemistry is the science of inventing and applying the concepts, principles, and strategies for measuring the characteristics of chemical systems. Recently, science and technology have attained a swift development in industry which contributes significantly towards growing the value of life along with polluting the environment and consequently posing injurious effects on living organisms and balance of environmental systems. Thus, the cleaning of environment and its protection from pollutants are the major concern to the scientists and various agencies so as to keep the level of pollution below permissible limits [1–3].

In order to attain this assignment, analytical chemistry extents almost all areas of chemistry however engage with the development of tools and methods to evaluate physical and chemical properties of substances or composition of matter and applying those techniques in their qualitative as well as quantitative estimation. Therefore, numerous techniques for determining the concentration of biomolecules, cations and anions in solutions viz. atomic absorption spectrometry, electrothermal atomic absorption spectrometry, inductively coupled plasma atomic emission spectrometry, inductively coupled plasma mass spectrometry, inductively coupled plasma optical emission spectrometry, electrospray ionization mass spectrometry, high performance liquid chromatography, gas chromatography, X-ray photoelectron spectroscopy have been developed. Although some of these techniques are very precise and selective for the determination of a number of cations, anions and biomolecules in the solution, but their applications are limited by various factors such as cost, complex infrastructure and consumption of time [4–18].

Therefore, proposing a number of unquestionable advantages such as simplicity, low cost, quick response, wide working concentration range, and analytically relevant selectivity; ion concentration determination with electrochemical (voltammetric and potentiometric) and spectrophotometric methods comfortably took a leading place among all the above methods of analysis. Voltammetric sensors measure current as a function of a potential applied between a reference and a working electrode that causes oxidation or reduction of the analyte while in potentiometric sensors potential of the cell set up with an indicator electrode (ISE) in conjunction with a reference electrode is measured. On the other hand, the spectrophotometric sensors are based on measurement of absorbance or fluorescence emission caused by analyte directly or by a reaction/irradiation. However, analysis of viscous and colored samples can also be carried out by means of these

techniques without any difficulty. Therefore, these techniques can be employed in the analysis of ions/molecules in various fields including clinical, environmental, industrial effluents, wastewater, soil, fertilizers and agricultural studies. Keeping these advantages in mind, sensors which generally provide convenient, fast and low cost analysis are preferred, if available.

1.2. Historical review of electrochemical and spectrophotometric sensors

1.2.1. Historical review of voltammetry

The beginning of voltammetry was assisted by Nobel laureate Sir Jaroslav Heyrovský who proposed the innovation in polarography while recording the first dependence of the current flowing through the dropping mercury electrode on the applied potential and drew the first polarogram. Later on, development of modern polarographic and voltammetric methods on mercury electrodes were proceeded from classical dropping mercury electrode through mercury streaming electrode, hanging mercury drop electrode, mercury film electrode, static mercury drop electrode, mercury amalgam electrodes, mercury microelectrodes, controlled growth mercury electrodes and contractible mercury drop electrodes [19–24]. Nowadays, reliable mercury electrodes for nanomolar and subnanomolar concentrations are commercially available.

Further, development of measuring techniques which proceeded from classical DC polarography, through oscillopolarography, Kalousek's switcher, AC polarography, tast polarography, normal pulse polarography, differential pulse polarography, square-wave voltammetry, cyclic voltammetry, anodic stripping voltammetry, adsorptive stripping voltammetry, convolution techniques and elimination methods [25–29], played a conclusive role in this process resulting in the decrease of the detection limit from 10^{-5} M for DC polarography through 10^{-7} M for pulse techniques to 10^{-11} M for stripping methods [30]. Following the various advantages of voltammetry, industry reacts with the production of cheaper potentiostats, electrodes, and cells that could be effectively used in routine analytical work.

1.2.2. Historical review of ion selective electrodes

The electric potential was first observed by Luigi Galvani in 1791 during the dissection of a frog. Further, du Bois-Reymond proposed that living cell membranes have properties similar to an electrode of galvanic cell. However, the scientific reason to this phenomenon was given in 1890 when Ostwald explained that the semi-permeability of the membrane was the main cause of potential generation [31]. The discovery of hydrogen ion

sensing glass electrode in 1906 by Cremer set a landmark in history of ion selective electrodes (ISEs). Efforts to develop other ISEs were initiated by Kolthoff and Sanders [32] who made first silver halide disk sensors. In the early 1960s, Pungor characterized Ag-I based heterogeneous membrane electrodes which were used as commercial solid state ISEs. These electrodes exhibited good selectivity and gave a thermodynamically reversible Nernstian response with respect to the primary ion. Many researchers continued their work towards the fabrication of various ISEs of heterogeneous membranes consisting of an electroactive material supported in an inert matrix of silicone rubber [33]. However, active research in the field of ISEs was performed with the discovery of fluoride ISEs by Frant and coworkers [34]. This electrode was based on lanthanum fluoride doped with europium fluoride and considered as the second best electrode after glass electrode.

Afterwards, a widespread research was started in the field of precipitate based ion-selective electrodes as well as on the application of complexing agents based liquid membrane electrodes [35]. Bloch and coworkers developed the first ionophore-based polymeric membrane based on PVC [36]. The procedure for compounding, casting, drying and mounting PVC membranes was introduced by Moody *et al.* [37]. Finally, the origin of host-guest chemistry [38, 39] explored various materials in developing ISEs for various cations and anions.

1.2.3. Historical review of UV–vis spectrophotometry

Spectrophotometry measures quantitatively the reflection or transmission properties of a material as a function of wavelength. In 1666 Sir Isaac Newton studied the nature of light by allowing sunlight to enter a small hole in a window shutter passing it through a glass prism and observed a spectrum of color lines. Further, William Wollaston employed a narrow slit instead of a round aperture and produced a series of visible spectral lines, each one an image of the slit and representing a different color of the visible spectrum. Afterwards, the spectroscope was developed by a German optician Joseph von Fraunhofer during the study of light. After various developments, in 1930's, a new instrument called colorimeter or spectrophotometer was developed that used a grating or prism to isolate a specific wavelength for absorption spectral analysis and eventually photo detectors replaced the inaccurate human eyes [40]. In 2002, Varian Inc. developed a double beam 6000i UV–vis–NIR spectrophotometer which involves an InGaAs detector that improves signal to noise ratio over conventional lead sulfide detectors. Its operating range of 175 nm to 1800 nm is applicable to materials science research. In 2003, Thermo Scientific introduces the 'Evolution 300' spectrophotometer, based on xenon lamp technology.

In 2004, Shimadzu introduces the SolidSpec-3700/3700DUV series of UV–vis–NIR spectrophotometers involving three detectors. In 2011, Agilent Technologies releases the Cary 60 UV–vis spectrophotometer with xenon lamp typically lasts 10 years and remote sampling options that minimize sample handling. Although modern UV–vis spectrometers differ greatly from the first DUs, all operate on the same basic principle.

1.2.4. Historical review of fluorescence spectrophotometry

In 1833, Sir David Brewster recognized a red emission from green leaf extracts, dispersive-scattering phenomenon; known as characteristic fluorescence emission from chlorophyll. In 1845, Herschel recorded the first "fluorescence emission spectrum" of quinine. In 1852, George Gabriel Stokes determined that the emission from quinine was at a longer wavelength than the excitation and used fluorescence as an analytical tool. In 1867, Goppelsroder performed a fluorescence-based analysis and developed a method for the quantization of non-luminescent Al(III) by forming a strongly fluorescent Al(III) complex. In 1877, evidence of the power of luminescence was demonstrated when Adolf Baeyer used fluorescence to demonstrate a link between the Rhine and Danube rivers [41, 42]. R. Meyer in 1897 introduced the term "fluorophores" to describe those compounds or the specific functional groups responsible for the phenomenon of fluorescence. Heimstaedt and Heinrich Lehmann (1911-1913) developed the first fluorescence microscope to investigate the auto fluorescence of biosamples such as bacteria, protozoa, plant, and animal tissues. A lot of development in fluorescence stream in subsequent years and first commercial fluorometer was developed by an American Instrument Company (AMINCO) collaborated with Dr. Robert Bowman who designed the instrument and marketed first ever spectrophotofluorimeter (SPF) in 1956. Invention of spectrophotofluorimeter was indeed an exciting journey which started with a need to destroy the malaria parasite effectively during World War II. The basic spectroscopic techniques were invited in the early 20th century and became well developed in the late 20th century and found applications in the field, including forensic, environmental, industrial and medical questions.

1.3. Sensor

Sensors are sophisticated devices that are frequently employed to detect and respond to electrical, physical, chemical or optical signals. Sensors are usually designed to operate under well defined conditions for individual analytes in certain sample types. Technically, a sensor provides a certain type of response directly related to the quantity of

a specific chemical species. There are certain features which have to be considered when we choose a sensor. These are as follows:

i.   Sensor should provide accurate, inexpensive and easy handling.

ii.   Sensors have usually limits for temperature/humidity.

iii. Sensors have a range of measurement limits.

iv.   Calibration – Essential for most of the measuring devices as the readings changes with time.

v.   Resolution – Smallest increment in signal detected by the sensor.

vi.   Repeatability – The reading that varies is repeatedly measured under the same environment.

vii. Sensors should satisfy a strong and large market need.

1.3.1. Classification of sensors

Depending upon the nature of properties under investigation, the sensors have been classified into three main categories:

(A) Physical Sensors

(B) Biochemical Sensors

(C) Chemical Sensors

(A) Physical sensors

A physical sensor provides information about a physical property of the system and no chemical reaction takes place. Typical examples are those based upon measurement of conductivity, refractive index, temperature, pressure or mass change. Currently, a number of physical sensors are available and uses for temperature monitoring and pressure control in various industrial process.

(B) Biochemical sensors

In such type of sensors, a biochemical process is the source of the analytical signal. In other words, a device that utilizes biological components such as organisms, tissues, cells, membranes, enzymes, antibodies etc. to indicate the amount of a biomaterial. They may be considered as a subgroup of the chemical ones because the mechanisms on which they are based is similar to other chemical sensors besides they are developing at such a rapidity that they deserve their own category. Such sensors are also called biosensors. Typical examples are microbial potentiometric sensors, immunosensors, and glucose sensors. They are applied for food testing, medical care device, environmental monitoring, water testing and biological warfare agent detection.

(C) Chemical sensors

According to the IUPAC recommendations, 1991, chemical sensor is a device that transforms chemical information, ranging from the concentration of a specific sample component to the total composition analysis, into an analytically useful signal [43]. All the chemical sensors are composed of a transducer, which transforms the response into a noticeable signal on modern instrumentation, and a chemically selective layer, that separates the response of the analyte from its instantaneous environment.

Chemical sensors produce an electrical signal in response to the presence of a particular analyte which give information about the chemical composition of its environment in the form of a molecular, ionic or atomic species. Moreover in such type of sensors, a chemical reaction with the contribution of the analyte gives rise to the analytical signal.

Classification of chemical sensors

The development of instrumentation and computers makes it possible to design chemical sensors utilizing operating principles of the transducer that have been used in chemistry. Further, chemical sensors may be classified in the following categories:

1) Optical sensors

An optical sensor is a device which changes optical signal into electronic signals. This group may be further subdivided according to the type of optical properties which have been applied in chemical sensors:

a) Absorbance, measured in a transparent medium, caused by the absorptivity of the analyte itself or by a reaction with some suitable indicator.

b) Fluorescence, measured as the positive emission effect caused by irradiation. Also, selective quenching of fluorescence may be the basis of such devices.

c) Luminescence, based on the measurement of the intensity of light emitted by a chemical reaction in the receptor system.

d) Reflectance, measured in non-transparent media, usually using an immobilized indicator.

e) Refractive index, measured as the result of a change in solution composition. This may include also a surface plasmon resonance effect.

f) Optothermal effect, based on a measurement of the thermal effect caused by light absorption.

g) Light scattering, based on effects caused by particles of definite size present in the sample.

2) Electrochemical sensors

Devices transform the effect of the electrochemical interaction analyte–electrode into a useful signal. Such effects may be stimulated electrically or may result in a spontaneous interaction at the zero-current condition. The following subgroups may be distinguished:

a) Voltammetric sensors, in which current is measured in an electrochemical reaction at the sensing electrode and the voltage, measured by the reference electrode, at which it occurs depends on the potential between the sensing electrode and the electrolyte. This subgroup may include sensors based on chemically inert electrodes, chemically active electrodes and modified electrodes. In this group are included sensors with and without (galvanic sensors) external current source.

b) Potentiometric sensors, in which the potential of the indicator electrode (ion-selective electrode, redox electrode, metal/metal oxide electrode) is measured in the solution against a reference electrode and the voltage difference between the two electrodes is measured.

c) Chemically sensitized field effect transistor, in which the effect of the interaction between the analyte and the active coating is transformed into a change of the source-drain current. The interactions between the analyte and the coating are, from the chemical point of view, similar to those found in potentiometric ion-selective sensors.

d) Potentiometric solid electrolyte gas sensors work in high temperature solid electrolytes and are usually applied for gas sensing measurements.

1.4. Literature survey

Forever since the discovery of electrochemical and optical sensors has provoked a great deal of interest owing to their substantial role in analytical chemistry steadily increasing. In recent years, the field of sensors is perhaps one of the most eminent examples of interdisciplinary research in analytical chemistry. A number of some significant papers [44–56] have appeared in the recent past. Progress in this field, including principles, theory, and applications of electrochemical and optical sensors have been described in the periodic reviews [57–64]. The list is absolutely comprehensive and it is improbable to report the total bibliography on these sensors. Therefore, merely some latest and considerable publications, that highlight various aspects of sensors developed for various biomolecules and metal ions, and are presented here.

1.4.1. Voltammetric sensors for biomolecules and pharmaceutical formulations

Considerable efforts have been made by researchers to develop voltammetric sensors for biomolecules and pharmaceutical formulations due to their occurrence in diverse samples including food, industry, medical, environmental and clinical. Although a large number of sensors for these formulations have been reported, a brief review on voltammetric sensors for these formulations is given in the following paragraphs.

A number of reviews [65–69] have been reported which summarize the different types of electrometric methods and represent their mechanisms in the determination of biological samples. The reviews are focused on a comparative description of the applications of carbon-based nanomaterials towards detection of biomolecules and hence present the results in a critical manner, future challenges of better sensor design and implementation are evaluated. Radovan and coworkers [70] reported ascorbic acid and acetaminophen simultaneously on bare boron-doped diamond electrode by a differential pulse voltammetry using aqueous buffered media. The working concentration range for both the analytes were obtained in the concentration range 0.01–0.1 mM for anodic current peaks. The potential applicability of the technique was associated with pharmaceutical products. Further, a voltammetric sensor was developed by Alizadeh *et al.* [71] for the determination of caffeine owing to differential pulse voltammetry using a carbon paste electrode prepared by a molecularly imprinted polymer. The linear working concentration range and detection limit of the sensor was calculated as 6×10^{-8} to 2.5×10^{-5} mol L^{-1} and 1.5×10^{-8} mol L^{-1} respectively. Ragupathy *et al.* [72] reported an electrocatalytic oxidation at multiwalled carbon nanotube-silica network-gold nanoparticles based nanohybrid modified electrode for determination of ascorbic acid in the presence of dopamine. The sensor electrode presented a high sensitivity (8.59 µA/mM) and selectivity for ascorbic acid by differential pulse voltammetry in the presence of a large excess of dopamine with a large potential separation of ~0.26 V. Sanghavi *et al.* [73] have determined acetaminophen, aspirin and caffeine simultaneously by voltammetric technique employing an in situ surfactant-modified multiwalled carbon nanotube paste electrode. Later on, Jain and coworkers [74] have investigated cefixime in pharmaceutical and biological fluids by a number of voltammetric techniques. Lu and coworkers [75] used a novel nanocomposites sensor for electrocatalystic investigation of epinephrine in the presence of uric acids and ascorbic acids. Similarly, Raoof *et al.* [76] constructed a carbon nanotubes and ruthenium oxide hexacyanoferrate film modified glassy carbon electrode sensor for simultaneous determination of ascorbic acid, epinephrine and uric acid.

The differential pulse voltammetric sensor prepared by Habibi and coworkers [77] based on single-walled carbon nanotube-modified carbon-ceramic electrode performed excellent electrochemical catalytic activities toward acetaminophen and ascorbic acid; and gives linear responses over ranges of 0.2 to 150.0 μM and 5.0 to 700.0 μM respectively. Further, Chatraei *et al.* [78] studied an acetaminophen-modified glassy carbon electrode for the simultaneous determination of ascorbic acid, glutathione, tryptophan and adrenaline by voltammetric methods. Mazloum-Ardakani *et al.* [79] employed electropolymerization of a thin film of para-phenylenediamine at a glassy carbon electrode and applied for the simultaneous determination of ascorbic acid, dopamine and uric acid. The detection limits were found to be 0.4, 1.0 and 2.5 μM for ascorbic acid, dopamine and uric acid, respectively. Later on, Zhang and coworkers [80] developed a sensitive differential pulse stripping voltammetric sensor for the determination of caffeine using glassy carbon electrode modified by multi-walled carbon nanotubes and nafion. The modified electrode was successfully utilized for real samples of pharmaceuticals and cola.

Recently Amare and coworkers [81] reported a glassy carbon electrode modified by 4-Amino-3-hydroxynaphthalene sulfonic acid for the determination of caffeine by electrochemical techniques. The enhancement in the peak current of caffeine concentration was found to be 6×10^{-8} to 4×10^{-5} mol L^{-1} with a detection limit of 1.37×10^{-7} mol L^{-1}. The results achieved from coffee extracts indicated the applicability of the developed method for analysis of real samples. Later on, Ba *et al.* [82] used poly(sulfosalicylic acid) modified glassy carbon electrode for the determination of L-tryptophan in the presence of ascorbic acid and dopamine by electrochemical methods. The proposed method exhibited a wide measuring concentration range of 5×10^{-8} to 1×10^{-5} M with a detection limit of 6.8×10^{-9} M. Raj *et al.* [83] introduced graphene oxide modified glassy carbon electrode for the electrocatalytic determination of purine derivatives as uric acid, xanthine, hypoxanthine and caffeine at physiological pH. Not only this, the synthesized sensor was successfully demonstrated in real samples such as human blood plasma and urine samples. Rezaei *et al.* [84] reported electrochemical sensor for caffeine using imprinted film based on polypyrrole, sol-gel, and gold nanoparticles hybrid nanocomposite modified pencil graphite electrode. The proposed method was applied successfully in the real samples viz., plasma, urine, tablet, green tea, energy and soda drink for the determination of caffeine.

Later on, a selective and sensitive electrometric method at a glassy carbon electrode modified with polyaniline–zinc oxide nanocomposite for betahistine hydrochloride have been reported by Jain and coworkers [85] in solubilized system. Herein, the lower the

detection limit of 19.57 μg/mL established the sensitivity of the proposed method. Zhu *et al.* [86] introduced a novel multi-nanopore graphene modified glassy carbon electrode for the determination of dopamine and uric acid simultaneously in the presence of ascorbic acid. Another graphene-gold nanoparticles composite coated with nafion film modified glassy carbon electrode was developed by Sanghavi and coworkers [87] for the voltammetric quantification of sumatriptan drug. Deng *et al.* [88] explored an acetylene black paste electrode modified with graphene–polyvinylpyrrolidone composite film for the determination and study of the electrochemical behavior of vanillin. Under the optimal conditions, the oxidation peak current was proportional to vanillin concentration and the detection limit was found to be 10 nM.

Furthermore, a novel voltammetric sensor was prepared by Arabzadeh *et al.* [89] for femtomolar determination of lysozyme based on a glassy carbon electrode modified by metal–chelate affinity immobilized onto gold nanoparticles. The proposed electrochemical sensor showing the high selectivity, good sensitivity and stability toward lysozyme detection and was satisfactorily applied to the determination of lysozyme in real samples such as hen egg white, a great deal in developing other electrochemical sensors. Kalambate *et al.* [90] developed a graphene–platinum nanoparticles coated nafion film composite modified glassy carbon electrode for the estimation of paracetamol and domperidone simultaneously. The reported method allowed for the determination of these drugs in the linear working range of 8.2×10^{-6}–1.6×10^{-9} M with detection limits of 1.06×10^{-10} M and 4.37×10^{-10} M, respectively. Vidya *et al.* [91] determined an electrochemical sensor for the determination of dopamine in the presence of ascorbic acid and uric acid at carbon paste electrode modified by sodium dodecyl sulphate-reduced graphene oxide. On the basis of the sweep rate effect, it was concluded that the diffusion and adsorption controlled process was taken place in the electrochemical study of the reported sensor.

Carbon nanotubes have also gained attention to a great extent during the last two decades and various biomolecules and drugs were reported for the preparation of voltammetric sensors. Therefore, some other multi-walled carbon nanotubes modified glassy carbon electrode for, gemifloxacin [92], 4-aminohippuric acid and uric acid [93], mycophenolate mofetil and mycophenolic acid [94], *N*-acetyl-L-cysteine and tryptophan [95], verapamil [96] were also investigated to develop voltammetric sensors with a good linear working concentration range. Similarly, some other important glassy carbon electrode fabricated with multi-walled carbon nanotubes functionalized with polymeric membrane for, ascorbic acid [97], ascorbic acid, dopamine, uric acid and tryptophan [98],

paracetamol in the presence of dopamine and folic acid [99], olanzapine [100], paracetamol [101, 102], clenbuterol [103], epinephrine in the presence of serotonin and folic acid [104], norfloxacin [105] were determined by electrometric methods. The developed sensors were efficiently applied towards the determination of these drugs in human real samples and pharmaceutical formulations.

On the other hand, some voltammetric sensors for, salbutamol [106], clonazepam [107], dopamine and ascorbic acid [108], carbohydrates (glucose, xylose, galactose and mannose) [109] using glassy carbon electrode fabricated via self-assembled of nanoparticles on multi-walled carbon nanotubes were also developed. Further, some carbon paste electrode fabricated with multi-walled carbon nanotubes for pharmaceutical formulations such as morphine [110], ascorbic acid, acetaminophen and tryptophan [111], 6-mercaptopurine [112], acetaminophen [113], meloxicam [114] were developed. On the other hand, a variety of voltammetric sensors based on single-walled carbon nanotubes modified electrode for drugs viz., caffeine [115], 3,4-dihydroxyphenylalanine [116], codeine and caffeine [117], neohesperidin dihydrochalcone [118], natamycin [119] were also developed having a good agreement with the linear concentration range.

Recently, Khoshhesab [120] developed a novel nanocomposite based on CuO nanoparticles/graphene nanosheets and applied as an electrode material for the simultaneous electrochemical determination of acetaminophen, caffeine and ascorbic acid followed by the differential pulse voltammetry. The proposed sensor was successfully applied for their determination in urine, blood serum and pharmaceutical samples. Similarly, Daneshinejad *et al.* [121] introduced a selective and sensitive voltammetric sensor for simultaneous determination of dopamine and acetaminophen on a glassy carbon electrode modified with a thin film of poly(solochrome black T). The modified electrode was found to be free from the interference effect of other analytes such as ascorbic acid and uric acid. The detection limits were calculated to be 0.092 and 0.142 μmol L^{-1} for dopamine and acetaminophen, respectively. Wierzbicka *et al.* [122] reported highly ordered nanoporous thin Au film electrochemical sensor for the determination of epinephrine. That work includes the calculations of total number of electrons involved in the oxidation of epinephrine, transfer coefficient and diffusion coefficient of epinephrine. Further, a voltammetric sensor for the simultaneous determination of acetaminophen and ascorbic acid based on carbon paste electrode modified with Fe(III)-clinoptilolite nano-particles was reported by Sharifian and coworkers [123]. In this the working concentration ranges by square wave peak current were found to be 1.0×10^{-9}–1.0×10^{-2} mol L^{-1} for

ascorbic acid and 1.0×10^{-10}–1.0×10^{-2} mol L^{-1} for acetaminophen with detection limits of 1.8×10^{-9} mol L^{-1} and 9.9×10^{-10} mol L^{-1}, respectively. Bouabi and coworkers [124] reported chitosan modified carbon paste electrode for square wave voltammetric determination of paracetamol. The reported method was applied successfully in natural water samples, commercial tablets and human urine samples.

1.4.2. Ion selective sensors for transition metal ions

The determination of metals in various samples is essential in view of their toxicity above certain concentration level. Such efforts have been made by many researchers in the field of ion selective electrodes (ISEs) to develop selective sensors which allow their quick and reliable determination. We have reported an ion selective electrode for Cd^{2+} and detailed literature survey on ISEs for Cd^{2+} is presented in the subsequent Chapter of the thesis. Here a brief review of recently developed ISEs for various transition elements viz., Ti^{3+}, Cr^{3+}, Mn^{2+}, Fe^{3+}, Co^{2+}, Ni^{2+}, Cu^{2+}, Zn^{2+}, Mo^{6+}, Ag^{+}, Cd^{2+}, Pt^{2+}, Hg^{2+} etc. has been presented.

Abbas *et al.* [125] reported tetraiodo- and tetrabromo-ion pairs with cetylpyridinium based novel cadmium solid-state ion-selective electrodes employing by a graphite rod electrode. The developed sensors revealed near-Nernstian anionic slopes of – 29.8 and –25.1 mV/concentration decade over a wide pH range. The tetraiodocadmate and tetrabromocadmate electrodes showed linear ranges of 1.5×10^{-6}–1.0×10^{-1} and 1.0×10^{-6}–1.0×10^{-1} M and detection limits of 6×10^{-7} and 8×10^{-7} M respectively. Singh *et al.* [126] reported pentaazamacrocyclic manganese complex based PVC membrane electrode for selective determination of Mn^{2+} ion over other mono-, di-, and trivalent cations. The working concentration range of the sensor was found to be 1.25×10^{-5} to 1.0×10^{-1} M and had a fast response time of 20 s with a lifetime of 4 months. Jain *et al.* [127] synthesized two new salen type Schiff base based ionophores for the development of Ni^{2+}–selective PVC membrane ion sensors. The developed sensor exhibited a Nernstian response in the concentration range of 3.2×10^{-6} to 5.0×10^{-2} M nickel(II) and used adequately over a wide pH range (2.2–5.9) with a fast response time (~10 s). The sensor was also employed successfully for the trace level estimation of nickel in biological and environmental samples. Fakhari and coworkers [128] synthesized salen type Schiff bases as carriers using cresol derivatives for the development of copper(II)–selective PVC membrane sensors. The developed sensors gave a linear potential response in the concentration range of 1.0×10^{-5} to 1.0×10^{-1} M without any significant deviation in potential upto 9 weeks and also applied successfully for the determination of copper in real sample analysis. Gupta *et al.*

[129] used dibenzo-24-crown-8 ion active material for the development of a PVC matrix zinc selective sensors which worked well in the pH range of 4.8–6.2 and working concentration range was calculated to be 9.2×10^{-5} to 1.0×10^{-1} M. The potentiometric titration of Zn^{2+} with ethylenediaminetetraacetic acid (EDTA) demonstrated the practical utility of the sensor as well as utilized for the determination of Zn^{2+} in real wastewater samples.

Gupta *et al.* [130] fabricated chromium(III)-selective PVC matrix sensor using tri-o-thymotide as an electroactive material. Zamani *et al.* [131] developed 4-amino-3-hydrazino-6-methyl-1,2,4-triazin-5-one based selective and sensitive chromium(III) PVC membrane sensors. Similarly, cobalt(II)-selective PVC membrane sensors based on a salicylidene Schiff base [132] and pyridine derived macrocyclic compound [133] were also introduced. The developed sensors worked effectively in the wide pH range and applied in the real samples for the estimation of cobalt(II) ions. Further, Gupta *et al.* [134] reported PVC matrix membranes containing porphyrins carrier Cu(II)-selective potentiometric sensors. Additionally, Gupta and coworkers [135] developed a zinc(II)-selective PVC membrane electrode based on *N,N'*-bis(acetylacetone)ethylenediimine ionophore. The developed sensor worked linearly in the concentration range of 1.0×10^{-6} to 1.0×10^{-1} M and the selectivity of the proposed electrode was also calculated employing by the fixed interference method. Mashhadizadeh *et al.* [136] described a silver(I) ion selective electrode based on a modified carbon paste electrode and a coated wire PVC membrane electrode using a synthesized Schiff base as a suitable carrier.

Khan *et al.* [137] prepared a sensitive polyaniline Sn^{4+} phosphate composite cation-exchanger material for the sensitive determination of Hg^{2+} ions in aqueous solutions owing to ion-selective membrane electrode. Another some mercury(II) ion selective electrodes [138, 139] were established in the presence of interfering cations which showed wide dynamic working range, near-Nernstian slope, fast potential response and long lifetime. Similarly, some new Mn^{2+}-selective PVC matrix membrane electrodes [140, 141] based on distinct type of Schiff bases have been investigated. The developed sensors were successfully established the selectivity of Mn^{2+} over a wide variety of interfering cations and thus could be used for the determination of Mn^{2+} in a lot of samples by direct potentiometry. Wang *et al.* [142] reported novel PVC membrane electrodes for the selective determination of molybdate(VI) via triheptyl dodecyl ammonium iodide ionophore. The developed electrodes revealed near-Nernstian responses over a wide

working concentration range of 2.0×10^{-6} to 5.0×10^{-3} M and used in the pH range of 5.0–7.0.

Further, Zamani and coworkers [143] presented a novel ionophore N-(2-hydroxyethyl) ethylenediamine-*N,N',N''*-triacetic acid based PVC membrane potentiometric sensor having high affinity for iron(III). The designed sensor was successfully utilized in the concentration range of 1.0×10^{-9}–1.0×10^{-2} mol L^{-1} with a slope of 19.5 ± 0.4 mV per decade and the detection limit was illustrated to be 3.0×10^{-10} mol L^{-1} of Fe^{3+} ions concentration. In the same way, several PVC membrane ion selective sensors prepared based on various types of ionophores viz., quinoline [144], salicylidene [145] and pyridine diamide [146] derivatives for cadmium(II) ions.

Another, PVC matrix membrane ion selective sensors have been proposed utilizing imidazole [147] and triazene [148] based ionophores for selective determination of Hg^{2+} ions. The proposed electrodes showed a good Nernstian response, wide working concentration range, and excellent selectivity over a wide variety of alkali, alkaline earth, transition and heavy metal ions. Similarly, Gholivand *et al.* [149] reported a Pt^{2+} selective membrane electrode using 1,3-bis(2-cyanobenzene)triazene as an ionophore. Further, new PVC based membranes consisting of *p*-(4-*n*-butylphenylazo)calix[4]arene [150] as an electroactive material were employed to fabricate a cobalt(II)-selective sensor which exhibited Nernstian slope of 29.0 ± 1.0 mV/decade of activity with a wide concentration range of 9.2×10^{-6} to 1.0×10^{-1} M and the detection limit was found to be 4.0×10^{-6} M. It was also utilized in partially non-aqueous medium (up to 10%, v/v) without considerable change in the slope of the working concentration range.

Similarly, numerous PVC membrane sensors based on different type of ionophores viz., bis-benzilthiocarbohydrazide [151], naphthalene derivative [152], 1-phenyl-3-pyridin-2-yl-thiourea [153], di-tert-butylazodicarboxylate [154] and heptadentate Schiff's base (tris(3-(thiophenal)propyl)amine) [155] have been evolved for the selective determination of Fe^{3+} ions. The developed sensors showed high selectivity, faster response time, wide iron ion concentration range, relatively low detection limit, high stability, low cost and simple design. The reported electrodes were also utilized to the determination of iron in different real water samples.

Zhang *et al.* [156] synthesized and utilized monoazathiacrown ethers as ionophores for PVC membrane Ag^+-selective electrodes. Furthermore, some chromium(III)-selective PVC membrane sensors have been fabricated based on different types of ionophores viz., imidazole derivative [157] and methyl violet [158]. The developed electrodes exhibited

good selectivity and sensitivity with respect to alkali, alkaline earth, transition and heavy metal ions. The electrodes were effectively employed as an indicator in the potentiometric titration of Cr^{3+} with EDTA and were also applied to the direct determination of chromium(III) content in real water samples. Later on, Isa *et al.* [159] developed an ISE based on palladium(II) dichloro acetylthiophene fenchone azine for cobalt(II) ions. This electrode revealed Nerstian response of 1.0×10^{-1}–1.0×10^{-6} M with a detection limit and slope of 8.0×10^{-7} M and 29.6 ± 0.2 mV per decade respectively. Some ISEs based on different types of ionophores viz., disufanylphenylimine [160], phenylhydrazine [161], and hydroxyacetophenone [162] derivatives have been proposed for selective determination of Cu^{2+} ions. The proposed sensors were successfully applied for the determination of Cu^{2+} in various real and environmental samples and as indicator electrode for potentiometric titration of Cu^{2+} ions with EDTA.

Sheikhshoaie *et al.* [163] synthesized and utilized 2-(hydroxyl-5-methoxybenzylideneamino) phenol Schiff base as an ionophore for development of a Mn^{2+} selective membrane in PVC matrix. The proposed membrane sensor worked well over a wide concentration range of 6×10^{-6}–2×10^{-2} M with a slope of 29 ± 1 mV per decade showing a Nernstian response for Mn^{2+} ions. In addition, Gupta *et al.* [164] constructed a new thioallophanate based copper(II) PVC membrane sensor.

Several PVC based membrane sensors for silver(I) cation have been fabricated via various types of ionophores viz., p-tert-butylcalix[4]arene [165], 15-crown-5 [166] and benzophenone hydrazone derivative [167]. The developed electrodes revealed a wide linear concentration range, good Nernstian response, excellent selectivity towards Ag^{+} ions over a range of alkali, alkaline earth, and transition metal ions. The prepared electrodes were used as an indicator electrode in potentiometric titration and successfully applied for the determination of Ag^{+} ions in real water samples. Similarly, a number of mercury(II) ion selective PVC membrane electrodes have also been proposed based on different types of ionophores such as poly-o-toluidine Zr(IV) tungstate [168], symmetrical thiourea derivatives [169], quinoline derivative [170], and oxime derived compounds [171] giving a good response in the presence of interfering ions. Further, several tetrazole di- and triamide derivatives have been synthesized by Pazik *et al.* [172] and utilized as ion carriers in the development of ion-selective membrane electrodes. The developed electrodes were applied for the selective and sensitive determination of alkali, alkaline earth, transition and heavy metal cations.

Recently, Wardak *et al.* [173] proposed a novel cadmium ion selective PVC membrane electrode through solid contact based on ionic liquid and multi-walled carbon nanotubes. The detection limit of this electrode was found to be 2.3×10^{-9} mol L^{-1} and measuring range 10^{-2}–1.0×10^{-8} mol L^{-1} with slope of 30.2 mV/decade. In addition, Ahmadzadeh *et al.* [174] have successfully fabricated calix[4]pyrrole derivative ionophore doped highly selective PVC membrane electrode for Ti^{3+} ions in the presence of alkali, alkaline earth and transition metal cations. The proposed sensor was effectively applied in tab water and industrial wastewater samples for the detection of titanium(III) ions.

1.4.3. Optical sensors for metal ions

The determination of metal ions using optical sensors has been reported by numerous researchers. Detailed literature survey on optical sensors for various metals is presented in the subsequent Chapter of the thesis. Here a brief review of recently developed optical sensors for various elements viz., Na^+, K^+, Cs^+, Be^{2+}, Mg^{2+}, Al^{3+}, Cr^{3+}, Mn^{2+}, Fe^{3+}, Co^{2+}, Ni^{2+}, Cu^{2+}, Zn^{2+}, Pd^{2+}, Ag^+, Au^{3+}, Hg^{2+}, UO_2^{2+} etc. has been presented.

Xiang *et al.* [175] reported a highly selective and sensitive copper(II) fluorescent sensor at micromolar levels with salicylaldehyde rhodamine B hydrazone in neutral buffered media. The spirolactam ring-opening was taking place upon addition of copper(II) and a 1:1 metal–ligand complex was formed. Singh *et al.* [176] introduced a first polymeric sensor for chromogenic naked eye detection of silver and ratiometric fluorescent recognition of manganese. The linear working concentration range for silver via UV–vis spectra were established 10–60 μM whereas for manganese 0–50 nM by the fluorescence emission spectra. Bhalla *et al.* [177] reported a fluorescence 'Turn–On' sensor for mercury with a new pyrene–substituted terphenyl based derivative. The reported chemosensor exhibited photo-induced electrone transfer process upon addition of Hg^{2+} ions. Wang *et al.* [178] fabricated a binaphthyl-derived salicylidene Schiff base for copper and zinc ions sensing. It presents integrated molecular logic gates by monitoring fluorescence and absorbance mode. Further, a pyrrolidine constrained bipyridyl-dansyl chemosensor conjugate by triazole moiety was synthesized by Maity and coworkers [179]. The synthesized chemosensor worked as a selective colorimetric and ratiometric sensor for Al^{3+} followed by internal charge transfer mechanism. Later on, Xie and coworkers [180] developed a near infrared fluorescence probe for detection of copper and aluminum ions by a photo-induced electron transfer process based on 4,4-difluoro-4-bora-3a,4a-diaza-s-indacene dye. The linear working concentration range by fluorescence emission were found to be 10–50 μM and 30–110 μM for Cu^{2+} and Al^{3+} ions respectively. Mahapatra and

coworkers [181] reported triphenylamine-based indolylmethane unit as a colorimetric and fluorogenic probe for selective determination of Cu^{2+} over other heavy and transition metal cations in CH_3CN/H_2O (70/30, v/v) solution.

Similarly, Tang *et al.* [182] reported a reversible and sensitive rhodamine B fluorophore based "turn-on" chromogenic and fluorogenic chemosensor for selective sensing of Cu^{2+} in aqueous acetonitrile solution. Liu and coworkers [183] developed a new fluorescent probe for zinc(II) based on a Schiff base synthesis. The fluorescence intensity for zinc(II) ion was linear in the range of 1×10^{-7} $molL^{-1}$ to 1.2×10^{-5} mol L^{-1} promising for the preparation of new fluorescent probes for the recognition of zinc(II) ion. Liu *et al.* [184] reported a sensitive and selective colorimetric and fluorescent "turn-on" probes based on a photochromic diarylethene with a fluorescent rhodamine unit for Al^{3+} and Cr^{3+} ions. The reported sensors were utilized in environmental pollutants and biological systems for recognition of Al^{3+} and Cr^{3+} owing to its reversible and fluorescent switch cycle. Similarly, a highly selective fluorescent "turn-on" rhodamine based sensor for Fe^{3+} and Cu^{2+} was developed by Weerasinghe and coworkers [185].

In addition, Liu *et al.* [186] reported a simple and sensitive fluorescence turn-on probe utilizing berberine-G-quadruplex complex as sensing element for the detection of potassium cation despite being a high concentration of sodium cations. Hosseini and coworkers [187] reported a novel fluorogenic turn-on chemosensor for selective and sensitive determination of beryllium over other common mono, di- and trivalent cations. The enhancement in the fluorescence emission intensity of beryllium was found to be linear in the concentration range of 1.6×10^{-8}–1.6×10^{-7} M with a detection limit of 1.5×10^{-9} M. Moreover, a ratiometric fluorescence sensor for beryllium(II) has been fabricated by Ji *et al.* [188] using naphthylazo derivative as a sensing material. Later on, Kaur *et al.* [189] reported a dipodal chemosensor for detection of aluminium and the resultant complex demonstrated a highly selective response to perchlorate anion. The conditions were satisfied for AND molecular logic gate by the chemical inputs of aluminum and perchlorate. Further, You *et al.* [190] reported a highly fluorescent triazine-bridged polymer for the selective determination of Al^{3+} though in the presence of competing metal ions. Jung *et al.* [191] reported the first fluorescent chemosensor based on thiazolothiazole derivatives for Cr^{3+} and Al^{3+} metal ions.

Similarly, several sensitive and selective fluorescent probes based on a variety of chemosensor derivatives viz., 4-aminoantipyrine [192], thiazole [193], pyrazole [194, 195], pyrimidine [196], quinazoline [197], naphthalene [198–204], chromone [205, 206],

quinoline [207, 208] reported for the trace level determination of aluminium. The possible binding mode of the system between probe and Al^{3+} was evaluated by the job's plot. Moreover, the reported probes show linear fluorescence enhancement with the addition of aluminium metal ions. On the other hand, a number of fluorometric sensors based on rhodamine fluorophore derivatives were successfully explored for various metal ions [209–221]. The results indicated that the ring-opening of the rhodamine spirolactam fluorophore, induced by metal ion binding, dramatically enhanced in the absorbance and fluorescence of the mixed solution.

Chopra *et al.* [222] reported the first fluorescent organic nanoparticles based chemosensor in aqueous medium for nanomolar detection of Cs^+ cation over other competing metal ions. Further, Wang *et al.* [223] synthesized a multianalyte probe based on diketopyrrolopyrrole Schiff base for the detection of Al^{3+} and Fe^{3+} selectively. The reported Schiff base showed a good colorimetric as well as a fluorescence turn-on response to Al^{3+} and Fe^{3+} metal ions. Kim *et al.* [224] reported the solvent dependent fluorescence enhancement probe for Al^{3+} and Zn^{2+} ions with a naphthaldehyde derivative Schiff base receptor. The binding properties of the reported probe with metal ions were investigated by UV–vis, fluorescence, electrospray ionization mass spectroscopy and ^{1}H–NMR titration. Jiang *et al.* [225] described a highly selective and sensitive new fluorescence turn-on probe for aluminum. Moreover, the applicability of the probe in living systems was also evaluated in Escherichia coli and Gram-negative bacteria. Further, two simply and highly selective fluorescent probes based on 4-aminoantipyrine derivative for aluminium ions were derived by Li *et al.* [226]. The association constants for the probes are 1.58×10^6 M^{-1} and 8.72×10^6 M^{-1} obtained by fluorescent titration experiments. Qin *et al.* [227] synthesized a new quinoline derivative fluorescent chemosensor selective for Al^{3+} ions. The significant enhancement in the fluorescence intensity upon addition of Al^{3+} might be ascribed due to the formation of 1:2 ligand–metal complexes inhibiting photoinduced electron transfer progress.

In addition, Chang *et al.* [228] designed a novel bifunctional Schiff base for selective sensing of Al^{3+} and CN^- ions by colorimetric and fluorometric techniques. A fluorescence turn-on chemosensor for Al^{3+}, F^- and CN^- ions was developed by Ding and coworkers [229] using a pyridine derivative Schiff base in dimethyl sulfoxide media. The developed sensor was also successfully applied in the bioimaging studies of the living cell. Qin *et al.* [230] synthesized two pyrazolone derivative Schiff base fluorescent sensors for sensing of aluminium(III). The theoretical calculations were employed for the

identification of the proposed mode of binding between sensors and aluminium(III). Similarly, Guo *et al.* [231] reported a naphthalene derivative Schiff base based fluorescent turn-on chemosensor selective for Al^{3+} ions. The detection limit of the reported chemosensor for Al^{3+} was found to be 1.0×10^{-7} M. Kim and coworkers [232] designed and synthesized a rhodamine B based Schiff base receptor for recognition of Cu^{2+} and Al^{3+} ions as an "OFF–ON–OFF" logic function dual sensor. The detection limits of the receptor for Cu^{2+} and Al^{3+} were found to be 4.726×10^{-7} and 4.43×10^{-7} M respectively. Moreover, the confocal laser scanning microscopy and scanning electron microscopy was employed to investigate the sensitivity of the solid sensor.

Huerta-Aguilar and coworkers [233] synthesized organic nanoparticles of *N,N′*-ethylenebis(salicylimine) as chemosensor for the recognition of Zn^{2+} and Al^{3+} ions in aqueous medium. The synthesized system was utilized in biological and environmental samples as a novel three inputs logic gate supported by the fluorescence. A fluorescence 'turn-on' chemosensor reported by Sarkar *et al.* [234] for the sensitive and selective detection of Zn^{2+} based on quinoline derivative and the limit of detection was found to be 5.0×10^{-9} M. The reported sensor was successfully applied in living cells and also demonstrated an INHIBIT logic gate with Zn^{2+} and EDTA as chemical inputs by means of fluorescence emission mode. Ponnuvel *et al.* [235] developed a quinolone tetrazole based fluorescence turn-on chemosensor for the selective recognition of Zn^{2+}. The enhancement in the fluorescence intensity upon addition of chemosensor to the Zn^{2+} ions took place due to the internal charge transfer mechanism which was further explained by the Density Functional Theory (DFT). Similarly, a reversible fluorescence turn-on receptor for detection of Zn^{2+} ions based on an amino acid Schiff base was developed by Subha and coworkers [236] and DFT calculations were carried out to understand the binding mechanism. Not only this, the receptor was also successfully applied in living cells as a microbial sensor for Escherichia coli and Staphylococcus aureus. Further, Park *et al.* [237] reported a new quinoline derived dual chemosensor for detection of Zn^{2+} and Co^{2+} in aqueous media. The reported chemosensor was applied to quantify Zn^{2+} and Co^{2+} in water samples as well as for Zn^{2+} in living cells.

Çimen *et al.* [238] developed a novel on-off fluorescent sensor by benzimidazole–benzothiadiazole derivative for recognition of Co^{2+} and Cu^{2+} in ethanol solution. The detection limits were estimated to be 4.1×10^{-7} M and 5.5×10^{-7} M for Co^{2+} and Cu^{2+} ions respectively. Recently, several colorimetric and fluorescent sensors have been developed based on different types of chemosensor derivatives viz., isophorone [239], pyridine [240]

and coumarin [241] for the selective determination of copper(II) ions. These sensors showed micromolar sensing ability towards the copper(II) ions. Further, Sharma *et al.* [242] reported a Schiff base chemosensor derived from vitamin B_6 cofactor pyridoxal-5-phosphate for colorimetric sensing of Cu^{2+} and fluorescence turn-off sensing of Fe^{3+} in aqueous medium at the micromolar detection limit. Similarly, Wang *et al.* [243] synthesized a rhodamine derivative bifunctional optical sensor for pH and Cu^{2+} ions. The synthesized sensor was applied successfully in the living cells and real water samples. Yang *et al.* [244] developed a tetraphenylethene functionalized rhodamine derivative chemosensor for colorimetric and fluorescent turn-on signal towards Fe^{3+} and 'naked eye' detection of Cu^{2+} ions. The binding mode of the metal–ligand complexes showed a 1:1 stoichiometry attributed to spirolactam ring-opening process.

Similarly, two fluorometric probes have been introduced based on a variety of chemosensors derivatives viz., bithiazole [245], pyridine [246] for the sensitive and selective sensing investigation of Fe^{3+} ions. The binding analysis liable for the enhancement in the fluorescence intensity was calculated through the method of continuous variations (Job's plot). Zhao *et al.* [247] investigated fluorescent sensors based on two new naphthalimide derivatives for pH and Fe^{3+} ions. The photoinduced electron transfer process was observed between the fluorophore and the donor and this process could be reversibly switched by repeated protonation and deprotonation. The geometrical structure and electronic structure of the sensors were reorganized by Density Functional Theory (DFT)/Time-Dependent Density Functional Theory (TDDFT) calculations. In addition, Wu *et al.* [248] reported a highly selective and sensitive fluorescent sensor for Fe^{3+}/F^- ions. The limit of detection was found to be 5.87×10^{-8} M for Fe^{3+} and 4.84×10^{-8} M for F^- respectively. Further, Janakipriya *et al.* [249] developed fluorescence turn-on probe for selective interactions of trivalent cations Fe^{3+}, Al^{3+} and Cr^{3+} based on naphthalimide derivative. Gupta and coworkers [250] reported two new aminopyridine Schiff bases based chemosensors for colorimetric and optical sensing investigation towards Zn^{2+}, Ni^{2+}, Fe^{3+} and UO_2^{2+} ions. The colorimetric behavior of chemosensors with different sensing aspects such as binding constant, sensitivity, pH range, stoichiometry and interference effect was investigated towards these ions. Moreover, the reported probes also exhibited excellent "off-on" fluorogenic selectivity with Zn^{2+} ions.

Further, a highly selective and sensitive mercuric ion ratiometric fluorescent sensor with imidazole derivative fluorophore was demonstrated by Ma and coworkers [251]. The limit of detection by this method was calculated to be 6.5 nM and the probe was also

applied successfully for the determination of mercuric ion in real water samples. Niu *et al.* [252] reported a fluorescence quenching sensor for highly selective and sensitive recognition of Hg^{2+} based on phenylamine-oligothiophene derivative demonstrating no significant interference effect in the presence of competing metal ions as Na^+, K^+, Ca^{2+}, Ag^+, Fe^{3+}, Al^{3+}, Cr^{3+}, Co^{2+}, Ni^{2+}, Zn^{2+}, Pb^{2+}, Cd^{2+} and Fe^{2+}. The detection limit of the sensor was found to be as low as 4.392×10^{-7} M.

In addition, a naphthalene derivative macrocyclic Schiff base was synthesized by Azadbakht *et al.* [253] and utilized for the development of fluorescent chemosensor for cesium ions. Kambam *et al.* [254] reported a highly sensitive and selective fluorescence probe based on fluorescein derivative for Au^{3+} in aqueous solution. The confocal fluorescence images revealed the probe as a cell permeable and were used to monitor Au^{3+} in living cells. Huang *et al.* [255] developed a rhodamine B derivative based off-on fluorescent probe for Pd^{2+} in aqueous medium which showed an excellent selectivity to Pd^{2+} over other metal ions owing to the rigid hydrazone binding site and the spirolactam ring-opening. Additionally, the probe has been successfully applied in detection of Pd^{2+} in natural water samples, palladium containing catalyst and imaging of Pd^{2+} in living cells. Later on, Li *et al.* [256] introduced a fluorescent turn-on chemosensor based on rosamine derivative for selective sensing of silver(I) ion over other competing metal ions. The binding properties between silver ion and chemosensor were further studied by Job's plot and ^{1}H–NMR titration experiments.

Recently, two new fluorescence turn-on sensors reported in the presence of other competing metal ions based on chemosensor derivatives viz., chromone [257] and quinoline [258] for the selective recognition of Mg^{2+} ions in organic solvents. The association constants for complexes were estimated to be 3.33×10^4 M^{-1} and 1.91×10^7 M^{-1} respectively, on the basis of the fluorescence titration curve assuming a 1:1 stoichiometry by the Benesi–Hildebrand method.

1.5. The problem

On the basis of the previously reported literature it was found that numerous types of electrochemical and optical sensors were developed for biomolecules and pharmaceutical formulations, alkali, alkaline earth and transition metals, and other elements. The researchers tried to improve the validation parameters viz., working concentration range, detection limit, binding constant, selectivity, life time and response time of previously reported electrochemical and optical sensors using newer materials. Consequently, a number of sensors are available using diverse type of materials. Though,

for most of the biomolecules and cations, yet the best sensor so far developed is not the final word and can forever be improved in some aspects by the accessibility of newer selective materials. Additionally, the literature survey demonstrates that the most of the sensors reported for biomolecules AA and CAF, and Al^{3+}, Cd^{2+} metal cations are not of very high selectivity and usually demonstrate high response time, high detection limit and limited working concentration range. Since the determination of these biomolecules and cations are significant, therefore attempts have been made to develop some new electrochemical and optical sensors for biomolecules and cations which illustrate enhanced the performance compared to the existing ones.

The performance of the every sensor largely depends on the selectivity of the sensing material utilized during the preparation. It is vastly significant and necessary that the sensing material employed should have high affinity for a particular biomolecule/cation/anion and poor for others. The high affinity of the sensing material for a particular ion may be because of numerous processes such as applied potential, excitation wavelength, selective ion exchange, ion-ionophore complexation or hydrogen bonding. However, the problem is that very few sensing materials are accessible which demonstrate high affinity to a particular ion as a result of these processes. Though, the newer materials such as calixarenes, porphyrins, Schiff bases, macrocyclic compounds, metal chelates and biomolecules are being continually synthesized. In the present investigations, some of such materials have been utilized as sensing material for the fabrication of voltammetric sensors, PVC membrane ion selective electrodes and optical sensors for CAF, AA, Al^{3+} and Cd^{2+} metal ions. The attempts have been made successfully to a considerable extent as evident from the results reported in the following chapters.

- Biomolecules and pharmaceutical formulations are the compounds of a huge attention in the field of development of voltammetric sensors owing to their biological relevance and numerous biochemical and industrial aspects. In view of the applications mentioned earlier, we thought it is significant to develop voltammetric sensor employing modified electrode and to examine as molecular recognition materials for simultaneous determination of AA and CAF. Consequently, glassy carbon electrode modified by multiwall carbon nanotube was employed for the determination of AA and CAF by means of cyclic and square wave voltammetry. The results obtained are given in Third chapter, which obviously reveals that efforts have been substantially successful.

- Chelating ligand is an additional class of compounds which have been employed as sensing material for the development of many sensors. The chelating ligand p-tert-butylcalix[6]arene having six oxygen donor sites for complexation with metal ions was procured. The selectivity coefficients of its complexes with numerous metal cations were established and it was observed that the ionophore showed high affinity towards Cd(II) cations. Therefore, it was used as a potential ionophore for the preparation of PVC membrane Cd(II)–selective electrode. The results are summarized in Fourth Chapter which clearly indicates that attempts have been successful to a remarkable extent and the developed Cd(II)–selective PVC membrane electrode illustrates better performance compared to the existing ones in a range of aspects.

- Some novel aza compound and Schiff bases viz. 1-(2-pyridylazo)-2-naphthol (**R1**), *N,N′*-bis(salicylidene)-m-phenylenediamine (**R2**), *N,N′*-bis(salicylidene)-o-phenylenediamine (**R3**), *N,N′*-bis(o-hydroxyacetophenone)-m-phenylenediamine (**R4**) and *N*-(o-hydroxyacetophenone)-o-phenylenediamine (**R5**) were synthesized and used as highly selective receptors in the development of optical sensors for the trace level detection of Al^{3+} ions. The complexation behavior of the reported receptors over a number of competing metal ions disclosed their high affinity for Al^{3+} ions. The reversibility of these receptors was also investigated by EDTA titration. The results obtained are incorporated in Fifth Chapter which suggests that efforts are successful over a remarkable extent and newly developed optical sensors demonstrate better performance than the existing ones in several aspects.

References

1. A. Bogusz, P. Oleszczuk, R. Dobrowolski, Application of laboratory prepared and commercially available biochars to adsorption of cadmium, copper and zinc ions from water, *Bioresour. Technol.* **196** (2015) 540–549.

2. M. Khan, E. Yilmaz, B. Sevinc, E. Sahmetlioglu, J. Shah, M.R. Jan, M. Soylak, Preparation and characterization of magnetic allylamine modified graphene oxide-poly(vinyl acetate-co-divinylbenzene) nanocomposite for vortex assisted magnetic solid phase extraction of some metal ions, *Talanta* **146** (2016) 130–137.

3. N. Atar, A. Olgun, S. Wang, Adsorption of cadmium(II) and zinc(II) on boron enrichment process waste in aqueous solutions: Batch and fixed-bed system studies, *Chem. Eng. J.* **192** (2012) 1–7.

4. V.K. Singh, K.P. Singh, D. Mohan, Status of heavy metals in water and bed sediments of river Gomti – A tributary of the Ganga River, India, *Environ. Monit. Assess.* **105** (2005) 43–67.

5. K.P. Singh, D. Mohan, V.K. Singh, A. Malik, Studies on distribution and fractionation of heavy metals in Gomti river sediments – A tributary of the Ganges, India, *J. Hydrol.* **312** (2005) 14–27.

6. D. Bohrer, U. Heitmann, M.D. Huang, H. Becker-Ross, S. Florek, B. Welz, D. Bertagnolli, Determination of aluminum in highly concentrated iron samples: Study of interferences using high-resolution continuum source atomic absorption spectrometry, *Spectrochim. Acta B* **62** (2007) 1012–1018.

7. K.P. Singh, A. Malik, N. Basant, V.K. Singh, A. Basant, Multi-way data modeling of heavy metal fractionation in sediments from Gomti River (India), *Chemometr. Intell. Lab.* **87** (2007) 185–193.

8. A. Zioła-Frankowska, M. Frankowski, J. Siepak, Development of a new analytical method for online simultaneous qualitative determination of aluminium (free aluminium ion, aluminium-fluoride complexes) by HPLC-FAAS, *Talanta* **78** (2009) 623–630.

9. G.A. Zachariadis, E. Sahanidou, Multi-element method for determination of trace elements in sunscreens by ICP-AES, *J. Pharm. Biomed. Anal.* **50** (2009) 342–348.

10. Q. Tu, T. Wang, C.J. Welch, High-throughput metal screening in pharmaceutical samples by ICP-MS with automated flow injection using a modified HPLC configuration, *J. Pharm. Biomed. Anal.* **51** (2010) 90–95.

11. M. Rezaee, Y. Yamini, A. Khanchi, M. Faraji, A. Saleh, A simple and rapid new dispersive liquid–liquid microextraction based on solidification of floating organic drop combined with inductively coupled plasma-optical emission spectrometry for preconcentration and determination of aluminium in water samples, *J. Hazard. Mater.* **178** (2010) 766–770.

12. N. Lewen, D. Nugent, The use of inductively coupled plasma-atomic emission spectroscopy (ICP-AES) in the determination of lithium in cleaning validation swabs, *J. Pharm. Biomed. Anal.* **52** (2010) 652–655.

13. L.A. Portugal, G.D. Matos, D.C. Lima, G.B. Brito, A.P. Fernandes, S.L.C. Ferreira, Determination of lead in aluminum and magnesium antacids using electrothermal atomic absorption spectrometry, *Microchem. J.* **98** (2011) 29–31.

14. I. Ali, W.A. Wani, A. Khan, A. Haque, A. Ahmad, K. Saleem, N. Manzoor, Synthesis and synergistic antifungal activities of a pyrazoline based ligand and its copper(II) and nickel(II) complexes with conventional antifungals, *Microb. Pathogenesis* **53** (2012) 66–73.

15. Q. Tu, T. Wang, V. Antonucci, High-efficiency sample preparation with dimethylformamide for multi-element determination in pharmaceutical materials by ICP-AES, *J. Pharm. Biomed. Anal.* **52** (2010) 311–315.

16. M. Araya-Farias, A. Gaudreau, E. Rozoy, L. Bazinet, Rapid HPLC-MS method for the simultaneous determination of tea catechins and folates, *J. Agric. Food Chem.* **62** (2014) 4241–4250.

17. R.M. Nejem, M.M. Issa, M.H. AL-Kholy, A.A. Saleh, A.A. Shanab, R.I.S.V. Staden, H.Y. Aboul-Enein, Development and validation of kinetic and atomic absorption spectrophotometric methods for the determination of salbutamol sulphate, *RSC Adv.* **5** (2015) 57164–57170.

18. Y. Yao, F. Lu, Y. Zhu, F. Wei, X. Liu, C. Lian, S. Wang, Magnetic core–shell $CuFe_2O_4@C_3N_4$ hybrids for visible light photocatalysis of Orange II, *J. Hazard. Mater.* **297** (2015) 224–233.

19. T. M. Florence, Anodic stripping voltammetry with a glassy carbon electrode mercury-plated *in situ, J. Electroanal. Chem. Interfacial Electrochem.* **27** (1970) 273–281.

20. Z. Kowalski, J. Migdalski, Increasing the signal to noise ratio in amperometry and polarography using the controlled-growth mercury drop electrode, *Talanta* **41** (1994) 309–316.

21. L. Novotny, Development of renewed mercury multi-purpose (multi-mode, versatile) microelectrodes, a part of PC-controlled measuring systems (including the PC-ETP), *Fresenius J. Anal. Chem.* **362** (1998) 184–188.

22. J. Migdalski, Z. Kowalski, Application of current-time relationship recorded on the controlled growth mercury drop electrode for determination of trace surfactants, *Chem. Anal. (Warsaw)* **44** (1999) 635–645.

23. L. Novotny, Voltammetry of biologically active species and surfactants on new miniaturized and contractible (compressible) mercury electrodes, Fresenius *J. Anal. Chem.* **363** (1999) 55–58.

24. B. Yosypchuk, L. Novotny, Nontoxic Electrodes of Solid Amalgams, *Crit. Rev. Anal. Chem.* **32** (2002) 141–151.

25. E. Wahlin, A. Bresle, On the instantaneous polarographic current. I. Automatic recording of selected parts of the current-time curve of the individual mercury drop, *Acta Chem. Scand.* **10** (1956) 935–942.

26. E.P. Parry, R.A. Osteryoung, Evaluation of analytical pulse polarography, *Anal. Chem.* **37** (1965) 1634–1637.

27. D.K. Gosser Jr., Cyclic voltammetry: Simulation and analysis of reaction mechanisms, 1st Edition, *Wiley–VCH*, New York, 1993.

28. L. Trnkova, O. Dracka, Elimination voltammetry. Experimental verification and extension of theoretical results, *J. Electroanal. Chem.* **413** (1996) 123–129.

29. P. Zuman, Role of mercury electrodes in contemporary analytical chemistry, *Electroanal.* **12** (2000) 1187–1194.

30. J. Barek, J. Zima, Eighty Years of Polarography – History and Future, *Electroanal.* **15** (2003) 467–472.

31. J. Koryta, Theory and applications of ion-selective electrodes part 4, *Anal. Chim. Acta* **139** (1982) 1–51.

32. I.M. Kolthoff, H.L. Sanders, Electric Potentials at Crystal Surfaces, and at Silver Halide Surfaces in Particular, *J. Am. Chem. Soc.* **59** (1937) 416–420.

33. A.M.U. Macdonald, K. Toth, The development of fluoride-sensitive membrane electrodes: Part I. Membranes containing thorium, lanthanum or calcium fluoride, *Anal. Chim. Acta* **41** (1968) 99–106.

34. M.S. Frant, J.W. Ross Jr., Electrode for sensing fluoride ion activity in solution, *Science* **154** (1966) 1553–1555.

35. T. Higuchi, C.R. Illian, J.L. Tossounian, Plastic electrodes specific for organic ions, *Anal. Chem.* **42** (1970) 1674–1676.

36. R. Bloch, A. Shatkay, H.A. Saroff, Fabrication and evaluation of membranes as specific electrodes for calcium ions, *Biophys. J.* **7** (1967) 865–877.

37. G.J. Moody, R.B. Oke, J.D.R. Thomas, A calcium-sensitive electrode based on a liquid ion exchanger in a poly(vinyl chloride) matrix, *Analyst* **95** (1970) 910–918.

38. M.E. Farago, Thallium(I) complexes with some macrocyclic "crown" polyethers, *Inorg. Chim. Acta* **23** (1977) 211–213.

39. M.S. Whittingham, Chemistry of intercalation compounds: Metal guests in chalcogenide hosts, *Prog. Solid State Chem.* **12** (1978) 41–99.

40. N.C. Thomas, The Early History of Spectroscopy, *J. Chem. Educ.* **68** (1991) 631–634.

41. F.V. Bright, Bioanalytical applications of fluorescence spectroscopy, *Anal. Chem.* **60** (1988) 1031A–1039A.

42. B. Valeur, M.N. Berberan-Santos, A brief history of fluorescence and phosphorescence before the emergence of quantum theory, *J. Chem. Educ.* **88** (2011) 731–738.

43. A. Hulanicki, S. Glab, F. Ingman, Chemical sensors definitions and classification, *Pure Appl. Chem.* **63** (1991) 1247–1250.

44. R.K. Mahajan, I. Kaur, T.S. Lobana, A mercury(II) ion-selective electrode based on neutral salicylaldehyde thiosemicarbazone, *Talanta* **59** (2003) 101–105.

45. A. Beiraghi, S. Babaee, M. Roshdi, A selective optical sensor for beryllium determination based on incorporating of 1,8-dihydroxyanthrone in a poly(vinyl chloride) membrane, *J. Hazard. Mater.* **190** (2011) 962–968.

46. M. Shamsipur, T. Poursaberi, M. Hassanisadi, M. Rezapour, F. Nourmohammadian, K. Alizadeh, A new chelation induced enhanced fluorescence-type optical sensor based on parared immobilized in a plasticized PVC membrane for selective determination of Zn(II) ions, *Sens. Actuators B* **161** (2012) 1080–1087.

47. B. Çeken, M. Kandaz, A. Koca, Electrochemical metal-ion sensors based on a novel manganese phthalocyanine complex, *Synth. Met.* **162** (2012) 1524–1530.

48. A.X. Oliveira, S.M. Silva, F.R.F. Leite, L.T. Kubota, F.S. Damos, R.D.C.S. Luz, Highly sensitive and selective basal plane pyrolytic graphite electrode modified with 1,4-naphthoquinone/MWCNT for simultaneous determination of dopamine, ascorbate and urate, *Electroanal.* **25** (2013) 723–731.

49. A.P.P. Eisele, D.N. Clausen, C.R.T. Tarley, L.H.D. Antonia, E.R. Sartori, Simultaneous square-wave voltammetric determination of paracetamol, caffeine and orphenadrine in pharmaceutical formulations using a cathodically pretreated boron-doped diamond electrode, *Electroanal.* **25** (2013) 1734–1741.

50. S. Tajik, M.A. Taher, H. Beitollahi, Application of a new ferrocene-derivative modified-graphene paste electrode for simultaneous determination of isoproterenol, acetaminophen and theophylline, *Sens. Actuators B* **197** (2014) 228–236.

51. A.A.A. Aziz, S.H. Seda, Detection of trace amounts of Hg^{2+} in different real samples based on immobilization of novel unsymmetrical tetradentate Schiff base within PVC membrane, *Sens. Actuators B* **197** (2014) 155–163.

52. X. Wang, J. Yang, Y. Wang, Y. Li, F. Wang, L. Zhang, Studies on electrochemical oxidation of estrogenic disrupting compound bisphenol AF and its interaction with human serum albumin, *J. Hazard. Mater.* **276** (2014) 105–111.

53. C. Kokkinos, A. Economou, T. Speliotis, Tin-film mini-sensors fabricated by a thin-layer microelectronic approach for stripping voltammetric determination of trace metals, *Electrochem. Commun.* **38** (2014) 96–99.

54. P. Deng, Z. Xu, R. Zeng, C. Ding, Electrochemical behavior and voltammetric determination of vanillin based on an acetylene black paste electrode modified with graphene–polyvinylpyrrolidone composite film, *Food Chem.* **180** (2015) 156–163.

55. M. Rong, L. Lin, X. Song, Y. Wang, Y. Zhong, J. Yan, Y. Feng, X. Zeng, X. Chen, Fluorescence sensing of chromium(VI) and ascorbic acid using graphitic carbon nitride nanosheets as a fluorescent "switch", *Biosens. Bioelectron.* **68** (2015) 210–217.

56. E. Khaled, M.S. Kamel, H.N. Hassan, S.H.A. El-Alim, H.Y. Aboul-Enein, Novel screen printed potentiometric sensors for the determination of oxicams, *RSC Adv.* **5** (2015) 12755–12762.

57. P. Bühlmann, E. Pretsch, E. Bakker, Carrier-based ion-selective electrodes and bulk optodes. 2. Ionophores for potentiometric and optical sensors, *Chem. Rev.* **98** (1998) 1593–1687.

58. J. Tria, E.C.V. Butler, P.R. Haddad, A.R. Bowie, Determination of aluminium in natural water samples, *Anal. Chim. Acta* **588** (2007) 153–165.

59. B.J. Privett, J.H. Shin, M.H. Schoenfisch, Electrochemical sensors, *Anal. Chem.* **82** (2010) 4723–4741.

60. D.W. Kimmel, G. LeBlanc, M.E. Meschievitz, D.E. Cliffel, Electrochemical sensors and biosensors, *Anal. Chem.* **84** (2012) 685–707.

61. M. Guziński, G. Lisak, J. Kupis, A. Jasiński, M. Bocheńska, Lead(II)-selective ionophores for ion-selective electrodes: A review, *Anal. Chim. Acta* **791** (2013) 1–12.

62. S. Sahana, P.K. Bharadwaj, Detection of alkali and alkaline earth metal ions by fluorescence spectroscopy, *Inorg. Chim. Acta* **417** (2014) 109–141.

63. W.A. Zoubi, N.A. Mohanna, Membrane sensors based on Schiff bases as chelating ionophores–A review, *Spectrochim. Acta A* **132** (2014) 854–870.

64. C. Yang, M.E. Denno, P. Pyakurel, B.J. Venton, Recent trends in carbon nanomaterial-based electrochemical sensors for biomolecules: A review, *Anal. Chim. Acta* **887** (2015) 17–37.

65. C.B. Jacobs, M.J. Peairs, B.J. Venton, Review: Carbon nanotube based electrochemical sensors for biomolecules, *Anal. Chim. Acta* **662** (2010) 105–127.

66. A. Cernat, M. Tertis, R. Sandulescu, F. Bedioui, A. Cristea, C. Cristea, Electrochemical sensors based on carbon nanomaterials for acetaminophen detection: A review, *Anal. Chim. Acta* **886** (2015) 16–28.

67. C. Yang, M.E. Denno, P. Pyakurel, B.J. Venton, Recent trends in carbon nanomaterial-based electrochemical sensors for biomolecules: A review, *Anal. Chim. Acta* **887** (2015) 17–37.

68. M.M. Barsan, M.E. Ghica, C.M.A. Brett, Electrochemical sensors and biosensors based on redox polymer/carbon nanotube modified electrodes: A review, *Anal. Chim. Acta* **881** (2015) 1–23.

69. B.J. Sanghavi, O.S. Wolfbeis, T. Hirsch, N.S. Swami, Nanomaterial-based electrochemical sensing of neurological drugs and neurotransmitters, *Microchim. Acta* **182** (2015) 1–41.

70. C. Radovan, C. Cofan, D. Cinghita, Simultaneous determination of acetaminophen and ascorbic acid at an unmodified boron-doped diamond electrode by differential pulse voltammetry in buffered media, *Electroanal.* **20** (2008) 1346–1353.

71. T. Alizadeh, M.R. Ganjali, M. Zare, P. Norouzi, Development of a voltammetric sensor based on a molecularly imprinted polymer (MIP) for caffeine measurement, *Electrochim. Acta* **55** (2010) 1568–1574.

72. D. Ragupathy, A.I. Gopalan, K.P. Lee, Electrocatalytic oxidation and determination of ascorbic acid in the presence of dopamine at multiwalled carbon nanotube–silica

network–gold nanoparticles based nanohybrid modified electrode, *Sens. Actuators B* **143** (2010) 696–703.

73. B.J. Sanghavi, A.K. Srivastava, Simultaneous voltammetric determination of acetaminophen, aspirin and caffeine using an in situ surfactant-modified multiwalled carbon nanotube paste electrode, *Electrochim. Acta* **55** (2010) 8638–8648.

74. R. Jain, V.K. Gupta, N. Jadon, K. Radhapyari, Voltammetric determination of cefixime in pharmaceuticals and biological fluids, *Anal. Biochem.* **407** (2010) 79–88.

75. X. Lu, Y. Li, J. Du, X. Zhou, Z. Xue, X. Liu, Z. Wang, A novel nanocomposites sensor for epinephrine detection in the presence of uric acids and ascorbic acids, *Electrochim. Acta* **56** (2011) 7261–7266.

76. J.B. Raoof, R. Ojani, M. Baghayeri, A selective sensor based on a glassy carbon electrode modified with carbon nanotubes and ruthenium oxide/hexacyanoferrate film for simultaneous determination of ascorbic acid, epinephrine and uric acid, *Anal. Methods* **3** (2011) 2367–2373.

77. B. Habibi, M. Jahanbakhshi, M.H. Pournaghi-Azar, Differential pulse voltammetric simultaneous determination of acetaminophen and ascorbic acid using single-walled carbon nanotube-modified carbon–ceramic electrode, *Anal. Biochem.* **411** (2011) 167–175.

78. F. Chatraei, H.R. Zare, Electrodeposited acetaminophen as a bifunctional electrocatalyst for simultaneous determination of ascorbic acid, glutathione, adrenaline and tryptophan, *Analyst* **136** (2011) 4595–4602.

79. M. Mazloum-Ardakani, M.A. Sheikh-Mohseni, A. Benvidi, Electropolymerization of thin film conducting polymer and its application for simultaneous determination of ascorbic acid, dopamine and uric acid, *Electroanal.* **23** (2011) 2822–2831.

80. J. Zhang, L.P. Wang, W. Guo, X.D. Peng, M. Li, Z.B. Yuan, Sensitive differential pulse stripping voltammetry of caffeine in medicines and cola using a sensor based on multi-walled carbon nanotubes and nafion, *Int. J. Electrochem. Sci.* **6** (2011) 997–1006.

81. M. Amare, S. Admassie, Polymer modified glassy carbon electrode for the electrochemical determination of caffeine in coffee, *Talanta* **93** (2012) 122–128.

82. X. Ba, L. Luo, Y. Ding, X. Liu, Determination of L-tryptophan in the presence of ascorbic acid and dopamine using poly(sulfosalicylic acid) modified glassy carbon electrode, *Sens. Actuators B* **187** (2013) 27–32.

83. M.A. Raj, S.A. John, Simultaneous determination of uric acid, xanthine, hypoxanthine and caffeine in human blood serum and urine samples using electrochemically reduced graphene oxide modified electrode, *Anal. Chim. Acta* **771** (2013) 14–20.

84. B. Rezaei, M.K. Boroujeni, A.A. Ensafi, Caffeine electrochemical sensor using imprinted film as recognition element based on polypyrrole, sol-gel, and gold nanoparticles hybrid nanocomposite modified pencil graphite electrode, *Biosens. Bioelectron.* **60** (2014) 77–83.

85. R. Jain, D.C. Tiwari, P. Karolia, Highly sensitive and selective polyaniline–zinc oxide nanocomposite sensor for betahistine hydrochloride in solubilized system, *J. Mol. Liq.* **196** (2014) 308–313.

86. X. Zhu, Y. Liang, X. Zuo, R. Hu, X. Xiao, J. Nan, Novel water-soluble multi-nanopore graphene modified glassy carbon electrode for simultaneous determination of dopamine and uric acid in the presence of ascorbic acid, *Electrochim. Acta* **143** (2014) 366–373.

87. B.J. Sanghavi, P.K. Kalambate, S.P. Karna, A.K. Srivastava, Voltammetric determination of sumatriptan based on a graphene/gold nanoparticles/nafion composite modified glassy carbon electrode, *Talanta* **120** (2014) 1–9.

88. P. Deng, Z. Xu, R. Zeng, C. Ding, Electrochemical behavior and voltammetric determination of vanillin based on an acetylene black paste electrode modified with graphene–polyvinylpyrrolidone composite film, *Food Chem.* **180** (2015) 156–163.

89. A. Arabzadeh, A. Salimi, Novel voltammetric and impedimetric sensor for femtomolar determination of lysozyme based on metal–chelate affinity immobilized, onto gold nanoparticles, *Biosens. Bioelectron.* **74** (2015) 270–276.

90. P.K. Kalambate, B.J. Sanghavi, S.P. Karna, A.K. Srivastava, Simultaneous voltammetric determination of paracetamol and domperidone based on a graphene/platinum nanoparticles/nafion composite modified glassy carbon electrode, *Sens. Actuators B* **213** (2015) 285–294.

91. H. Vidya, B.E.K. Swamy, Voltammetric determination of dopamine in the presence of ascorbic acid and uric acid at sodium dodecyl sulphate/reduced graphene oxide modified carbon paste electrode, *J. Mol. Liq.* **211** (2015) 705–711.

92. R. Jain, J.A. Rather, Voltammetric determination of antibacterial drug gemifloxacin in solubilised systems at multi-walled carbon nanotubes modified glassy carbon electrode, *Colloids Surf. B* **83** (2011) 340–346.

93. J.B. Raoof, R. Ojani, M. Baghayeri, F. Ahmadi, Fabrication of a fast, simple and sensitive voltammetric sensor for the simultaneous determination of 4-aminohippuric acid and uric acid using a functionalized multi-walled carbon nanotube modified glassy carbon electrode, *Anal. Methods* **4** (2012) 1825–1832.

94. T. Madrakian, M. Soleimani, A. Afkhami, Simultaneous determination of mycophenolate mofetil and its active metabolite, mycophenolic acid, by differential pulse voltammetry using multi-walled carbon nanotubes modified glassy carbon electrode¸ *Mater. Sci. Eng. C* **42** (2014) 38–45.

95. B. Jahanshahi, J.B. Raoof, M. Amiri-Aref, R. Ojani, A voltammetric sensor based on modified multi-walled carbon nanotubes for N-acetyl-L-cysteine determination in the presence of tryptophan using 4-chlorocatechol as a homogenous electrochemical catalyst, *J. Nanosci. Nanotechnol.* **15** (2015) 3429–3436.

96. M.A. Chamjangali, N. Goudarzi, G. Bagherian, A.A. Reskety, Development of a new electrochemical sensor for verapamil based on multi-walled carbon nanotube immobilized on glassy carbon electrode, *Measurement* **71** (2015) 23–30.

97. I. Tiwari, K.P. Singh, M. Singh, C.E. Banks, Polyaniline/polyacrylic acid/multi-walled carbon nanotube modified electrodes for sensing ascorbic acid, *Anal. Methods* **4** (2012) 118–124.

98. H. Li, Y. Wang, D. Ye, J. Luo, B. Su, S. Zhang, J. Kong, An electrochemical sensor for simultaneous determination of ascorbic acid, dopamine, uric acid and tryptophan based on MWNTs bridged mesocellular graphene foam nanocomposite, *Talanta* **127** (2014) 255–261.

99. P.V. Narayana, T.M. Reddy, P. Gopal, G.R. Naidu, Electrochemical sensing of paracetamol and its simultaneous resolution in the presence of dopamine and folic acid at a multi-walled carbon nanotubes/poly(glycine) composite modified electrode, *Anal. Methods* **6** (2014) 9459–9468.

100. S. Shahrokhian, M. Azimzadeh, P. Hosseini, Modification of a glassy carbon electrode with a bilayer of multiwalled carbon nanotube/benzene disulfonate-doped polypyrrole: Application to sensitive voltammetric determination of olanzapine, *RSC Adv.* **4** (2014) 40553–40560.

101. Y. Peng, Z. Wu, Z. Liu, An electrochemical sensor for paracetamol based on an electropolymerized molecularly imprinted o-phenylenediamine film on a multi-walled carbon nanotube modified glassy carbon electrode, *Anal. Methods* **6** (2014) 5673–5681.

102. J.I. Gowda, D.G. Gunjiganvi, N.B. Sunagar, M.N. Bhat, S.T. Nandibewoor, MWCNT–CTAB modified glassy carbon electrode as a sensor for the determination of paracetamol, *RSC Adv.* **5** (2015) 49045–49053.

103. H. Zhai, Z. Liu, Z. Chen, Z. Liang, Z. Su, S. Wang, A sensitive electrochemical sensor with sulfonated graphene sheets/oxygen-functionalized multi-walled carbon nanotubes modified electrode for the detection of clenbuterol, *Sens. Actuators B* **210** (2015) 483–490.

104. P.V. Narayana, T.M. Reddy, P. Gopal, M.M. Reddy, G.R. Naidu, Electrocatalytic boost up of epinephrine and its simultaneous resolution in the presence of serotonin and folic acid at poly(serine)/multi-walled carbon nanotubes composite modified electrode: A voltammetric study, *Mater. Sci. Eng. C* **56** (2015) 57–65.

105. H.D. Silva, J. Pacheco, J. Silva, S. Viswanathan, C. Delerue-Matos, Molecularly imprinted sensor for voltammetric detection of norfloxacin, *Sens. Actuators B* **219** (2015) 301–307.

106. Y. Li, Z. Ye, P. Luo, Y. Li, B. Ye, A sensitive voltammetric sensor for salbutamol based on MWNTs composite nano-Au film modified electrode, *Anal. Methods* **6** (2014) 1928–1935.

107. B. Habibi, M. Jahanbakhshi, Silver nanoparticles/multi walled carbon nanotubes nanocomposite modified electrode: Voltammetric determination of clonazepam, *Electrochim. Acta* **118** (2014) 10–17.

108. V. Vinoth, J.J. Wu, A.M. Asiri, S. Anandan, Simultaneous detection of dopamine and ascorbic acid using silicate network interlinked gold nanoparticles and multi-walled carbon nanotubes, *Sens. Actuators B* **210** (2015) 731–741.

109. A.C.D. Sá, A. Cipri, A. González-Calabuig, N.R. Stradiotto, M.D. Valle, Resolution of galactose, glucose, xylose and mannose in sugarcane bagasse employing a voltammetric electronic tongue formed by metals oxy-hydroxide/MWCNT modified electrodes, *Sens. Actuators B* **222** (2016) 645–653.

110. A.A. Ensafi, M. Izadi, B. Rezaei, H. Karimi-Maleh, N-hexyl-3-methylimidazolium hexafluoro phosphate/multiwall carbon nanotubes paste electrode as a biosensor for voltammetric detection of morphine, *J. Mol. Liq.* **174** (2012) 42–47.

111. M. Keyvanfard, R. Shakeri, H. Karimi-Maleh, K. Alizad, Highly selective and sensitive voltammetric sensor based on modified multiwall carbon nanotube paste electrode for simultaneous determination of ascorbic acid, acetaminophen and tryptophan, *Mater. Sci. Eng. C* **33** (2013) 811–816.

112. M. Keyvanfard, V. Khosravi, H. Karimi-Maleh, K. Alizad, B. Rezaei, Voltammetric determination of 6-mercaptopurine using a multiwall carbon nanotubes paste electrode in the presence of isoprenaline as a mediator, *J. Mol. Liq.* **177** (2013) 182–189.

113. E. Haghshenas, T. Madrakian, A. Afkhami, A novel electrochemical sensor based on magneto Au nanoparticles/carbon paste electrode for voltammetric determination of acetaminophen in real samples, *Mater. Sci. Eng. C* **57** (2015) 205–214.

114. S. Azodi-Deilami, E. Asadi, M. Abdouss, F. Ahmadi, A.H. Najafabadi, S. Farzaneh¸ Determination of meloxicam in plasma samples using a highly selective and sensitive voltammetric sensor based on carbon paste electrodes modified by molecularly imprinted polymer nanoparticle–multiwall carbon nanotubes, *Anal. Methods* **7** (2015) 1280–1292.

115. B. Habibi, M. Abazari, M.H. Pournaghi-Azar, A carbon nanotube modified electrode for determination of caffeine by differential pulse voltammetry, *Chin. J. Catal.* **33** (2012) 1783–1790.

116. L. Chen, F. Chang, L. Meng, M. Li, Z. Zhu, A novel electrochemical chiral sensor for 3,4-dihydroxyphenylalanine based on the combination of single-walled carbon nanotubes, sulfuric acid and square wave voltammetry, *Analyst* **139** (2014) 2243–2248.

117. B. Habibi, M. Abazari, M.H. Pournaghi-Azar, Simultaneous determination of codeine and caffeine using single-walled carbon nanotubes modified carbon-ceramic electrode, *Colloids Surf. B* **114** (2014) 89–95.

118. L. Yang, L. Wang, K. Li, B. Ye, Sensitive voltammetric determination of neohesperidin dihydrochalcone based on SWNTs modified glassy carbon electrode, *Anal. Methods* **6** (2014) 9410–9418.

119. Z. Ye, L. Yang, J. Wen, B. Ye, Sensitive determination of natamycin based on a new voltammetric sensor: A single-walled carbon nanotube composite poly(L-serine) film modified electrode, *Anal. Methods* **7** (2015) 2855–2861.

120. Z.M. Khoshhesab, Simultaneous electrochemical determination of acetaminophen, caffeine and ascorbic acid using a new electrochemical sensor based on CuO–graphene nanocomposite, *RSC Adv.* **5** (2015) 95140–95148.

121. H. Daneshinejad, M.A. Chamjangali, N. Goudarzi, A. Roudbari, Application of a thin film of poly(solochrome black T) as a redox mediator for the electro-catalytic

simultaneous determination of dopamine and acetaminophen in the pharmaceutical and biological samples, *Mater. Sci. Eng. C* **58** (2016) 532–540.

122. E. Wierzbicka, G.D. Sulka, Fabrication of highly ordered nanoporous thin Au films and their application for electrochemical determination of epinephrine, *Sens. Actuators B* **222** (2016) 270–279.

123. S. Sharifian, A. Nezamzadeh-Ejhieh, Modification of carbon paste electrode with Fe(III)-clinoptilolite nano-particles for simultaneous voltammetric determination of acetaminophen and ascorbic acid, *Mater. Sci. Eng. C* **58** (2016) 510–520.

124. Y.E. Bouabi, A. Farahi, N. Labjar, S.E. Hajjaji, M. Bakasse, M.A.E. Mhammedi, Square wave voltammetric determination of paracetamol at chitosan modified carbon paste electrode: Application in natural water samples, commercial tablets and human urines, *Mater. Sci. Eng. C* **58** (2016) 70–77.

125. M.N. Abbas, E. Zahran, Novel solid-state cadmium ion-selective electrodes based on its tetraiodo- and tetrabromo-ion pairs with cetylpyridinium, *J. Electroanal. Chem.* **576** (2005) 205–213.

126. A.K. Singh, P. Saxena, A. Panwar, Manganese(II)-selective PVC membrane electrode based on a pentaazamacrocyclic manganese complex, *Sens. Actuators B* **110** (2005) 377–381.

127. A.K. Jain, V.K. Gupta, P.A. Ganeshpure, J.R. Raisoni, Ni(II)-selective ion sensors of salen type Schiff base chelates, *Anal. Chim. Acta* **553** (2005) 177–184.

128. A.R. Fakhari, T.A. Raji, H. Naeimi, Copper-selective PVC membrane electrodes based on salens as carriers, *Sens. Actuators B* **104** (2005) 317–323.

129. V.K. Gupta, M.A. Khayat, A.K. Minocha, P. Kumar, Zinc(II)-selective sensors based on dibenzo-24-crown-8 in PVC matrix, *Anal. Chim. Acta* **532** (2005) 153–158.

130. V.K. Gupta, A.K. Jain, P. Kumar, S. Agarwal, G. Maheshwari, Chromium(III)-selective sensor based on tri-o-thymotide in PVC matrix, *Sens. Actuators B* **113** (2006) 182–186.

131. H.A. Zamani, G. Rajabzadeh, M.R. Ganjali, Highly selective and sensitive chromium(III) membrane sensors based on 4-amino-3-hydrazino-6-methyl-1,2,4-triazin-5-one as a new neutral ionophore, *Sens. Actuators B* **119** (2006) 41–46.

132. V.K. Gupta, A.K. Singh, S. Mehtab, B. Gupta, A cobalt(II)-selective PVC membrane based on a Schiff base complex of N,N´-bis(salicylidene)-3,4-diaminotoluene, *Anal. Chim. Acta* **566** (2006) 5–10.

133. A.K. Singh, R.P. Singh, P. Saxena, Cobalt(II)-selective electrode based on a newly synthesized macrocyclic compound, *Sens. Actuators B* **114** (2006) 578–583.

134. V.K. Gupta, A.K. Jain, G. Maheshwari, H. Lang, Z. Ishtaiwi, Copper(II)-selective potentiometric sensors based on porphyrins in PVC matrix, *Sens. Actuators B* **117** (2006) 99–106.

135. V.K. Gupta, S. Agarwal, A. Jakob, H. Lang, A zinc-selective electrode based on *N,N'*-bis(acetylacetone)ethylenediimine, *Sens. Actuators B* **114** (2006) 812–818.

136. M.H. Mashhadizadeh, A. Mostafavi, H. Allah-Abadi, I. Sheikhshoai, New Schiff base modified carbon paste and coated wire PVC membrane electrode for silver ion, *Sens. Actuators B* **113** (2006) 930–936.

137. A.A. Khan, Inamuddin, Applications of Hg(II) sensitive polyaniline Sn(IV) phosphate composite cation-exchange material in determination of Hg^{2+} from aqueous solutions and in making ion-selective membrane electrode, *Sens. Actuators B* **120** (2006) 10–18.

138. X. Yu, Z. Zhou, Y. Wang, Y. Liu, Q. Xie, D. Xiao, Mercury(II)-selective polymeric membrane electrode based on the 3-[4-(dimethylamino)phenyl]-5-mercapto-1,5-diphenylpentanone, *Sens. Actuators B* **123** (2007) 352–358.

139. F. Bakhtiarzadeh, S.A. Ghani, An ion selective electrode for mercury(II) based on mercury(II) complex of poly(4-vinyl pyridine), *J. Electroanal. Chem.* **624** (2008) 139–143.

140. V.K. Gupta, A.K. Jain, G. Maheshwari, Manganese (II) selective PVC based membrane sensor using a Schiff base, *Talanta* **72** (2007) 49–53.

141. M.H. Mashhadizadeh, E.P. Taheri, I. Sheikhshoaie, A novel Mn^{2+} PVC membrane electrode based on a recently synthesized Schiff base, *Talanta* **72** (2007) 1088–1092.

142. J. Wang, L. Wang, Y. Han, J. Jia, L. Jiang, W. Yang, Q. Sun, H. Lv, PVC membrane electrode based on triheptyl dodecyl ammonium iodide for the selective determination of molybdate(VI), *Anal. Chim. Acta* **589** (2007) 33–38.

143. H.A. Zamani, M.T. Hamed-Mosavian, E. Hamidfar, M.R. Ganjali, P. Norouzi, A novel iron(III)-PVC membrane potentiometric sensor based on *N*-(2-hydroxyethyl) ethylenediamine-*N,N',N''*-triacetic acid, *Mater. Sci. Eng. C* **28** (2008) 1551–1555.

144. B. Rezaei, S. Meghdadi, R.F. Zarandi, A fast response cadmium-selective polymeric membrane electrode based on *N,N'*-(4-methyl-1,2-phenylene)diquinoline-2-carboxamide as a new neutral carrier, *J. Hazard. Mater.* **153** (2008) 179–186.

145. A.K. Singh, S. Mehtab, Polymeric membrane sensors based on Cd(II) Schiff base complexes for selective iodide determination in environmental and medicinal samples, *Talanta* **74** (2008) 806–814.

146. M. Shamsipur, A.S. Dezaki, M. Akhond, H. Sharghi, Z. Paziraee, K. Alizadeh, Novel PVC-membrane potentiometric sensors based on a recently synthesized sulfur-containing macrocyclic diamide for Cd^{2+} ion. Application to flow-injection potentiometry, *J. Hazard. Mater.* **172** (2009) 566–573.

147. R.K. Mahajan, R.K. Puri, A. Marwaha, I. Kaur, M.P. Mahajan, Highly selective potentiometric determination of mercury(II) ions using 1-furan-2-yl-4-(4-nitrophenyl)-2-phenyl-5H-imidazole-3-oxide based membrane electrodes, *J. Hazard. Mater.* **167** (2009) 237–243.

148. M.K. Rofouei, M. Mohammadi, M.B. Gholivand, Mercury(II) selective membrane electrode based on 1,3-bis(2-methoxybenzene)triazene, *Mater. Sci. Eng. C* **29** (2009) 2154–2159.

149. M.B. Gholivand, M. Mohammadi, M. Khodadadian, M.K. Rofouei, Novel platinum(II) selective membrane electrode based on 1,3-bis(2-cyanobenzene)triazene, *Talanta* **78** (2009) 922–928.

150. P. Kumar, Y.B. Shim, A novel cobalt(II)-selective potentiometric sensor based on p-(4-n-butylphenylazo)calix[4]arene, *Talanta* **77** (2009) 1057–1062.

151. H.A. Zamani, M.R. Ganjali, H. Behmadi, M.A. Behnajady, Fabrication of an iron(III) PVC-membrane sensor based on bis-benzilthiocarbohydrazide as a selective sensing material, *Mater. Sci. Eng. C* **29** (2009) 1535–1539.

152. A. Babakhanian, M.B. Gholivand, M. Mohammadi, M. Khodadadian, A. Shockravi, M. Abbaszadeh, A. Ghanbary, Fabrication of a novel iron(III)–PVC membrane sensor based on a new 1,1'-(iminobis(methan-1-yl-1-ylidene))dinaphthalen-2-ol synthetic ionophore for direct and indirect determination of free iron species in some biological and non-biological samples, *J. Hazard. Mater.* **177** (2010) 159–166.

153. M.G. Motlagh, M.A. Taher, A. Ahmadi, PVC membrane and coated graphite potentiometric sensors based on 1-phenyl-3-pyridin-2-yl-thiourea for selective determination of iron(III), *Electrochim. Acta* **55** (2010) 6724–6730.

154. M. Masrournia, H.A. Zamani, H.A. Mirrashid, M.R. Ganjali, F. Faridbod, Di-tert-butylazodicarboxylate based PVC membrane sensor for Fe(III) ion measurement in pharmaceutical formulation, *Mater. Sci. Eng. C* **31** (2011) 574–578.

155. H.A. Zamani, M.R. Ganjali, F. Faridbod, M. Salavati-Niasari, Heptadentate Schiff-base based PVC membrane sensor for Fe(III) ion determination in water samples, *Mater. Sci. Eng. C* **32** (2012) 564–568.

156. J. Zhang, J. Ding, T. Yin, X. Hu, S. Yu, W. Qin, Synthesis and characterization of monoazathiacrown ethers as ionophores for polymeric membrane silver-selective electrodes, *Talanta* **81** (2010) 1056–1062.

157. A. Abbaspour, M. Refahi, A. Khalafi-Nezhad, N.S. Rad, S. Behrouz, Carbon composite–PVC based membrane coated platinum electrode for chromium determination, *J. Hazard. Mater.* **184** (2010) 20–25.

158. S.Y. Kazemi, A.S. Hamidi, N. Asanjarani, J. Zolgharnein, Optimization of a new polymeric chromium(III) membrane electrode based on methyl violet by using experimental design, *Talanta* **81** (2010) 1681–1687.

159. I.M. Isa, S. Mustafar, M. Ahmad, N. Hashim, S.A. Ghani, Cobalt(II) selective membrane electrode based on palladium(II) dichloro acetylthiophene fenchone azine, *Talanta* **87** (2011) 230–234.

160. A. Shokrollahi, A. Abbaspour, M. Ghaedi, A.N. Haghighi, A.H. Kianfar, M. Ranjbar, Construction of a new Cu^{2+} coated wire ion selective electrode based on 2-((2-(2-(2-(2-hydroxy-5-methoxybenzylidene amino)phenyl)disufanyl)phenylimino) methyl)-4-methoxyphenol Schiff base, *Talanta* **84** (2011) 34–41.

161. M.N. Kopylovich, K.T. Mahmudov, A.J.L. Pombeiro , Poly(vinyl) chloride membrane copper-selective electrode based on 1-phenyl-2-(2-hydroxyphenylhydrazo)butane-1,3-dione, *J. Hazard. Mater.* **186** (2011) 1154–1162.

162. M. Ghanei-Motlagh, M.A. Taher, V. Saheb, M. Fayazi, I. Sheikhshoaie, Theoretical and practical investigations of copper ion selective electrode with polymeric membrane based on *N,N'*-(2,2-dimethylpropane-1,3-diyl)-bis(dihydroxy acetophenone), *Electrochim. Acta* **56** (2011) 5376–5385.

163. I. Sheikhshoaie, T. Shamspur, S.Y. Ebrahimipur, Asymmetric Schiff base as carrier in PVC membrane electrodes for manganese(II) ions, *Arabian J. Chem.* **5** (2012) 201–205.

164. V.K. Gupta, L.P. Singh, R. Singh, N. Upadhyay, S.P. Kaur, B. Sethi, A novel copper(II) selective sensor based on dimethyl 4,4′ (o-phenylene) bis(3-thioallophanate) in PVC matrix, *J. Mol. Liq.* **174** (2012) 11–16.

165. Z. Yan, Y. Lu, H. Wang, S. Wu, B. Zhao, A heterocycle functionalized p-tert-butylcalix[4]arene as a neutral carrier for silver(I) ion-selective electrode, *J. Mol. Liq.* **183** (2013) 72–78.

166. F. Karimian, G.H. Rounaghi, M.H. Arbab-Zavar, Construction of a PVC based 15-crown-5 electrochemical sensor for Ag(I) cation, *Chin. Chem. Lett.* **25** (2014) 809–814.

167. A. Dadkhah, M.K. Rofouei, M.H. Mashhadizadeh, Synthesis and characterization of *N,N′*-bis(benzophenone imine)formamidine as ionophores for silver-selective electrodes, *Sens. Actuators B* **202** (2014) 410–416.

168. M. Naushad, Inamuddin, T.A. Rangreez, Z.A. ALOthman, A mercury ion selective electrode based on poly-o-toluidine Zr(IV) tungstate composite membrane, *J. Electroanal. Chem.* **713** (2014) 125–130.

169. M. Ghanei-Motlagh, M. Fayazi, M.A. Taher, On the potentiometric response of mercury(II) membrane sensors based on symmetrical thiourea derivatives–Experimental and theoretical approaches, *Sens. Actuators B* **199** (2014) 133–141.

170. S.M.J.M. Kermani, M. Ghanei-Motlagh, R. Zhiani, M.A. Taher, M. Fayazi, I. Razavipanah, Novel solid-state mercury(II)-selective electrode based on symmetrical sulfur-containing carrier, *J. Mol. Liq.* **206** (2015) 145–150.

171. T. Sardohan-Koseoglu, E. Kir, B. Dede, Preparation and analytical application of the novel Hg(II)-selective membrane electrodes based on oxime compounds, *J. Colloid Interface Sci.* **444** (2015) 17–23.

172. A. Pazik, A. Skwierawska, Synthesis and application of tetrazole di- and triamide derivatives in ion-selective membrane electrodes, *Sens. Actuators B* **196** (2014) 370–380.

173. C. Wardak, Solid contact cadmium ion-selective electrode based on ionic liquid and carbon nanotubes, *Sens. Actuators B* **209** (2015) 131–137.

174. S. Ahmadzadeh, M. Rezayi, E. Faghih-Mirzaei, M. Yoosefian, A. Kassim, Highly selective detection of titanium(III) in industrial waste water samples using meso-octamethylcalix[4]pyrrole-doped PVC membrane ion-selective electrode, *Electrochim. Acta* **178** (2015) 580–589.

175. Y. Xiang, A. Tong, P. Jin, Y. Ju, New fluorescent rhodamine hydrazone chemosensor for Cu(II) with high selectivity and sensitivity, *Org. Lett.* **8** (2006) 2863–2866.

176. N. Singh, N. Kaur, C.N. Choitir, J.F. Callan, A dual detecting polymeric sensor: Chromogenic naked eye detection of silver and ratiometric fluorescent detection of manganese, *Tetrahedron Lett.* **50** (2009) 4201–4204.

177. V. Bhalla, R. Tejpal, M. Kumar, R.K. Puri, R.K. Mahajan, Terphenyl based 'turn on' fluorescent sensor for mercury, *Tetrahedron Lett.* **50** (2009) 2649–2652.

178. S. Wang, G. Men, L. Zhao, Q. Hou, S. Jiang, Binaphthyl-derived salicylidene Schiff base for dual-channel sensing of Cu, Zn cations and integrated molecular logic gates, *Sens. Actuators B* **145** (2010) 826–831.

179. D. Maity, T. Govindaraju, Pyrrolidine constrained bipyridyl-dansyl click fluoroionophore as selective Al^{3+} sensor, *Chem. Commun.* **46** (2010) 4499–4501.

180. X. Xie, Y. Qin, A dual functional near infrared fluorescent probe based on the bodipy fluorophores for selective detection of copper and aluminum ions, *Sens. Actuators B* **156** (2011) 213–217.

181. A.K. Mahapatra, G. Hazra, N.K. Das, S. Goswami, A highly selective triphenylamine-based indolylmethane derivatives as colorimetric and turn-off fluorimetric sensor toward Cu^{2+} detection by deprotonation of secondary amines, *Sens. Actuators B* **156** (2011) 456–462.

182. R. Tang, K. Lei, K. Chen, H. Zhao, J. Chen, A rhodamine-based off–on fluorescent chemosensor for selectively sensing Cu(II) in aqueous solution, *J. Fluoresc.* **21** (2011) 141–148.

183. S.B. Liu, C.F. Bi, Y.H. Fan, Y. Zhao, P.F. Zhang, Q.D. Luo, D.M. Zhang, Synthesis, characterization and crystal structure of a new fluorescent probe based on Schiff base for the detection of Zinc(II), *Inorg. Chem. Commun.* **14** (2011) 1297–1301.

184. W. Liu, S. Pu, D. Jiang, S. Cui, G. Liu, C. Fan, Fluorescent probes for Al(III) and Cr(III) based on a photochromic diarylethene bearing a fluorescent rhodamine unit, *Microchim. Acta* **174** (2011) 329–336.

185. A.J. Weerasinghe, F.A. Abebe, E. Sinn, Rhodamine based turn-on dual sensor for Fe^{3+} and Cu^{2+}, *Tetrahedron Lett.* **52** (2011) 5648–5651.

186. Y. Liu, B. Li, D. Cheng, X. Duan, Simple and sensitive fluorescence sensor for detection of potassium ion in the presence of high concentration of sodium ion using berberine–G-quadruplex complex as sensing element, *Microchem. J.* **99** (2011) 503–507.

187. M. Hosseini, Z. Vaezi, M.R. Ganjali, F. Faridbod, S.D. Abkenar, Fluorescence "turn-on" chemosensor for the selective detection of beryllium, *Spectrochim. Acta A* **83** (2011) 161–164.

188. X. Ji, W. Shi, S. Zhang, M. Wei, D.G. Evans, X. Duan, A ratiometric fluorescence sensor for Be^{2+} based on Beryllon II/layered double hydroxide ultrathin films, *Anal. Chim. Acta* **728** (2012) 77–85.

189. K. Kaur, V.K. Bhardwaj, N. Kaur, N. Singh, Fluorescent chemosensor for Al^{3+} and resultant complex as a chemosensor for perchlorate anion: First molecular security keypad lock based on Al^{3+} and ClO_4^- inputs, *Inorg. Chem. Commun.* **26** (2012) 31–36.

190. J. You, J. Kim, T. Park, B. Kim, E. Kim, Highly fluorescent conjugated polyelectrolyte nanostructures: Synthesis, self-assembly, and Al^{3+} ion sensing, *Adv. Funct. Mater.* **22** (2012) 1417–1424.

191. J.Y. Jung, S.J. Han, J. Chun, C. Lee, J. Yoon, New thiazolothiazole derivatives as fluorescent chemosensors for Cr^{3+} and Al^{3+}, *Dyes Pigm.* **94** (2012) 423–426.

192. Y. Zhou, J. Zhang, H. Zhou, X. Hu, L. Zhang, M. Zhang, A highly selective fluorescent probe for Al^{3+} based on 4-aminoantipyrine, *Spectrochim. Acta A* **106** (2013) 68–72.

193. A. Helal, S.H. Kim, H.S. Kim, A highly selective fluorescent turn-on probe for Al^{3+} via Al^{3+}-promoted hydrolysis of ester¸ *Tetrahedron* **69** (2013) 6095–6099.

194. X.Y. Cheng, M.F. Wang, Z.Y. Yang, Y. Li, T.R. Li, C.J. Liu, Q.X. Zhou, A highly sensitive and selective Schiff base fluorescent chemodosimeter for aluminium(III), *J. Coord. Chem.* **66** (2013) 1847–1853.

195. X.Y. Cheng, R. Fang, Z.Y. Yang, M.F. Wang, Q.X. Zhou, T.R. Li, Y. Li, Interaction of a Schiff-base fluorescent sensor with Al^{3+}: Experimental and computational studies, *J. Coord. Chem.* **67** (2014) 737–744.

196. V.D. Suryawanshi, A.H. Gore, P.R. Dongare, P.V. Anbhule, S.R. Patil, G.B. Kolekar, A novel pyrimidine derivative as a fluorescent chemosensor for highly selective detection of aluminium(III) in aqueous media, *Spectrochim. Acta A* **114** (2013) 681–686.

197. Z. Liu, Z. Yang, Y. Li, T. Li, B. Wang, Y. Li, X. Jin, An effective mutli-wavelength emissive aluminium ion fluorescence chemosensor based on 3-[1′-(2′-hydroxy-α-methylbenzylidene-imino)]-2-(p-N,N-dimethylaminophenyl)-1,2-dihydroquinazolin-4-(3H)-one, *Inorg. Chim. Acta* **395** (2013) 77–80.

198. C.Y. Lu, Y.W. Liu, P.J. Hung, C.F. Wan, A.T. Wu, A turn-on and reversible schiff-base fluorescence sensor for Al^{3+} ion, *Inorg. Chem. Commun.* **35** (2013) 273–275.

199. R. Azadbakht, J. Khanabadi, A highly sensitive and selective off–on fluorescent chemosensor for Al^{3+} based on naphthalene derivative, *Inorg. Chem. Commun.* **30** (2013) 21–25.

200. R. Azadbakht, J. Khanabadi, A novel aluminum-sensitive fluorescent nano-chemosensor based on naphthalene macrocyclic derivative, *Tetrahedron* **69** (2013) 3206–3211.

201. A. Sahana, A. Banerjee, S. Lohar, S. Das, I. Hauli, S.K. Mukhopadhyay, J.S. Matalobos, D. Das, Naphthalene based highly selective off–on–off type fluorescent probe for Al^{3+} and NO_2^- ions for living cell imaging at physiological pH, *Inorg. Chim. Acta* **398** (2013) 64–71.

202. Z. Liu, Y. Li, Y. Ding, Z. Yang, B. Wang, Y. Li, T. Li, W. Luo, W. Zhu, J. Xie, C. Wang, Water-soluble and highly selective fluorescent sensor from naphthol aldehyde-tris derivate for aluminium ion detection, *Sens. Actuators B* **197** (2014) 200–205.

203. D.P. Singh, V.P. Singh, A dihydrazone based fluorescent probe for selective determination of Al^{3+} ions, *J. Lumin.* **155** (2014) 7–14.

204. R. Azadbakht, J. Khanabadi, A novel fluorescent nano-chemosensor for Al(III) ions using a new macrocyclic receptor, *Spectrochim. Acta A* **124** (2014) 249–255.

205. C. Liu, Z. Yang, M. Yan, A highly selective and sensitive fluorescent turn-on chemosensor for Al^{3+} based on a chromone Schiff base, *J. Coord. Chem.* **65** (2012) 3845–3850.

206. L. Fan, J.C. Qin, T.R. Li, B.D. Wang, Z.Y. Yang, A chromone Schiff-base as Al(III) selective fluorescent and colorimetric chemosensor, *J. Lumin.* **155** (2014) 84–88.

207. L. Fan, X.H. Jiang, B.D. Wang, Z.Y. Yang, 4-(8´-Hydroxyquinolin-7´-yl)methyleneimino-1-phenyl-2,3-dimethyl-5-pyzole as a fluorescent chemosensor for aluminium ion in acid aqueous medium, *Sens. Actuators B* **205** (2014) 249–254.

208. K. Zhang, Z.Y. Yang, B.D. Wang, S.B. Sun, Y.D. Li, T.R. Li, Z.C. Liu, J.M. An, A highly selective chemosensor for Al^{3+} based on 2-oxo-quinoline-3-carbaldehyde Schiff-base, *Spectrochim. Acta A* **124** (2014) 59–63.

209. S. Pu, T. Wang, G. Liu, W. Liu, S. Cui, A new photoinduced fluorescent switch based on a photochromic diarylethene with a rhodamine fluorophore, *Dyes Pigm.* **94** (2012) 416–422.

210. A. Dhara, A. Jana, S. Konar, S.K. Ghatak, S. Ray, K. Das, A. Bandyopadhyay, N. Guchhait, S.K. Kar, A novel rhodamine-based colorimetric chemodosimeter for the rapid detection of Al^{3+} in aqueous methanol: Fluorescent 'off–on' mechanism, *Tetrahedron Lett.* **54** (2013) 3630–3634.

211. J. Bordini, I. Calandreli, G.O. Silva, K.Q. Ferreira, D.P.S. Leitão-Mazzi, E.M. Espreafico, E. Tfouni, A rhodamine-B-based turn-on fluorescent sensor for biological iron(III), *Inorg. Chem. Commun.* **35** (2013) 255–259.

212. C.Y. Li, Y. Zhou, Y.F. Li, C.X. Zou, X.F. Kong, Efficient FRET-based colorimetric and ratiometric fluorescent chemosensor for Al^{3+} in living cells, *Sens. Actuators B* **186** (2013) 360–366.

213. A. Dhara, A. Jana, N. Guchhait, S.K. Kar, Isatin appended rhodamine scaffold as an efficient chemical tool to detect selectively Al^{3+}, *J. Lumin.* **154** (2014) 369–375.

214. A. Dhara, A. Jana, S.K. Mandal, A.R. Khuda-Bukhsh, N. Guchhait, S.K. Kar, A unique rhodamine-based 'off–on' molecular spy for selective detection of trivalent aluminium and chromium ions: Synthesis, crystal structure and spectroscopic properties along with living cell imaging, *Inorg. Chim. Acta* **423** (2014) 454–461.

215. Q. Huang, Y. Zhou, Q. Zhang, E. Wang, Y. Min, H. Qiao, J. Zhang, T. Ma, A new "off–on" fluorescent probe for Pd^{2+} in aqueous solution and live-cell based on spirolactam ring-opening reaction, *Sens. Actuators B* **208** (2015) 22–29.

216. N.R. Chereddy, P. Nagaraju, M.V.N. Raju, V.R. Krishnaswamy, P.S. Korrapati, P.R. Bangal, V.J. Rao, A novel FRET 'off–on' fluorescent probe for the selective detection of Fe^{3+}, Al^{3+} and Cr^{3+} ions: Its ultrafast energy transfer kinetics and application in live cell imaging, *Biosens. Bioelectron.* **68** (2015) 749–756.

217. R. Manjunath, E. Hrishikesan, P. Kannan, A selective colorimetric and fluorescent sensor for Al^{3+} ion and its application to cellular imaging, *Spectrochim. Acta A* **140** (2015) 509–515.

218. Y. Fang, Y. Zhou, J.Y. Li, Q.Q. Rui, C. Yao, Naphthalimide–Rhodamine based chemosensors for colorimetric and fluorescent sensing Hg^{2+} through different signaling mechanisms in corresponding solvent systems, *Sens. Actuators B* **215** (2015) 350–359.

219. F. Yan, T. Zheng, D. Shi, Y. Zou, Y. Wang, M. Fu, L. Chen, W. Fu, Rhodamine-aminopyridine based fluorescent sensors for Fe^{3+} in water: Synthesis, quantum chemical interpretation and living cell application, *Sens. Actuators B* **215** (2015) 598–606.

220. J.W. Jeong, B.A. Rao, Y.A. Son, Rhodamine-chloronicotinaldehyde-based "off–on" chemosensor for the colorimetric and fluorescent determination of Al^{3+} ions, *Sens. Actuators B* **208** (2015) 75–84.

221. Q. Huang, Q. Zhang, E. Wang, Y. Zhou, H. Qiao, L. Pang, F. Yu, A new ''off–on'' fluorescent probe for Al^{3+} in aqueous solution based on rhodamine B and its application to bioimaging, *Spectrochim. Acta A* **152** (2016) 70–76.

222. S. Chopra, N. Singh, P. Thangarasu, V.K. Bhardwaj, N. Kaur, Fluorescent organic nanoparticles as chemosensor for nanomolar detection of Cs^+ in aqueous medium, *Dyes Pigm.* **106** (2014) 45–50.

223. L. Wang, L. Yang, D. Cao, A visual and fluorometric probe for Al(III) and Fe(III) using diketopyrrolopyrrole-based Schiff base, *Sens. Actuators B* **202** (2014) 949–958.

224. D.H. Kim, Y.S. Im, H. Kim, C. Kim, Solvent-dependent selective fluorescence sensing of Al^{3+} and Zn^{2+} using a single Schiff base, *Inorg. Chem. Commun.* **45** (2014) 15–19.

225. Y. Jiang, L.L. Sun, G.Z. Ren, X. Niu, W.Z. Hu, Z.Q. Hu, A new fluorescence turn-on probe for aluminum(III) with high selectivity and sensitivity, and its application to bioimaging, *ChemistryOpen* **4** (2015) 378–382.

226. Y. Li, Z. Liu, W. Zhu, H. Fu, Y. Ding, J. Xie, W. Yang, L. Li, C. Cheng, Two different emission-wavelength fluorescent probes for aluminium ion based on tunable fluorophores in aqueous media, *J. Fluoresc.* **25** (2015) 603–611.

227. J.C. Qin, Z.Y. Yang, Selective fluorescent sensor for Al^{3+} using a novel quinoline derivative in aqueous solution, *Synth. Met.* **209** (2015) 570–576.

228. Y.J. Chang, S.S. Wu, C.H. Hu, C. Cho, M.X. Kao, A.T. Wu, A new bifunctional schiff base as a colorimetric and fluorescence sensor for Al^{3+} and CN^-, *Inorg. Chim. Acta* **432** (2015) 25–31.

229. W.H. Ding, D. Wang, X.J. Zheng, W.J. Ding, J.Q. Zheng, W.H. Mu, W. Cao, L.P. Jin, A turn-on fluorescence chemosensor for Al^{3+}, F^- and CN^- ions, and its application in cell imaging, *Sens. Actuators B* **209** (2015) 359–367.

230. J.C. Qin, X.Y. Cheng, R. Fang, M.F. Wang, Z.Y. Yang, T.R. Li, Y. Li, Two schiff-base fluorescent sensors for selective sensing of aluminium(III): Experimental and computational studies, *Spectrochim. Acta A* **152** (2016) 352–357.

231. A. Guo, R. Zhu, Y. Ren, J. Dong, L. Feng, A "turn-on" fluorescent chemosensor for aluminum ion and cell imaging application, *Spectrochim. Acta A* **153** (2016) 530–534.

232. H.S. Kim, S. Angupillai, Y.A. Son, A dual chemosensor for both Cu^{2+} and Al^{3+}: A potential Cu^{2+} and Al^{3+} switched YES logic function with an INHIBIT logic gate and a novel solid sensor for detection and extraction of Al^{3+} ions from aqueous solution, *Sens. Actuators B* **222** (2016) 447–458.

233. C.A. Huerta-Aguilar, T. Pandiyan, N. Singh, N. Jayanthi, Three novel input logic gates supported by fluorescence studies: Organic nanoparticles (ONPs) as chemosensor for detection of Zn^{2+} and Al^{3+} in aqueous medium, *Spectrochim. Acta A* **146** (2015) 142–150.

234. D. Sarkar, A. Pramanik, S. Jana, P. Karmakar, T.K. Mondal, Quinoline based reversible fluorescent 'turn-on' chemosensor for the selective detection of Zn^{2+}: Application in living cell imaging and as INHIBIT logic gate, *Sens. Actuators B* **209** (2015) 138–146.

235. K. Ponnuvel, V. Padmini, R. Sribalan, A new tetrazole based turn-on fluorescence chemosensor for Zn^{2+} ions and its application in bioimaging, *Sens. Actuators B* **222** (2016) 605–611.

236. L. Subha, C. Balakrishnan, S. Natarajan, M. Theetharappan, B. Subramanian, M.A. Neelakantan, Water soluble and efficient amino acid schiff base receptor for reversible fluorescence turn-on detection of Zn^{2+} ions: Quantum chemical calculations and detection of bacteria, *Spectrochim. Acta A* **153** (2016) 249–256.

237. G.J. Park, J.J. Lee, G.R. You, L. Nguyen, I. Noh, C. Kim, A dual chemosensor for Zn^{2+} and Co^{2+} in aqueous media and living cells: Experimental and theoretical studies, *Sens. Actuators B* **223** (2016) 509–519.

238. O. Çimen, H. Dinçalp, C. Varlıklı, Studies on UV–vis and fluorescence changements in Co^{2+} and Cu^{2+} recognition by a new benzimidazole–benzothiadiazole derivative, *Sens. Actuators B* **209** (2015) 853–863.

239. R. An, D. Zhang, Y. Chen, Y.Z. Cui, A "turn-on" fluorescent and colorimetric sensor for selective detection of Cu^{2+} in aqueous media and living cells, *Sens. Actuators B* **222** (2016) 48–54.

240. X. Zheng, K.H. Lee, H. Liu, S.Y. Park, S.S. Yoon, J.Y. Lee, Y.G. Kim, A bis(pyridine-2-ylmethyl)amine-based selective and sensitive colorimetric and fluorescent chemosensor for Cu^{2+}, *Sens. Actuators B* **222** (2016) 28–34.

241. A. Bekhradnia, E. Domehri, M. Khosravi, Novel coumarin-based fluorescent probe for selective detection of Cu(II), *Spectrochim. Acta A* **152** (2016) 18–22.

242. D. Sharma, A. Kuba, R. Thomas, R. Kumar, H.J. Choi, S.K. Sahoo, An aqueous friendly chemosensor derived from vitamin B_6 cofactor for colorimetric sensing of Cu^{2+} and fluorescent turn-off sensing of Fe^{3+}, *Spectrochim. Acta A* **153** (2016) 393–396.

243. E. Wang, Y. Zhou, Q. Huang, L. Pang, H. Qiao, F. Yu, B. Gao, J. Zhang, Y. Min, T. Ma, 5-Hydroxymethylfurfural modified rhodamine B dual-function derivative: Highly sensitive and selective optical detection of pH and Cu^{2+}, *Spectrochim. Acta A* **152** (2016) 327–335.

244. Y. Yang, C.Y. Gao, N. Zhang, D. Dong, Tetraphenylethene functionalized rhodamine chemosensor for Fe^{3+} and Cu^{2+} ions in aqueous media, *Sens. Actuators B* **222** (2016) 741–746.

245. J. Geng, Y. Liu, J. Li, G. Yin, W. Huang, R. Wang, Y. Quan, A ratiometric fluorescent probe for ferric ion based on a 2,2´-bithiazole derivative and its biological applications, *Sens. Actuators B* **222** (2016) 612–617.

246. M.S.H. Faizi, S. Gupta, V.K. Mohan, V.K. Jain, P. Sen, Highly selective visual detection of Fe^{3+} at ppm level, *Sens. Actuators B* **222** (2016) 15–20.

247. Y. Zhao, G. Zhang, Z. Liu, C. Guo, C. Peng, M. Pei, P. Li, Benzimidazo[2,1-a]benz[de]isoquinoline-7-one-12-carboxylic acid based fluorescent sensors for pH and Fe^{3+}, *J. Photochem. Photobiol. A* **314** (2016) 52–59.

248. X. Wu, Q. Niu, T. Li, A novel urea-based "turn-on" fluorescent sensor for detection of Fe^{3+}/F^- ions with high selectivity and sensitivity, *Sens. Actuators B* **222** (2016) 714–720.

249. S. Janakipriya, N.R. Chereddy, P. Korrapati, S. Thennarasu, A.B. Mandal, Selective interactions of trivalent cations Fe^{3+}, Al^{3+} and Cr^{3+} turn on fluorescence in a naphthalimide based single molecular probe, *Spectrochim. Acta A* **153** (2016) 465–470.

250. V.K. Gupta, A.K. Singh, L.K. Kumawat, N. Mergu¸ An easily accessible switch-on optical chemosensor for the detection of noxious metal ions Ni(II), Zn(II), Fe(III) and UO_2(II), *Sens. Actuators B* **222** (2016) 468–482.

251. F. Ma, M. Sun, K. Zhang, S. Wang, A ratiometric fluorescence sensor for highly selective and sensitive detection of mercuric ion, *Sens. Actuators B* **209** (2015) 377–383.

252. Q. Niu, X. Wu, S. Zhang, T. Li, Y. Cui, X. Li, A highly selective and sensitive fluorescent sensor for the rapid detection of Hg^{2+} based on phenylamine-oligothiophene derivative, *Spectrochim. Acta A* **153** (2016) 143–146.

253. R. Azadbakht, J. Khanabadi, A novel fluorescent nano-chemosensor for cesium ions based on naphthalene macrocyclic derivative, *Spectrochim. Acta A* **139** (2015) 279–285.

254. S. Kambam, B. Wang, F. Wang, Y. Wang, H. Chen, J. Yin, X. Chen, A highly sensitive and selective fluorescein-based fluorescence probe for Au^{3+} and its application in living cell imaging, *Sens. Actuators B* **209** (2015) 1005–1010.

255. Q. Huang, Y. Zhou, Q. Zhang, E. Wang, Y. Min, H. Qiao, J. Zhang, T. Ma, A new "off–on" fluorescent probe for Pd^{2+} in aqueous solution and live-cell based on spirolactam ring-opening reaction, *Sens. Actuators B* **208** (2015) 22–29.

256. L.Q. Li, L.J. Gao, A novel rosamine based fluorescent sensor for Ag^{+} recognition, *Spectrochim. Acta A* **152** (2016) 426–430.

257. G.Q. Wang, J.C. Qin, L. Fan, C.R. Li, Z.Y. Yang, A turn-on fluorescent sensor for highly selective recognition of Mg^{2+} based on new Schiff's base derivative, *J. Photochem. Photobiol. A* **314** (2016) 29–34.

258. M.H. Kao, T.Y. Chen, Y.R. Cai, C.H. Hu, Y.W. Liu, Y. Jhong, A.T. Wu, A turn-on Schiff-base fluorescence sensor for Mg^{2+} ion and its practical application, *J. Lumin.* **169** (2016) 156–160.

CHAPTER 2
Principles, Theory and Practice of Sensors

2.1. Introduction

A number of various types of instrumental analytical techniques are available to the analysis of industrial, chemical, biomedical, drug formulations and environmental research. Consequently, the basic concepts of some analytical techniques applied in the present communications are described here:

2.1.1. Voltammetric techniques

2.1.2. Potentiometric ion selective electrodes

2.1.3. Spectrophotometric techniques

2.1.1. Voltammetric techniques

Voltammetry is a group of electroanalytical methods employed in numerous industrial processes. In these techniques, a time-dependent potential (E) excitation signal to the working electrode about an analyte is applied and the resulting current (i), with respect to the fixed potential of the reference electrode, flowing among the working and auxiliary electrodes is measured as a function of that potential [1, 2]. Hence, consequently the plot among applied potential versus measuring current is known as voltammogram. In some cases, the applied potential is varied or the current is monitored over a period of time (t). The arrangement of a modern typical voltammetric electrochemical cell is shown in Figure 2.1(a). In the present communications we have utilized glassy carbon electrode as working electrode shown in Figure 2.1(b).
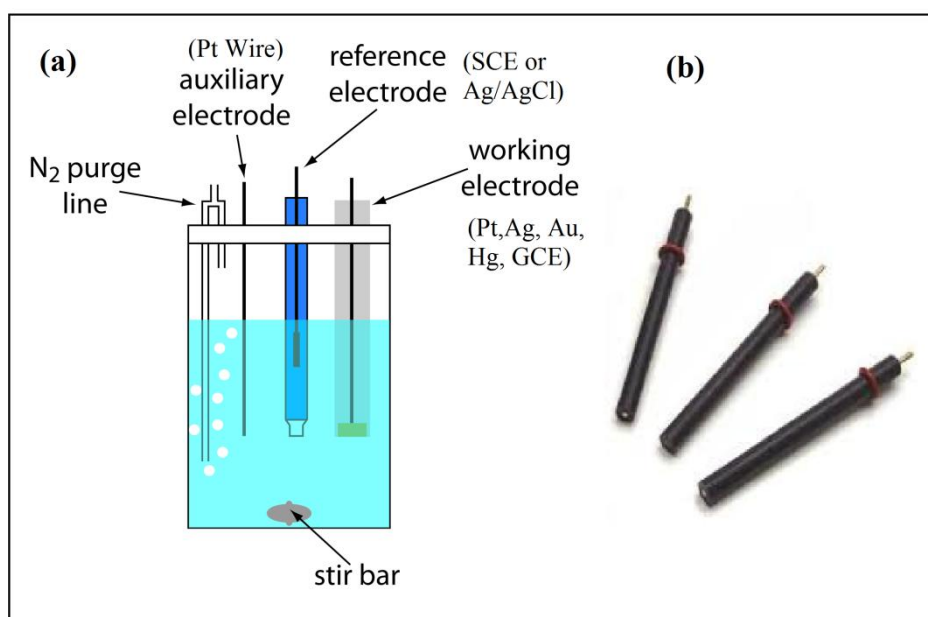
Figure 2.1. Schematic arrangement of a typical electrochemical cell for voltammetry (a) and (b) Glassy carbon electrode as working electrode.

2.1.1.1. Cyclic voltammetry

Cyclic voltammetry (CV) is an electrochemical technique that measures the current developed in an electrochemical cell under higher voltage compared to predicted by the Nernst equation. The potential generated on the working electrode is measured with respect to a reference electrode, and the resultant applied potential produces an excitation signal shown in Figure 2.2 [3, 4]. In the Figure 2.2(A), the forward scan of the potential first scans negatively, starting from a greater potential (a) and ending at a lower potential (d). The potential extrema (d) is the point where the voltage is sufficient enough to have caused an oxidation or reduction of an analyte, is called the switching potential. The reverse scan arises from (d) to (g), and where the potential scans are positively. The Figure 2.2 (A) shows a typical reduction occurring from (a) to (d) and an oxidation occurring from (d) to (g). This cycle can be repeated, and the scan rate can be varied. The slope of the excitation signal gives the scan rate used.
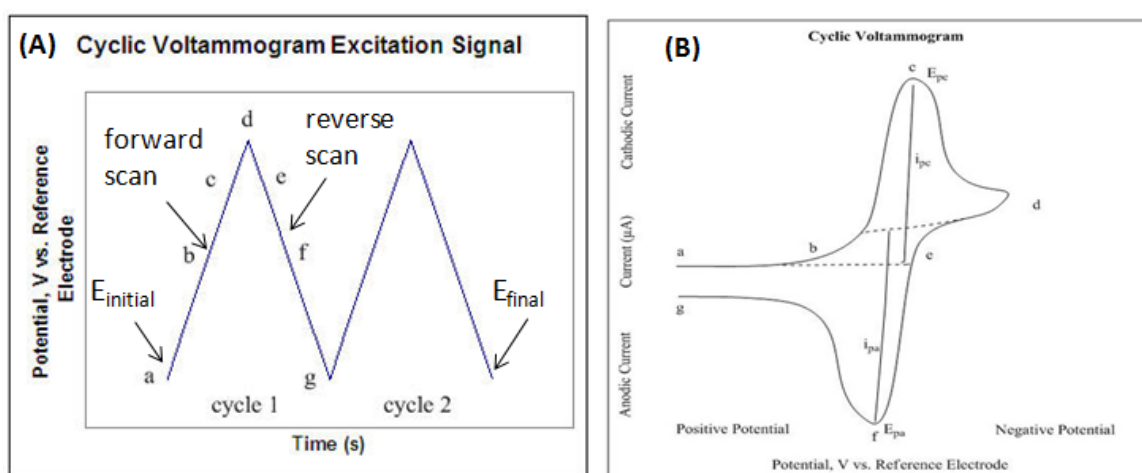
Figure 2.2. (A) Typical CV excitation signal (B) Voltammogram of a single electron oxidation–reduction.

In Figure 2.2 (B), the reduction process occurs from (a) the initial potential to (d) the switching potential. In this region the potential is scanned negatively to cause a reduction. The resulting current is called cathodic current (i_{pc}). The corresponding peak potential occurs at (c), and is called the cathodic peak potential (E_{pc}). The E_{pc} is reached when all of the substrate at the surface of the electrode has been reduced. After the switching potential has been reached (d), the potential scans positively from (d) to (g). This results in anodic current (I_{pa}) and oxidation to occur. The peak potential at (f) is called the anodic peak potential (E_{pa}), and is reached when all of the substrate at the surface of the electrode has been oxidized. Further, a useful information is that, if the diffusion constants

for the oxidized and reduced species are similar, the value of peak potential (E^o) can be estimated from the mean of E_{pa} and E_{pc}, and the separation of both the peaks is approximately (59/n) mV at 25 °C (n = number of electrons participating in the redox process). The peak current in cyclic voltammetry [5–7], for a reversible reaction is given by the Randles-Sevcik equation (at 25 °C):

$$i_p = (2.69 \times 10^5)n^{3/2}AD^{1/2}C \, v^{1/2} \qquad\qquad (2.1)$$

where,

i_p = peak current

n = number of electrons in the redox reaction

A = surface area of the working electrode (cm²)

D = diffusion coefficient for the electroactive species (cm²/s)

v = scan rate (V/s)

C = concentration of the electroactive species at the electrode (mol/cm³)

Consequently, cyclic voltammetry can be employed to study qualitative information about electrochemical processes under numerous conditions like; the presence of intermediates in oxidation-reduction reactions, the reversibility of a reaction. CV can also be used to determine the diffusion coefficient of an analyte, the electron stoichiometry of a system and the formal reduction potential.

2.1.1.2. Pulse voltammetric techniques

The basis of all the pulse voltammetric techniques is the difference in the rate of the decay of the charging and the faradaic currents followed by a potential step or pulse. The decays in the charging current is exponentially, while the faradaic current (for a diffusion-controlled current) decays as a function of $1/(time)^{1/2}$. The important parameters for pulse techniques are as follows:

1. Pulse amplitude – height of the potential pulse in mV. This may or may not be constant depending upon the technique.

2. Pulse width – duration of the potential pulse in ms.

3. Sample period – time at the end of the pulse during which the current is measured (ms).

4. Pulse period or drop time – the time required for one potential cycle (ms), and is particularly significant for voltammetry.

A lot of diverse pulse techniques (like normal pulse voltammetry, reverse pulse voltammetry, differential pulse voltammetry, staircase voltammetry and square wave

voltammetry) are accessible, which differ in their potential pulse wave forms, the number of sampling points, and whether a solid electrode (voltammetry) or a mercury drop electrode (polarography) is used. The discrimination against the charging current that is inherent in these techniques leads to lower detection limits (when compared to linear sweep techniques), which makes these techniques suitable for quantitative analysis. In the present communications differential pulse voltammetry and square wave voltammetry are described here:

2.1.1.2.1. Differential pulse voltammetry

Differential pulse voltammetry (DPV) is considered as a derivative of linear sweep voltammetry or staircase voltammetry, with a series of regular voltage pulses superimposed on the potential linear sweep or stair steps depicted in Figure 2.3. The current is measured immediately before each potential change, and the current difference is plotted as a function of potential. By sampling the current just before the potential is changed, the effect of the charging current can be decreased. Further, the reversible reactions exhibit symmetrical peaks, and irreversible reactions exhibit asymmetrical peaks. In this technique an analyte can be detected at a level of about 10^{-8} M. The detailed study of DPV is described in the literature [8, 9].
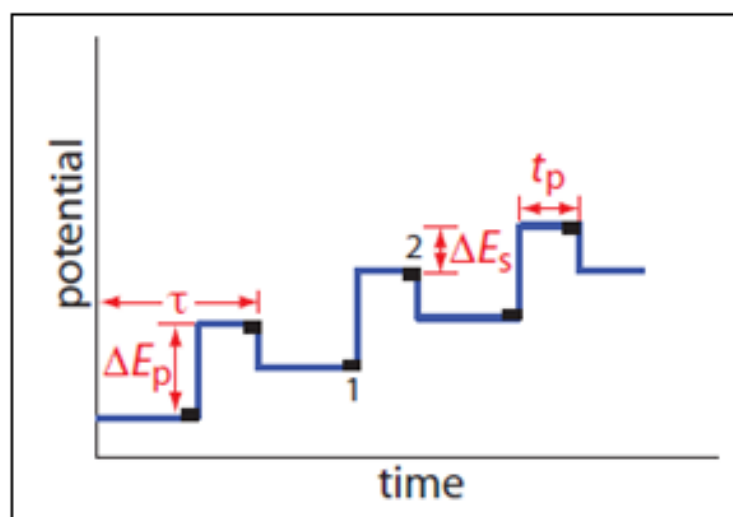
Figure 2.3. Potential-excitation signals for differential pulse voltammetry.

The current is sampled at the time intervals shown by the black rectangles. When measuring a change in current, Δi, the current at point 1 is subtracted from the current at point 2. The symbols shown in the diagrams are as follows: τ is the cycle time (pulse period); ΔE_p is a fixed or variable pulse potential (pulse amplitude); ΔE_s is the fixed change in potential per cycle, and t_p is the pulse time (pulse width).

2.1.1.2.2. Square wave voltammetry

Square wave voltammetry (SWV) is a form of linear potential sweep voltammetry. In a square wave voltammetric experiment, the potential waveform can be viewed as a superposition of a regular square wave onto an underlying staircase (Figure 2.4). Thus SWV can be considered a modification of staircase voltammetry.
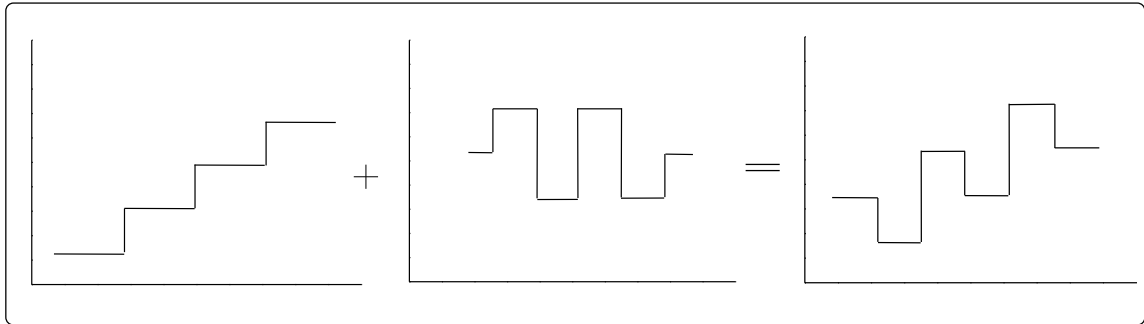
Figure 2.4. Image explaining origins of the potential waveform in square wave voltammetric analysis.

In square wave voltammetric process the current is sampled at two times; once at the end of the forward potential pulse and again at the end of the reverse potential pulse (in both cases immediately before the potential direction is reversed). This difference current is displayed as a function of the applied potential. As a result of this current sampling technique, the contribution to the current signal resulting from capacitive (sometimes referred to as non-faradaic or charging) current is minimal [10]. The potential wave form for square wave voltammetry (SWV) is shown in Figure 2.5 and the terms are explained in the section 2.1.1.2.1.
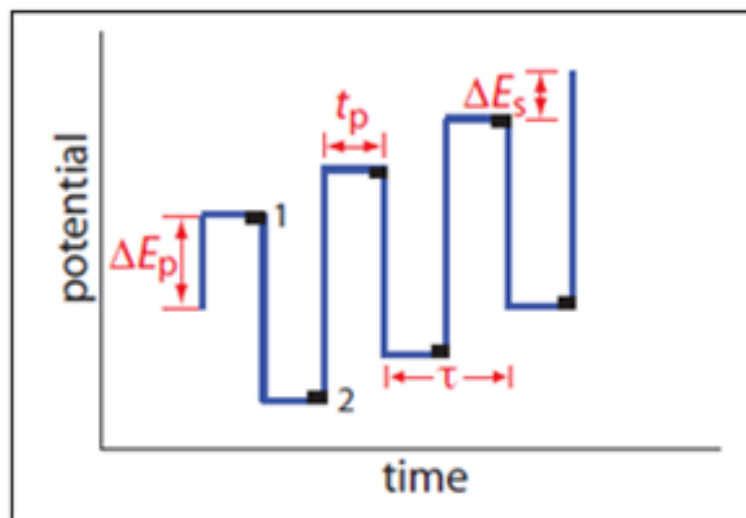
Figure 2.5. Potential-excitation signals for square wave voltammetry.

Square wave voltammetry has been employed in various electrochemical measurements owing to its characteristics such as minimal contributions from non-faradaic currents, the use of a differential current plot instead of separate forward and reverse current plots, high sensitivity and viewed as an improvement to other electroanalytical techniques. For instance, SWV suppressed background currents much more effectively than cyclic voltammetry, hence, analyte concentrations on the nanomolar scale can be recorded utilizing SWV.

2.1.2. Potentiometric ion selective electrodes

In an ion selective electrode, a semipermeable membrane is used for separation of two differently concentrated solutions of an appropriate electrolyte and the electric potential evolved across the membrane is observed under zero current condition; i.e., when there is no transport of charge at any point in the system. The generation of membrane potential usually depends upon the ratio of activity of diffusible ions present on the two sides of membrane. Therefore, the membrane potential can be employed for determination of activity/concentration of an ion by an appropriate membrane setup [11]. The theory and methodology of ion selective electrodes assumed in such determinations is briefly discussed here.

When, a semipermeable cation-exchange membrane placed between two solutions having different concentration of an electrolyte AY allows the diffusion of A^+ from higher to lower concentration side as membrane is more permeable to these ions and hinders partially or totally the diffusion of other ion Y^-. Hence, an electrical double layer is formed across the membrane, results electrical potential gradient generated. This potential is the sum of Donnan and diffusion potential known as membrane potential (E_m). Since potential developed across a membrane depends upon the activity of a particular charged species, and is given by the expression [12]:

$$E_m = \frac{2.303 RT}{Z_A F}\left[\log \frac{(a_A)_2}{(a_A)_1} - (z_Y - z_A)\int_1^2 t_Y^- d\log a^{\pm}\right] \qquad (2.2)$$

where z_A and z_Y are the charges on the ion A and Y, respectively, t_y^- is the transport number of Y, $a^{\pm}$ is the mean activity of electrolyte and $(a_A)_1$ and $(a_A)_2$ represent the activities of A^+ in solutions 1 and 2, respectively.

First term on the right hand side of the equation (2.2) gives the thermodynamic limiting value of the concentration potential, i.e., Donnan potential while the second term

denotes the diffusion potential due to co-ion flux in the membrane. However, if the membrane is believed to be ideally permselective ($t_y^- = 0$), then equation (2.2) takes the form of the Nernst equation:

$$E_m = \pm \frac{2.303RT}{Z_A F} \log \frac{(a_A)_2}{(a_A)_1}$$

(2.3)

The equation (2.3) represents Donnan potential for an ideally permselective membrane. The sign will be +ve for cation selective and −ve for anion selective membranes. The following cell set up is usually employed for the measurement of membrane potential using saturated calomel electrodes (SCE) or other reference electrodes.

External Reference Electrode (SCE)	External or Test Solution of AY	Membrane	Internal Solution of AY	Internal reference electrode (SCE)
2				1
$E_{L(2)}$				$E_{L(1)}$
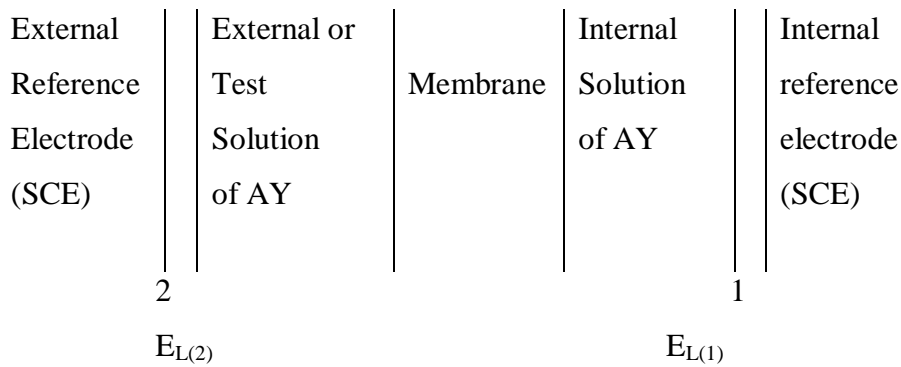
In general, compartment 1 contains reference or internal solution whose concentration is kept constant. The saturated calomel electrode dipped in this solution is known as internal reference electrode. The membrane together with internal solution and internal reference electrode is known as membrane electrode or membrane sensor. The saturated calomel electrode dipped in external solution, which is generally referred to as test solution or sample, is known as external reference electrode. The electromotive force (emf) across this cell is the sum of all individual potential contributions. Many of these are sample-independent and the calculated emf can frequently be described by the following expression

$$E_{cell} = E_{cal} + E_{L(2)} + E_m + E_{L(1)} - E_{cal}$$

(2.4)

where E_{cal}, E_L and E_m are the saturated calomel electrode potential, liquid junction potential and membrane potential, respectively. From equations (2.3) and (2.4):

$$E_{cell} = E_{cal} - E_{cal} + E_{L(1)} + E_{L(2)} \pm \frac{2.303RT}{Z_A F} \log \frac{(a_A)_2}{(a_A)_1}$$

$$E_{cell} = [E_{L(1)} + E_{L(2)} - \frac{2.303RT}{Z_A F} \log (a_A)_1] + \frac{2.303RT}{Z_A F} \log (a_A)_2 \quad (2.5)$$

(For cation exchange membrane)

The values of $E_{L(1)}$ and $E_{L(2)}$ are small and generally remain constant. Also the term $\frac{2.303RT}{Z_A F} \log (a_A)_1$ remains constant if the concentration of internal solution is not changed.

Consequently, in a given experimental setup, all the terms in parenthesis of equation (2.5) are constant and can be substituted by a constant E'_0. The value of E'_0 would change only when experimental conditions are changed. The equation (2.5) is reduced to well-known Nernst equation:

$$E_{cell} = E'_0 + \frac{2.303RT}{Z_A F} \log (a_A)_2 \quad (2.6)$$

Thus, it is clear from equation (2.6) that the cell potential is directly proportional to the concentration or activity of the sample ions in aqueous solution under investigation. Usually attempts are not made to determine the membrane potential by subtracting external SCE potential. The whole electrochemical cell as described above is taken as a sensor and the value of E_{cell} gives activity of the ion of interest. If for a developed membrane sensor, the slope of the plot between E_{cell} and $\log (a_A)_2$ comes out to be equal to theoretical slope i.e., $\frac{0.0591}{Z_A}$, then the membrane is said to be ideal as it has responded according to Nernst equation (2.6) [13, 14]. The slope of such a membrane is called Nernstian slope.

Before further discussion on the performance of ion-selective electrodes, some of the terms used require to be defined. IUPAC compendium of nomenclature [15, 16] is helpful in sorting out the terms.

2.1.2.1 Membrane

Generally, ion selective electrodes employ homogeneous/heterogeneous membranes of chemical compounds. The capability to differentiate between numerous permeating species is the principal characteristics of a membrane applied in electrochemical sensors. This differentiation leads to the formation of an electrical double

layer, which is the source of electric potential. The potential developed is basically due to two processes: (i) different mobilities of the ions through the membrane resulting in the generation of diffusion potential, (ii) Donnan or phase boundary potential arising from non-transport of one or more kind of ions. The potential developed is a function of activity ratios of the interchangeable ions on the two sides of the membrane.

In general, the polymeric membrane used in ISEs consists of four components: Electroactive material (ionophore), lipophilic additive, plasticizer and the polymer matrix depicted in Figure 2.6. The detailed description is described in subsequent sections.
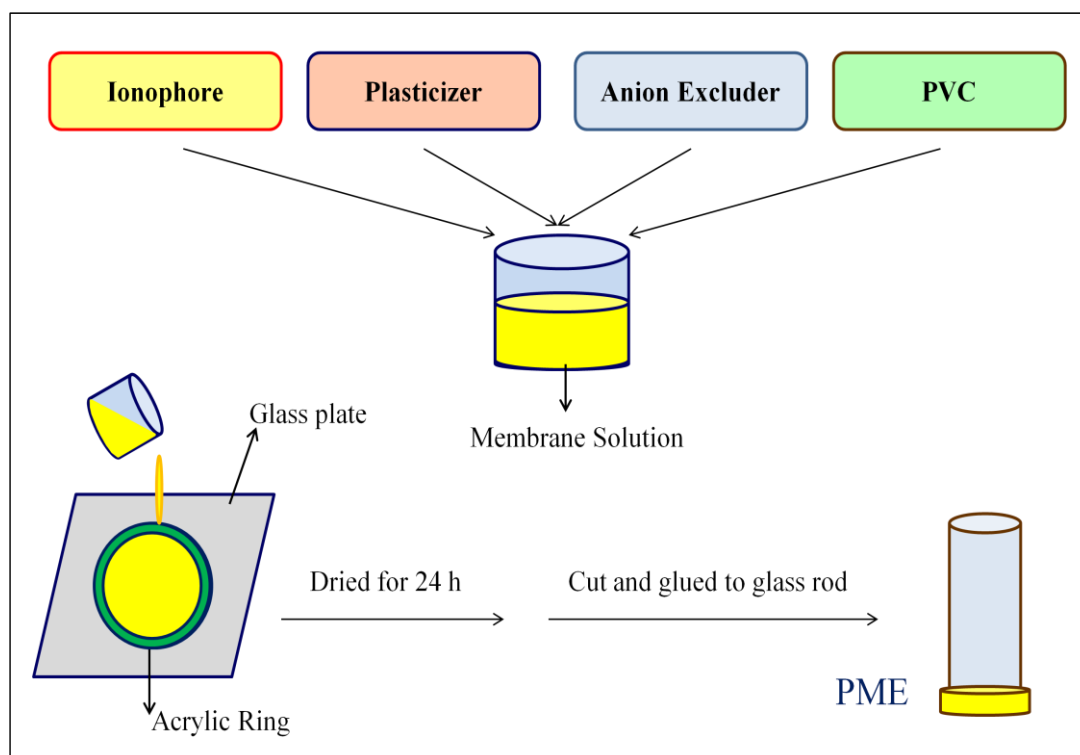
Figure 2.6. Schematic presentation of preparation of polymeric membrane electrode.

i. Electroactive Material (Ionophore)

Ion carrier or ionophore is the key components of polymeric membrane ion-selective electrodes that govern the ion selectivity and sensitivity because the molecular-level phenomenon, sensed by the ISE is the binding between the ionophore and target ion. Ideally, it forms reversible and relatively strong complex with target ion and not with the other ions. A range of substances viz., solid electrolyte, inorganic and organic ion exchanger, salts of multivalent atoms, metal chelates, polythia macrocycles, polyaza, crown ethers, cryptands and calixarenes which have been employed as ion carriers for the preparation of ISEs. Depending upon the nature of ionophore, ISEs are classified into three different classes as shown in Figure 2.7. Top: electrically neutral carrier (L) and lipophilic

cation exchanger (R–); center: charged carrier (L–) and anion exchanger (R+); and bottom: cation exchanger (R–) based ion selective electrodes [17].

Neutral carrier based ion-selective electrode

Sample solution   **Polymeric membrane**   **Inner filling solution**

I^+ IL^+ $R–$ I^+

     L

$A–$ $A–$

$R–$ IL^+ IL^+ L

Charged carrier based ion-selective electrode

I^+ IL IL R^+ I^+

     R^+

$A–$ $A–$

$L–$ $L–$ IL

Ion exchanger based ion-selective electrode

I^+ $R–$ I^+ $R–$ I^+

$A–$ $A–$

I^+ I^+ $R–$
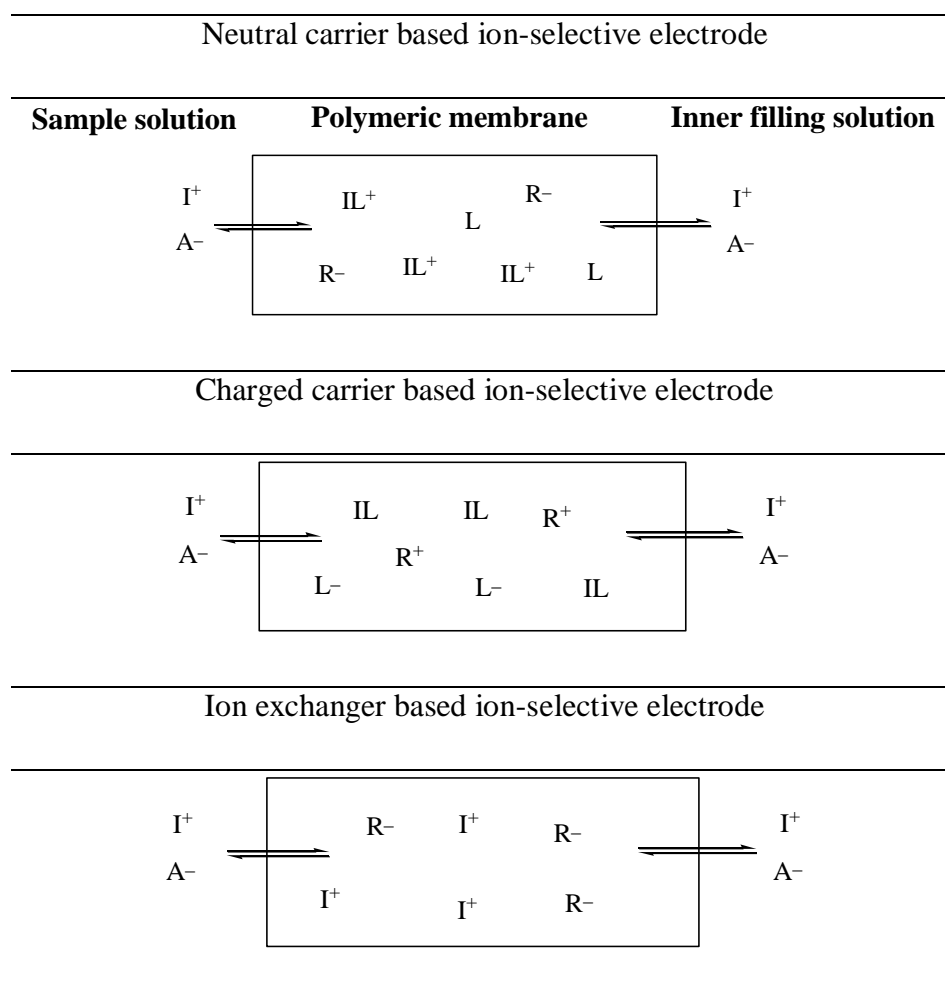
Figure 2.7. Schematic representation of equilibria between sample, ion-selective membrane and inner filling solution.

ii. *Polymeric (Inert) Matrix*

The matrix utilized provides an inert base which imparts physical-mechanical stability and elasticity to the membrane. As it was mentioned above, polymer membrane provides a unique opportunity to obtain a variety of electrodes selective towards particular ions by doping membrane with certain ionophore. Polymer matrix should be chemically inert, hydrophobic, flexible, non-porous; stable and crack resistant. Moreover, it should not swell in sample solutions. Polymers as homogenous membrane matrices first came in use with charged carriers. Poly(vinyl chloride) (PVC), Silicon rubber, some methacrylates, polyurethanes and polystyrene [18–20] have been demonstrated as polymer matrices meeting this requirement. Though, the most commonly used polymer is PVC due to simplicity of membrane preparation. Of the various binders used for preparing

heterogeneous solid state membranes, PVC has been most widely used due to its relatively cheap cost, good mechanical properties, inertness and amenability to plasticization. It also provides good flexibility to mechanical and pressure damage as well as the electroactive materials is highly compatible with the matrix resulting in their reduced leaching from the membrane and the electrode life is increased to a substantial extent.

iii. *Solvent mediator or Plasticizer*

Plasticizers are the high molecular weight compounds, used in polymeric membranes to enhance its flexibility and softness and provide mobility of membrane constituents within the membrane phase. A good plasticizer should exhibit high lipophilicity, low tendency to exudate from the polymer matrix, low vapor pressure and high capacity to dissolve the membrane components [21]. Extension of plasticizer alkyl chains may be a partial solution, as it may lead to incompatibility of plasticizer with membrane components. The membrane polarity, which may give a selectivity modifying influence because of the improved solvation of high valence ions by more polar media, depends also on the nature of membrane plasticizer. A number of organic solvents such as phthalates, dioctylsebacate, 2-nitrophelyl octyl ether, acetophenone and benzyl acetate have been utilized suitably and efficiently as plasticizer to enhance the performance of ISEs.

iv.   *Lipophilic additive or lipophilic ionic sites*

The prerequisite for obtaining a theoretical response with ISE membranes is their perm-selectivity, which means that no significant amount of counter ions may enter the membrane phase. Lipophilic ionic additive is a salt of non-exchangeable lipophilic anion/cation and an exchangeable counter ion. Their main function is to provide the ion selective membrane permselective by reducing interference owing to foreign ions, to optimize sensing selectivity (by defining the ratio of complexed to uncomplexed ionophore concentration in the membrane) and to reduce the bulk membrane impedance [22]. Moreover, the presence of lipophilic additive in ion selective membrane not only reduces the ohmic resistance but also increase the sensitivity of membrane electrodes. These additives may also catalyze the exchange kinetics at the sample-membrane interface [23]. Lipophilic ion exchangers traditionally used for polymeric membrane preparation are the anionic tetraphenylborate derivatives viz., sodium tetrakis-[3,5-bis- (1,1,1,3,3,3-hexafluoro-2-methoxy-2-propyl)-phenyl]borate trihydrate (NaHFPB), sodium tetraphenyl borate (NaTPB) and potassium tetrakis p-(chloro phenyl)borate (KTpClPB) and the

cationic tetraalkylammonium salts viz., tridodecyl methylammonium chloride (TDDMACl), hexadecyl trimethylammonium bromide (HTAB) and tributylammonium chloride (TBAC).

2.1.2.2. Combination electrode/Cell assembly

It is an electrochemical apparatus that incorporates an ion-selective electrode and a reference electrode in a single assembly, thereby avoiding the need for a separate reference electrode. A simple schematic format of the cell assembly is depicted in Figure 2.8.
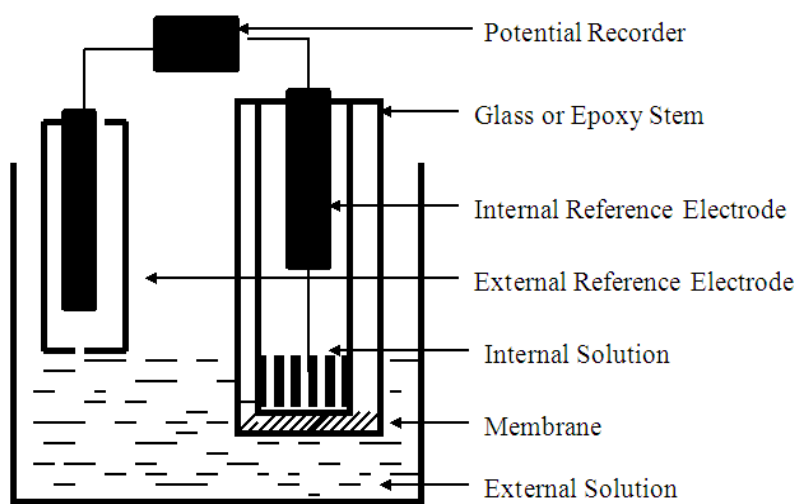
Figure 2.8. Schematic representation of membrane electrode cell assembly.

2.1.2.3. Calibration curve
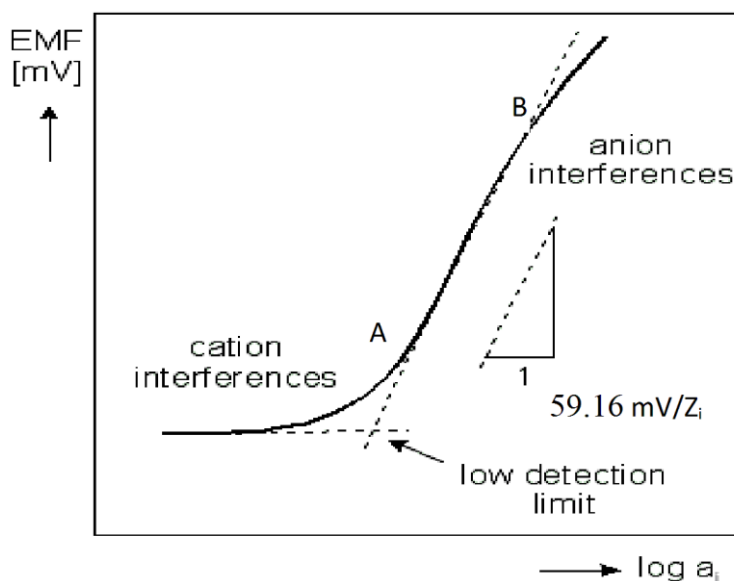
Figure 2.9. Calibration Curve of an ion-selective electrode.

The cell potential of the assembly is changed when the activity of the solution of primary ion is altered. A plot between cell potential and logarithm of the activity or

concentration of the primary ion is generally referred as calibration curve. It determines the performance characteristics of the ion selective electrode and is used in the determination of primary ion concentration. For a primary ion A, the logarithm of its activity (log a_A) is usually plotted along the abscissa of the graph and the cell potential is plotted along the ordinate. A Typical calibration curve ordinarily is shown in Figure 2.9.

2.1.2.4. Limit of detection

According to the IUPAC recommendation of 1976, detection limit can be defined as the minimum concentration which can be determined for the primary ion. It is obtained from the point of intersection of two extrapolated linear segments of the calibration curve as shown in Figure 2.9. The potential response of ISEs becomes stable below the detection limit.

2.1.2.5. Working concentration range/Linear range/Measuring range

The working concentration range of ISEs is generally defined as the activity range over which the potential response of the cell is linear. In this range the electrode responds according to the Nernst equation. A maximum range will be attained if the interfering ion is not complexed at all by the carrier. A typical linear range of the calibration curve of the ISE shown in Figure 2.9 is considered to be its linear part between A and B.

2.1.2.6. Slope of the ISE

In general, slope is defined as the gradient of the linear portion of the calibration curve. According to Nernst equation (2.6)

$$\text{E}_{\text{cell}} = \text{E}_0' + \frac{2.303RT}{Z_A F} \log(a_A)$$

If the slope is equal to 2.303 RT/ z_AF, the slope is normally called Nernstian slope. If the slope of an ISE Nernstian, it is said that the electrode behavior is ideal. The theoretical values of the slope is 59.1 mV decade^{-1} activity at 298 K for monovalent ion, 29.5 mV decade^{-1} activity for divalent ion and 19.7 mV decade^{-1} activity for trivalent ion.

2.1.2.7. Response time

According to recommendations for nomenclature of ion-selective electrodes [11], the response time is the time elapses between the instant at which an ion-selective electrode and a reference electrode are brought into contact with a sample solution and the

first instant at which emf/time slope ($\Delta E/\Delta t$) becomes equal to a limiting value on the basis of the experimental conditions and/or requirements concerning the accuracy.

The IUPAC recommendations outline two experimental procedures for measuring the response time. According to first method so called dipping method, the electrode is instantaneously immersed into a solution of known activity of the target ion; simultaneously the response time is recorded. The response time determined by this method is called as static response time. In second method response time is recorded by varying standard test solutions with different target ion concentrations. The measurement sequence is from lower to higher concentration. To evaluate the reversibility of the electrodes, a similar procedure in the opposite direction can also be adopted.

2.1.2.8. Lifetime of ISE

The lifetime of an ion-selective electrode may be defined as the time interval between the conditioning of the membrane and the moment when at least one parameter of the functionality characteristics of the device changes detrimentally. The working shelf life of an ISE can vary from a few days to a few months. After this time the slope and detection limit of the sensor get changed significantly. It will depend on the nature of the samples analyzed and the lipophilicity of the ingredients of ion selective membrane.

2.1.2.9. Potentiometric selectivity

Selectivity is an important characteristic of an ISE that describes the extent to which the device may be used in the estimation of analyte ion in the presence of other ions. The ion for which the sensor is designed is called primary ion and all other ions are referred to as interfering ions or foreign ions or secondary ions. In fact, no ISE responds exclusively to primary ion i.e., specific to it. However, in practice it is more selective to primary ions than to interfering ions. Therefore, it is a necessary parameter to determine as it indicates the commercial potential of any sensor. The degree of selectivity of the sensor for primary ions A, with respect to interfering ion B, is expressed in terms of potentiometric selectivity coefficient ($K_{A,B}^{Pot}$) which is defined by the semi-empirical Nicolsky-Eisenman equation (2.7)

$$E = E° \pm \frac{2.303RT}{Z_A F} \log \left[a_A + \sum K_{A,B}^{Pot} \, a_B^{z_A/z_B} \right] \qquad (2.7)$$

where z_A, z_B, a_A and a_B are the charges and activity of ions A and B, respectively. It is apparent from equation (2.7) that a value of $K_{A,B}^{Pot} = 1$ at $z_A = z_B$ indicates equal response

to both A and B. Similarly, the value of $K_{A,B}^{Pot} < 1$ indicates that the sensor responds more to A in comparison to B i.e., the sensor is selective to A over B. Smaller is the value of selectivity coefficient better is the selectivity. On the other hand, $K_{A,B}^{Pot} > 1$ indicates that the sensor's response is more towards B rather than A and in such a case it is said that the ion B causes considerable interference.

When the charges $z_A \neq z_B$, the values of selectivity coefficient $K_{A,B}^{Pot} \cong 1$ does not indicate equal response to primary and interfering ions as per equation (2.7), but now it depends on the values of z_A and z_B. For different values of z_A and z_B, $K_{A,B}^{Pot}$ values showing equal response to both A and B have been computed from equation (2.7).

It is important to highlight that selectivity coefficient values signify the selectivity only at the conditions of determination but in actual practice the interference caused depends on the relative concentration of the primary and interfering ions and other experimental conditions. Though the selectivity coefficient may not reflect exactly the interference level but still it is a very important parameter to estimate the likely performance of a sensor. However, it has been seen that the deviation between the expected performance of a sensor on the basis of selectivity coefficient and the experimental performance is not large. Therefore, it is essential to evaluate the performance of a sensor in the presence of other ions by determining selectivity coefficient. A number of methods have been described to determine selectivity coefficient [24–26] and are grouped into the following categories.

      (a) Separate solution method (SSM)

      (b) Fixed interference method (FIM)

      (c) Matched potential method (MPM)

(a) Separate solution method (SSM)

In SSM method, the potential of the cell containing test solution of primary ion A of activity a_A is first determined. The emf of this cell E_A is related to the activity of primary ion by the equation (2.8)

$$E_A = E^0 + \frac{2.303RT}{z_A F} \log a_A \tag{2.8}$$

Further, the emf of a separate cell containing test solution of interfering ion B of activity a_B is determined. Its emf E_B is related to activity a_B by the equation:

$$E_B = E^0 + \frac{2.303RT}{z_A F} \log \mathrm{K}_{A,B}^{Pot} (a_B)^{z_A/z_B} \tag{2.9}$$

From equations (2.8) and (2.9)

$$\log \mathrm{K}_{A,B}^{Pot} = \frac{E_B - E_A}{2.303RT/z_A F} + \log \frac{a_A}{(a_B)^{z_A/z_B}} \tag{2.10}$$

When $E_A = E_B$

$$\mathrm{K}_{A,B}^{Pot} = \frac{a_A}{(a_B)^{z_A/z_B}} \tag{2.11}$$

Even though the separate solution method is simple to perform, is not usually applied for the determination of $\mathrm{K}_{A,B}^{Pot}$ values, because it does not represent the actual conditions under which the ion selective electrode is used [27].

(b) Fixed interference method (FIM)

In this procedure, the potential of the cell is measured for a number of solutions containing interfering ion of constant activity a_B but varying values of activity of primary ion a_A. The plot of potential so obtained against activity a_A is shown in Figure 2.10. This plot generally has three distinct regions. In the first region PQ, the linear response of the sensor indicates that it is responding only to primary ion, A, with no interference caused by B in this concentration range.

In the second region QR, deviation from linearity is caused because now the sensor is also responding to the activity of B as the concentration of primary ion decreases. So in this region (QR), the response of the sensor is mixed and is owing to both the ions A and B. The third region RS of the plot is linear and the potential is constant. Constancy in the potential indicates that the sensor is now only responding to interfering ion B with no contribution arising owing to primary ion A. This generally occurs at lower activity of A. Since the activity of B is constant and A is not affecting the potential in this concentration range, the potential of the sensor remains constant. The linear portion PQ and RS are then extrapolated and meet at the intersection point T. The potential corresponding to point T can be generated by constant activity of B or by the activity of A. Thus, for point T, E_A is equal to E_B (E_A is generated by A of activity a_A and E_B by B of activity a_B). Under this condition of $E_A = E_B$, the $\mathrm{K}_{A, B}$ can be calculated by the following equation (2.11) already derived under separate solution method.

$$K_{A,B}^{Pot} = \frac{a_A}{(a_B)^{z_A/z_B}}$$

This procedure is the most extensively utilized procedure as per IUPAC recommendation for determining selectivity coefficients [28, 29].
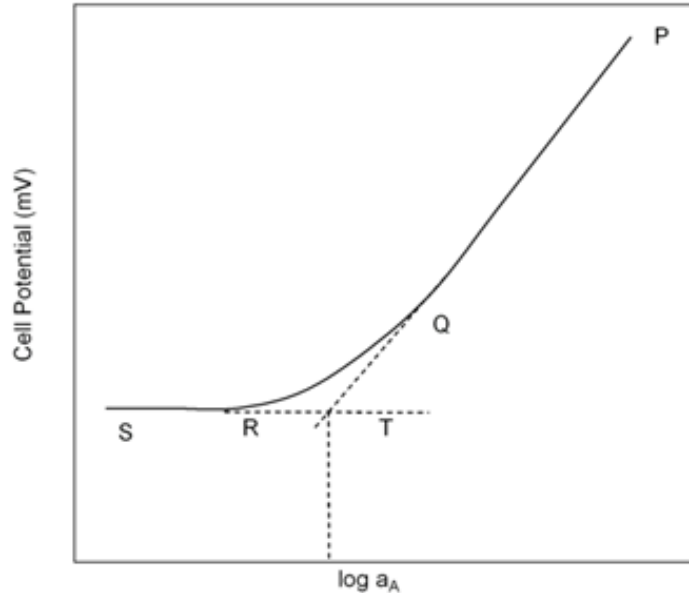
Figure 2.10. Potential vs. ($\log_{10} a_A$) plot illustrating the determination of selectivity coefficient by fixed interference method.

(c) Matched potential method (MPM)

This method is independent of the Nicolsky-Eisenman equation, was proposed by Gadzekpo and Christian [30] to overcome the difficulties in obtaining accurate selectivity coefficients when ions of unequal charge are involved. In this method, the selectivity coefficient $K_{A,B}^{Pot}$ is given by the following expression:

$$K_{A,B}^{Pot} = \frac{a'_A - a_A}{a_B} = \frac{\Delta a_A}{a_B} \tag{2.12}$$

and is determined by measuring the change in potential upon increasing by a definite amount the primary ion activity from an initial value of a_A to a'_A and a_B represents the activity of interfering ion added to same reference solution of activity a_A which brings about same potential change. The potential response curve obtained in the matched potential method is depicted in Figure 2.11. This method provides practically realistic values of $K_{A,B}^{Pot}$. The characteristics of matched potential method are that the charge number

on primary and interfering ions is not taken into consideration and Nernstian responses are assumed neither to the primary nor interfering ions. These characteristics lead to the following advantages: (i) the power term problem for ions of unequal charge disappears, and (ii) the method is applicable even to non-Nernstian interfering ions. However, as this method is independent of the Nicolsky-Eisenman equation or its modified forms, and it is therefore difficult to correlate the values of $K_{A,B}^{Pot}$ obtained by this method with any particular phenomena such as ion exchange [31].
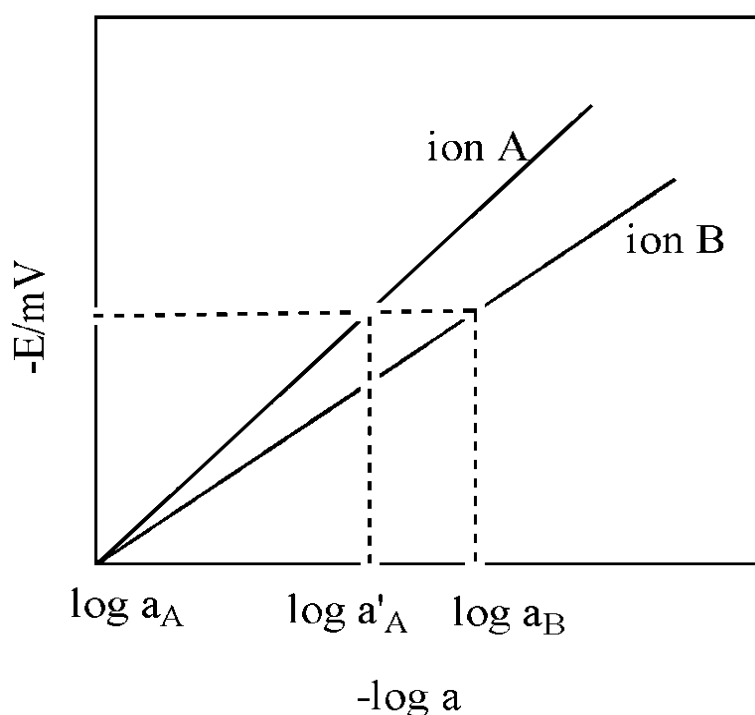
Figure 2.11. Potential vs. log a_A plot illustrating the determination of selectivity coefficient by matched potential method (activity of B = a_B).

It is seen from the above paragraphs that the selectivity of ion selective electrode depends on the experimental conditions, usually the concentration of ions and the method of determination. It is for this reason, $K_{A,B}^{Pot}$ is not called selectivity constant, but selectivity coefficient. Further, different methods give different values of selectivity coefficient as the conditions prevailing at the membrane-solution interface are not same [32, 33]. In this thesis, the selectivity coefficients values have been determined using fixed interference method and the values have been worked out from the experimental data using equation (2.11).

2.1.3. Spectrophotometric techniques

Spectrophotometry deals with visible light, near-ultraviolet and near-infrared. It measures the light intensity transmitted or reflected by a chemical substance as a function of wavelength quantitatively and the device which can employed for measuring light intensity is known as spectrophotometer.

2.1.3.1. Photoluminescence

At room temperature most of the elementary particles reside in their ground state. When these ground stated particles irradiated with an electromagnetic radiation, they absorb photons with proper energy. The energy absorbed by the particles leads to a rapid formation of an electronically excited state followed by the dissipation of the excess energy in different ways (Figure 2.12). The phenomenon occurs emission followed by the absorption of a photon is known as photoluminescence whereas another one that followed by a chemical reaction is known as chemiluminescence [34]. Basically, depending on the nature of the excited state, the emission light can be divided into two major categories as phosphorescence and fluorescence. A detailed study of the photoluminescence process is discussed under the following subsections.
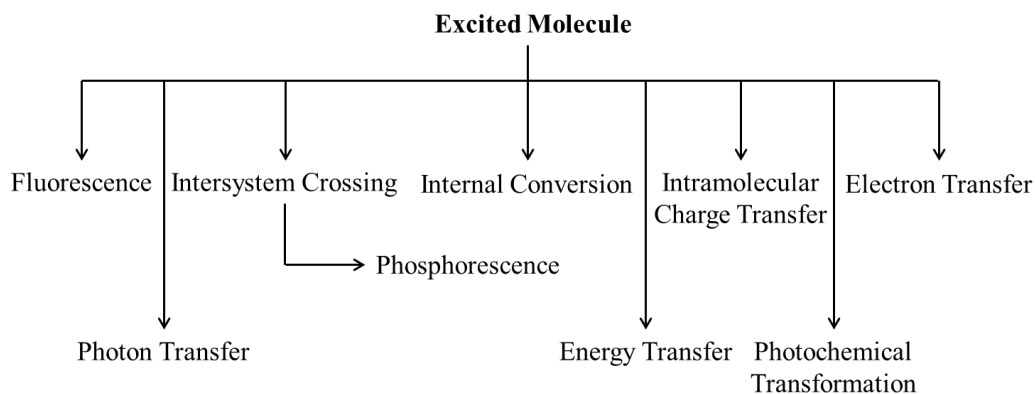
Figure 2.12. Typical possible excitation and de-excitation of the molecules.

As previously discussed atom or molecule absorb photons when irradiated by electromagnetic radiation, hence a rapid transition of an electron occur from highest occupied molecular orbital (HOMO, HOMO−1 etc.) to the lowest unoccupied molecular orbital (LUMO, LUMO+1 etc.) of the molecule. In the majority of cases, for such electronic transitions the UV−Visible region (200–800 nm) of the electromagnetic spectrum is sufficient. In addition, the other regions of the electromagnetic spectrum may induce exciting changes upon irradiation of the molecule and results are roughly outlined in the Figure 2.13.
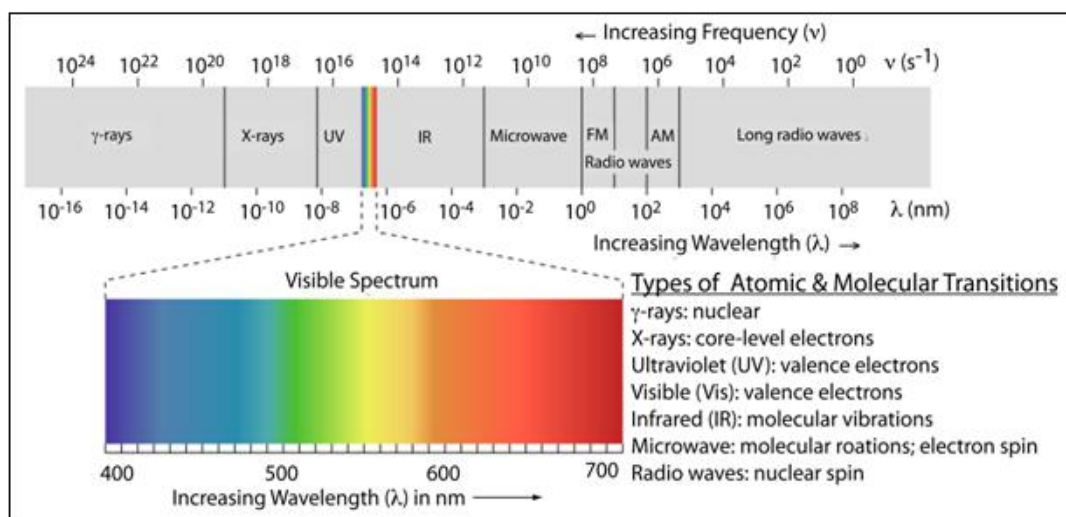
Figure 2.13. Typical electromagnetic spectrum showing different regions and type of transition responsible for the change in energy. The visible spectrum shown in colored band.

Optical radiation is subdivided into ultraviolet, visible light and near-infrared (NIR, 750–1000 nm). Near-infrared absorption can be achieved in extended conjugation [35] or mixed-valence system [36].

When matter hits by radiation, it might be absorbed, scattered, transmitted or reflected the radiation. The matter may absorb radiation of a distinct frequency; the energy of the frequency relates to the difference between two electron energy-levels. Therefore, the relationship between absorbance, the concentration of the absorber and the path length is described by the Lambert-Beer Law:

$$A = \varepsilon \times c \times l = -\log_{10}\frac{I}{I_0} = -\log_{10}T \qquad (2.13)$$

where, A = Absorbance, ε = molar absorption coefficient or molar extinction coefficient, c = concentration, l = absorption path length, I_0 = Incident light, I = Transmitted light

At a specific wavelength, the intensity of the absorption depends on the molar absorption coefficient (ε) of the molecule. Its value gives us the information of how 'allowed' a transition is. 'Allowed' and 'forbidden' terms are beyond the classical physics, as they represent the results of quantum mechanical calculations. As mentioned earlier, the value of absorption coefficient indicates the probability of an electronic transition from the ground state to an excited state of a molecule. The low probability ($\varepsilon < 100$) exhibits spin forbidden and symmetry allowed transition. Whereas, the high probability of absorption coefficient ($\varepsilon < 10^4$) shows spin and symmetry allowed transition resulting a strong absorption band.

2.1.3.2. The physical deactivation of excited states

Once the molecules disclose having a particular energy photons, excitation may occur, i.e. an electron from lower-energy to higher-energy molecular orbitals can be encouraged in the molecule. In the visible and/or ultraviolet range, such types of excitations are typical for the photon energies and produce electronically excited states. Aforesaid excited states are unstable and instantly lose their excess energy via a range of deactivation processes. To ease understand the photon absorption and deactivation processes, it is recommended to visualize a typical way which may happen is depicted in the Perrin-Jablonski diagram (Figure 2.14).

The Perrin-Jablonski diagram demonstrates the properties of excited states as well as their relaxation processes. After light absorption by the molecules in ground states, the vibrational levels in the excited states will be crowded with electrons. Owing to volatility of this state, the electrons instantly calm down to the lowest vibrational level of S_1 within picosecond or less through vibrational relaxation, and this process (non-radiative loss of energy as heat to the surroundings) is known as the internal conversion. According to Kasha's rule, the residuary photochemical processes namely fluorescence, quenching etc., are more possibly to happen from the vibrational level of S_1 [34]. On the basis of this rule, after excitation all the photochemical reactions forever will originate from the $v = 0$ of S_1, because the relaxation rate to the lowest vibrational level of S_1 is the fastest deactivation process. Now, the excited electron at S_1 of the excited molecule may undergo either fluorescence via emitting photons or intersystem crossing to the triplet state or it may just relax to the ground singlet state S_0 through releasing by the excess energy via internal conversion.

In idealized conditions, the intersystem crossing (non-radiative transition between states of different spin multiplicity) transitions from singlet state S_1 to the triplet state T_1 is forbidden and it will occur when the electron in the S_1 state undergo a spin conversion. These transitions favoured in some conditions such as presence of heavy atom and/or exciton coupling within a molecule. The relaxation of electron from triplet state T_1 to singlet state S_0 is a radiative process, named as "phosphorescence". The rate of radiative decay from T_1 to S_0 state is much slower than the fluorescence process owing to its spin multiplicity and additionally it is a lower-energetic radiation. The details of these processes including timescales are depicted in the Figure 2.14.

The fluorescence is a spin-allowed radiative relaxation process owing to the same spin multiplicity of the excited (S_1) and the ground (S_0) states. Thus, it occurs in a very

short period within the range of picoseconds to microseconds. The emitted light always has a longer wavelength (less energetic) compared to absorbed light because loss of limited energy by the molecule during this process. This energy difference or red-shift of the fluorescence spectrum contrast to the absorption spectrum is called the Stokes shift.
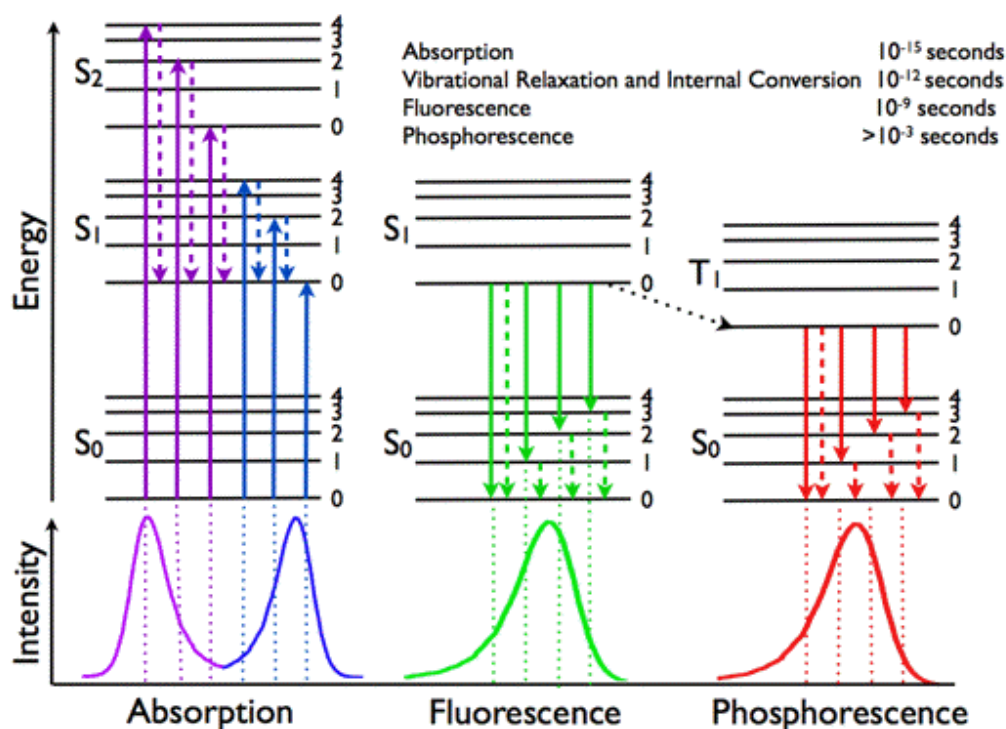
Figure 2.14. The typical view of Perrin-Jablonski diagram representing energy levels and spectra.

In the Figure 2.14 the solid arrows occurring by absorption (violet, blue) or emission (green for fluorescence; red for phosphorescence) designate radiative transitions of a photon whereas non-radiative transitions represented by dashed arrows (violet, blue, green, red).

2.1.3.3. Fluorescent chemosensors

To the invent of a fluorescent chemosensors, the synthesis of signalling moieties (fluorophore) and recognition of analyte (the receptor unit) are the major significant things. During the recognition process the analyte part is covalently connected to the receptor. The consequence of the receptor occurs from its impact on binding and selectivity [37]. Therefore, it is concluded that a receptor should be sensitive and should provide a strong and selective affinity towards the target analyte. Further, the fluorophore part in the chemosensor works as a signal transformer, since it can transform the information into a useful optical signal. The considerable changes arise in the photophysical properties of a

fluorophore during the binding of an analyte to the receptor, the changes can be observed and processed in the right way to determine a given analyte. The design of the chemosensor affects the variations in the fluorescence signal and this signal can be examined while complexed with the targeted analyte. The signal could be in the form of quenching or enhancement in the fluorescence intensity, in addition the certain shift in the emission wavelength [38].

The fluorescent probes or receptors are two types to construct, they are integrated and spacer types (Figure 2.15). In the first case, the receptor and fluorophore are attached through spacer that prevents the conjugation while in the latter case, both the receptor unit and the signalling moieties (both having π-electron system), are connected to each other conjugatively [39].
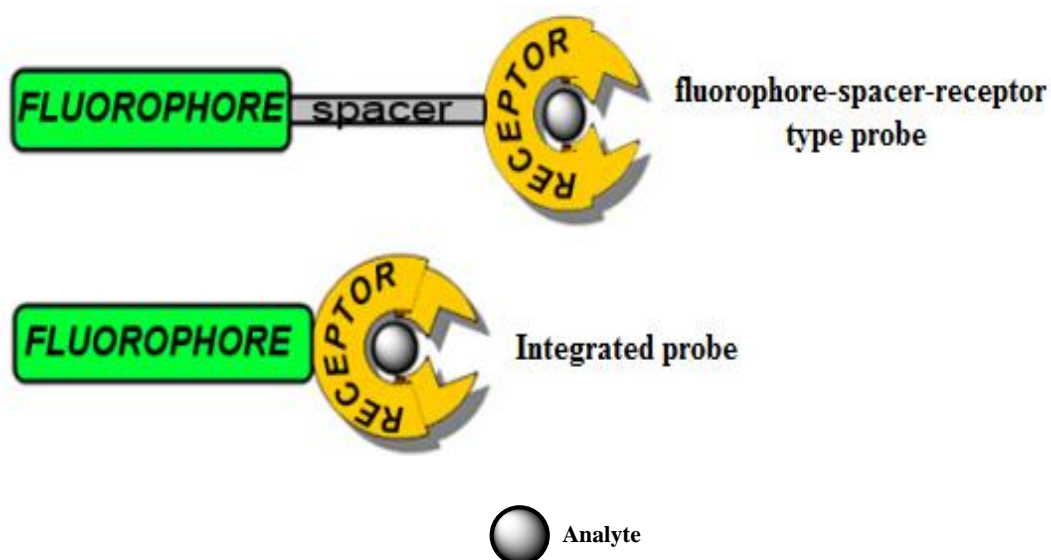
Figure 2.15. Simple illustration of a chemosensor.

2.1.3.4. Mechanisms of signal transduction

The fluorescence emission process appears from the electronic excited states of analytes. Though, owing to the high reactivity of the electrons in these states, reactions which generally do not take place in the ground states are able to occur. Some of these reactions are established to be interesting, in the point of view of chemical sensing, as they allow a one-step deactivation of the excited state (quenching) and occasionally, formation of new emission bands resembling to the products of these reactions. Upon binding of analyte to chemosensors, it is probable to modulate some of these reactions (since they depend on the interaction of reaction sites through enhancers or quenchers of their emission), and hence take advantage of the different mechanisms for signal transduction.

2.1.3.4.1. Photoinduced electron transfer (PET)

The extensive range of analytes such as cations, anions and neutral molecules can be detected by employing a simple, sensitive and naked-eye fluorescent sensor. In some cases, during the relaxation of the excited molecule, it may transfer an electron from potential donor unit to low-lying vacant orbital or either it may transfer to another system that is generally named as quencher. Additionally, the luminophore that absorbs the light after excitation process accept an electron into its unfulfilled ground state or it may donate an electron to the vacant orbital of receptor from its excited state. This process has been studied well, owing to its important role in photosynthesis [40]. Subsequent to the absorption of light the electron is transferred, this process is entitled as photo-induced electron transfer (PET). In case of PET-type chemosensor both the fluorophore and the receptor units linked by a non-conjugated bridge existing in the same molecule and receptor accepts/donates an electron from/to the fluorophore.

A typical model of allowed and forbidden PET-type mechanisms in the forms of frontier molecular orbital is depicted in Figure 2.16. The PET-type model chemosensor is incorporated of three units, as fluorophore, spacer and receptor. The nature of the receptor unit which fluorophore will give upon analyte binding, determines the type of the response. In this case, the receptor unit performs as the electron donating unit and the PET process is activated through the electron transfer from fulfilled HOMO of the receptor unit to the semi vacant ground state orbital of the fluorophore. This process blocks the customary relaxation pathway of excited fluorophore and hence quenches emission. This can also said to be reductive photo-induced electron transfer. When donor orbital of the receptor unit can be controlled or somehow stabilized, an off–on type fluorescence emission will be accomplished. Further, when bonded to the targeted analyte, the weakly fluorescent sensor will become strongly fluorescent. Thus, the probes which display such PET type mechanism are employed widely in the field of chemosensing [41, 42].

In a practical application, the fluorescence of unbound chemosensor **1** was quenched and it may donate an electron to the excited state HOMO of the chemosensor **1** moiety depicted in Scheme 2.1 based on a PET switching mechanism. A PET sensor based on nitrogen donors was extremely sensitive to environmental pH stimuli owing largely to the protonation extent of the nitrogen being strongly dependent on environmental pH. At low pH conditions, the quenching of fluorescence **1** designated due to the lone pairs of the sulphur donors and performed an important role in the modulation of the PET processes. In neutral and acidic conditions, the PET process from a nitrogen donor to the fluorophore

was blocked owing to intramolecular hydrogen bonding or by protonation of the nitrogen donor. The PET derived from the sulphur donors to the fluorophore is always switched on and hence resulted in the fluorescence being quenched. Further, the PET processes from both the nitrogen donor and the sulphur donors to the fluorophore in the basic media were switched on owing to the deprotonation of the phenol hydroxy, leading to the complete quenching of the fluorescence. The phenolic O, N, and S donors are probably coordinate to Al^{3+} ion subsequent to bonding with the Al^{3+} ion. Hence, the PET processes were entirely blocked, obtained from the lone electron pairs of both the sulfur and nitrogen donors to the fluorophore and generated strong fluorescence enhancements [43]. PET systems can exhibit either ON–OFF or OFF–ON switching, but systems exhibiting OFF–ON behavior are preferred for signalling binding events.
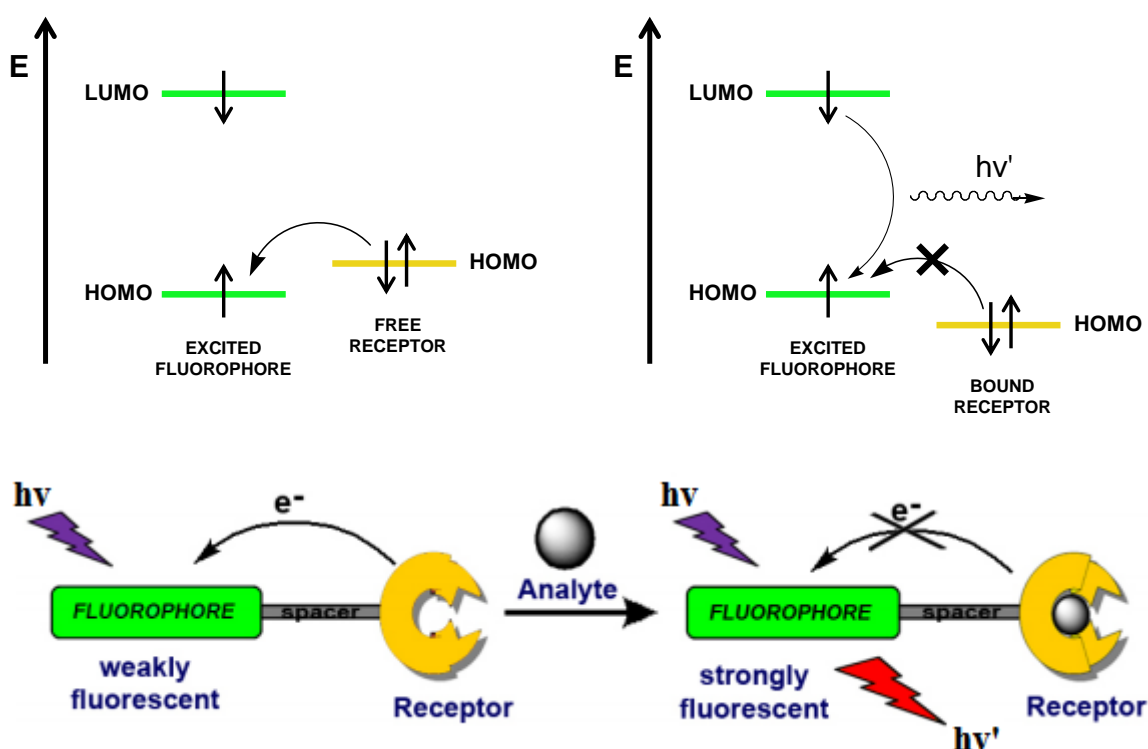
Figure 2.16. Typical view of PET mechanism.
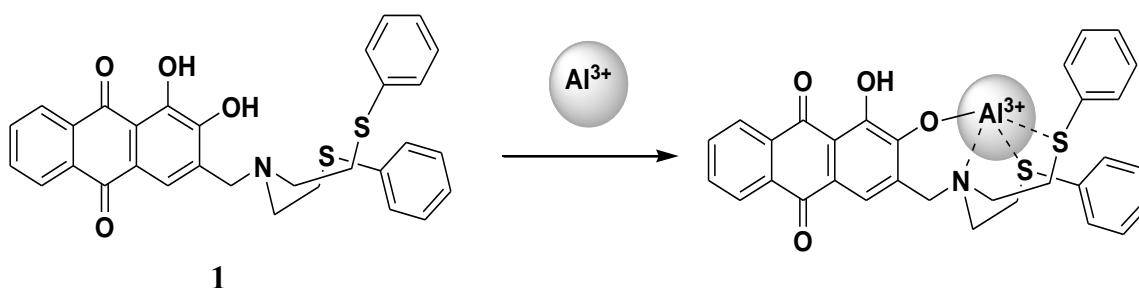
Scheme 2.1. Anthraquinone based Al^{3+} sensor displaying a PET fluorescence response.

In the excited state a molecule is an electron acceptor as well as a better electron donor owing to the promotion of electron to a higher energy level. The principle of a simple PET type chemosensor which contains electron accepting fluorophore from receptor is briefly discussed. What if the receptor moiety accepts electron from excited fluorophore?
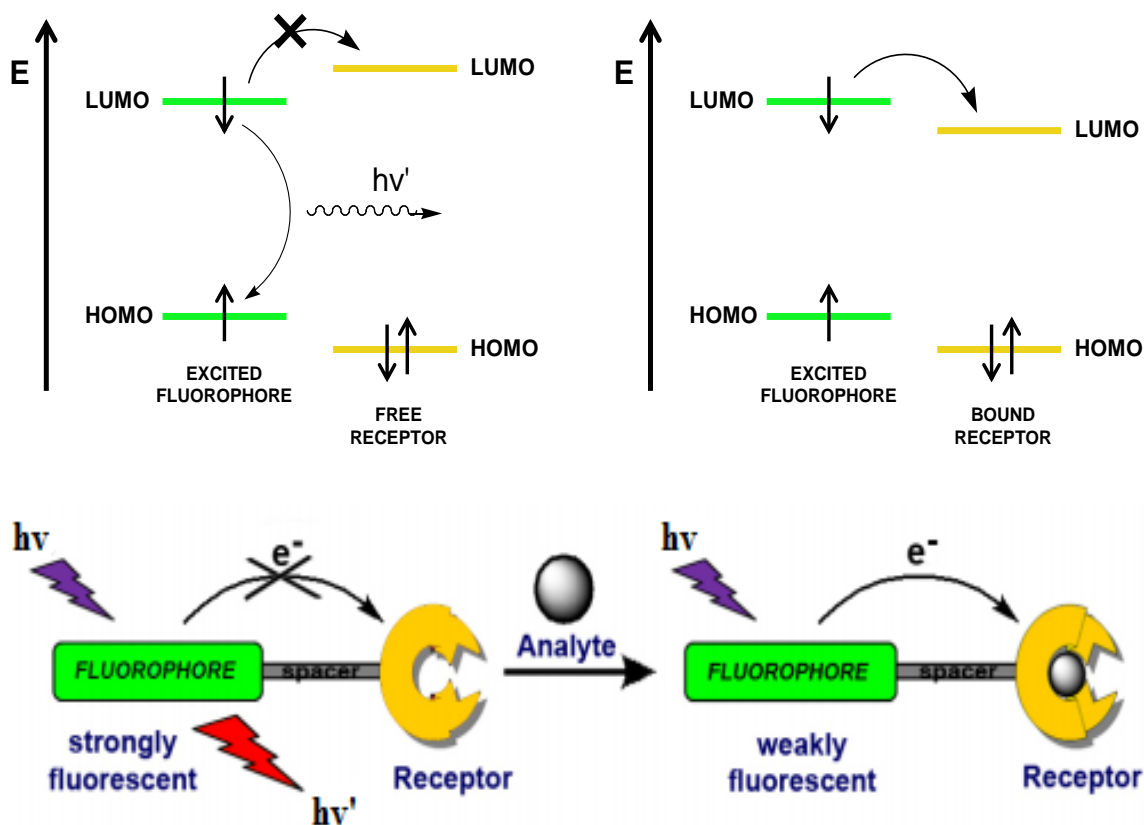
Figure 2.17. Typical view of oxidative PET mechanism.

2

bright-green fluorescence   **very weak fluorescence**
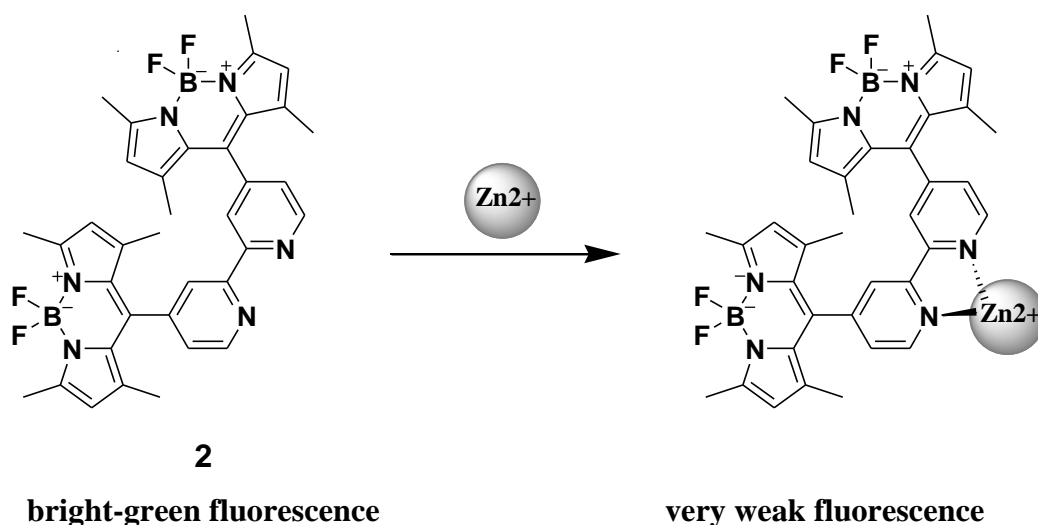
Scheme 2.2. Oxidative PET mechanism generated after coordination with zinc.

The oxidative PET depends on redox potentials of both the receptor and fluorophore units. The probable oxidative PET mechanism in terms of the molecular orbitals involved exhibits in Figure 2.17. Contradictory to the earlier mechanism, the unbound form of the chemosensor exhibits strong fluorescence, whereas the fluorescence of the bound species is quenched and this is termed as an on–off system. Therefore, in the presence of an analyte the emission intensity of such system decreases extensively.

Compound **2** [44] demonstrates the oxidative PET mechanism in the presence of zinc cation. As shown in Scheme 2.2, Bodipy dye and 2,2ˡ-bipyridine were selected as the fluorophore and the receptor, respectively in the sensing probe. The fluorophore shows bright green fluorescence in the absence of zinc cation, beyond complexation with zinc ion quenches the fluorescence through oxidative PET mechanism.

The PET process and its projected mechanisms were exhibited technically within the above figures. In this section the principles of a range of photo-induced electron transfer (PET) type mechanisms and its utilization in the field of development of molecular sensing have been examined in the previous papers. Therefore, PET has been the most extensively used mechanism amongst other conventional sensing mechanisms in the design of fluorescent chemosensors.

2.1.3.4.2. Intramolecular charge transfer (ICT)

It is an electron transfer process in which the fluorophore is directly connected to the receptor and is a part of the fluorophore π–electron system where one terminal is possibly to be electron rich (electron donor) while the other one is electron poor (electron acceptor). The two phenomena (PET and ICT) are simply differentiated with their absorption and emission spectra [38]. In PET, strong quenching occurs and no spectral shifts are noticed. On the other hand, binding of a cation to the receptor, alters the fluorescence emission intensity and lifetime, as well as induces a spectral shift of the absorption and emission bands. In cases of cation sensing, it is predictable that a complexed cation will reduce the electron-donating character of the electron donor (such as amino group), causing a reduction in conjugation, resulting blue-shift of the absorption spectrum. Conversely, if the acceptor group (e.g. a carbonyl group) interrelates with a cation, its electron withdrawing character is increased, the conjugation is augmented, and a red-shift in the absorption spectrum is noticed. Generally, the fluorescence spectra are shifted in the same way like the absorption spectra.

The changes in photophysical properties can also be described by charge dipole interactions [45]. The electron donating group will be positively charged in the excited

state and upon binding with the cation, the excited state is destabilized than the ground state. Consequently, the energy gap between the excited and ground states will increase showing a blue shift in both the absorption and emission spectra. Moreover, in the presence of electron accepting group (such as carbonyl group) on the receptor unit, the interaction towards cation will stabilize the excited state more than the ground state, reducing the energy gap between the ground and excited states and hence a red shift appears in both the absorption and emission spectra. Thus, the energy (ΔE) needed for the electron transition from ground state to excited state is less, and so the wavelength corresponding to this energy is increased and a red-shift will be observed in the absorption as well as in the emission spectra (Figure 2.18).
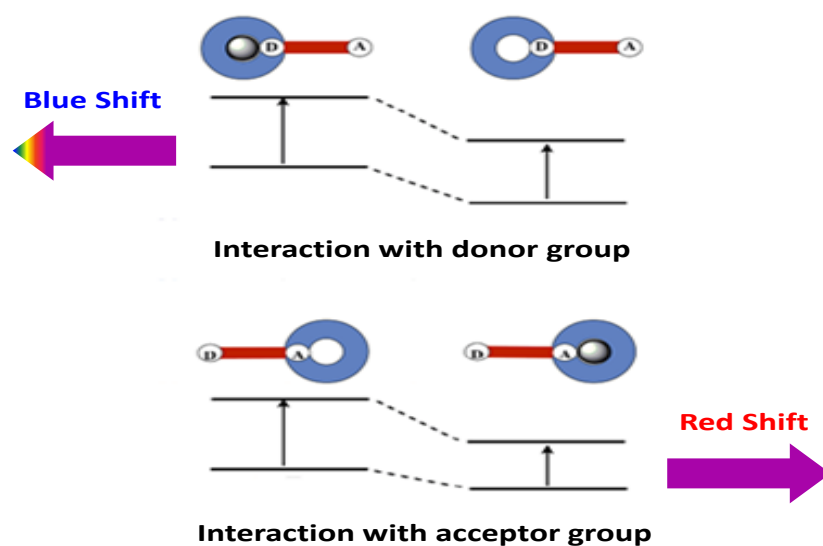
Figure 2.18. Simple spectral displacements of ICT type sensors.

Compounds those are structurally similar but varied in receptor unit can demonstrate different spectral shifts upon binding with the same analyte. For example, two Bodipy dyes alone show similar spectral properties, whereas upon protonation display opposite spectral shifts [46]. One of those dyes contains electron donating aniline moiety whereas another contains electron accepting pyridine moiety as receptor units (Figure 2.19). As a result, in their protonation form, these two compounds show spectral shifts in the opposite directions owing to the reasons as described earlier.

A number of numerous fluorophores have been designed and reported in accordance with the ICT mechanism. Conjugated compounds containing both electron donor (D) and electron accepting (A) groups which show ICT mechanism via the π-conjugated link are also said to be 'Push-Pull' system (D-π-A system). Besides this, the applications of chemosensing and analyte monitoring discussed earlier, this kind of

systems has also been found in numerous optical-electrical applications together with organic light emitting devices [47, 48], and solar cell materials [49, 50].
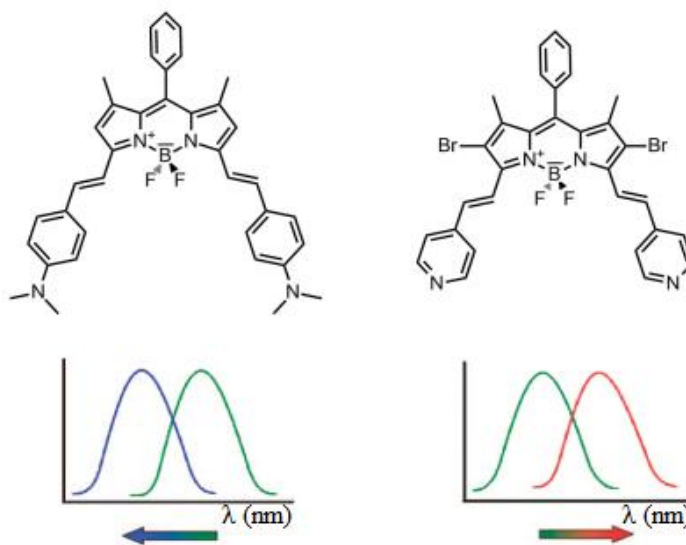
Figure 2.19. Characteristics bidirectional switching dyes associated to ICT donor and acceptor.

2.1.3.4.3. Energy transfer (ET)

The energy transfer is an additional signalling mechanism which can be categorized as fluorescence resonance (FRET) and electronic energy transfer (EET) derived from the interaction distance between donor and acceptor moieties and it is merely feasible when the system is multichromophoric. In this process, the energy of donor chromophore is transferred to acceptor chromophore as the donor unit absorbs light at comparatively short wavelength and the acceptor unit fluoresces at longer wavelength (Figure 2.20). Moreover, the energy of the donor at its excited state is employed to excite the acceptor via energy transfer.
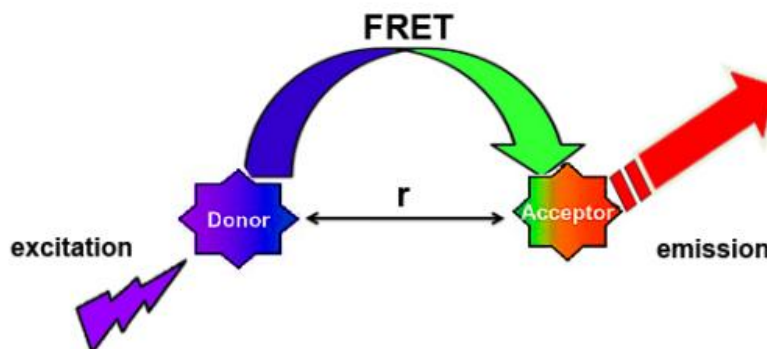
Figure 2.20. A schematic representation of the FRET process.

As depicted in Scheme 2.3 displays FRET fluorescence when unbound; the phenanthrene group is excited and emission from the pyrene is viewed. The unbound sensor has free rotation through the hexyl spacer which permits the fluorophores to associate because of hydrophobic interactions. Binding of a carbohydrate forces the fluorophores aside by rigidifying the system and excitation of the phenanthrene yields phenanthrene emission.

Over the past three decades, the utility of FRET has established applications in numerous fields like light frequency conversion, artificial photosynthetic antenna, cascade systems, singlet oxygen generation and switching element in molecular machines.
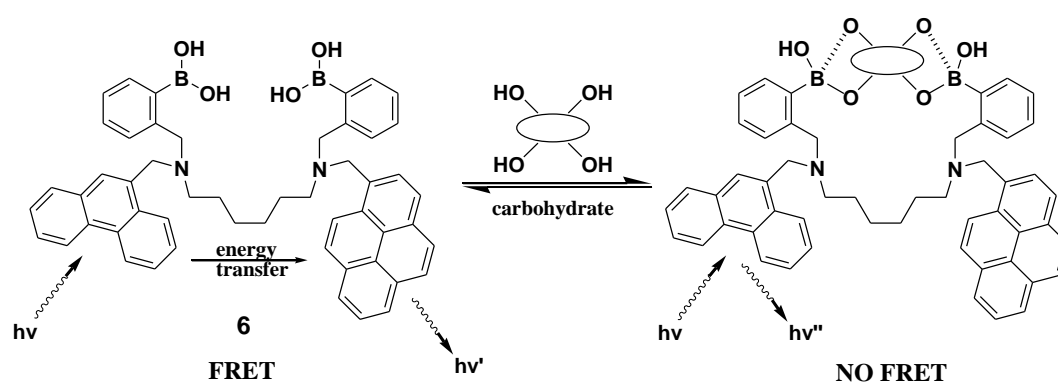
Scheme 2.3. FRET fluorescence response showing in a carbohydrate sensor.

2.1.3.4.4. Excimer and exciplex formation

A molecule in the excited state can overlap with an unexcited molecule similar to itself, giving rise to a dimer in the excited state [38], so-called as excimer (from "excited dimer"). The excimer emission spectrum differs significantly from that of monomers; it is generally broad, shifted to longer wavelengths and does not demonstrate vibrational resolution. If the collision occurs between molecules which vary in structure an excited state complex is produced which is called exciplex (from "excited complex"). The formation of excimers and exciplexes is reversible (subsequent to emission they separate and are free to form again upon excitation) and requires close location and sufficient orientation of the two molecules engaged (in the case of excimers, generally two heterocycles rich in π-electrons are needed, which form two parallel planes via π-π stacking).

A band demonstrating the monomer fluorescence of naphthalene, is depicted on the left side in Figure 2.21. The fluorescence emission changes (right of Figure 2.21) and a new red-shifted band is apparent at the high concentrations of naphthalene. The new band is the consequence of a lower energy complex which forms when an excited naphthalene

moiety transfers energy to an adjacent cofacially stacked naphthalene molecule to form an excited state complex (exciplex).
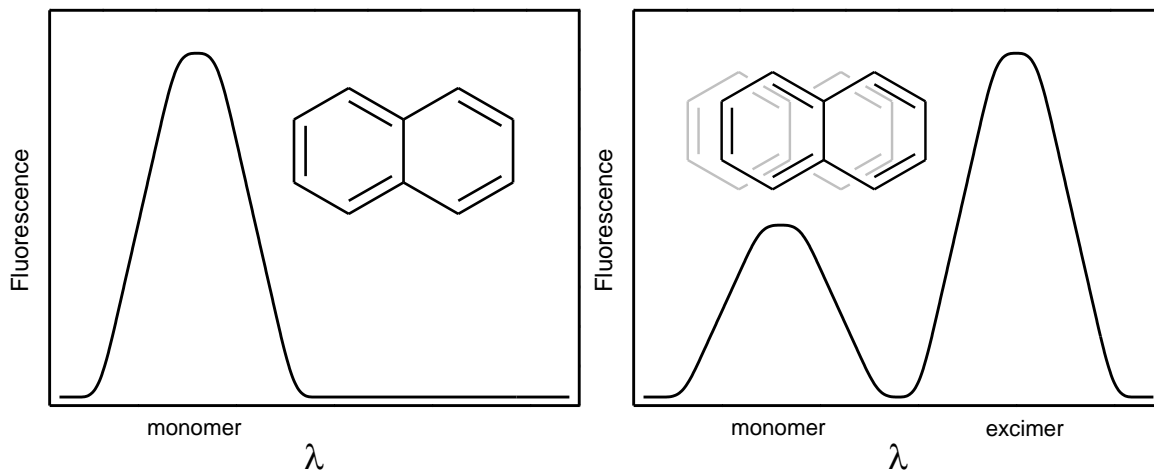
Figure 2.21. Excimer fluorescence of naphthalene.

2.1.3.5. Association constant (K)

The binding affinity between the two molecules at equilibrium is described by the mathematical constant named as association constant. For a fluorescence enhancement process the association constant can be calculated employing Benesi-Hildebrand equation [38]:

$$\frac{1}{F-F_0} = \frac{1}{F_{MAX}-F_0} + \frac{1}{F_{MAX}-F_0} \times \frac{1}{K[M^{n+}]} \qquad (2.14)$$

where F_0, F, and F_{MAX} are the fluorescence intensities of the fluorophore without analyte, intensity with varying concentrations of analyte, and intensity with the maximum concentration of analyte, respectively. K is the association constant, and $[M^{n+}]$ is the analyte concentration. The linear relationship was attained from the fluorescence titration plotted $[1/(F-F_0)]$ as a function of $1/[M^{n+}]$ and slope is equal to $[1/(F-F_0)K]$.

Whereas, in case of a fluorescence quenching process, the association constant is described by the Stern-Volmer equation [34] which is given by

$$\frac{F_0}{F} = 1 + K[M^{n+}] \qquad (2.15)$$

where, F_0 and F are the observed fluorescence intensity of fluorophore in the absence and presence of analyte, respectively. K is the association constant and $[M^{n+}]$ is the concentration of analyte. A plot of F_0/F versus $[M^{n+}]$ is named as a Stern-Volmer (SV) plot that yields a straight line by means of a slope equal to K.

2.1.3.6. Limit of detection (LOD)

The lowest concentration of an analyte which can be reliably measured is known as limit of detection and could be calculated based on Signal-to-Noise ratio = 3. Signal to Noise ratio (S/N) is a dimensionless measure of the relative strength of an analytical signal (S) to the average strength of the background instrumental noise (N) for a particular sample and is closely associated to the detection level. The general formula of limit of detection is given by:

$$\mathbf{LOD} = \frac{3\mathbf{SD}}{\mathbf{m}} \qquad (2.16)$$

where, **SD** is the standard deviation from the blank measurement (fluorophore without analyte) and **m** is the slope from the calibration curve of the fluorophore with varying concentrations of analyte.

The detection limit is calculated from the standard deviation of the blank. The sample Standard Deviation is a measure of the degree of agreement, or precision, among replicate analyses of a sample. The standard deviation is defined as:

$$\mathbf{SD} = \sqrt{\frac{\sum(\mathbf{x} - \mathbf{x'})^2}{\mathbf{N} - 1}}$$

where, **x** is the emission intensity of the blank solution, x' is the mean of the intensity of all blank solutions and N is the number of measurements.

References

1. P.T. Kissinger, W.R. Heineman, Laboratory techniques in electroanalytical chemistry, 2nd Edition, Revised and expanded, *CRC Press*, New York, 1996.

2. C.G. Zoski, Handbook of Electrochemistry, 1st Edition, *Elsevier,* Amsterdam, 2007.

3. P.T. Kissinger, W.R. Heineman, Cyclic voltammetry, *J. Chem. Educ.* **60** (1983) 702–706.

4. G.A. Mabbott, An introduction to cyclic voltammetry, *J. Chem. Educ.* **60** (1983) 697–702.

5. D.A. Skoog, F.J. Holler, S.R. Crouch, Principles of instrumental analysis, 6th Edition, *Thomson Brooks Cole*, 2007.

6. R.K. Mahajan, N. Kaur, M.S. Bakshi, Cyclic voltammetry investigation of the mixed micelles of conventional surfactants with L64 and F127, *Colloids Surf. A* **276** (2006) 221–227.

7. A. Sinha, Dhanjai, R. Jain, Electrocatalytic determination of α 2-adrenergic agonist tizanidine at graphene–silicon dioxide nanocomposite sensor, *Mater. Res. Bull.* **65** (2015) 307–314.

8. K.F. Drake, R.P.V. Duyne, Cyclic differential pulse voltammetry: A versatile instrumental approach using a computerized system, *J. Electroanal. Chem.* **89** (1978) 231–246.

9. B.J. Sanghavi, A.K. Srivastava, Adsorptive stripping differential pulse voltammetric determination of venlafaxine and desvenlafaxine employing nafion–carbon nanotube composite glassy carbon electrode, *Electrochim. Acta* **56** (2011) 4188–4196.

10. A.J. Bard, L.R. Faulkner, Electrochemical methods: Fundamentals and applications, 2nd Edition, *John Wiley & Sons, Inc.*, New York, 2001.

11. G.E. Baiulescu, V.V. Cosofret, Applications of ion-selective membrane electrodes in organic analysis (Ellis horwood series in analytical chemistry), *Ellis Horwood Ltd.*, 1977.

12. G.J. Moody, J.D.R. Thomas, Selective ion sensitive electrodes, *Merrow Publishing Co. Ltd.*, 1971.

13. P.L. Bailey, Analysis with ion-selective electrodes, 2nd Edition, *Heyden*, 1980.

14. J. Inczedy, T. Lengyel, A.M. Ure, Compendium of analytical nomenclature, definitive rules 1997, 3rd Edition, *Blackwell Science*, 1998.

15. R.P. Buck, V.V. Cosofret, Recommended procedures for calibration of ion-selective electrodes, *Pure Appl. Chem.* **65** (1993) 1849–1858.

16. A.K. Covington, Terminology and conventions for microelectronic ion-selective field effect transistor devices in electrochemistry (IUPAC recommendations 1994), *Pure Appl. Chem.* **66** (1994) 565–569.

17. X. Zhang, H. Ju, J. Wang, Electrochemical sensors, biosensors and their biomedical applications, 1st Edition, *Elsevier*, 2008.

18. Y. Tsujimura, T. Sunagawa, M. Yokoyama, K. Kimura, Sodium ion-selective electrodes based on silicone-rubber membranes covalently incorporating neutral carriers, *Analyst* **121** (1996) 1705–1709.

19. Y. Qin, S. Peper, E. Bakker, Plasticizer-free polymer membrane ion-selective electrodes containing a methacrylic copolymer matrix, *Electroanal.* **14** (2002) 1375–1381.

20. A.K. Singh, G. Bhattacharjee, M. Singh, S. Chandra, A new macrocyclic polystyrene based membrane sensor for zinc, *Electroanal.* **9** (1997) 1005–1008.

21. M.A. Simon, R.P. Kusy, The molecular, physical and mechanical properties of highly plasticized poly(vinyl chloride) membranes, *Polymer* **34** (1993) 5106–5115.

22. O.M. Petrukhin, A.B. Kharitonov, E.V. Frakiisky, Y.I. Urusov, A.F. Zhukov, A.N. Shipway, V.E. Baulin, The effect of lipophilic anionic additives on detection limits of ion-selective electrodes based on ionophores with phosphoryl complexing groups, *Sens. Actuators B* **76** (2001) 653–659.

23. S.I. Wakida, T. Masadome, T. Imato, Y. Shibutani, K. Yakabe, T. Shono, Y. Asano, Additive-salt effect on low detection limit and slope sensitivity in response of potassium- and sodium-selective neutral carrier based electrodes and their liquid-membrane based ion-sensitive field-effect transistor, *Anal. Sci.* **15** (1999) 47–51.

24. Y. Umezawa, CRC handbook of ion-selective electrodes: Selectivity coefficients, 1st Edition, *CRC Press*, Boca Raton, 1990.

25. Y. Umezawa, K. Umezawa, H. Sato, Selectivity coefficients for ion-selective electrodes: Recommended methods for reporting $K_{A,B}^{Pot}$ values, *Pure Appl. Chem.* **67** (1995) 507–518.

26. C. Macca, Determination of potentiometric selectivity, *Anal. Chim. Acta* **321** (1996) 1–10.

27. R.P. Buck, E. Lindner, Recommendations for nomenclature of ion-selective electrodes, *Pure Appl. Chem.* **66** (1994) 2527–2536.

28. E. Bakker, Selectivity of liquid membrane ion-selective electrodes, *Electroanal.* **9** (1997) 7–12.

29. E. Bakker, E. Pretsch, P. Buhlmann, Selectivity of potentiometric ion sensors, *Anal. Chem.* **72** (2000) 1127–1133.

30. V.P.Y. Gadzekpo, G.D. Christian, Determination of selectivity coefficients of ion-selective electrodes by a matched-potential method, *Anal. Chim. Acta* **164** (1984) 279–282.

31. G. Horvai, The matched potential method, a generic approach to characterize the differential selectivity of chemical sensors, *Sens. Actuators B* **43** (1997) 94–98.

32. E. Bakker, P. Buhlmann, E. Pretsch, Carrier-based ion-selective electrodes and bulk optodes. 1. General characteristics, *Chem. Rev.* **97** (1997) 3083–3132.

33. C. Macca, The current usage of selectivity coefficients for the characterization of ion-selective electrodes. A critical survey of the 2000/2001 literature, *Electroanal.* **15** (2003) 997–1010.

34. J.R. Lakowicz, Principles of fluorescence spectroscopy, 3rd Edition, *Springer Science & Business Media*, New York, 2006.

35. M. Adachi, Y. Nagao, Design of near-infrared dyes based on π-conjugation system extension 2. Theoretical elucidation of framework extended derivatives of perylene chromophore, *Chem. Mater.* **13** (2001) 662–669.

36. M.F. Rastegar, E.K. Todd, H. Tang, Z.Y. Wang, A new class of near-infrared electrochromic oxamide-based dinuclear ruthenium complexes, *Org. Lett.* **6** (2004) 4519–4522.

37. Z. Xu, J. Yoon, D.R. Spring, Fluorescent chemosensors for Zn^{2+}, *Chem. Soc. Rev.* **39** (2010) 1996–2006.

38. B. Valeur, Molecular fluorescence: Principles and applications, 1st Edition, *Wiley-VCH*, Weinheim, 2002.

39. K. Rurack, U. Resch-Genger, Rigidization, preorientation and electronic decoupling– the 'magic triangle' for the design of highly efficient fluorescent sensors and switches, *Chem. Soc. Rev.* **31** (2002) 116–127.

40. M.R. Wasielewski, J.M. Fenton, Govindjee, The rate of formation of $P_{700}^{+}-A_0^{-}$ in photosystem I particles from spinach as measured by picosecond transient absorption spectroscopy, *Photosynth. Res.* **12** (1987) 181–190.

41. A.W. Czarnik, Fluorescent chemosensors for ion and molecule recognition, *American Chemical Society*, Washington, DC, 1993.

42. A.P.D. Silva, T.S. Moody, G.D. Wright, Fluorescent PET (Photoinduced Electron Transfer) sensors as potent analytical tools, *Analyst* **134** (2009) 2385–2393.

43. Y. Lu, S. Huang, Y. Liu, S. He, L. Zhao, X. Zeng, Highly selective and sensitive fluorescent turn-on chemosensor for Al^{3+} based on a novel photoinduced electron transfer approach, *Org. Lett.* **13** (2011) 5274–5277.

44. B. Turfan, E.U. Akkaya, Modulation of boradiazaindacene emission by cation-mediated oxidative PET, *Org. Lett.* **4** (2002) 2857–2859.

45. H.G. Lohr, F. Vogtle, Chromo- and fluoroionophores. A new class of dye reagents, *Acc. Chem. Res.* **18** (1985) 65–72.

46. E. Deniz, G.C. Isbasar, O.A. Bozdemir, L.T. Yildirim, A. Siemiarczuk, E.U. Akkaya, Bidirectional switching of near IR emitting boradiazaindacene fluorophores, *Org. Lett.* **10** (2008) 3401–3403.

47. Y. Zhou, Y. Xiao, S. Chi, X. Qian, Isomeric boron-fluorine complexes with donor-acceptor architecture: Strong solid/liquid fluorescence and large Stokes shift, *Org. Lett.* **10** (2008) 633–636.

48. Y. Dong, A. Bolduc, N. McGregor, W.G. Skene, Push-pull aminobithiophenes – Highly fluorescent stable fluorophores, *Org. Lett.* **13** (2011) 1844–1847.

49. S. Erten-Ela, M.D. Yilmaz, B. Icli, Y. Dede, S. Icli, E.U. Akkaya, A panchromatic boradiazaindacene (BODIPY) sensitizer for dye-sensitized solar cells, *Org. Lett.* **10** (2008) 3299–3302.

50. H. Burckstummer, N.M. Kronenberg, K. Meerholz, F. Wurthner, Near-infrared absorbing merocyanine dyes for bulk heterojunction solar cells, *Org. Lett.* **12** (2010) 3666–3669.

CHAPTER 3
Simultaneous Determination of Ascorbic Acid and Caffeine by a Voltammetric Sensor

3.1. Introduction

Ascorbic acid (AA) (2-(1, 2-dihydroxyethyl)-4,5-dihydroxyfuran-3-one), commonly known as vitamin-C [1], is one of the most important and widespread natural compounds. It plays an important role in the formation and maintenance of collagen, and as a powerful antioxidant defending the body against oxidative stress [2]. Therefore, these materials are employed extensively in skin care products and as important agents in the treatment of skin pigmentation and aging [3]. It strengthens and protects the immune system, increases iron bioavailability, and is thought to assist diminish cholesterol levels [4]. Owing to these properties, it is used for the prevention and treatment of common cold, mental illness, infertility, cancer, Alzheimer's disease, atherosclerosis, and AIDS [5–7]; thus it is essential for humans, since its absence can cause damage, known as the syndrome of scurvy [8]. However, guinea pigs, humans and other primates are not capable to synthesize vitamin C owing to the final enzyme (L-gulonolactone oxidase) of the vitamin C synthesis pathway is missing. Because of the absence of this enzyme, humans are dependent on vitamin C from their diet [9–11]. However, at higher concentration levels, AA contributes to the formation of kidney stones.

Caffeine (CAF) (1,3,7-trimethylpurine-2,6-dione), is an alkaloid; a class of naturally occurring compounds containing nitrogen and having the basic properties of an organic amine called xanthenes [12–14]. Other common members of this class include theophylline and theobromine. It's found naturally in many food products such as coffee, tea, yerbamate, guarana berries, cola nuts and cacao beans etc. [15–18]. For the plant, caffeine acts as a natural pesticide since it paralyzes and kills some of the insects that attempt to feed on the plant [19]. However, there may appear some undesirable and toxic consequences to their consumers due to overdose of CAF like; hypertension, nausea, anxiety, hyperactivity, oversensitivity, irritability, nervousness, insomnia, depression, seizure, and inhibition of DNA which acutely threaten people's health and therefore, lowers quality of life in the long run [20, 21]. It promotes many physiological functions such as gastric acid secretion, dieresis, cardiac stimulant and stimulates the central nervous system by increasing the release of adrenaline and results in the absorption of body fat as fuel and spares glycogen [22–28]. CAF was banned by the World Anti Doping Agency (WADA) at a level of 12 µg/ml in urine because of its use by professional athletes to give them endurance, alertness and sense of extra energy needed for their workouts. However, its other formulations are used for the treatment of migraine and for anti-inflammatory and diuretic action.

In addition to several important applications of AA and CAF separately, their combinations are widely used for analgesic and antipyretic effects [29, 30]. As a result of widespread use of AA and CAF they are present in many environmental samples. In view their adverse effects it is important to determine them in environmental samples, human body fluids and pharmaceutical preparations.

A number of techniques such as spectrophotometry [31, 32], gas chromatography-mass spectrometry (GC–MS) [33], high-performance liquid chromatography (HPLC) [34, 35], ion chromatography [36], and solid phase analysis [37] are available for the determination of AA and CAF. These techniques are highly sophisticated, time consuming and expensive, and require large infrastructure back up and expert knowledge. Thus, they are not very appropriate for the analysis of large number of samples, whereas electrometric methods provide a faster and convenient route for the determination of drugs. A number of drugs have been accurately determined separately by voltammetric technique using modified glassy carbon electrode (MGCE) [38–40].

Simultaneous determination of AA and CAF in many pharmaceutical formulations is important as they are widely used for treatment of various diseases. It has been attempted by differential pulse voltammetry using boron doped diamond electrode (BDD) [41] and glassy carbon electrode (GCE) [42]. The detection limit for BDD has been found 19 μM and 7.0 μM and for MGCE 1.0×10^{-2} μM and 3.52×10^{-3} μM for AA and CAF, respectively and therefore these methods are not very appropriate for trace determination of these drugs.

In order to estimate the concentration of AA and CAF simultaneously, we have made attempts to employ square wave voltammetry (SWV) using both bare GCE and MGCE for their determination up to low level concentration. As the sensitivity of bare GCE was found to be poor, the electrode was modified by multiwall carbon nanotubes (MWCNT) to give better results.

After the discovery of carbon nanotubes (CNTs) by Iijima in 1991 [43], they have received increasing employment to prepare electrodes. Recently CNTs have obtained remarkable attention in chemical, physical and material fields because of their unique structure and extraordinary properties, such as high electrical conductivity, tubular structure, large surface area, excellent adsorptive ability and efficient catalytic activity [44–46], indicating that they can facilitate charge transfer reaction and make contributions to the higher current response of AA and CAF; when they are used as electrode materials in electroanalytical chemistry.
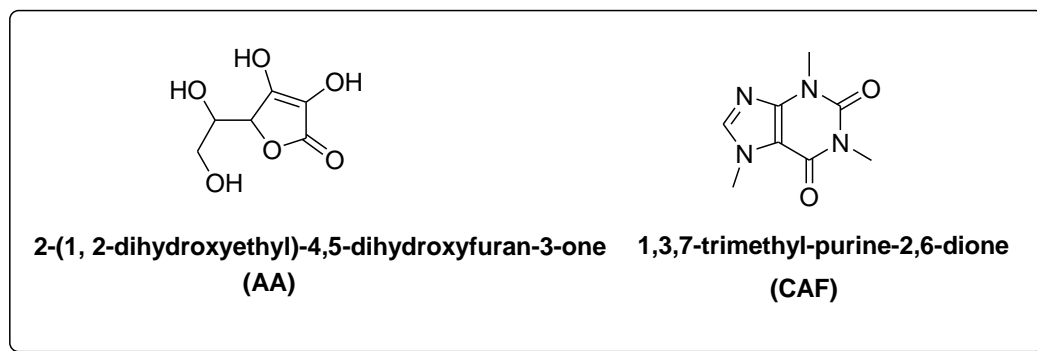
Scheme: 3.1. Chemical structure of the studied compounds.

3.2. Material and methods

3.2.1. Chemicals, reagents and instrumentation

CAF and AA (Scheme 3.1) were procured from Adams, USA and Sigma Aldrich, respectively. Phosphate buffer (PBS) of different pH values was prepared according to the method of Christian and Purdy [47]. All reagents used were of analytical grade. Tablets of different pharmaceutical companies containing AA and CAF were procured from the local market. Ag/AgCl (BAS Model MF–2052 RB–5B), GCE and MWCNT (purity > 98%, outer diameter 10–15 nm and inner diameter 2–6 nm) were procured from BAS, USA. All the solutions were prepared in double distilled water.

All the electrochemical experiments were conducted in a single cell assembly having three electrodes: Ag/AgCl (3M NaCl) electrode, glassy carbon electrode and Pt wire electrode as reference, working and counter electrodes, respectively. The voltammetric experiments were carried out on a bioanalytical system (BAS, West Lafayette, USA) Epsilon EC–USB voltammetric analyzer. All pH measurements were made on a digital pH meter (Model CP–901, Century India Ltd.).

3.2.2. Preparation of modified glassy carbon electrode (MGCE)

The bare GCE was modified by the reported method with a slight modification [48]. The bare GCE was polished carefully using zinc oxide and alumina mixture with the help of a silky pad. The polished electrode was washed with doubly distilled water and then dried. A suspension of MWCNT (0.5 mg/ml) in *N,N′*-dimethyl formamide (DMF) was prepared by the dispersion of MWCNT using ultrasonic churning. Small amount (40µl) of this suspension was put on the surface of bare polished GCE. It was seen that the suspension covered total surface area of the GCE. The suspension was allowed to desiccate by keeping the electrode in open at room temperature (25 ± 2 °C). Within about half an hour, the solvent evaporated off leaving a thin layer of MWCNT all around the electrode

surface. This process was repeated a number of times till a smooth layer formed all around the electrode surface. The electrode so obtained is called MGCE. Further, modified electrode was cleaned by applying a potential of –200 mV for 180 seconds after each run to remove the adsorbed analyte.

3.2.3. Voltammetric procedure

One mmol per liter of stock solutions of AA and CAF were equipped in double distilled water. In the electrolytic cell, 2 ml of phosphate buffer solution (PBS) pH 7.2 and needed amount of stock solution was added and the total volume made up to 4 ml with double distilled water. Voltammograms were then recorded using voltammetric analyzer under gilt-edged parameters. Voltammetric parameters were gilt-edged for a better electrode response and these gilt-edged parameters were used throughout the experiment. Gilt-edged parameters for SWV were: initial (E): –200 mV, final (E): 1000 mV, step (E): 4 mV, square wave amplitude (Esw): 25 mV, square wave frequency (f): 15 Hz, Quit time: 2 s and full scale (+/–): 1 mA and initial (E): 0 mV, final (E): 1600 mV, step (E): 4 mV, square wave amplitude (Esw): 25 mV, square wave frequency (f): 15 Hz, Quit time: 2 s and full scale (+/–): 1 mA for AA and CAF, respectively.

Gilt-edge conditions for cyclic voltammetry (CV) were initial (E): 0 mV, switching potential 1 (E): 1600 mV, switching potential 2 (E): –1600 mV, final (E): 0 mV, scan rate (v): 10 mV/s and full scale (+/–): 1 mA. All the potentials are recorded at an ambient temperature of 25 ± 2 ℃ with reference to Ag/AgCl electrode.

3.3. Results and discussion

3.3.1. Cyclic voltammetry

The electrochemical behavior of ascorbic acid and caffeine on the modified GCE was estimated by cyclic voltammetry at a scan rate of 100 mV/s and the other parameters were, initial (E): –200 mV, Switching potential (1): 1600 mV, Switching potential (2): –1600 mV, final (E): –200 mV, Quit time: 2 s, No. of segments: 3, full scale (+/–): 1mA using modified GCE. Well established peaks were obtained for ascorbic acid and caffeine in anodic region at ~ 190 mV and ~ 1400 mV, respectively as shown in Figure 3.1 and there were no reduction peaks were obtained in reverse scan indicates the irreversibility of the electrode reaction. In addition to obtained better results, further study of ascorbic acid and caffeine samples were carried out by using square wave voltammetry, as it has well established rewards such as low background current, low detection limit and high sensitivity [49].
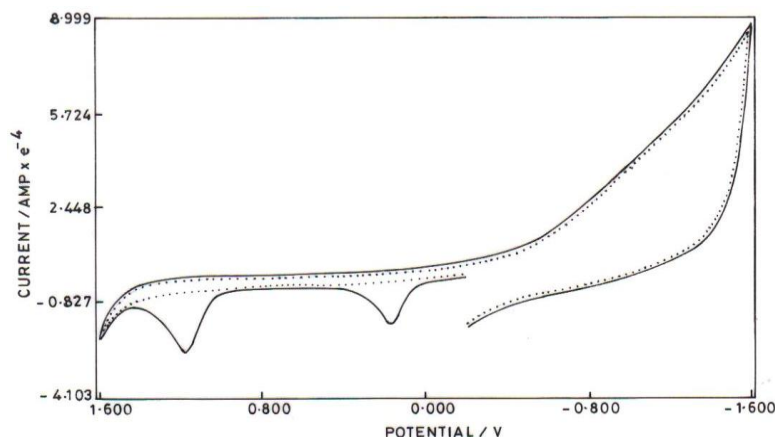
Figure 3.1. A cyclic voltammogram recorded at MWCNT modified GCE using 0.1 mM concentration (solid line —). The dotted line (……) shows blank at pH 7.20.

3.3.2. Square wave voltammetry

The voltammetric response of mixture of AA and CAF in phosphate buffer was investigated using square wave frequency at 15 Hz in the pH range 2.15–9.15 and 4.0–10.0, respectively. The voltammograms, in dashed line and solid line for bare GCE and MGCE, respectively at pH 7.0 are given in Figure 3.2. It is seen that the oxidation peaks obtained with MGCE are sharper than those obtained with bare GCE. Further, the peak potentials obtained with MGCE are lower (~−10 mV and ~1103 mV for AA and CAF, respectively) than the peak potentials with bare GCE (~202 mV and ~1402 mV). Not only
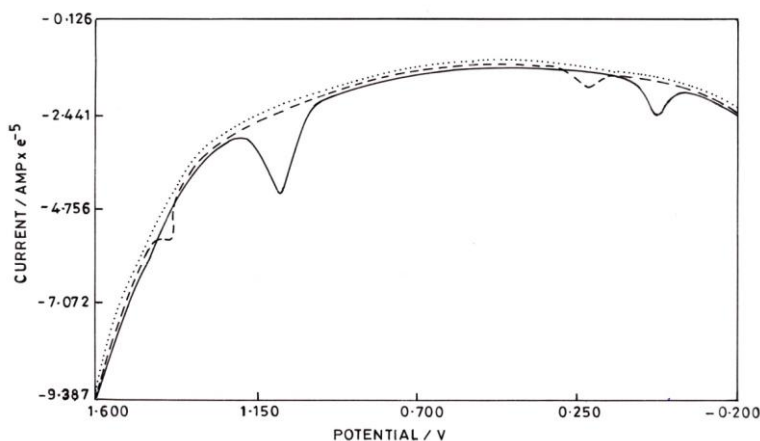
Figure 3.2. The square wave voltammograms of AA and CAF in a mixture, obtained with bare GCE (dashed line – – – –), MGCE (solid line —) and (dotted line ……) for blank solution.

this, the peak current obtained with MGCE for both the drugs is higher than that obtained with bare GCE. Similar observations were also obtained in case of an oxidation study by multiwalled carbon nanotubes modified basal plane pyrolytic graphite electrode (MWCNT/BPPGE) [50]. As carbon nanotubes exhibit high electrical conductivity, it

89

appears that the carbon nanotubes accelerate electron transfer reaction rate in the oxidation process at some exposed walls of MWCNTs owing to its aromatic structure with the sp^2– like planes and thus lowering the peak potential for modified electrode [51–54].

The effect of increasing concentration of AA and CAF on the voltammogram is shown in Figures 3.3 and 3.4. It is seen from the voltammograms that the peak current increases with increase in the concentration of the drug. The increase in the current with concentration of the drug is linear as evidenced by the linear plots (shown in insets in the same figures).
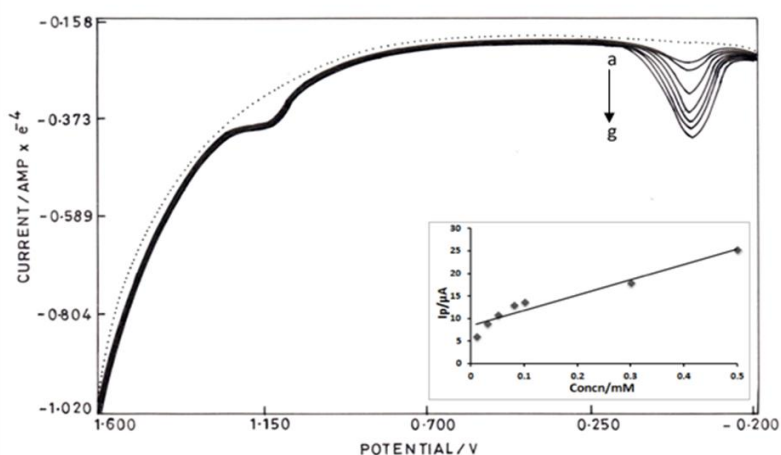
Figure 3.3. The square wave voltammograms obtained with blank solution (dotted line…) and with MGCE (solid line —) in phosphate buffer solution 7.2 pH; (a) containing constant concentration of CAF (30 µM) and increasing concentration of AA: (a) 10, (b) 30, (c) 50, (d) 80, (e) 100, (f) 300 and (g) 500 µM. Inset is the plot between peak current versus concentration of the AA.
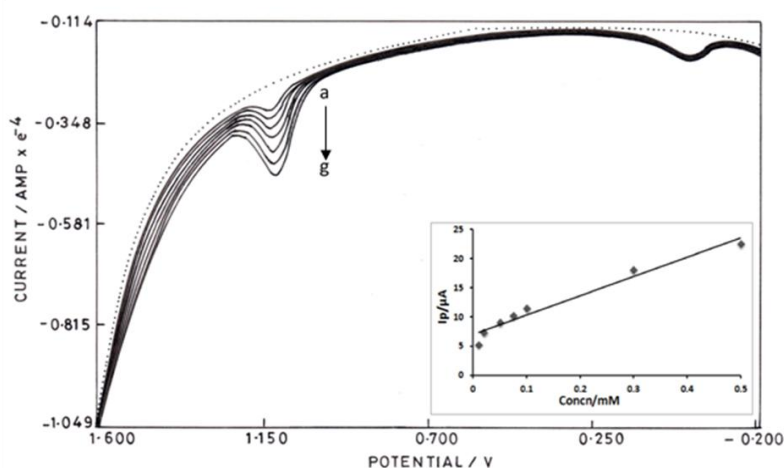
Figure 3.4. The square wave voltammograms obtained with blank solution (dotted line…) and with MGCE (solid line —) in phosphate buffer solution 7.2 pH; (a) containing constant concentration of AA (80 µM) and increasing concentration of CAF: (a) 10, (b) 30, (c) 50, (d) 80, (e) 100, (f) 300 and (g) 500 µM. Inset is the plot between peak current versus concentration of the CAF.

In order to determine AA and CAF in various samples, calibration plots are needed. Calibration plots were drawn (Figures 3.5a and 3.5b) from the voltammograms obtained by the oxidation study of AA and CAF taken separately. Calibration characteristics evaluated from the figures (3.5a and 3.5b) are summarized in Table 3.1. The following equations obtained on regression analysis fit these linear plots:

$$i_p \, (\mu A) = 17.17C \, (\mu M) + 2.603 \text{ For AA} \tag{3.1}$$

$$i_p \, (\mu A) = 48.54C \, (\mu M) + 3.319 \text{ For CAF} \tag{3.2}$$

where, C is the concentration of analytes and the correlation coefficients are 0.992 and 0.995 for AA and CAF, respectively.
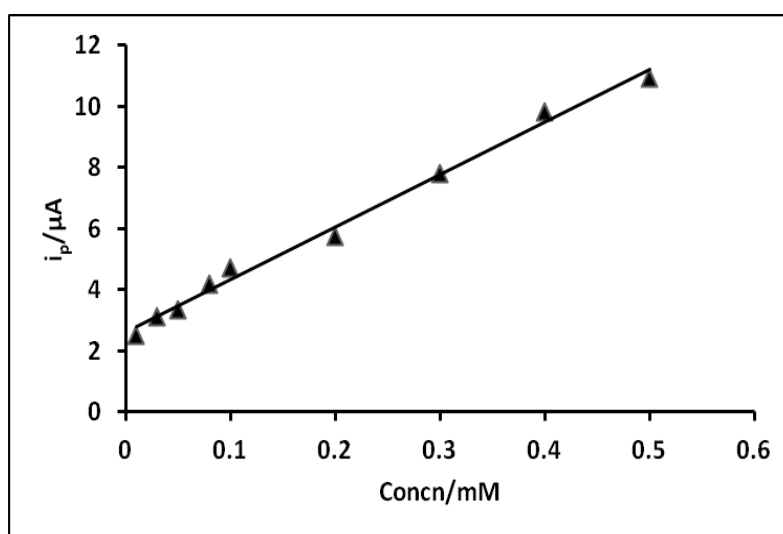
Figure 3.5a. Plot between peak current versus concentration as obtained in oxidation of AA taken separately by square wave voltammetry with MGCE.
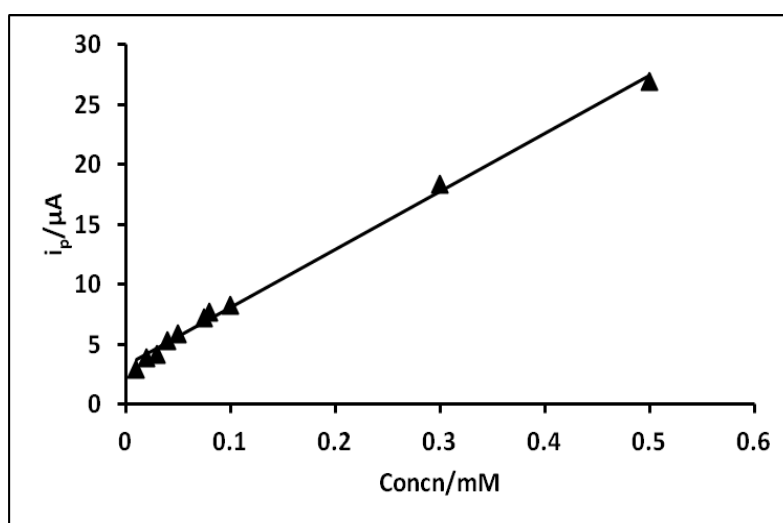
Figure 3.5b. Plot between peak current versus concentration as obtained in oxidation of CAF taken separately by square wave voltammetry with MGCE.

Table 3.1. Calibration characteristics for the determination of AA and CAF by SWV using MWCNT modified glassy carbon electrode.

Characteristics	AA	CAF
Calibration range	10 μM−500 μM	10 μM−500 μM
Detection limit	1.0×10^{-2} μM	3.52×10^{-3} μM
Limit of quantification	3.33×10^{-2} μM	11.73×10^{-3} μM
Sensitivity	17.17 μA μM^{-1}	48.54 μA μ M^{-1}
Intercept	2.603	3.219
RSD of slope	2.97	5.35
RSD of intercept	0.45	0.02

3.3.3. Effect of pH

The effect of pH on peak potential was studied by determining the voltammograms of the drugs separately at various pH values. The peak potential values were evaluated from the voltammograms at different pH values, and are plotted as a function of pH in Figures 3.6a and 3.6b for AA and CAF, respectively.
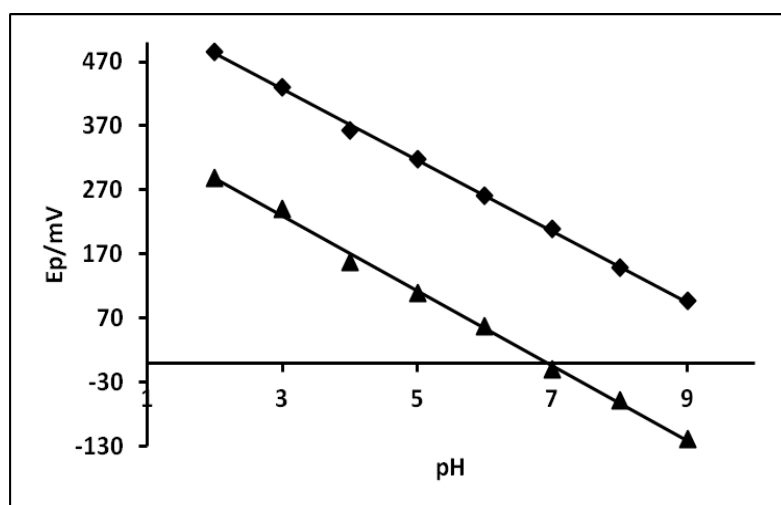
Figure 3.6a. Plot between peak potential versus pH as obtained in oxidation of AA by square wave voltammetry with MGCE (▲) and bare GCE (■).

The following equations obtained on regression analysis fit these linear plots with correlation coefficients 0.997, 0.999, 0.998 and 0.994, respectively.

$Ep / mV = -58.36pH + 404.4$ versus Ag/AgCl for AA on MGCE (pH 2.15–9.15)   (3.3)

$Ep / mV = -55.39pH + 593.5$ versus Ag/AgCl for AA on bare GCE (pH 2.15–9.15)   (3.4)

$Ep / mV = -55.44pH + 1748.0$ versus Ag/AgCl for CAF on MGCE (pH 4.0–10.0)   (3.5)

$Ep / mV = -58.98pH + 1818.0$ versus Ag/AgCl for CAF on bare GCE (pH 4.0–10.0)   (3.6)
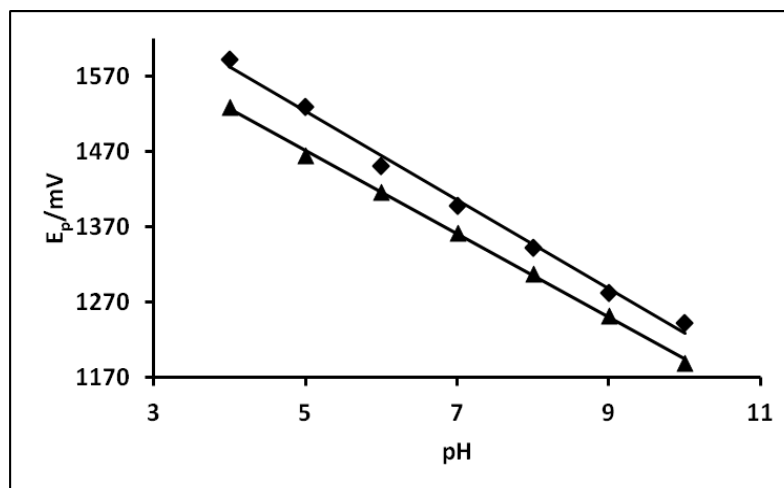
Figure 3.6b. Plot between peak potential versus pH as obtained in oxidation of CAF by square wave voltammetry with MGCE (▲) and bare GCE (■).

It is seen that the values of dEp/dpH obtained from the linear plots are ~58 and ~55 mV which indicate that equal number of protons and electrons are involved in the electrochemical oxidation of these drugs at the electrode. Further, similar values of ~55 and ~59 mV are obtained for AA and CAF respectively, for bare GCE indicate that the equal number of electrons and protons are involved in the oxidation reaction at this electrode also [55].

3.3.4. Effect of square wave frequency
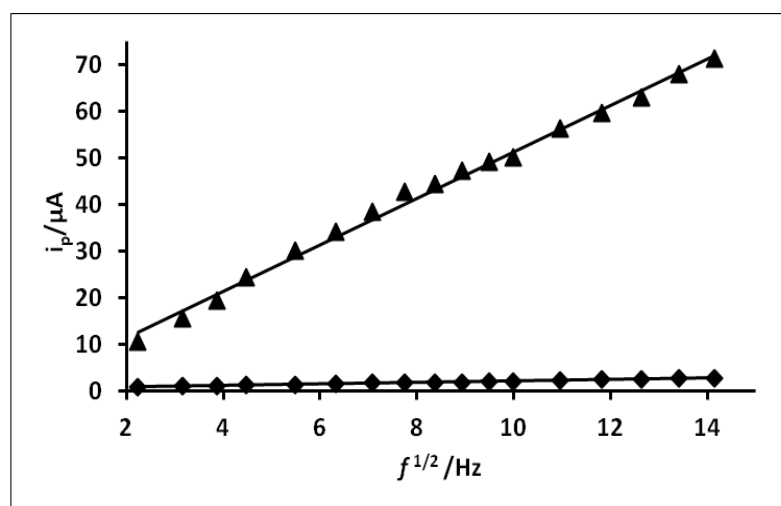
Figure 3.7a. Plot between peak current versus $f^{1/2}$ as obtained in oxidation of AA by square wave voltammetry with MGCE (▲) and bare GCE (■).

Voltammograms of AA and CAF were also obtained as a function of frequency at pH 7.2. The peak currents were evaluated from these voltammograms and are plotted against frequency in Figures 3.7a and 3.7b respectively. The linear nature of i_p versus $f^{1/2}$

shows that the oxidation process at the electrode is diffusion controlled for both the drugs. The following equations obtained on regression analysis fit the linear plots with correlation coefficient 0.994, 0.983, 0.989 and 0.990, respectively.

$$i_p (\mu A) = 4.982\, f^{\frac{1}{2}}\, (Hz) + 1.589 \text{ for AA on MGCE} \tag{3.7}$$

$$i_p (\mu A) = 0.161\, f^{\frac{1}{2}}\, (Hz) + 0.576 \text{ for AA on bare GCE} \tag{3.8}$$

$$i_p (\mu A) = 11.19\, f^{\frac{1}{2}}\, (Hz) - 21.74 \text{ for CAF on MGCE} \tag{3.9}$$

$$i_p (\mu A) = 2.920\, f^{\frac{1}{2}}\, (Hz) - 1.081 \text{ for CAF on bare GCE} \tag{3.10}$$
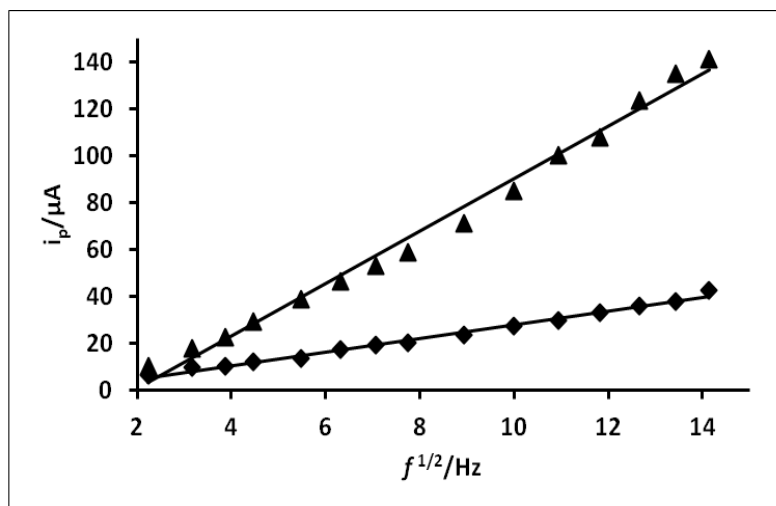
**Figure 3.7b.** Plot between peak current versus $f^{1/2}$ as obtained in oxidation of CAF by square wave voltammetry with MGCE (▲) and bare GCE (■).

3.3.5. Analytical utility

3.3.5.1. Determination of CAF in real samples as coffee, tea leaves and mountain dew

The MWCNT modified glassy carbon electrode was also used to determine CAF in coffee (Instant Coffee of Nescafe Sunrise), tea leaves (Mohani Tea Leaves) and cold drink (mountain dew), which were procured from local market. 25 mg of coffee powder or tea leaves were heated with 25 ml of double distilled water with constant stirring. After about 6 hours CAF was extracted in water in aqueous phase and the mixture was then filtered using whatman filter paper 42. Then 2 ml of PBS of pH 7.2 was added to 2 ml of the filtrate and square wave voltammograms were recorded for this mixture. The amount of CAF determined in coffee, tea leaves and cold drink (mountain dew) is reported in Table 3.2.

2 ml of the cold drink (mountain dew) was taken and volume made up to 4 ml with PBS (pH 7.2) for the determination of CAF and subjected to SWV. The peak currents were evaluated from the voltammograms and used to determine amount of CAF using calibration plot Figure 3.5b obtained for the oxidation of CAF separately.

Table 3.2. Determination of CAF in tea leaves, coffee and cold drink (mountain dew) by SWV using MWCNT modified glassy carbon electrode.

Sample	Determined amount (mg/gm)
Tea leaves	28.00 ± 0.02
Coffee	96.44 ± 0.03
Cold drink (Mountain dew)	0.145 ± 0.003

3.3.5.2. Determination of AA and CAF in pharmaceutical preparations

Table 3.3. Determination of AA and CAF in pharmaceutical formulations by SWV using MWCNT modified glassy carbon electrode.

Compound	Tablet name/ company	Amount Reported mg/gm of the tablets	Amount Determined mg/gm of the tablets
AA	Limacee (Abbott Healthcare Pvt. Ltd., Ahmedabad)	727.273	715.345 ± 0.02
	Berocin-C (Micro Labs Ltd., Banglore)	541.541	549.946 ± 0.14
CAF	Nimutal Cold + (Elder Pharm. Ltd., Mumbai)	39.370	41.024 ± 0.21
	Sinarest (Centaur Pharm. Pvt. Ltd., Goa)	55.351	52.934 ± 0.04
	Cozy Plus (Ind-Swift Ltd., H.P.)	55.866	54.674 ± 0.18
	CC-GO (G.S. Pharm. Pvt. Ltd., Uttrakhand)	56.866	58.250 ± 0.03

The electrode was also used to determine the quantity of the AA and CAF in various pharmaceutical tablets as available in the local market. Tablets containing AA and CAF were procured from the local market. The tablets were powdered and the known quantity of tablets were dissolved in 25 ml double distilled water and the total volume of this solution was made up of 50 ml by adding of PBS pH 7.2 . The square wave voltammograms of this solution were recorded under gilt-edged parameters. The peak current of voltammograms evaluated and used to calculate AA and CAF from the calibration plots Figures 3.5a and 3.5b. The amount so determined is given in Table 3.3, where it is compared with the amount reported as per specification of the drug. It is seen

from the Table 3.3 that there is a close agreement between the amount determined and amount reported indicating that the proposed electrode is an efficient tool for quantification of AA and CAF in pharmaceutical preparations.

3.3.5.3. Determination of AA and CAF in human urine samples

The utility of the biosensor (MGCE) was further explored by using it for the simultaneous determination of AA and CAF in urine samples of patients. Patients who were taking AA and CAF in some form in the treatment of the disease were selected. Urine samples were collected from the patients undergoing treatment in the hospital of Indian Institute of Technology Roorkee, Roorkee. The urine sample was diluted twenty times by PBS pH 7.2 and square wave voltammograms of the samples were recorded using MGCE. A typical voltammogram obtained is shown in Figure 3.8, which shows well defined oxidation peaks at ~ −10mV and ~ 1103 mV for AA and CAF, respectively. Other peaks present in the same voltammogram could be due to oxidation of other compounds present in urine but not identified. The amount of AA and CAF determined is shown in Table 3.4.
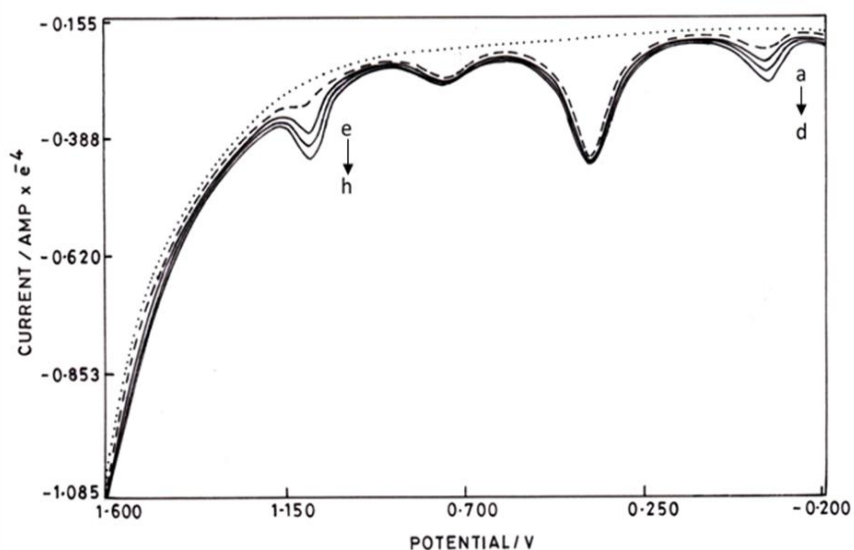
Figure 3.8. The square wave voltammograms for blank solution (dotted line ......), urine sample without addition of drugs (dashed line − − − −) and after addition of AA and CAF (solid line ─). Amount added of AA (a) 0.00, (b) 0.002215, (c) 0.004403, and (d) 0.006605 mg/ml and amount added CAF (e) 0.00, (f) 0.002428, (g) 0.004855, and (h) 0.007282 mg/ml.

3.3.6. Reproducibility and stability of the modified electrode

The sensing reproducibility and stability of a sensor increases its reliability and therefore MWCNT modified GCE was used by measuring voltammetric current for a fixed concentration of AA and CAF in phosphate buffer solution (pH 7.2). Five repetitive

measurements at MGCE under the optimal conditions were performed. The relative standard deviations (RSD) were found to be 1.45% and 1.74% for AA and CAF, respectively at MGCE, which showed that the electrode have good reproducibility. The electrode was stored in the laboratory before and after its continuous use for 20 days and it was observed that it could retain 96.3% and 95.8% current of its original response for AA and CAF, respectively, suggesting acceptable stability of the electrode [56, 57]. The results showed that the developed electrochemical sensor can be used as an alternative method for the quantification of AA and CAF in real samples because of its simplicity and good reproducibility.

Table 3.4. Determination of AA and CAF in human urine sample by SWV using MWCNT modified glassy carbon electrode.

Urine sample	Added AA amount (mg/ml)	Added CAF amount (mg/ml)	Determined AA amount (mg/ml)	Determined CAF amount (mg/ml)
Sample	0.00	0.00	0.078 ± 0.0016	0.150 ± 0.0037
	0.002215	0.002428	0.091 ± 0.0053	0.187 ± 0.0041
	0.004403	0.004855	0.099 ± 0.0032	0.197 ± 0.003
	0.006605	0.007282	0.141 ± 0.0027	0.215 ± 0.0018

3.4. Conclusion

The cyclic voltammogram indicates well established oxidation peaks for ascorbic acid and caffeine in anodic region and the absence of reduction peaks in reverse scan shows the irreversibility of the electrode reaction. Further, the square wave voltammetric studies have shown that the peak potentials and detection limits for modified glassy carbon electrode for the determination of AA and CAF are ~ -10 mV and ~ 1103 mV, and 1.0×10^{-2} μM and 3.52×10^{-3} μM respectively and for bare glassy carbon electrode are ~ 202 mV and ~ 1402 mV and 5.29×10^{-1} μM and 9.41×10^{-2} μM respectively. The lower value shows that the modified glassy carbon electrode is superior to bare glassy carbon electrode. The mechanistic study has shown that the equal number of electrons and protons are involved in the oxidation of drugs. In view of high sensitivity for the detection of the drugs, the technique has been used for the reliable determination of AA and CAF in tea leaves, coffee, cold drink (mountain dew), pharmaceutical preparations and urine samples. Further, it is believed that the determination of AA and CAF by square wave voltammetry is convenient, faster, accurate and low cost analysis. It is thus superior to existing spectrophotometric and chromatographic methods which are expensive and time

consuming. Thus it can be said that this biosensor is a useful addition in the field of analytical chemistry for the determination of drugs.

References

1. E. Ergun, S. Kart, D.K. Zeybek, B. Zeybek, Simultaneous electrochemical determination of ascorbic acid and uric acid using poly(glyoxal-bis(2-hydroxyanil)) modified glassy carbon electrode, *Sens. Actuators B* **224** (2016) 55–64.

2. S.J. Padayatty, A. Katz, Y. Wang, P. Eck, O. Kwon, J.H. Lee, S. Chen, C. Corpe, A. Dutta, S.K. Dutta, M. Levine, Vitamin C as an antioxidant: Evaluation of its role in disease prevention, *J. Am. Coll. Nutr.* **22** (2003) 18–35.

3. M.L. Chang, C.M. Chang, Simultaneous voltammetric determination of ascorbic acid and its derivatives in cosmetics using epoxy-carbon composite electrodes, *J. Food Drug Anal.* **13** (2005) 205–211.

4. F. Buhl, B. Szpikowska-Sroka, M. Galkowska, Determination of L-ascorbic acid after chromatographic separation, *J. Planar Chromatogr.* **18** (2005) 368–371.

5. A.A. Ensafi, M. Taei, T. khayamian, A differential pulse voltammetric method for simultaneous determination of ascorbic acid, dopamine, and uric acid using poly (3-(5-chloro-2-hydroxyphenylazo)-4,5-dihydroxynaphthalene-2,7-disulphonic   acid) film modified glassy carbon electrode, *J. Electroanal. Chem.* **633** (2009) 212–220.

6. S. Chitravathi, B.E.K. Swamy, G.P. Mamatha, B.S. Sherigara, Simultaneous electrochemical determination of dopamine and ascorbic acid using poly (L-serine) modified carbon paste electrode, *J. Mol. Liq.* **160** (2011) 193–199.

7. W. Ren, H.Q. Luo, N.B. Li, Simultaneous voltammetric measurement of ascorbic acid, epinephrine and uric acid at a glassy carbon electrode modified with caffeic acid, *Biosens. Bioelectron.* **21** (2006) 1086–1092.

8. E.H. Duarte, L.T. Kubota, C.R.T. Tarley, Carbon nanotube based sensor for simultaneous determination of acetaminophen and ascorbic acid exploiting multiple response optimization and measures in the presence of surfactant, *Electroanal.* **24** (2012) 2291–2301.

9. H. Moteki, Y. Shimamura, M. Kimura, M. Ogihara, Signal transduction pathway for L-ascorbic acid- and L-ascorbic acid 2-glucoside-induced DNA synthesis and cell proliferation in primary cultures of adult rat hepatocytes, *Eur. J. Pharmacol.* **683** (2012) 276–284.

10. H. Moteki, M. Kimura, K. Sunaga, T. Tsuda, M. Ogihara, Signal transduction mechanism for potentiation by α_1- and β_2-adrenoceptor agonists of L-ascorbic acid-induced DNA synthesis and proliferation in primary cultures of adult rat hepatocytes, *Eur. J. Pharmacol.* **700** (2013) 2–12.

11. J. Mandl, A. Szarka, G. Bánhegyi, Vitamin C: Update on physiology and pharmacology, *Brit. J. Pharmacol.* **157** (2009) 1097–1110.

12. Y. Yardlm, E. Keskin, Z. Senturk, Voltammetric determination of mixtures of caffeine and chlorogenic acid in beverage samples using a boron-doped diamond electrode, *Talanta* **116** (2013) 1010–1017.

13. M. Amiri-Aref, J.B. Raoof, R. Ojani, A highly sensitive electrochemical sensor for simultaneous voltammetric determination of noradrenaline, acetaminophen, xanthine and caffeine based on a flavonoid nanostructured modified glassy carbon electrode, *Sens. Actuators B* **192** (2014) 634–641.

14. K. Tyszczuk-Rotko, I. Beczkowska, Nafion covered lead film electrode for the voltammetric determination of caffeine in beverage samples and pharmaceutical formulations, *Food Chem.* **172** (2015) 24–29.

15. S. Yang, R. Yang, G. Li, L. Qu, J. Li, L. Yu, Nafion/multi-wall carbon nanotubes composite film coated glassy carbon electrode for sensitive determination of caffeine, *J. Electroanal. Chem.* **639** (2010) 77–82.

16. J.M. Zen, Y.S. Ting, Simultaneous determination of caffeine and acetaminophen in drug formulations by square-wave voltammetry using a chemically modified electrode, *Anal. Chim. Acta* **342** (1997) 175–180.

17. S. Guo, Q. Zhu, B. Yang, J. Wang, B. Ye, Determination of caffeine content in tea based on ploy(safranine T) electroactive film modified electrode, *Food Chem.* **129** (2011) 1311–1314.

18. S.Y. Ly, C.H. Lee, Y.S. Jung, Voltammetric bioassay of caffeine using sensor implant, *Neuromol. Med.* **11** (2009) 20–27.

19. M. Aklilu, M. Tessema, M. Redi-Abshiro, Indirect voltammetric determination of caffeine content in coffee using 1,4-benzoquinone modified carbon paste electrode, *Talanta* **76** (2008) 742–746.

20. J.Y. Sun, K.J. Huang, S.Y. Wei, Z.W. Wu, F.P. Ren, A graphene-based electrochemical sensor for sensitive determination of caffeine, *Colloid. Surface. B* **84** (2011) 421–426.

21. L. Jiang, Y. Ding, F. Jiang, L. Li, F. Mo, Electrodeposited nitrogen-doped graphene/carbon nanotubes nanocomposite as enhancer for simultaneous and sensitive voltammetric determination of caffeine and vanillin, *Anal. Chim. Acta* **833** (2014) 22–28.

22. N. Spataru, B.V. Sarada, D.A. Tryk, A. Fujishima, Anodic voltammetry of xanthine, theophylline, theobromine and caffeine at conductive diamond electrodes and its analytical application, *Electroanal.* **14** (2002) 721–728.

23. B.C. Lourencao, R.A. Medeiros, R.C. Rocha-Filho, L.H. Mazo, O. Fatibello-Filho, Simultaneous voltammetric determination of paracetamol and caffeine in pharmaceutical formulations using a boron-doped diamond electrode, *Talanta* **78** (2009) 748–752.

24. A.J. Jeevagan, S.A. John, Electrochemical determination of caffeine in the presence of paracetamol using a self-assembled monolayer of non-peripheral amine substituted copper(II) phthalocyanine, *Electrochim. Acta* **77** (2012) 137–142.

25. X. Kan, T. Liu, C. Li, H. Zhou, Z. Xing, A. Zhu, A novel electrochemical sensor based on molecularly imprinted polymers for caffeine recognition and detection, *J. Solid State Electrochem.* **16** (2012) 3207–3213.

26. L. Svorc, Determination of caffeine: A comprehensive review on electrochemical methods, *Int. J. Electrochem. Sci.* **8** (2013) 5755–5773.

27. G. Yang, F. Zhao, B. Zeng, Facile fabrication of a novel anisotropic gold nanoparticle-chitosan-ionic liquid/graphene modified electrode for the determination of theophylline and caffeine, *Talanta* **127** (2014) 116–122.

28. A.C. Torres, M.M. Barsan, C.M.A. Brett, Simple electrochemical sensor for caffeine based on carbon and nafion-modified carbon electrodes, *Food Chem.* **149** (2014) 215–220.

29. M. Amiri, A. Bezaatpour, Z. Pakdel, K. Nekoueian, Simultaneous voltammetric determination of uric acid and ascorbic acid using carbon paste/cobalt Schiff base composite electrode, *J. Solid State Electrochem.* **16** (2012) 2187–2195.

30. A.A. Ensafi, H. Karimi-Maleh, S. Mallakpour, Simultaneous determination of ascorbic acid, acetaminophen, and tryptophan by square wave voltammetry using N-(3,4-dihydroxyphenethyl)-3,5-dinitrobenzamide-modified carbon nanotubes paste electrode, *Electroanal.* **24** (2012) 666–675.

31. M.M. Sena, J.C.B. Fernandes, L. Rover Jr., R.J. Poppi, L.T. Kubota, Application of two- and three-way chemometric methods in the study of acetylsalicylic acid and ascorbic acid mixtures using ultraviolet spectrophotometry, *Anal. Chim. Acta* **409** (2000) 159–170.

32. A. Belay, K. Ture, M. Redi, A. Asfaw, Measurement of caffeine in coffee beans with UV/vis spectrometer, *Food Chem.* **108** (2008) 310–315.

33. J. Zou, H. Zhang, M. Ding, Z. Shang, Large phase ratio spontaneous extraction followed by GC-MS for the determination of caffeine in beverages, *Chromatographia* **71** (2010) 323–326.

34. Y. Yamauchi, A. Nakamura, I. Kohno, K. Hatanaka, M. Kitai, T. Tanimoto, Quasi-flow injection analysis for rapid determination of caffeine in tea using the sample pre-treatment method with a cartridge column filled with polyvinylpolypyrrolidone, *J. Chromatogr. A* **1177** (2008) 190–194.

35. M.A. Rostagno, N. Manchon, M. D'Arrigo, E. Guillamon, A. Villares, A. Garcia-Lafuente, A. Ramos, J.A. Martinez, Fast and simultaneous determination of phenolic compounds and caffeine in teas, mate, instant coffee, soft drink and energetic drink by high-performance liquid chromatography using a fused-core column, *Anal. Chim. Acta* **685** (2011) 204–211.

36. Q.C. Chen, J. Wang, Simultaneous determination of artificial sweeteners, preservatives, caffeine, theobromine and theophylline in food and pharmaceutical preparations by ion chromatography, *J. Chromatogr. A* **937** (2001) 57–64.

37. A.B. Moreira, I.L.T. Dias, G.O. Neto, E.A.G. Zagatto, M.M.C. Ferreira, L.T. Kubota, Solid-phase spectrofluorimetric determination of acetylsalicylic acid and caffeine in pharmaceutical preparations using partial least-squares multivariate calibration, *Talanta* **67** (2005) 65–69.

38. R. Jain, Vikas, Voltammetric determination of cefpirome at multiwalled carbon nanotube modified glassy carbon sensor based electrode in bulk form and pharmaceutical formulation, *Colloids Surf. B* **87** (2011) 423–426.

39. X. Chen, J. Zhu, Q. Xi, W. Yang, A high performance electrochemical sensor for acetaminophen based on single-walled carbon nanotube–graphene nanosheet hybrid films, *Sens. Actuators B* **161** (2012) 648–654.

40. S. Shahrokhian, M. Azimzadeh, M.K. Amini, Modification of glassy carbon electrode with a bilayer of multiwalled carbon nanotube/tiron-doped polypyrrole: Application to sensitive voltammetric determination of acyclovir, *Mater. Sci. Eng. C* **53** (2015) 134–141.

41. B.C. Lourencao, R.A. Medeiros, R.C. Rocha-Filho, O. Fatibello-Filho, Simultaneous differential pulse voltammetric determination of ascorbic acid and caffeine in pharmaceutical formulations using a boron-doped diamond electrode, *Electroanal.* **22** (2010) 1717–1723.

42. O.W. Lau, S.F. Luk, Y.M. Cheung, Simultaneous determination of ascorbic acid, caffeine and paracetamol in drug formulations by differential-pulse voltammetry using a glassy carbon electrode, *Analyst* **114** (1989) 1047–1051.

43. S. Iijima, Helical microtubules of graphitic carbon, *Nature* **354** (1991) 56–58.

44. P.M. Ajayan, Nanotubes from carbon, *Chem. Rev.* **99** (1999) 1787–1799.

45. B. Habibi, M. Jahanbakhshi, M. Abazari, A modified single-walled carbon nanotubes/carbon-ceramic electrode for simultaneous voltammetric determination of paracetamol and caffeine, *J. Iran. Chem. Soc.* **11** (2014) 511–521.

46. J.M.P.J. Garrido, V. Rahemi, F. Borges, C.M.A. Brett, E.M.P.J. Garrido, Carbon nanotube β-cyclodextrin modified electrode as enhanced sensing platform for the determination of fungicide pyrimethanil, *Food Control* **60** (2016) 7–11.

47. G.D. Christian, W.C. Purdy, The residual current in orthophosphate medium, *J. Electroanal. Chem.* **3** (1962) 363–367.

48. Y. Wang, X. Wei, F. Wang, M. Li, Sensitive voltammetric detection of caffeine in tea and other beverages based on a DNA-functionalized single-walled carbon nanotube modified glassy carbon electrode, *Anal. Methods* **6** (2014) 7525–7531.

49. E. Molaakbari, A. Mostafavi, H. Beitollahi, Simultaneous electrochemical determination of dopamine, melatonin, methionine and caffeine, *Sens. Actuators B* **208** (2015) 195–203.

50. R.T. Kachoosangi, G.G. Wildgoose, R.G. Compton, Sensitive adsorptive stripping voltammetric determination of paracetamol at multiwalled carbon nanotube modified basal plane pyrolytic graphite electrode, *Anal. Chim. Acta* **618** (2008) 54–60.

51. S. Shahrokhian, E. Asadian, Simultaneous voltammetric determination of ascorbic acid, acetaminophen and isoniazid using thionine immobilized multi-walled carbon nanotube modified carbon paste electrode, *Electrochim. Acta* **55** (2010) 666–672.

52. G.G. Wildgoose, C.E. Banks, H.C. Leventis, R.G. Compton, Chemically modified carbon nanotubes for use in electroanalysis, *Microchim. Acta* **152** (2006) 187–214.

53. Y. Shao, J. Wang, H. Wu, J. Liu, I.A. Aksay, Y. Lin, Graphene based electrochemical sensors and biosensors: A review, *Electroanal.* **22** (2010) 1027–1036.

54. P.R. Dalmasso, M.L. Pedano, G.A. Rivas, Electrochemical determination of ascorbic acid and paracetamol in pharmaceutical formulations using a glassy carbon electrode modified with multi-wall carbon nanotubes dispersed in polyhistidine, *Sens. Actuators B* **173** (2012) 732–736.

55. B.J. Sanghavi, A.K. Srivastava, Simultaneous voltammetric determination of acetaminophen, aspirin and caffeine using an in situ surfactant-modified multiwalled carbon nanotube paste electrode, *Electrochim. Acta* **55** (2010) 8638–8648.

56. M.B. Gholivand, M. Khodadadian, Simultaneous voltammetric determination of theophylline and guaifenesin using a multiwalled carbon nanotube ionic liquid modified glassy carbon electrode, *Electroanal.* **26** (2014) 1975–1983.

57. B. Rafiee, A.R. Fakhari, M. Ghaffarzadeh, Impedimetric and stripping voltammetric determination of methamphetamine at gold nanoparticles-multiwalled carbon nanotubes modified screen printed electrode, *Sens. Actuators B* **218** (2015) 271–279.

CHAPTER 4
Preparation and Investigation of a Cadmium Selective Sensor

4.1. Introduction

Heavy metals are toxic to plants, animals and human beings as they pose a detrimental risk to human health even in trace concentrations [1]. In recent years, the analytical field has evolved, with growing concern for the welfare of the environment requiring that qualitative and quantitative information on the nature and concentration of pollutants needs to be explored [2]. In terms of environmental mobility and bioavailability, metal ions that are soluble in water are amongst the most dangerous contaminants because they are easily transported in aquifers, taken up by plants or aquatic organisms, and may interfere with any kind of dissolved organic or inorganic matter in water, e.g., humic substances. Cadmium is one of the metal ions which easily participate in biological processes and causes harmful health issues [3]. Cadmium is a non-essential and one of the most toxic metals and effect of its severe poisoning is manifested in a variety of symptoms which include high blood pressure, anaemia, kidney damage, bone marrow disorders, hypertension, and toxicity to aquatic biota etc. [4, 5]. It also causes a bone-related syndrome called itai-itai disease, metabolic disorders, and increased incidence of specific forms of cancer, possibly because of the direct inhibition of DNA mismatch remediation [6–8]. The provisional tolerable weekly input for cadmium recommended by the WHO on food additives is 0.4–5.0 mg based on a tolerable intake of 1µg/Kg of body weight per day [9]. It is released by various natural and anthropogenic sources to the atmosphere, aquatic environments (fresh and salt water environments) and terrestrial environments, such as from smelters, earth's crust, mantle, volcanic activity, weathering of rocks, and the disposal of cadmium bearing products. It enters natural water through industrial discharges from electroplating industries, metal finishing, nikel-cadmium (Ni-Cd) batteries, phosphate fertilizers, and mining, combustion of fossil fuels, pigments, solar cells, stabilizers and metallurgical alloying activities and finally it is bio-concentrated through the food chain [10–13].

Therefore, in consideration of various health problems caused by cadmium due to its increased industrial use, it is desirable to search for a fast, responsive and simple analytical technique for the detection and trace level monitoring of cadmium. Presently, sophisticated techniques, viz. atomic absorption spectroscopy (AAS), inductively coupled plasma mass spectrometry (ICP–MS) are employed for the determination of cadmium. However, these methods suffer disadvantages in terms of cost and unsuitability for routine analysis of large number of samples [14–16]. Ion-sensors are routinely used for such analysis, as these provide a convenient, fast and 'on-line' method for monitoring. A

number of Cd(II) ion-selective electrodes based on Ag_2S/CdS mixture [17, 18] have been reported but majority of them suffered serious interferences from various cations including Ag(I), Cu(II), Zn(II), Hg(II), and Fe(III). ISEs based on 3,6-dioxaoctanedithioamide offered a reasonable discrimination of all alkali and alkaline earth metal ions but are poisoned by Cu(II), Pd(II), Pt(II), Ag(I) and Hg(II) ions. A higher discrimination of Cd(II) ions was reported for an ISE based on benzo-15-crown-5 [19]. Jain and coworkers [20] reported inorganic ion-exchanger based on cerium(IV) vanadate in polystyrene matrix as Cd(II) ion-selective electrode. Gupta and coworkers exploited several crown molecules such as dibenzo-24-crown-8 [21], monoaza-18-crown-6 [22], dicyclohexano-18-crown-6 [23] and dicyclohexano-24-crown-8 [24], t-butyl thiacalix[4]arene and thiacalix[4]arene [25] in PVC matrix for construction of Cd(II)-selective electrodes. Khamjumphol et al. have worked on tripodal amine based ionophores [26] for cadmium determination. J. Sochor and coworkers reported bio-sensing of Cd(II) ions using commonly occurring potential pathogenic microorganism Staphylococcus aureus [27]. Recently, Karimi et al. have utilized multi-walled carbon nantotubes functionalized by dithizone as membrane material for ion sensing [28]. Among the various ligands available for ion-selective electrodes, the calixarenes met many of the requirements that an ionophore should satisfy for the use in ion-selective electrodes [29].

In the present studies p-tert-butyl calix[6]arene (Figure 4.1) was explored as a membrane material for the preparation of cadmium ion-selective electrode for selective determination of cadmium ions. This ionophore in molecular form exists in a cup-like shape having a well defined upper and lower rim resulting in the rigid confirmation which enables it to act as host molecule for Cd^{2+} ions because of the well performed cavities.
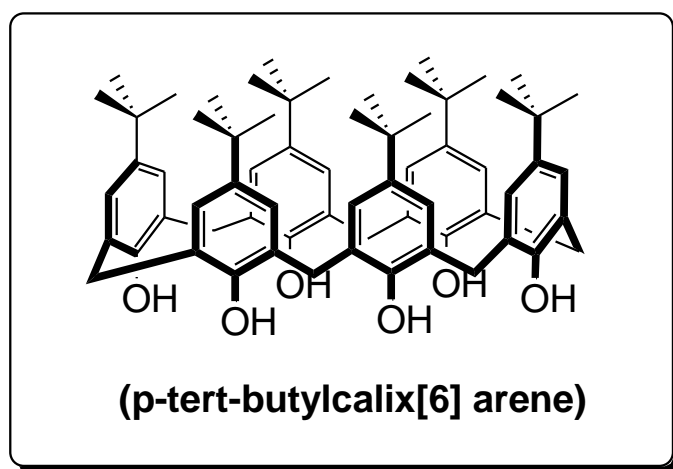

(p-tert-butylcalix[6] arene)

Figure 4.1. Structure of the studied compound (p-tert-butylcalix[6] arene).

4.2. Materials and methods

4.2.1. Reagents

All the reagents used were of analytical reagent grade and were used further without purification. P-tert-butyl calix[6]arene, and high molecular weight poly(vinyl chloride) (PVC) were procured from Aldrich, USA. Sodium tetraphenylborate (NaTPB) were procured from BDH, England; and dibutylphthalate (DBP) and dioctlyphthalate (DOP) were procured from Mobil, USA. 1-Chloronaphthalene (CN) and tetrahydrofuran (THF) were obtained from E. Merck, Germany and Ranbaxy (India), respectively. Metal nitrate solutions prepared were standardized according to appropriate methods. Solutions of different concentrations were made by diluting 0.1 M stock solutions.

4.2.2. Apparatus

Potentiometric measurements were carried out at 25 ± 0.1 °C on a Mettler Toledo pH/ion analyzer (model MA235). The membranes were equilibrated for 3–5 days in 1.0 M cadmium nitrate solution and potentials were measured by using PVC matrix membranes in conjunction with saturated calomel electrodes (SCE) by setting up the following cell assembly:

Internal reference electrode	Internal solution (0.1 M Cd^{2+})	PVC membrane	Test solution	External reference electrode

4.2.3. Membrane preparation

The membranes were prepared by adding THF (5–10 ml) to 1% of ionophore (p-tert-butyl calix[6]arene) and PVC (33%), anion excluder NaTPB (1%), solvent mediators (DBP, DOP, DBBP and CN) (65%) were further added to obtain membranes of different compositions (Table 4.1). The optimum composition of the membranes was obtained after a good deal of experimentation. After complete dissolution of all the components and thorough mixing, the homogeneous mixture obtained was concentrated by evaporation of THF. The oily viscous mixture obtained was poured into polyacrylate rings placed on a smooth glass plate. THF was allowed to evaporate at room temperature, after 24 hour, transparent membranes of about 0.5 mm thickness were obtained. A 5 mm diameter piece was cut out and glued to one end of a pyrex glass tube. The membranes prepared above were equilibrated with 1.0 M $Cd(NO_3)_2$ solution for 2 days. The membranes were further used for potential measurement studies.

4.3. Results and discussion

4.3.1. Potentiometric response

The plasticized PVC-based membrane electrode containing p-tert-butyl calix[6]arene as the neutral ion carrier, generated stable potential responses in solutions containing cadmium. Consequently, the performance of the membrane electrodes based on this carrier for Cd(II) ion in aqueous solution was studied. In the presence of the proposed carrier, the optimized membranes demonstrated Nernstian response and remarkable selectivity for Cd(II) ion over a wide variety of metal ions. The potentiometric response curves obtained for individual metal ions with ionophore under identical conditions are given in Figure 4.2. Among these ions, except for Cd(II) ion, for all other ions the slope of all the corresponding potential vs. log $[M^{n+}]$ plots is much different than the expected Nernstian slopes of 59.0, 29.5 mV per decade for the univalent and divalent cations respectively with very narrow linear range of concentration.
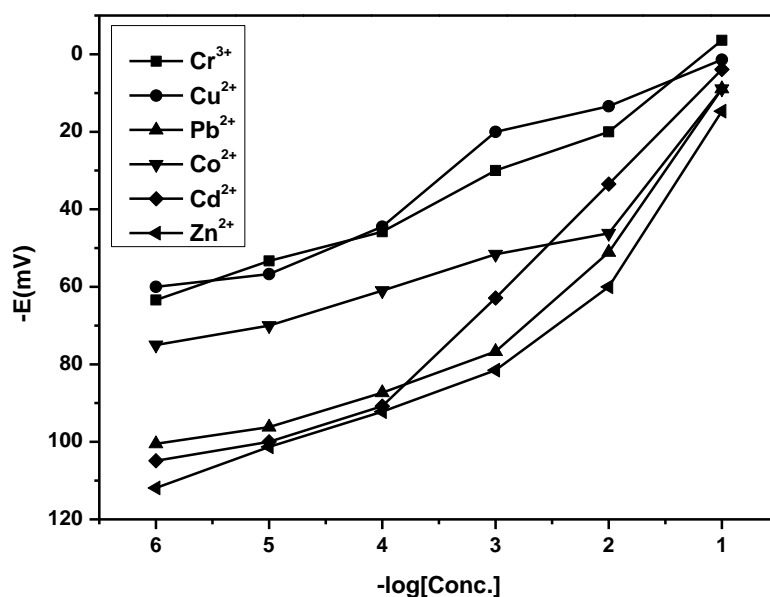
Figure 4.2. Potentiometric response curves of PVC-based electrodes containing I as ionophore towards various metal ions.

Membranes were prepared by dissolving the ionophore and PVC in THF. The ratio of ionophore and PVC was varied in order to obtain a composition which gives a membrane of best performance with regard to working concentration range, slope and response time. Further, the effect of anion discriminators (NaTPB) and plasticizers (solvent mediators), which are frequently used to improve the electrochemical properties of PVC membranes were also studied. For this purpose four solvent mediators viz. DOP, DBBP, CN and DBP were tried. Membranes having PVC-solvent, mediator-ionophore in different

compositions were prepared. The composition of the membranes showing the best results (wide working concentration, Nernstian/near-Nernstian slope, fast response time) are presented in Table 4.1.

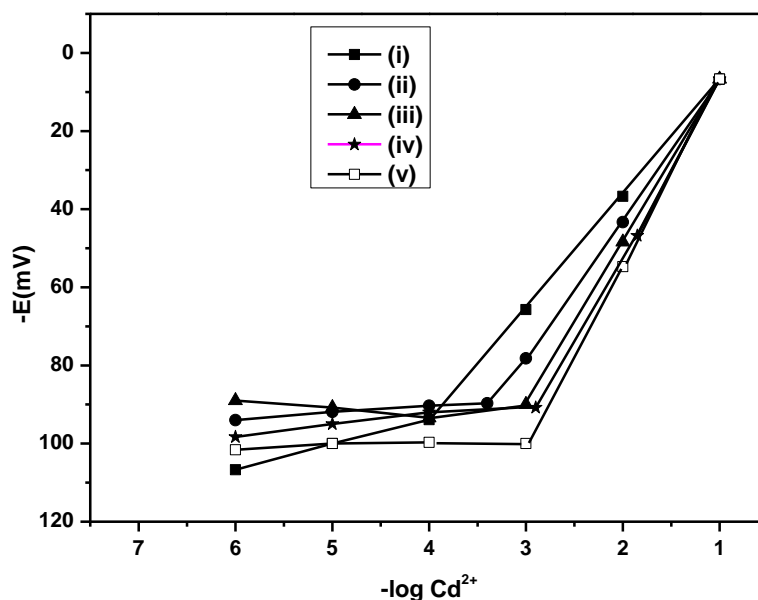### 4.3.2. Working concentration range and slope

Figure 4.3. Variation of cell potential with concentration of Cd^{2+} ions of PVC based membranes of (I) with different plasticizers (i): DOP (ii): DBP (iii): DBBP (iv): CN (v): without plasticizer.

The membranes were equilibrated with 1.0 M cadmium nitrate solution before carrying out potential studies. It was found that an equilibrium time of 2–3 days was optimum as the equilibrated membranes gave reproducible results and no drift in potentials were observed. The potentials of different membrane electrodes as a function of cadmium nitrate concentration are plotted in Figure 4.3. The working concentration range for different electrodes as evaluated from Figure 4.3 is given in Table 4.1. It is seen that electrode no. 1 having membrane without plasticizers exhibited a working concentration range of 7.8×10^{-4} to 1.0×10^{-1} mol dm^{-3} and non-Nernstian slope of 45 mV per decade of activity. However, upon addition of anion discriminator and plasticizers to the membranes (electrode nos. 2–5) the working concentration range changed. The membranes incorporating the solvent DBP (electrode no. 3), DBBP (electrode no. 4), CN (electrode no. 5) along with anion discriminator, NaTPB, exhibited linearity in the concentration ranges 3.7×10^{-4} to 1.0×10^{-1}, 1.0×10^{-3} to 1.0×0^{-1}, 1.0×10^{-3} to 1.0×10^{-1} mol dm^{-3} with slopes of 35, 40 and 43 mV per decade of activity; respectively. It can be inferred that the membrane no. 2 incorporating ionophore, PVC, NaTPB as anion discriminator and DOP as the solvent mediator in the ratio (w/w) 1:33:1:65 (I–PVC–NaTPB–DOP) gives the

best performance with regard to wide working concentration range of 9.7×10^{-5} to 1×10^{-1} mol dm^{-3} with a near-Nernstian slope of 29.0 ± 1 mV/decade of activity.

Table 4.1. Compositions and response characteristics of Cd^{2+} selective PVC based membrane containing p-tert-butylcalix[6]arene (I) as electroactive material.

Memb. no.	% Composition (w/w) of various components in membranes							Working concentration range	Slope (mV decade^{-1} activity)	Response time (s)
	I	PVC	NaT PB	DOP	DBP	DBBP	CN			
1	1	99	–	–	–	–	–	7.8×10^{-4}– 1.0×10^{-1}	45	80
2	1	33	1	65	–	–	–	9.7×10^{-5}– 1.0×10^{-1}	30	35
3	1	33	1	–	65	–	–	3.7×10^{-4}– 1.0×10^{-1}	35	40
4	1	33	1	–	–	65	–	1.0×10^{-3}– 1.0×10^{-1}	40	65
5	1	33	1	–	–	–	65	1.0×10^{-3}– 1.0×10^{-1}	43	57

4.3.3. Response and lifetime

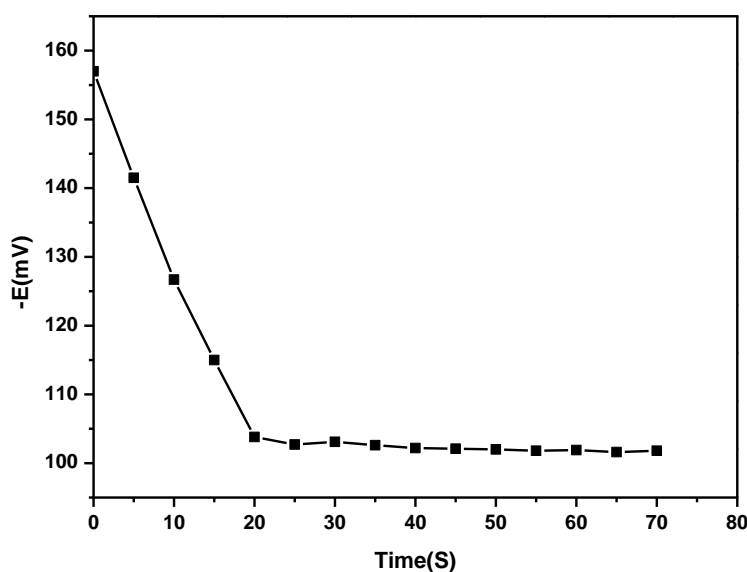**Figure 4.4.** Practical response time of the sensor from the time of addition of Cd^{2+} (1×10^{-5} M) solution.

The response is the time taken by the electrode to achieve a stable potential. Electrodes without solvent mediator gave a steady response in 75–90 s. However, the addition of solvent mediators improved the response time, as observed for membrane nos. 2–5. Though the response time of membranes with DBBP, CN, DBP were better (65, 57, 40 s respectively) over the whole concentration range, the fastest response (35 s) was shown by electrode no.2 (containing DOP as plasticizer) (Figure 4.4). The main factor for limited lifetime is the loss of ionophore from the membrane while contacting with aqueous solution. Sufficient lipophilicity of ionophores and plasticizer ensures stable potentials and long lifetimes [30, 31]. The membranes were studied over a period of 4 months without significant change in potentials. Whenever a drift in potential was observed, membranes were re-equilibrated with 1.0 M Cd^{2+} for 2–3 days. The membranes were stored in 0.1 M Cd^{2+} solution when not in use.

4.3.4. pH and non-aqueous effect

The dependence of electrode potential response on pH was tested over the range 2–8 for 1.0×10^{-3} M and 1.0×10^{-4} M Cd^{2+} ions (Figure 4.5). The operational range was studied by varying the pH of the test solutions with nitric acid or sodium hydroxide. Figure 4.5 shows that the potential is independent of pH in the range 2.8 to 6.2. The performance

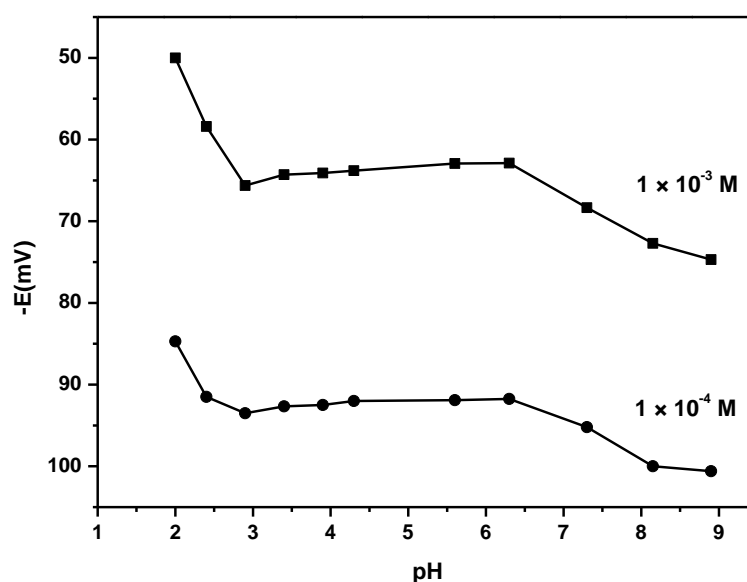**Figure 4.5.** Effect of pH on the potential response of the optimized Cd^{2+}-selective electrode.

of these sensor systems was also investigated in non-aqueous media by using water-methanol and water-ethanol mixtures. The membranes work satisfactorily up to maximum 20% (v/v) content of methanol and ethanol. In these mixtures, the working concentration range and slope remain unaltered; above a 20% non-aqueous content the slope was

appreciably decreased and the membranes were destroyed due to leaching of the ionophore from the PVC matrix.

4.3.5. Potentiometric selectivity

The most important characteristics of any ion selective electrode are its response to the primary ion in the presence of other ions in solution, which is usually expressed in terms of potentiometric selectivity coefficient. It illustrates the preference of the membrane for the interfering ion relative to a primary ion. In this work, the potentiometric selectivity coefficients were determined by 'fixed interference method' at 1.0×10^{-2} M concentration

Table 4.2. Selectivity coefficients of ions determined through 'fixed interference method'.

Interfering ion (B)	Selectivity coefficients $K_{A,B}^{Pot}$
Na^+	6.8×10^{-3}
K^+	6.5×10^{-3}
Ca^{2+}	7.9×10^{-2}
Sr^{2+}	6.3×10^{-2}
Ba^{2+}	8.5×10^{-2}
Ni^{2+}	1.1×10^{-1}
Zn^{2+}	3.3×10^{-1}
Cu^{2+}	2.4×10^{-3}
Pb^{2+}	3.5×10^{-3}
Co^{2+}	4.7×10^{-1}
Cr^{2+}	6.9×10^{-2}
Fe^{3+}	6.6×10^{-2}

of interfering ions (Table 4.2). This method was employed because the conditions prevailing at the membrane surface are the same while that analyzing the real samples. The selectivity coefficient values of the order of 0.001 are indicative that the sensor is selective for Cd^{2+} ions over a number of mono, bi and trivalent cations. Thus, the electrodes can be used for the determination of Cd^{2+} ions in the presence of these cations.

4.3.6. Analytical application

To assess the analytical applicability of the proposed sensor to real samples, the proposed sensor was used to measure Cd(II) in industrial waste water samples. The samples were collected and acidified with HNO_3 and used for further analysis. The potentials were measured by using the electrode cell assembly and calibration plots were

further employed to evaluate the concentration of Cd^{2+} in these samples (Table 4.3). Table 4.3 shows that the values of Cd^{2+} obtained by the proposed sensor are in good agreement with those obtained by standard AAS technique. Thus, the proposed sensor can be used for the determination of cd^{2+} in real samples.
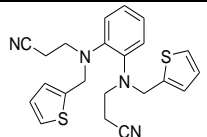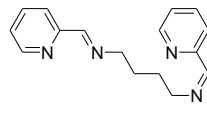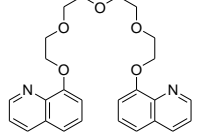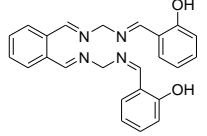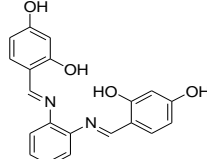
Table 4.3. Determination of cadmium in industrial waste water samples.

Sample	Cd^{2+} Conc. (M) proposed ISE	Cd^{2+} Conc. (M) AAS
1.	5.6×10^{-5}	5.9×10^{-5}
2.	5.8×10^{-5}	6.0×10^{-5}
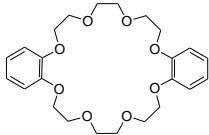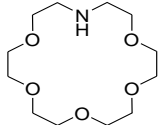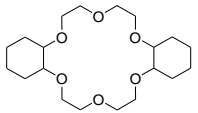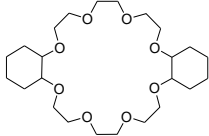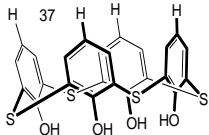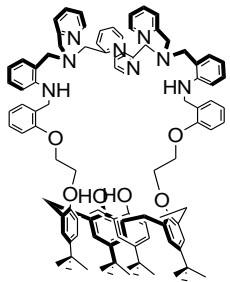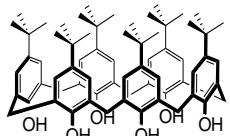
4.3.7. Comparative studies

The proposed sensor was compared with reported Cd(II)-ion selective electrodes depicted in Table. 4.4. The result shows that the proposed sensor is comparable to those reported in literature and even better in certain aspects.

Table 4.4. Comparison of the potentiometric parameters of the proposed Cd(II)-ISE with Cd(II)-ISEs reported previously.

Ref.	Ionophore	Linear range (M)	Lifetime of electrode	Response time (s)	Slope (mV/ decade)	pH range
4		1.7×10^{-8}– 1.0×10^{-1}	4–6 week	7	29.6±0.08	2.6–8.0
9		7.9×10^{-8}– 1.0×10^{-1}	2 month	10	30.0±0.2	2.0–8.0
13		1.0×10^{-5}– 1.0×10^{-1}	7 week	15	29.8±0.1	1.0–6.0
11		5.0×10^{-9}– 1.0×10^{-1}	2.5 month	11	30.0±0.2	2.0–8.5
12		1.0×10^{-6}– 1.0×10^{-1}	8 week	20	30.1±1.0	2.8–8.1

No.	Structure	Conc. range	Lifetime	Response time	Slope	pH range
21		3.9×10^{-5} – 1.0×10^{-1}	5 month	25	30.0 ± 1.0	3.2–7.5
22		1.0×10^{-5} – 1.0×10^{-1}	3 month	<10	29.0 ± 0.1	5.0–7.7
23		2.1×10^{-5} – 1.0×10^{-1}	6 month	17	29.0 ± 1.0	1.9–7.0
24		3.0×10^{-5} – 1.0×10^{-1}	5 month	23	30.0 ± 1.0	2.0–5.4
25		3.2×10^{-6} – 1.0×10^{-1}	3 month	8	29.5	4.5–6.5
26		1.6×10^{-6} – 1.0×10^{-2}	1 week	10	29.4 ± 0.6	6.0–9.0
28	MWCNT functionalized dithizone	1.8×10^{-7} – 1.0×10^{-4}	12 week	37	29.4 ± 1.3	3.0–7.0
This work		9.7×10^{-5} – 1.0×10^{-1}	> 4 month	35	29.0 ± 1	2.8–6.2

4.4. Conclusion

The molecular interaction between p-tert-butyl calix[6]arene and Cd(II) resulted in a sensor which exhibits fast (~35 s), stable, reproducible and selective response over prolong period. The sensor works well over a wide concentration range of 9.7×10^{-5} to 1.0×10^{-1} mol dm^{-3} with near Nernstian slope of 29.0 ± 1 mV/decade of activity. The working pH range of this sensor is 2.8 to 6.2. It can be used for more than 4 months without any

considerable change in response characteristics. It has excellent selectivity for Cd(II) over alkali, alkaline and other heavy metal cations.

References

1. K. Duarte, C.I.L. Justino, A.C. Freitas, A.M.P. Gomes, A.C. Duarte, T.A.P.Rocha-Santos, Disposable sensors for environmental monitoring of lead, cadmium and mercury, *TrAC–Trends Anal. Chem.* **64** (2015) 183–190.

2. M. Javanbakht, A. Shabani-Kia, M.R. Darvich, M.R. Ganjali, M. Shamsipur, Cadmium(II)-selective membrane electrode based on a synthesized tetrol compound, *Anal. Chim. Acta* **408** (2000) 75–81.

3. K. Rurack, U. Resch-Genger, W. Rettig, Global analysis of time-resolved emission – A powerful tool for the analytical discrimination of chemically similar Zn^{II} and Cd^{II} Complexes, *J. Photochem. Photobiol. A* **118** (1998) 143–149.

4. J. Singh, A.K. Singh, A.K. Jain, Fabrication of novel coated graphite electrodes for the selective nano-level determination of Cd^{2+} ions in biological and environmental samples, *Electrochim. Acta* **56** (2011) 9095–9104.

5. C. Dernane, A. Zazoua, I. Kazane, N. Jaffrezic-Renault, Cadmium-sensitive electrode based on tetracetone derivatives of p-tert-butylcalix[8]arene, *Mater. Sci. Eng. C* **33** (2013) 3638–3643.

6. S. Yu, F. Li, W. Qin, An All-solid-state Cd^{2+}-selective electrode with a low detection limit, *Sens. Actuators B* **155** (2011) 919–922.

7. R.A. Goyer, J. Liu, M.P. Waalkes, Cadmium and cancer of prostate and testis, *Biometals* **17** (2004) 555–558.

8. L. Wu, X. Fu, H. Liu, J. Li, Y. Song, Comparative study of graphene nanosheet- and multiwall carbon nanotube-based electrochemical sensor for the sensitive detection of cadmium, *Anal. Chim. Acta* **851** (2014) 43–48.

9. V.K. Gupta, A.K. Singh, B. Gupta, Schiff bases as cadmium(II) selective ionophores in polymeric membrane electrodes, *Anal. Chim. Acta* **583** (2007) 340–348.

10. G. Bertin, D. Averbeck, Cadmium: cellular effects, modifications of biomolecules, modulation of DNA repair and genotoxic consequences (a review), *Biochimie* **88** (2006) 1549–1559.

11. V.K. Gupta, M.A. Khayat, A.K. Singh, M.K. Pal, Nano level detection of Cd(II) using poly(vinyl chloride) based membranes of Schiff bases, *Anal. Chim. Acta* **634** (2009) 36–43.

12. A.A. Ensafi, S. Meghdadi, S. Sedighi, Sensitive cadmium potentiometric sensor based on 4-hydroxy salophen as a fast tool for water samples analysis, *Desalination* **242** (2009) 336–345.

13. A. Ghaemi, H. Tavakkoli, T. Mombeni, Fabrication of a highly selective cadmium(II) sensor based on 1,13-bis(8-quinolyl)-1,4,7,10,13-pentaoxatridecane as a supramolecular ionophore, *Mater. Sci. Eng. C* **38** (2014) 186–191.

14. D. Karunasagar, J. Arunachalam, Determination of cadmium by inductively coupled plasma mass spectrometry-reduction of molybdenum oxide interferences by addition of acetonitrile, *Anal. Chim. Acta* **441** (2001) 291–296.

15. G.G. Bortoleto, G.T. Macarovscha, S. Cadore, Determination of cadmium by flame-atomic absorption spectrometry after preconcentration on silica gel modified with cupferron, *J. Braz. Chem. Soc.* **15** (2004) 313–317.

16. W. Guo, S. Hu, Y. Xiao, H. Zhang, X. Xie, Direct determination of trace cadmium in environmental samples by dynamic reaction cell inductively coupled plasma mass spectrometry, *Chemosphere* **81** (2010) 1463–1468.

17. I.M.P.L.V.O. Ferreira, J.L.F.C. Lima, Tubular potentiometric detector for flow injection based on homogenous crystalline membranes sensitive to copper, cadmium and lead, *Analyst* **119** (1994) 209–212.

18. S. Ito, Y. Asano, H. Wada, Development of highly sensitive cadmium ion-selective electrodes by titration method and its application to cadmium ion determination in industrial waste water, *Talanta* **44** (1997) 697–704.

19. S.K. Srivastava, V.K. Gupta, S. Jain, A PVC-based benzo-15-crown-5 membrane sensors for cadmium, *Electroanal.* **8** (1996) 938–940.

20. A.K. Jain, L.P. Singh, A new polystyrene based heterogeneous membrane of cerium(IV) vanadate as cadmium(II) ion-selective electrode, *Indian J. Chem. A* **33** (1994) 1122–1123.

21. V.K. Gupta, P. Kumar, Cadmium(II)-selective sensors based on dibenzo-24-crown-8 in PVC matrix, *Anal. Chim. Acta* **389** (1999) 205–212.

22. V.K. Gupta, P. Kumar, R. Mangla, PVC based monoaza-18-crown-6 membrane potentiometric sensors for cadmium, *Electroanal.* **12** (2000) 752–756.

23. V.K. Gupta, S. Chandra, R. Mangla, Dicyclohexano-18-crown-6 as active material in PVC matrix membrane for the fabrication of cadmium selective potentiometric sensor, *Electrochim. Acta* **47** (2002) 1579–1586.

24. V.K. Gupta, A.K. Jain, P. Kumar, PVC-based membranes of dicyclohexano-24-crown-8 as Cd(II) selective sensor, *Electrochim. Acta* **52** (2006) 736–741.

25. V.K. Gupta, A.K. Jain, R. Ludwig, G. Maheshwari, Electroanalytical studies on cadmium(II) selective potentiometric sensors based on t-butyl thiacalix[4]arene and thiacalix[4]arene in poly(vinyl chloride), *Electrochim. Acta* **53** (2008) 2362–2368.

26. U. Khamjumphol, S. Watchasit, C. Suksai, W. Janrungroatsakul, S. Boonchiangma, T. Tuntulani, W. Ngeontae, New polymeric membrane cadmium(II)-selective electrodes using tripodal amine based ionophores, *Anal. Chim. Acta* **704** (2011) 73–86.

27. J. Sochor, O. Zitka, D. Hynek, E. Jilkova, L. Krejcova, L. Trnkova, V. Adam, J. Hubalek, J. Kynicky, R. Vrba, R. Kizek, Bio-sensing of Cadmium(II) ions using Staphylococcus aureus, *Sensors* **11** (2011) 10638–10663.

28. M. Karimi, F. Aboufazeli, H.R.L.Z. Zhad, O. Sadeghi, E. Najafi, Determination of cadmium(II) ions in environmental samples: A potentiometric sensor, *Curr. World Environ.* **7** (2012) 201–206.

29. D. Diamond, Calixarene-based sensing agents, *J. Incl. Phenom. Mol. Recognit. Chem.* **19** (1994) 149–166.

30. W. Zhang, L. Jenny, U.E. Spichiger, A comparison of neutral Mg^{2+}-selective ionophores in solvent polymeric membranes: Complex stoichiometry and lipophilicity, *Anal. Sci.* **16** (2000) 11–18.

31. O. Dinten, U.E. Spichiger, N. Chaniotakis, P. Gehrig, B. Rusterholz, W.E. Morf, W. Simon, Lifetime of neutral-carrier-based liquid membranes in aqueous samples and blood and the lipophilicity of membrane components, *Anal. Chem.* **63** (1991) 596–603.

CHAPTER 5
Determination of Aluminium by Fluorescent Sensors

5.1. Introduction

The quest of developing sensor of high selectivity and sensitivity for various metal ions is greatly increasing as a demand of analytical research in different areas of science [1, 2]. Presently in the modern analytical era, fluorescent sensors have widely shown their presence because of their numerous applications in therapeutic and ecological field. Generally, the florescent sensors have a combination of substrate-recognition functionality i.e. receptor and optical signalling capacities (chromophore), and its operational mechanism may follow two well distinct pathways. (1) It may get linked directly to the specific metal or (2) it may be appropriately associated with the metal in a non-covalent method [3]. Several fluorescent receptors which are highly specific and selective for Hg^{2+}, Cu^{2+}, Zn^{2+}, Fe^{3+} and other transition metal ions, have been reported [4–12]. However, still there is requirement of introducing good fluorescent receptors in the literature for the detection of Al^{3+} metal ions.

Aluminium is found in the earth crust widely in the form of polymorphous aluminosilicates (Al_2O_5Si) which upon acidification release the element into the environment and increases its bioavailability [13–15]. Being one of the most plentiful elements, aluminium metal is available cheaply and finds extensive use in home construction, food packing, cookware, deodorants, bleached flour, transport, house hold appliances, water treatment, phosphate binders, food additives, machinery and medicines such as buffered aspirins, antacids, vaccine, antiperspirant and allergen injection etc. [16–20]. According to a World Health Organization report, the average daily human intake of aluminium is approx. 3–10 mg per day. The tolerable weekly aluminium intake by the human being is estimated to be 7 mg per kg body weight [21, 22]. It is a good conductor of electricity and therefore used for the manufacture of electric wires, various electrical and electronic appliances. Biologically, it is not an essential element for human life and therefore high intake of aluminium can be toxic for human health. The excessive use of aluminium has resulted in its slow consumption by human beings where it causes many deadly effects; such as neurotoxicity, anaemia, dementia, Parkinson's and Alzheimer's diseases and cancer [23–29]. Also the ingestion of excessive amount of aluminium leads to its accumulation in target organs presenting damage of testicular tissue of both humans and animals. It has also been found that excess of aluminium in human spermatozoa and seminal plasma is directly correlated with decreased sperm motility and viability. In addition to it, long-term consumption of aluminium chloride in drinking water causes suppressive effects on both sexual and aggressive behavoir and fertility of male rats [30].

The results showed that aluminium significantly increased nitric oxide (NO) production and decreased both testicular adenosine 3',5'–cyclic monophosphate (cAMP) and testosterone levels. It also affects iron metabolism which may cause pernicious anaemic condition. In view of widespread applications of aluminium in domestic life, biological and environmental importance, toxicity of aluminium is highly considerable and therefore its determination in environment is desirable. Owing to the coordination and strong hydration ability of aluminium metal ions in water [31], it is easily interfered by the variation of pH value of solution and the coexistence of interfering ions.

There are several sophisticated analytical techniques viz. atomic absorption spectroscopy (AAS), inductively coupled plasma emission spectrometry (ICP–AES) and spectrophotometric sensors [32–37] for low concentration determination of metal ions. Among all of these techniques, determination of aluminium by spectrophotometric sensors has been found to be expedient, fast and can be used for the analysis of large number of samples in a very short period of time.

The problem is, that inspite of many merits of sensors, its use is limited due to poor selectivity and sensitivity. Thus a more selective and sensitive sensor is required to be developed. Our studies revealed that an azo compound and Schiff bases synthesized by us interacts strongly and selectively with aluminium metal ions. Therefore, these receptors have been used for preparing colorimetric and fluorometric sensors for aluminium metal ions. This chapter is divided in three parts (A), (B) and (C) and the results of these investigations are reported in present communication.

5.2. PART (A) Aluminium fluorescent sensor based on an azo compound (1-(2-pyridylazo)-2-naphthol)

5.2.1. Experimental

5.2.1.1. Reagents, materials and apparatus

2-aminopyridine, β-naphthol and sodium hydroxide of analytical grade were procured for synthesis of 1-(2-pyridylazo)-2-naphthol (PAN) (**R1**) from Merck (India) and further used without any purification. Sodium nitrite was procured from Samir tech-chem industry (India). Chloride and nitrate metal salts were purchased from SD-Fine chem. Limited.

The IR spectra of chemosensor were recorded on a Perkin Elmer FT–IR spectrometer in the range 4000–400 cm^{-1}. The CHNS data were collected on a Vario MICRO Cube and, ^{1}H–NMR and ^{13}C–NMR spectra of chemosensor were recorded on a Bruker 500 MHz (USA), using TMS as an internal standard, CD$_3$OD and CDCl$_3$ as

solvent. Mass spectra were recorded on Bruker-MicrOTOF II (USA). The differential pulse voltammetric experiments were performed using a CHI760E Electrochemical Workstation (USA) with a conventional three electrode cell assembly consisting of glassy carbon electrode, platinum wire and calomel electrode as working electrode, counter electrode and reference electrode, respectively. The UV–vis absorption spectra were recorded on a Shimadzu UV–2450 spectrophotometer and the fluorescent spectra on a Shimadzu RF–5301PC spectrofluorophotometer with slit width value of at 5.0 and 3.0 nm. The pH measurements were performed using a Eutech CyberScan pH 510 (Singapore). All the metal solutions for the study were prepared in methanol solution. Stock solution of **R1** and different metal chlorides and nitrates (10 mM) were prepared in methanol.

5.2.1.2. Synthesis of ligand (R1)

The ligand, (**R1**) (Scheme 5.1) was synthesized in aqueous media by the reported method with a slight modification [38]. 5.0 mmol of 2-aminopyridine was dissolved in 100 ml of water with concentrated HCl (5.0 ml). The resulting solution was cooled to 0–5 ºC with ice and an aqueous cold solution of sodium nitrite (24.0 mmol) was added under stirring. After about 2 min, a cold solution of β-naphthol (2.0 mmol) in aqueous sodium hydroxide (8.0 ml; 0.2 M) was added. The formation of a colored azo compound was observed. This mixture was stirred for about 10 min and then filtered and air-dried. Color: brick red; yield: 0.350 g (70%); state: solid; m.p.: 139–141 ºC.
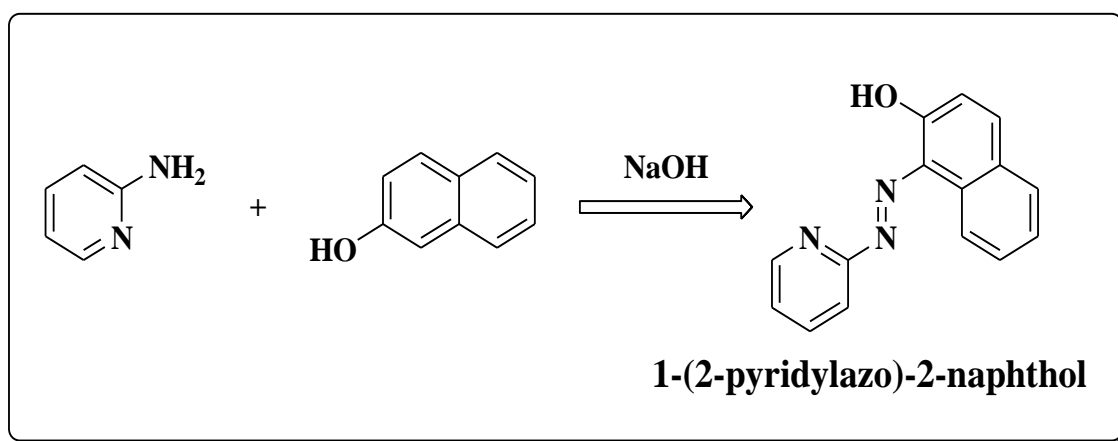
Scheme 5.1. Synthesis of receptor (**R1**) in methanol.

5.2.2. Results and discussion

The binding ability and mode of ligands with aluminium metal ions was investigated by FT–IR, HRMS, ^{1}H–NMR, UV–vis absorption and fluorescence emission spectroscopic experiments.

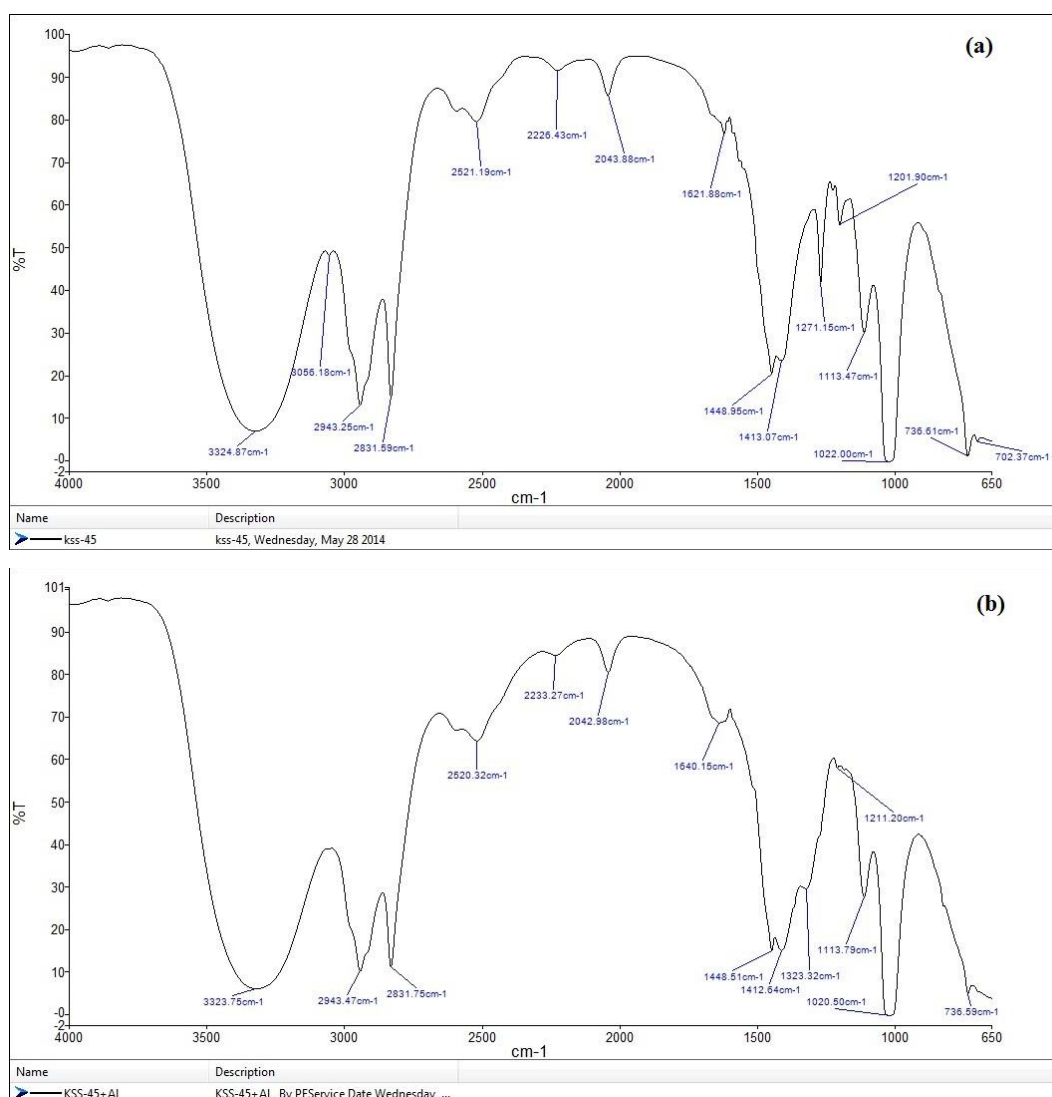### 5.2.2.1.Characterization of R1 and its complex with aluminium

Figure 5.1. FT–IR spectra of **R1** (a) and (b) **R1**–Al complex (in methanolic solution).

The FT–IR Spectrum of **R1** (Figure 5.1a) shows prominent peaks (v, cm^{-1}) at: 3324 (methanolic −O−H), 2943, 2831 (aliphatic −C−H), 1621 (−C=N), 1448, 1413 (aromatic −C=C−), 1271, 1201 (phenolic −O−H), 1113, 1022 (aliphatic −C−O), 736 (ortho substituted phenol). A comparison of FT–IR spectra (Figure 5.1a) of the ligand and spectra of the aluminium complex (Figure 5.1b) shows that the ligand peaks at 1621 cm^{-1} due to −C=N group are shifted at 1640 cm^{-1}; and 1271 and 1201 cm^{-1} due to −O−H group are merged into one and appears at 1323 cm^{-1} indicating −C=N and −O−H are coordinating sites. Thus FT–IR spectra support that Al forms, complex with **R1** with nitrogen and oxygen, acting as donor sites. The elemental analysis of the **R1**, was done and results are; Anal. calcd. % for $C_{15}H_{11}N_3O$: C=72.20, H=4.41, N=16.85, found %: C=71.52, H=4.4, N=16.71. The prominent ^{1}H–NMR peaks were found at; ((CD$_3$OD, 500 MHz), (δ, ppm) (J,

Hz)): 6.592–6.611 (d, J = 9.5, 1H), 7.200–7.226 (m, 1H), 7.405–7.422 (dt, J = 1.0, 7.5, 1H), 7.511–7.553 (m, 2H), 7.745–7.765 (d, J = 10.0, 1H), 7.911–7.935 (m, 2H), 8.341–8.374 (m, 2H); ^{13}C–NMR ((CDCl$_3$, 500 MHz), (δ, ppm)): 110.11, 120.30, 122.32, 127.07, 127.19, 128.50, 128.93, 129.42, 130.65, 133.54, 138.33, 142.82, 148.65, 155.57, 181.19 also support the structure of **R1** as shown in Scheme 5.1.
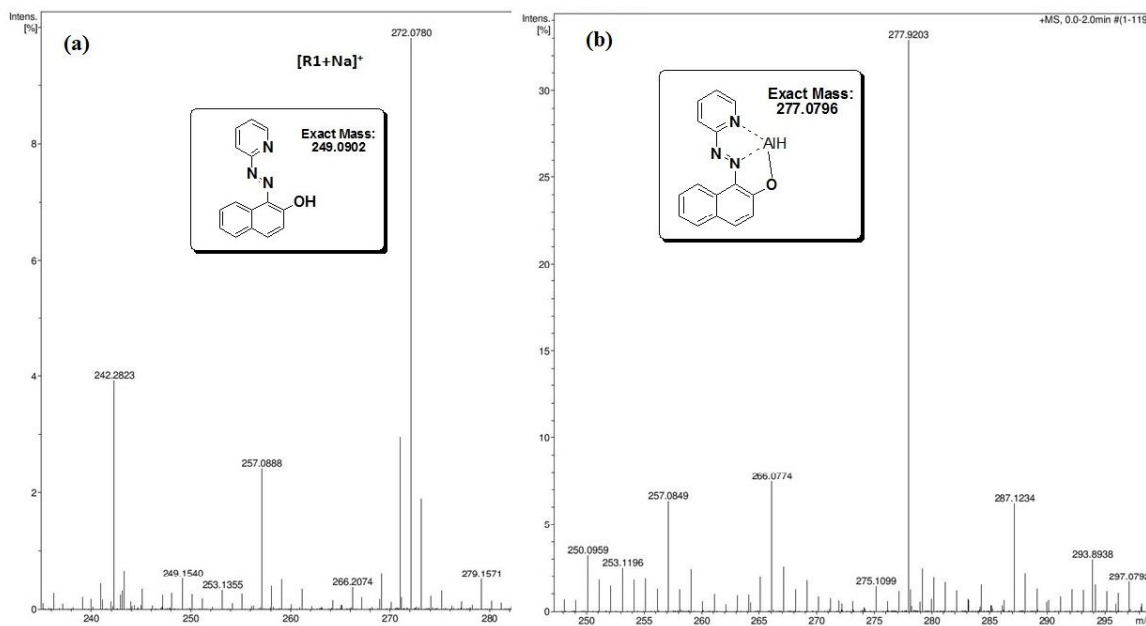

Figure 5.2. ESI–MS spectra of (a) ligand **R1** and (b) Al-complex with **R1**.

Further, HRMS spectra (Figure 5.2(a)) showing a prominent peak at 272.0780 due to [**R1**+Na]$^+$ also supports the alleged structure of **R1** as given in Scheme 5.1. The spectra of aluminium complex with **R1** also give a prominent peak at 277.9203 due to [**R1**+Al+H]$^+$ as shown in Figure 5.2(b). Hence the HRMS spectra indicate the stoichiometry of ligand and Al–complex is 1:1.

5.2.2.2. UV–vis absorption spectral studies

The UV–vis absorption spectrum of the metal and ligand mixture was recorded in methanolic solution (50 μM) is shown in Figure 5.3 which reveals absorption band at 464 nm. Different metal ions formed color complexes with the ligand that are exhibited in Figure 5.4, aluminium ions formed a dark red color complex whereas the other metal complexes were of different colors. It is clear that most of the metal ions (Mn^{2+}, Fe^{2+}, Fe^{3+}, Co^{2+}, Zn^{2+}, Cd^{2+}, Cu^{2+}, Ni^{2+}, Gd^{3+}, Nd^{3+}, Pb^{2+} and Al^{3+}) form complexes with **R1** in the absorption band region of 490–650 nm. Whereas other metal ions like Li$^+$, Na$^+$, K$^+$, Cs$^+$, Mg^{2+}, Ca^{2+}, Ba^{2+}, Cr^{3+}, Hg^{2+} and Sr^{2+} do not react significantly with the ligand.
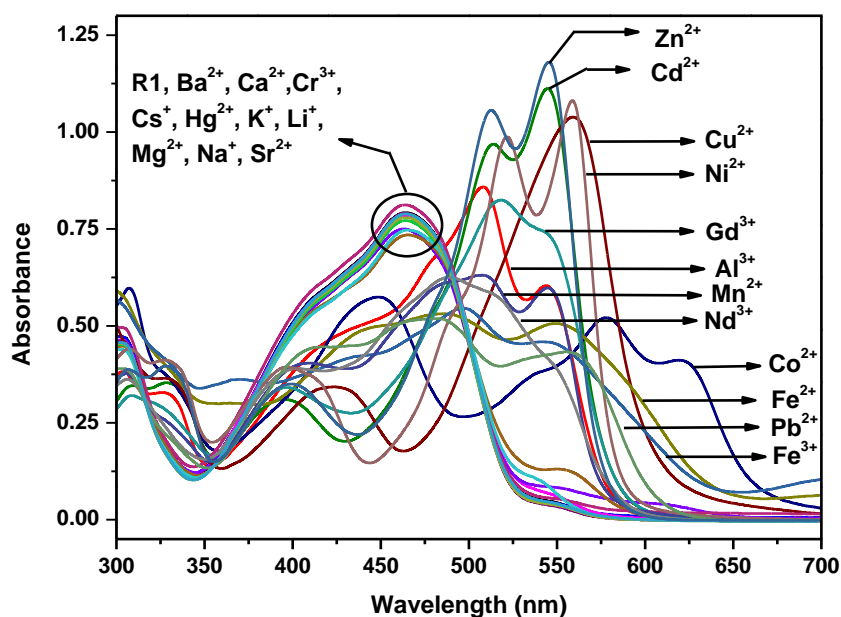
Figure 5.3. Absorption spectra of (50 μM) methanolic solution of ligand in the presence of different metals (Ba^{2+}, Ca^{2+}, Co^{2+}, Cd^{2+}, Cr^{3+}, Cs^{+}, Cu^{2+}, Fe^{2+}, Fe^{3+}, Hg^{2+}, K^{+}, Li^{+}, Na^{+}, Mg^{2+}, Mn^{2+}, Nd^{3+}, Pb^{2+}, Sr^{2+}, Gd^{3+}, Zn^{2+}, Ni^{2+} and Al^{3+}) (50 μM) in methanolic solution.
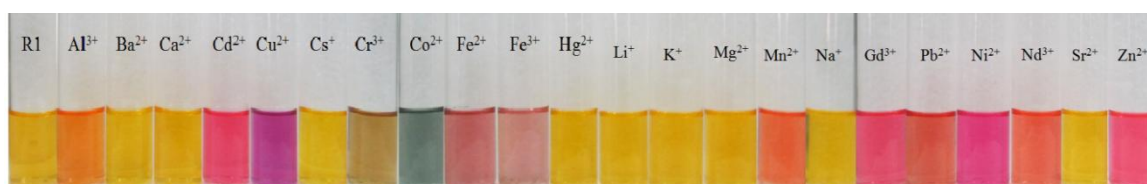

Figure 5.4. Color changes of (50 μM) concentration of ligand with different metal ions (50 μM) in methanol in 1:1 (v/v, mL) ratio.

5.2.2.3. Fluorescence emission studies

The reported ligand (10 μM) shows a weak fluorescence emission band at 521 nm with an excitation of 490 nm. However, upon addition of aluminium, significant fluorescence enhancement accompanied by a red shift of 48 nm from 521 to 569 nm was noticed (Figure 5.5). Whereas when other metal ions (10 μM) such as Li^{+}, Na^{+}, K^{+}, Cs^{+}, Mg^{2+}, Ca^{2+}, Ba^{2+}, Cr^{3+}, Co^{2+}, Mn^{2+}, Fe^{2+}, Fe^{3+}, Ni^{2+}, Cd^{2+}, Zn^{2+}, Cu^{2+}, Hg^{2+}, Nd^{3+}, Pb^{2+}, Sr^{2+}, and Gd^{3+} were added to the ligand, there were no significant changes observed in fluorescence emission spectra of metal ligand complex. The enhancement in fluorescence emission intensity is observed that exhibits "on–off" mode of high sensitivity towards Al^{3+} ions. Additionally, the receptor on UV light treatment shows remarkable changes from colorless to pinkish red fluorescence in the presence of aluminium within 5 s, which can be easily detected by the naked eye. Thus, this ligand can be used to detect aluminium visually.
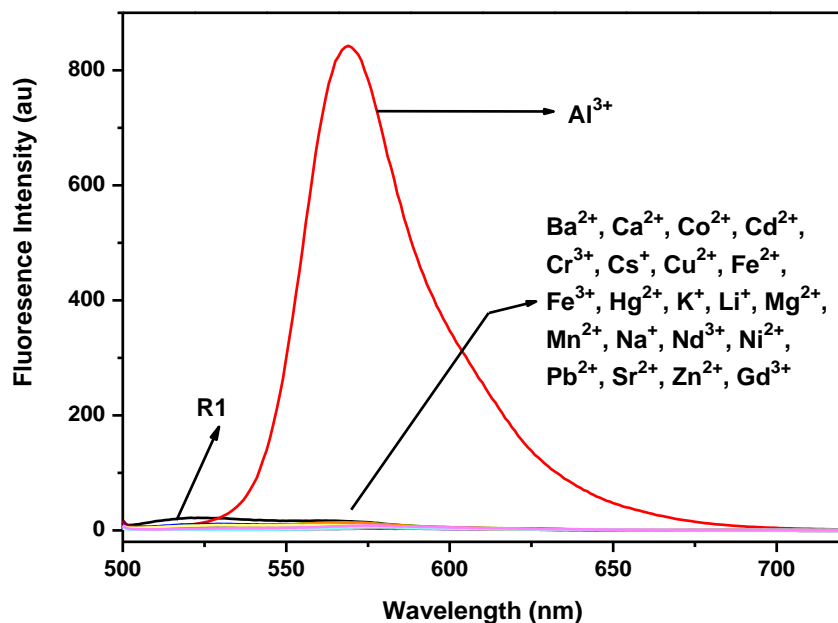
Figure 5.5. Fluorescence emission spectra of ligand (10 µM) in the presence of different metal ions (Ba^{2+}, Ca^{2+}, Co^{2+}, Cd^{2+}, Cr^{3+}, Cs^+, Cu^{2+}, Fe^{2+}, Fe^{3+}, Hg^{2+}, K^+, Li^+, Na^+, Mg^{2+}, Mn^{2+}, Nd^{3+}, Pb^{2+}, Sr^{2+}, Gd^{3+}, Zn^{2+}, Ni^{2+} and Al^{3+}) (10 µM) in methanol solvent using slit width 5.0 nm.

In addition, the fluorescence response of the ligand for various concentrations of Al^{3+} ions (0–50 µM) was also investigated. Upon addition of Al^{3+} ions, the fluorescence intensity centred at 569 nm of receptor gradually increased and remained approximately
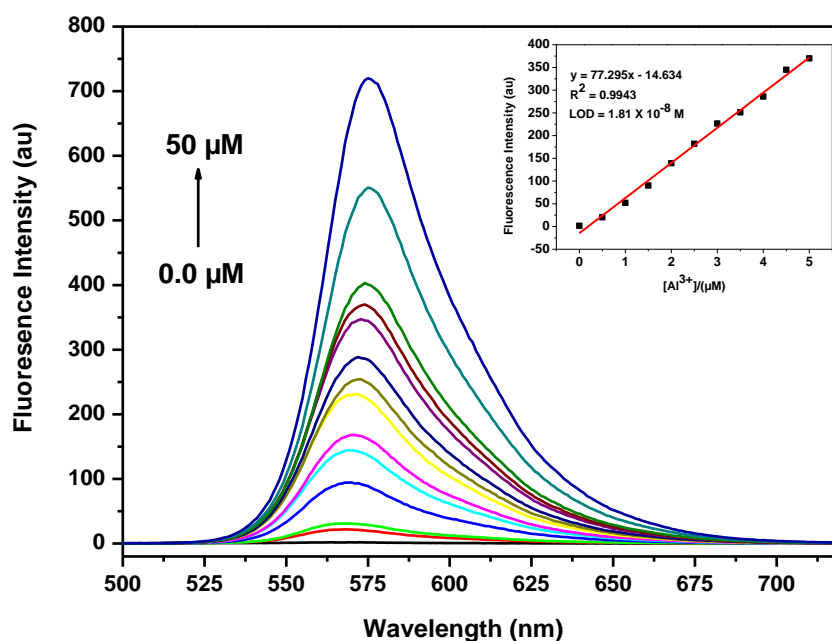

Figure 5.6. Fluorescence titration curve of the ligand (10 µM), on addition of increasing aluminium ion concentration (0.0, 0.5, 1.0, 1.5, 2.0, 2.5, 3.0, 3.5, 4.0, 4.5, 5.0, 10, 25 and 50 µM) with an excitation of 490 nm. Inset shows the linear relation for fluorescence change at 569 nm as a function of the amount added of Al^{3+} ions (0–5.0 µM) at a slit width of 3.0 nm.

steady when 1.0 equivalent of Al^{3+} ions was added, indicating the formation of a 1:1 bonding mode between ligand and Al^{3+} ions (Figure 5.6). In order to prove the selectivity of **R1** probe towards the Al^{3+} ions, the calculation of detection limit was performed by the help of standard deviation based on S/N = 3 and linear fittings (Inset in the Figure 5.6) by plotting the fluorescence intensity changes as a function of Al^{3+} concentration and detection limit was found to be 1.81×10^{-8} M.

Further, the binding constant of chemosensor **R1** with Al^{3+} has been calculated with the help of the Benesi–Hildebrand equation via the fluorescence titration [39, 40]. The principle and theory of the method have been described earlier in the section 2.1.3.5 in chapter 2. From curve fitting the fluorescence emission intensity of receptor **R1** against the reciprocal of the Al^{3+} concentration yielded a linear fit depicted in Figure 5.7. The value of the stability constant was calculated to be 1.025×10^4 M^{-1} ($R^2 = 0.9801$). The linear fit also exhibited the 1:1 complexation behavoir of receptor to metal ions.
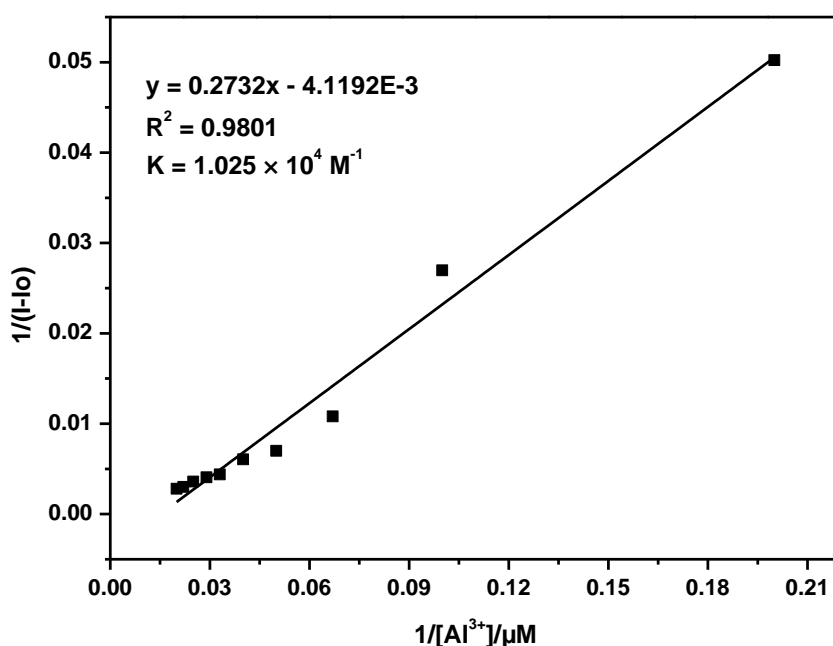

Figure 5.7. Benesi−Hildebrand plot recorded the fluorescence changes at 569 nm using slit width 3.0 nm.

5.2.2.3.1. Proposed binding mode

In this study the metal-to-ligand ratio of the chemosensor **R1**–Al^{3+} complex, Job's plot method was employed for the fluorescence emission spectra of chemosensor and Al^{3+} metal ions. A plot of fluorescence emission intensity versus molar fraction of [**R1**]/([**R1**]+[Al^{3+}]) depicted in Figure 5.8 and the results designated the formation of a 1:1 stoichiometric complexation between **R1**–Al^{3+}.
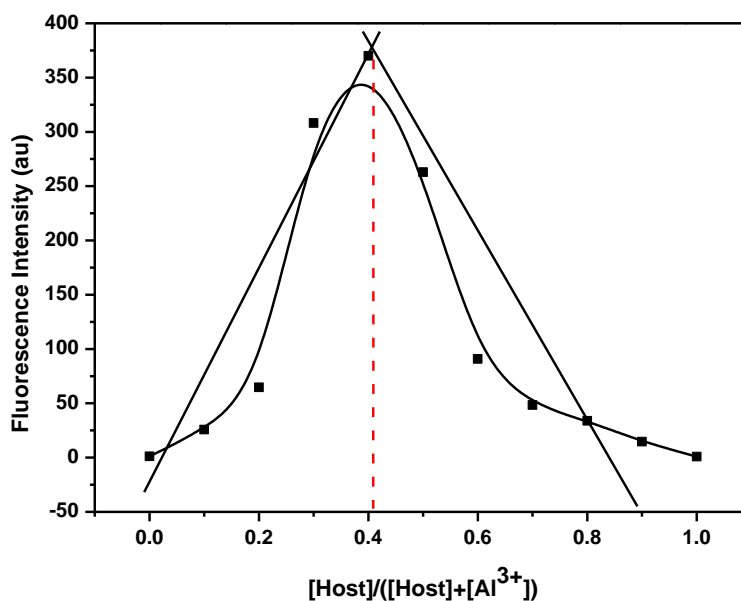
Figure 5.8. Job's plot for receptor by fluorescence method ($\lambda_{em} = 569$ nm) using slit width at 3.0 nm; and total concentration of receptor and metal is 10 µM.

In addition to this, the Figure 5.9 shows the changes in fluorescence intensity of the receptor before and after the addition of Al^{3+} ions in the presence of other sensed metal ions under UV lamp. It has exhibited that the other metal ions (Cd^{2+}, Co^{2+}, Cu^{2+}, Fe^{2+}, Ni^{2+} and Zn^{2+}) quenches the fluorescence intensity of the receptor–Al^{3+} complex, due to the similar binding ability towards these metal ions.
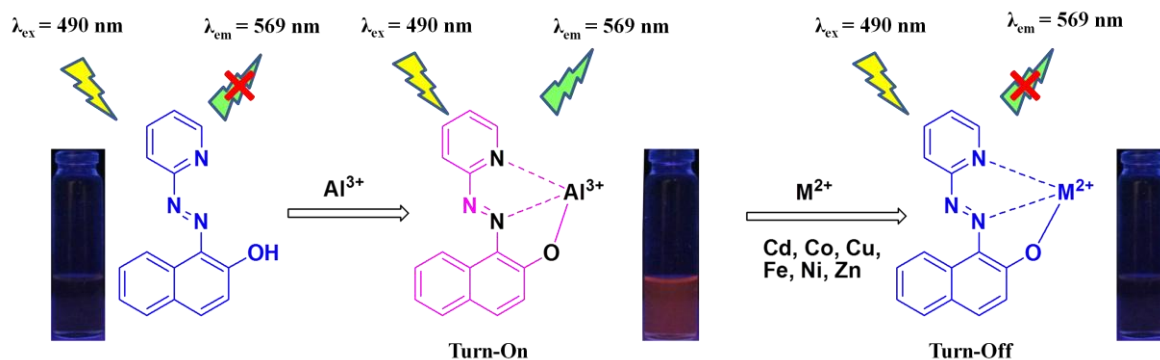

Figure 5.9. The fluorescence emission changes of sensor (10 µM) with 1.0 equivalent of Al^{3+}, and in the presence of other metal ions (Cd^{2+}, Co^{2+}, Cu^{2+}, Fe^{2+}, Ni^{2+}, Zn^{2+}) excited by a commercially available UV lamp ($\lambda_{ex} = 490$ nm).

The selectivity of the ligand (10 µM) for Al^{3+} ions over other metal ions was also investigated (Figure 5.10). It was seen that the fluorescence emission intensity of aluminium ligand mixture remained unaffected by Ba^{2+}, Ca^{2+}, Cr^{3+}, Cs^{+}, Fe^{3+}, Gd^{3+}, Hg^{2+}, K^{+}, Li^{+}, Na^{+}, Mg^{2+}, Mn^{2+}, Nd^{3+}, Pb^{2+} and Sr^{2+}. Therefore, aluminium has selectivity over these metals and the synthesized receptor can be used for its estimation in the presence of

these metals. On the other hand metal ions such as Co^{2+}, Cd^{2+}, Cu^{2+}, Fe^{2+}, Zn^{2+} and Ni^{2+} were found to decline emission intensity of **R1**–Al^{3+} complex and therefore expected to cause interference. This interference effect could be reduced by addition of higher concentration of Al^{3+} ions.
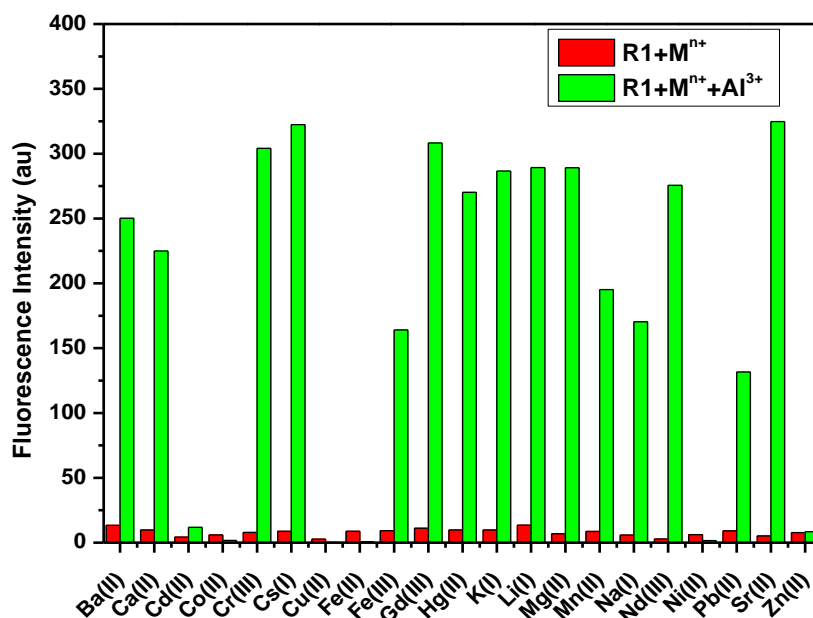

Figure 5.10. Selectivity of the receptor toward Al^{3+} and other metal ions. In the absence (red bars) and presence (green bars) of 1.0 equivalent Al^{3+} ion at $\lambda_{ex} = 490$ nm, slit width was taken at 3.0 nm during the experiment at room temperature in methanol.
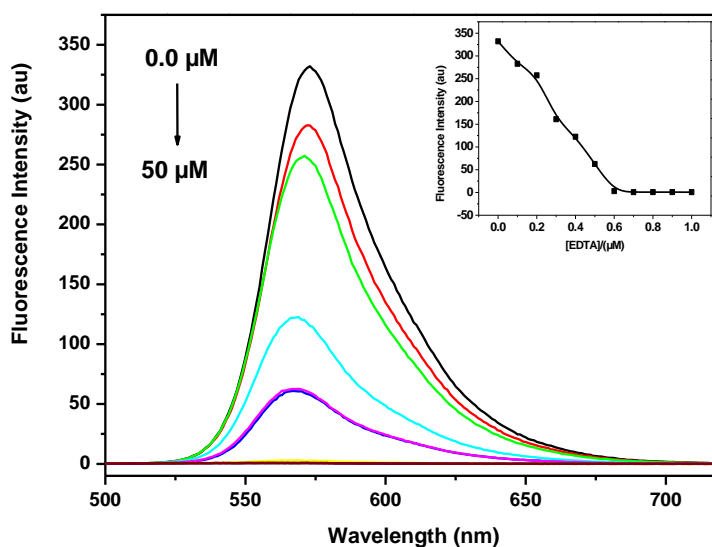
5.2.2.3.2. Reversibility of the ligand

Figure 5.11. The variation in the fluorescence intensity on the increasing concentration of EDTA (0.0, 5, 10, 15, 20, 25, 30, 35, 40, 45 and 50 μM) in the presence of the ligand (10 μM) with an excitation of 490 nm at slit width value of 3.0 nm. Inset is the plot between fluorescence intensity vs EDTA equivalent.

On the other hand, the reversibility of the ligand is considered as an important aspect in practical applications, therefore EDTA titration was conducted to examine the reversibility of the **R1**–Al^{3+} complexation in Figure 5.11. Results of the titration shows that, **R1**–Al^{3+} complex emission intensity declines after the addition of EDTA solution at 569 nm because EDTA reacts first with the available free metal ions in the solution and then it displaces the metal ions from the ligand–metal ion complex. Owing to this effect the fluorescence of metal ligand complex goes to "turn–off".
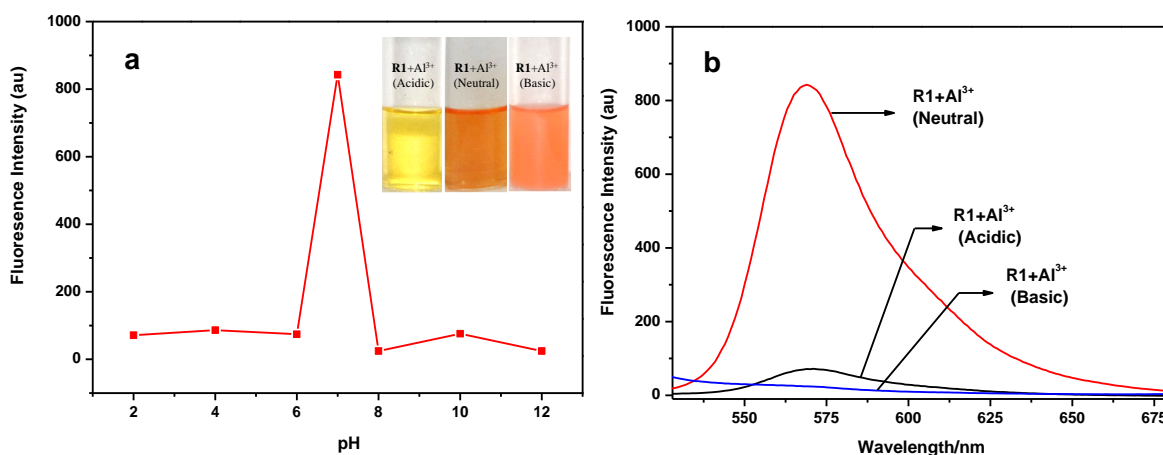
5.2.2.3.3. Effect of pH

Figure 5.12. (a) Fluorescence intensities of **R1** (10 µM) at λ_{max} = 569 nm in the presence of Al^{3+} (10 µM) under different pH conditions at slit width value of 5.0 nm. Inset: Photographs showing the colorimetric changes of **R1**–Al^{3+} in different pH conditions (left), (b) Spectral changes of **R1**–Al^{3+} as a function of pH (right).

Moreover, to examine the metal ion selectivity, for some biological applications, it is extremely necessary that the chemosensor should be suitable for measuring specific cations in the physiological pH range [41, 42]. Therefore, we measured the effect of pH between chemosensor and Al^{3+} ions in the pH range of 2.0 to 12.0 at 569 nm. The experiment was carried out at a fixed concentration of 10 µM of fluorescent probe (**R1**–Al^{3+}) and the results are depicted in Figure 5.12(a). The fluorescent probe showed color changes in acidic as well as in basic media which could be detected by naked-eye under UV lamp (Inset in the same figure). The fluorescence intensity reduced in acidic condition because of receptor could be protonated and its binding ability reduced. The decrease in fluorescence intensity was also observed in basic media, it may be due to formation of metal hydroxides and thus reducing the formation of **R1**–Al^{3+} complex. The spectral changes observed in different pH conditions are shown in Figure 5.12(b). As a result, chemosensor exhibited exceptionally good fluorescent nature for aluminium metal ions at

approximately neutral pH range in 30% aqueous solution revealing that the chemosensor could be applied for the detection of Al^{3+} ions in biological environment.

5.2.2.3.4. Solvent effect

In addition to this, the effect of a range of solvents such as dimethyl sulfoxide (DMSO), tetrahydrofuran (THF), dimethylformamide (DMF), acetone and methanol on the detection of Al^{3+} metal ions by **R1** was explored and the results are shown in Figure 5.13. From the figure it can be seen that the fluorescence intensity is changed owing to different binding mode of the chemosensor with Al^{3+} ions in different solvents. Thus, the best results were observed when methanol was treated as solvent.
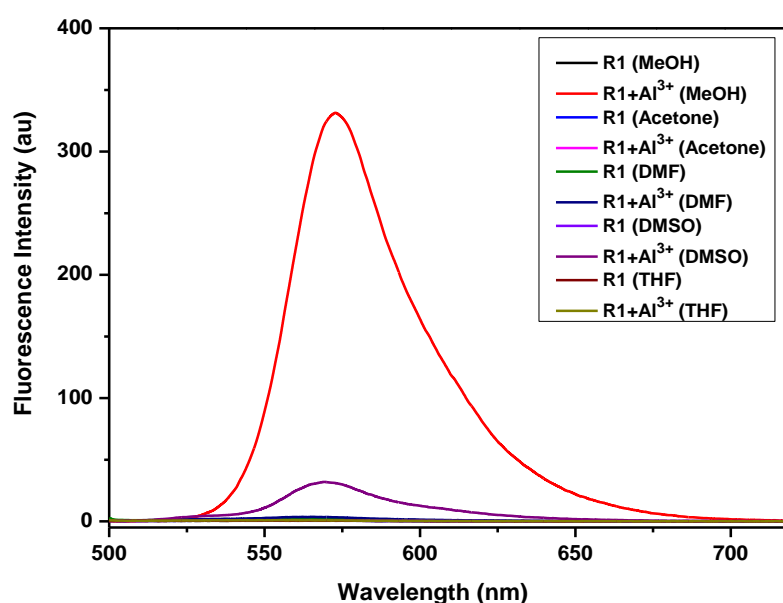

Figure 5.13. The effect on the fluorescence emission intensity of **R1**–Al^{3+} probe in the presence of different solvents recorded at a slit width value of 3.0 nm.

5.2.2.4. Electrochemical measurement

As depicted in Figure 5.14, the corresponding wavelength to the band gap energy can be calculated from the cross point of absorption and emission onset lines. The corresponding wavelength for **R1** is 508 nm and **R1**+Al^{3+} is 555 nm which are equal to 2.441 eV (for **R1**) and 2.234 eV (for **R1**+Al^{3+}) band gap energy. Figure 5.15 shows the current–voltage curve for **R1** and **R1**+Al^{3+} regarding to differential pulse voltammetric experiments. Based on results, **R1** shows $E_{ox} = 0.620$ eV which is equal to $E_{HOMO} = -5.420$ eV and **R1**+Al^{3+} shows $E_{ox} = 0.624$ eV which is equal to $E_{HOMO} = -5.424$ eV. The results show that upon addition of Al^{3+} ions increased the oxidation potential of **R1**, due to decrease in electron releasing nature of **R1**–Al^{3+} complex. LUMO energy levels (for **R1** is –2.979 eV, and for **R1**+Al^{3+} is –3.190 eV) were estimated from HOMO and band gap

energies (Figure 5.16). This experiment proves that increase in oxidation potential and decrease in band gap as a result of interaction in between **R1** and Al^{3+} ions [43].
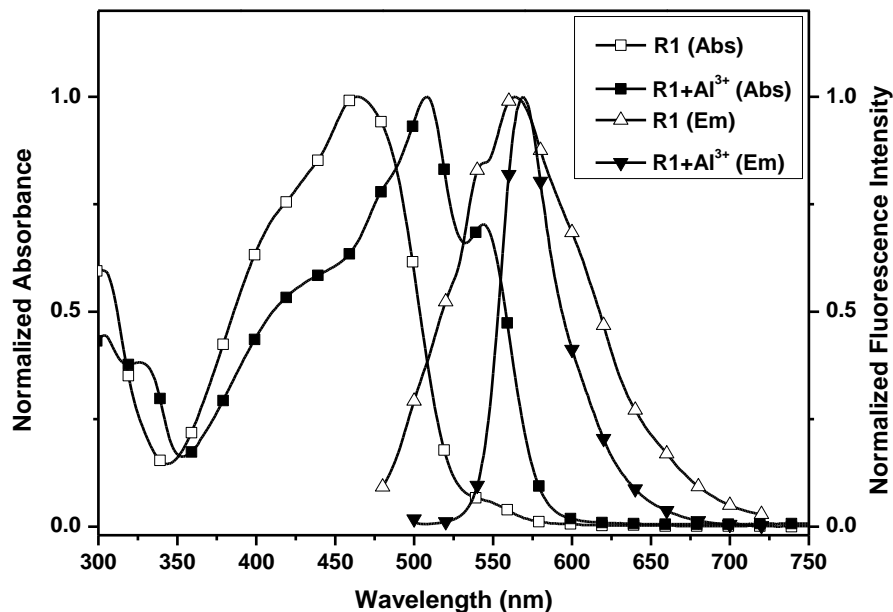
Figure 5.14. The normalized UV–vis absorption and fluorescence emission spectra of **R1** and **R1**–Al^{3+} recorded in methanol at a slit width of 3.0 nm.
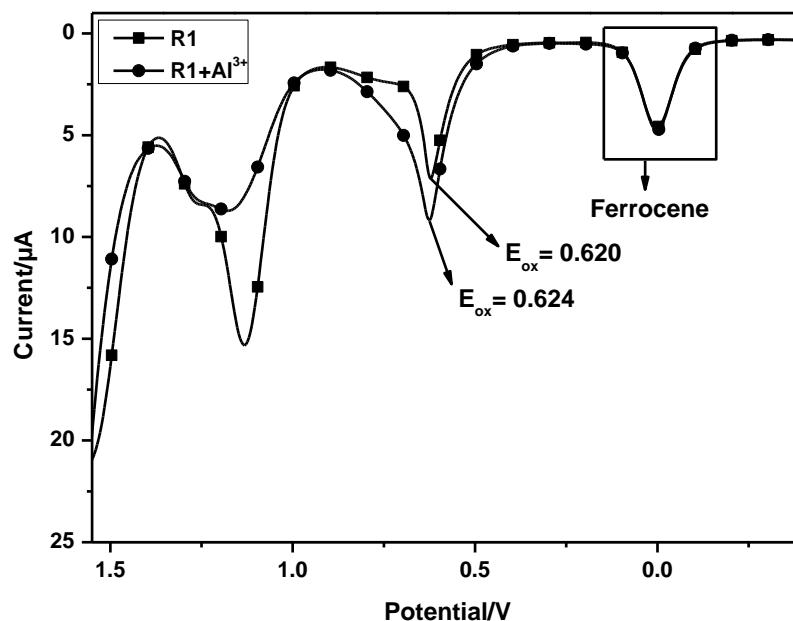
Figure 5.15. Differential pulse voltammograms recorded for the chemosensor **R1** and the corresponding Al^{3+} addition product in methanol.

5.2.2.5. ^{1}H−NMR titration

The ^{1}H–NMR spectra of **R1** with and without addition of Al^{3+} metal ions are shown in Figure 5.17. The results showed that when metal–ligand titrations were performed by the addition of different equivalents of Al^{3+} ions, some changes in the ^{1}H–

NMR-spectra were observed. It has been found that the peak of protons at about 8.05 and 7.95 ppm of ligand were shifted to upfield 8.0 and 7.90 ppm upon addition of Al^{3+} ions,
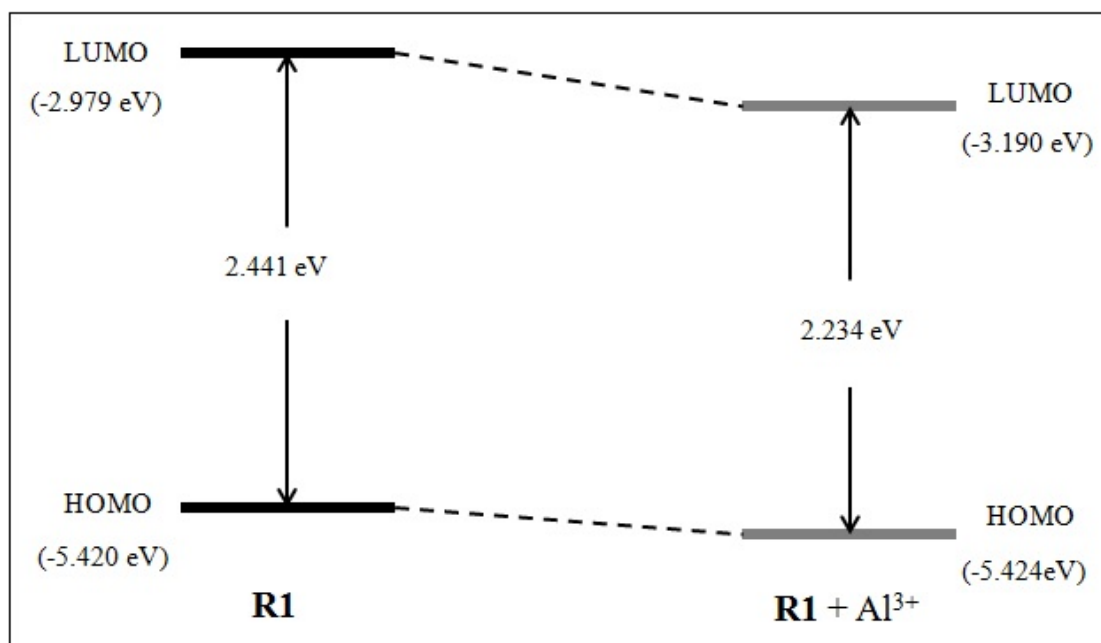

Figure 5.16. Energy level diagram of the chemosensor **R1** and it's corresponding complex with Al^{3+} metal ions.

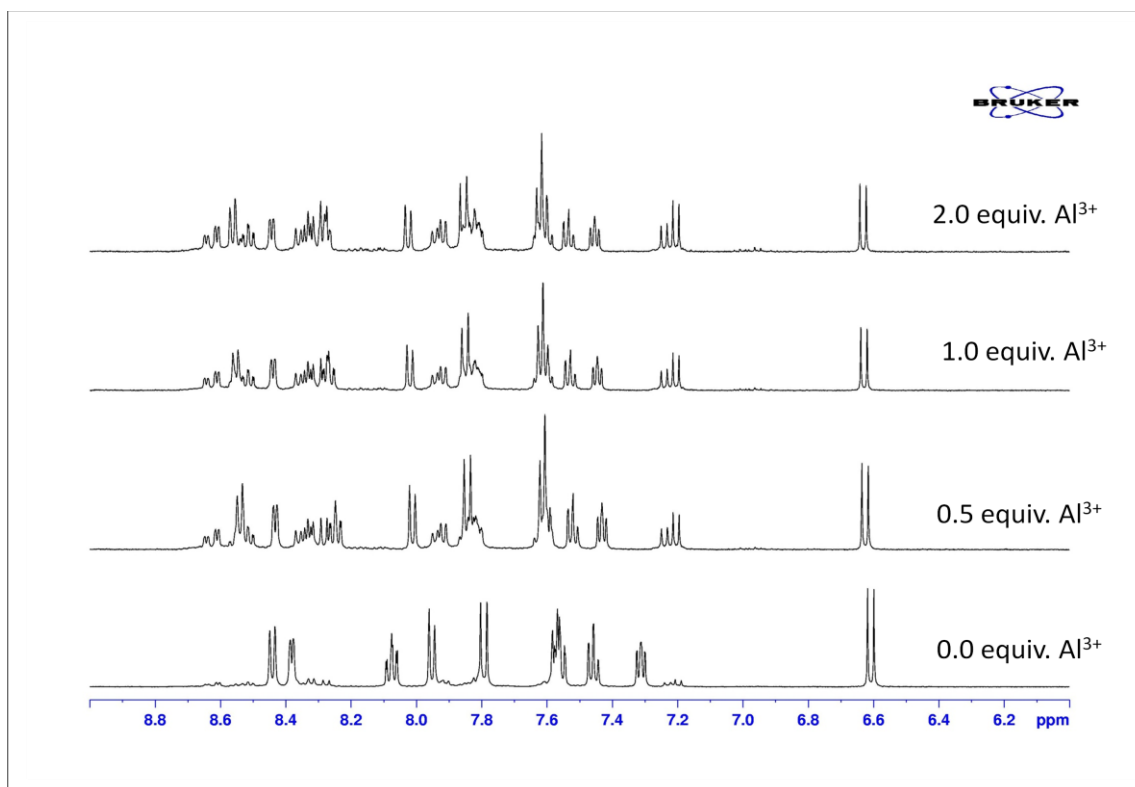**Figure 5.17.** ^1H–NMR (500 MHz) spectra of receptor and its complex, after addition of different quantities of Al^{3+} (0.0–2.0 equivalent) in CD_3OD.

owing to interruption of the intra-molecular hydrogen bonding between the phenolic hydroxyl group and the nitrogen of the azo moiety. Conversely, the protons of pyridine ring were shifted downfield with the addition of Al^{3+} ions, which indicated that the structure of receptors became more rigid after coordination with aluminium ions. This indicates that the phenolic hydroxyl group, nitrogen atom of the azo moiety and nitrogen of pyridine ring participated in complexation with aluminium ions. Therefore, it can be supposed that the aluminium ion may be chelated by the counter anion or solvent in order to satisfy the need of six-coordination [44].

5.2.3. Conclusion

The ligand prepared can be used to detect Al^{3+} ions qualitatively and quantitatively both by colorimetry and fluorescence spectrophotometry. However, fluorescence method shows higher selectivity and it can be used to estimate Al^{3+} ions concentration with a detection limit of 1.81×10^{-8} M. The receptor can also be employed to detect Al^{3+} ions in diverse samples under the UV light even though naked eye. The receptor gives exceptionally good results with aluminium metal ions at the physiological pH range. Consequently, it is of great utility for analysing large number of biological, analytical and environmental samples.

5.3. PART (B) Aluminium fluorescent sensor based on Schiff bases *N,N′*-bis(salicylidene)-m-phenylenediamine and *N,N′*-bis(salicylidene)-o-phenylenediamine

5.3.1. Experimental

5.3.1.1.Materials and apparatus

Salicylaldehyde, m-phenylenediamine and metal salts were of analytical grade reagent and procured from Merck, India and o-phenylenediamine was obtained from Loba Chemie (India), which were used without further purification. The FT–IR spectra were recorded using a Thermo Scientific Nicolet 6700 FT–IR spectrometer within the range 4000–400 cm^{-1}. The CHNS percentage was determined using a Vario MICRO Cube. The ^{1}H–NMR and ^{13}C–NMR spectra were documented on a Bruker 500 MHz (USA), using TMS as an internal standard, CDCl$_3$ and CD$_3$OD as solvents. The mass spectra were recorded on Bruker–MicrOTOF–Q II (USA). The UV–vis absorption spectra and fluorescence emission spectra were plotted using a Shimadzu UV–2450 spectrophotometer and Shimadzu RF–5301PC spectrofluorophotometer equipped with a quartz cuvette of 1.0 cm path length with a xenon lamp as the excitation source by means of slit width value of

at 3.0 nm, respectively. The differential pulse voltammetric experiments were carried out using a CHI760E Electrochemical Workstation (USA) with a predictable three electrode cell assembly consisting of glassy carbon electrode, platinum wire and calomel electrode as working electrode, counter electrode and reference electrode, respectively.

The stock solutions (10 mM) of receptors (**R2** and **R3**); and metal chlorides and nitrates were prepared in methanol. For all the fluorescence emission measurements, excitation wavelength was 410 nm.
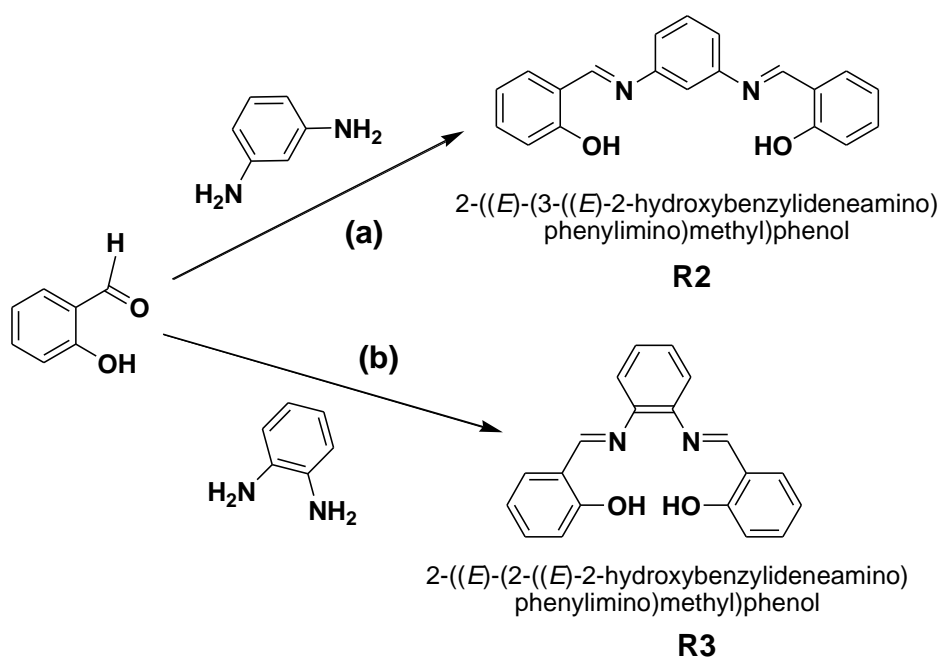
Scheme 5.2. Synthesis of receptors: path (a) for **R2** and (b) for **R3**.

5.3.1.2. Synthesis of receptor

The receptors (**R2** and **R3**) were synthesized using the reported method [45, 46] with a specific modification as shown in Scheme 5.2. A solution of (5.0 mmol, 0.541 g) corresponding phenylenediamine in 20 ml of ethanol was added slowly to 2-hydroxybenzaldehyde (1.221 g, 10.0 mmol) ethanolic solution (15 ml) under the nitrogen atmosphere with continuous stirring. The obtained mixture was refluxed for 3 h and the completion of the reaction was checked by TLC in hexane-ethyl acetate mixture. Then the resulting mixture was cooled to room temperature, evaporate the solvent at reduced pressure, and the resulting solid product was then washed with cold ethanol. The desired receptor products were recrystallized by using ethanol. The characterization of the synthesized compounds was done by various spectroscopic techniques such as FT–IR, ^{1}H–NMR, ^{13}C–NMR and HRMS.

N,N′-Bis(salicylidene)-m-phenylenediamine, (R2): Yield: 1.32 g (83%); color: yellow solid; m.p. 104–106 °C; Anal. calcd. for $C_{20}H_{16}N_2O_2$: C=75.93, H=5.10, N=8.86, found: C=75.22, H=5.08, N=8.84; FT–IR (KBr, v, cm^{-1}): 3429 (O−H), 1564 (C=N), 1500 (C=C), 1283 (C−N), 1197, 1146 (C−O); ^{1}H–NMR (CDCl$_3$, 500 MHz, δ ppm, J Hz): 6.946–6.977 (t, J = 7.5, 2H), 7.038–7.054 (d, J = 8.0, 2H), 7.182–7.209 (m, 3H), 7.383–7.424 (m, 4H), 7.451–7.482 (t, J = 7.5, 1H), 8.663 (s, 2H), 13.103 (s, 2H); ^{13}C–NMR (CDCl$_3$, 500 MHz, δ ppm): 113.96, 117.34, 119.10, 119.21, 119.62, 130.33, 132.48, 133.47, 149.75, 161.20, 163.37; HRMS (ESI, m/z): [M+H]$^+$ calcd. for $C_{20}H_{16}N_2O_2$: 317.1290; found: 317.1281.

N,N′-Bis(salicylidene)-o-phenylenediamine, (R3): Yield: 1.39 g (88%); color: orange yellow solid; m.p. 153–155 °C; Anal. calcd. for $C_{20}H_{16}N_2O_2$: C=75.93, H=5.09, N=8.86, found: C=75.28, H=5.14, N=8.82; FT–IR (KBr, v, cm^{-1}): 3427 (O−H), 1562 (C=N), 1411 (C=C), 1274 (C−N), 1192, 1103 (C−O); ^{1}H–NMR (CDCl$_3$, 500 MHz, δ ppm, J Hz): 6.907–6.939 (t, J = 7.5, 2H), 7.038–7.054 (d, J = 8.0, 2H), 7.230–7.249 (m, 2H), 7.338–7.390 (m, 6H), 8.639 (s, 2H), 13.051 (s, 2H); ^{13}C–NMR (CDCl$_3$, 500 MHz, δ ppm): 117.55, 119.03, 119.24, 119.71, 127.75, 132.37, 133.42, 142.52, 161.36, 163.71; HRMS (ESI, m/z): [M+H]$^+$ calcd. for $C_{20}H_{16}N_2O_2$: 317.1290; found: 317.1266.

5.3.2. Results and discussion

5.3.2.1. Spectral analysis

The UV−vis and Fluorescence spectra were recorded in methanol solvent for both the receptors (**R2** and **R3**) in which the simulations of Al^{3+} ion could induce dramatic spectral changes; however there were some perceptible distinction. Detailed spectral changes would be particularly discussed in the following sections.

5.3.2.1.1. UV−vis absorption spectral response of the receptors

The UV−vis absorption spectra of methanolic solution of the receptors **R2** and **R3** (50 μM) and their mixtures with various metal ions (50 μM) are depicted in Figure 5.18(a and b). Both the receptors exhibit weak absorption band in the ultraviolet region at about 340 nm and 328 nm, respectively. It is seen from spectral changes that the receptors show a high selectivity towards aluminium over the other metal ions studied (Ba^{2+}, Ca^{2+}, Co^{2+}, Cd^{2+}, Cs$^+$, Cr^{3+}, Cu^{2+}, Fe^{2+}, Fe^{3+}, Hg^{2+}, K$^+$, Li$^+$, Na$^+$, Mg^{2+}, Mn^{2+}, Gd^{3+}, Nd^{3+}, Pb^{2+}, Sr^{2+}, Zn^{2+} and Ni^{2+}). Since UV−vis absorption spectroscopy is the complementary part of fluorescence emission spectroscopy, thus for interpreting the more precised results, further we applied fluorescence emission studies.
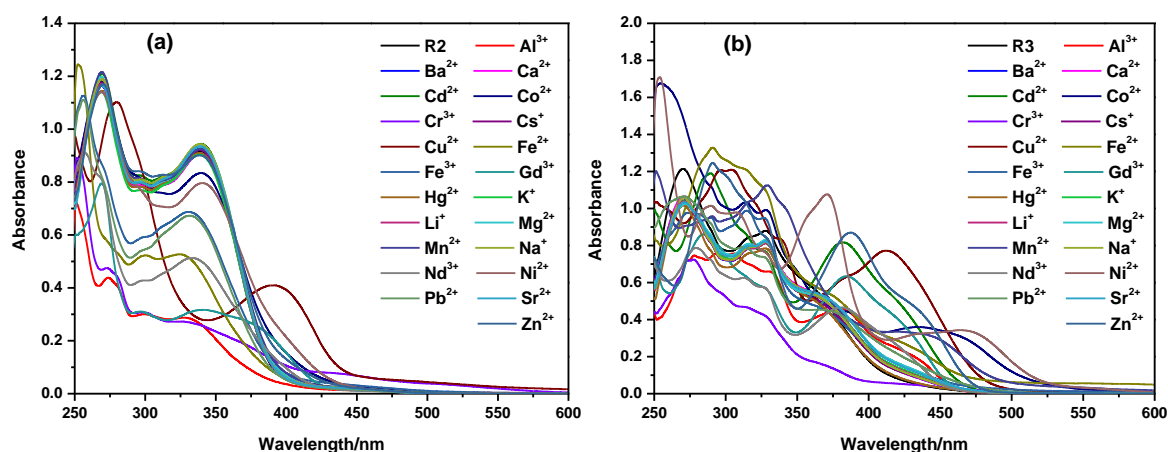
Figure 5.18. UV–vis absorption spectra of; (a) receptor **R2** and (b) receptor **R3** in the presence of (50 μM) several metal ions (1.0 equivalent for each metal ion).

5.3.2.1.2. Fluorescence emission spectral response of the receptors

In order to further examine the selectivity of receptors towards the metal ions, the fluorescence response of the receptors (**R2** and **R3**) in methanolic solution was also looked into. The fluorescence emission spectra were recorded after addition of 40 μM of each of various metal ions and depicted in Figure 5.19(a and b). It is seen that the receptors do not show a significant fluorescence emission band in the absence of metal ions. A remarkable enhancement in the fluorescence emission band is observed upon addition of Al^{3+} to the
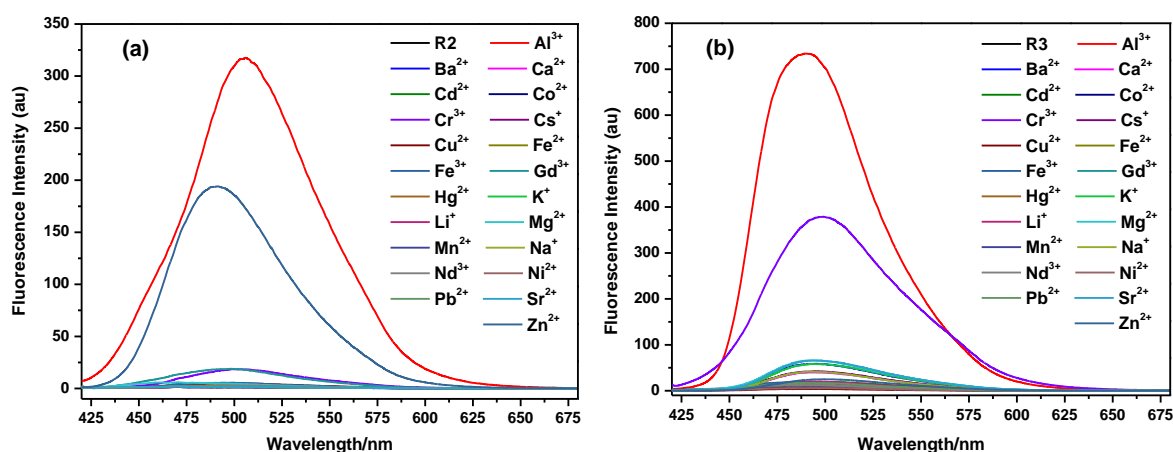

Figure 5.19. Fluorescence emission spectra of receptors (40 μM) in the presence of 1.0 equivalent of different metal ions (Ca^{2+}, Ba^{2+}, Co^{2+}, Cd^{2+}, Cs^+, Cr^{3+}, Cu^{2+}, Fe^{2+}, Fe^{3+}, Hg^{2+}, K^+, Li^+, Na^+, Mg^{2+}, Mn^{2+}, Nd^{3+}, Pb^{2+}, Sr^{2+}, Gd^{3+}, Al^{3+}, Ni^{2+} and Zn^{2+}) in methanol.

receptors at λ_{max} = 506 nm and 489 nm for receptor **R2** and **R3**, respectively. However, the addition of Zn^{2+} to receptor **R2** and of Cr^{3+} to receptor **R3** results in a small enhancement in fluorescence emission intensity. On the other hand, the addition of all other metal ions including Ba^{2+}, Ca^{2+}, Co^{2+}, Cd^{2+}, Cs^+, Cu^{2+}, Fe^{2+}, Fe^{3+}, Hg^{2+}, K^+, Li^+, Na^+, Mg^{2+}, Mn^{2+}, Nd^{3+}, Gd^{3+}, Pb^{2+}, Sr^{2+} and Ni^{2+} causes no significant fluorescence emission under the same

conditions. Thus the receptors show a selective emission response to Al^{3+} and they exhibit "ON–OFF" mode of high sensitivity. Additionally, on treatment with UV light they show incredible changes from colorless to sharp bright blue fluorescence in the presence of aluminium within 5 s which could easily be detected by naked eye.

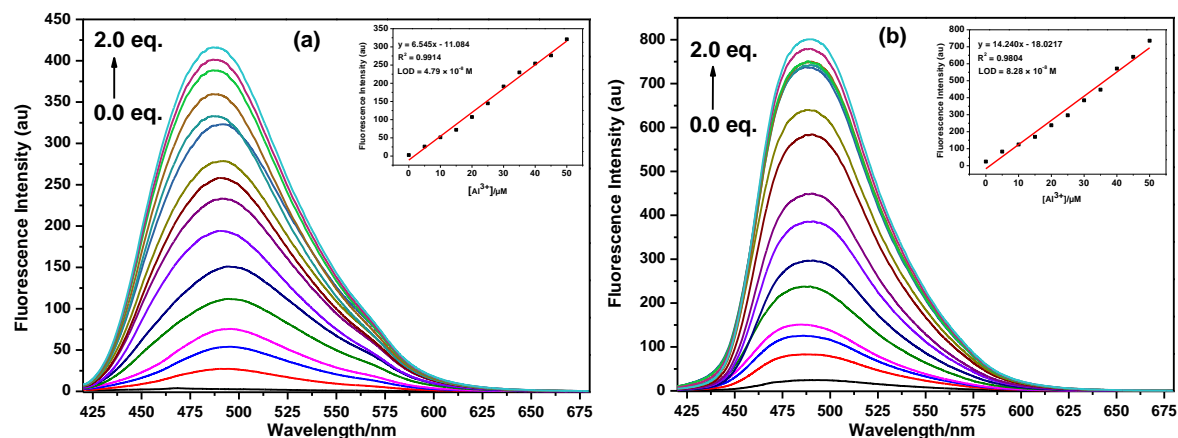### 5.3.2.1.2.1. Fluorescence titration on aluminium metal ions

Figure 5.20. Changes in the fluorescence emission spectra of receptor **R2** (a) and **R3** (b) (40 µM) with added $[Al^{3+}]$. $[Al^{3+}]$ = 0.0, 5, 10, 15, 20, 25, 30, 35, 40, 45, 50, 60, 70, 80, 90, 100 µM, (from bottom to top). Inset: linear plot between added amounts of metal ion (0.0–50 µM) and intensity (λ_{ex} = 410 nm; λ_{em} = 506 nm and 489 nm for **R2** and **R3**, respectively).

       The fluorescence response of the probe for increasing concentrations of Al^{3+} (0.0, 5, 10, 15, 20, 25, 30, 35, 40, 45, 50, 60, 70, 80, 90, 100 µM) was shown in Figure 5.20(a and b). It is seen that upon addition of Al^{3+}, the fluorescence emission intensity (at 506 nm and 489 nm) of receptor **R2** and **R3** gradually increased. The changes in the fluorescence intensity ratio lead to a continuous color change from colorless to sharp bright blue which can distinguished under the UV lamp allowing the fluorescence detection of Al^{3+}, which cannot be seen or distinguished by naked eyes. The fluorescence dose response of the probe with Al^{3+} metal ions were examined and shown inset in the same Figure. Noticeably, the fluorescence intensity with the concentration of the Al^{3+} ions added (0–50 µM) shows good linearity with a correlation coefficient of 0.9914 and 0.9804 which could be used for the quantification of Al^{3+}; and the detection limit is determined to be 4.79×10^{-8} M and 8.28×10^{-8} M on the basis of signal to noise ratio (S/N = 3) for receptors **R2** and **R3** respectively. The sensitivity of the studied method is comparable to or higher than reported methods using fluorescence probes.

       On the other hand, the binding constant of the receptors **R2** and **R3** with Al^{3+} has been established using the Benesi–Hildebrand equation by the fluorescence method [47].

The Benesi–Hildebrand equation plot yielded a linear fit Figure 5.21(a and b) and the stability constants for the receptors **R2** and **R3** are found to be 1.41×10^4 M^{-1} and 1.59×10^4 M^{-1}, respectively. The linear fit also indicates 1:1 complexation behavoir of receptors with metal ions.
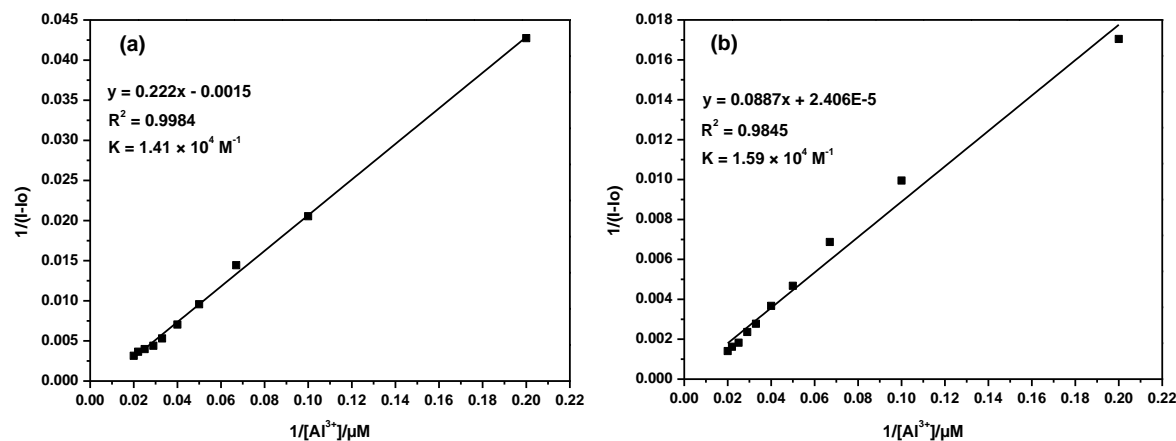

Figure 5.21. Benesi-Hildebrand plot for the determination of binding constant; of (a) receptor **R2** and (b) of **R3** for Al^{3+} in methanol at λ_{ex} = 410 nm.
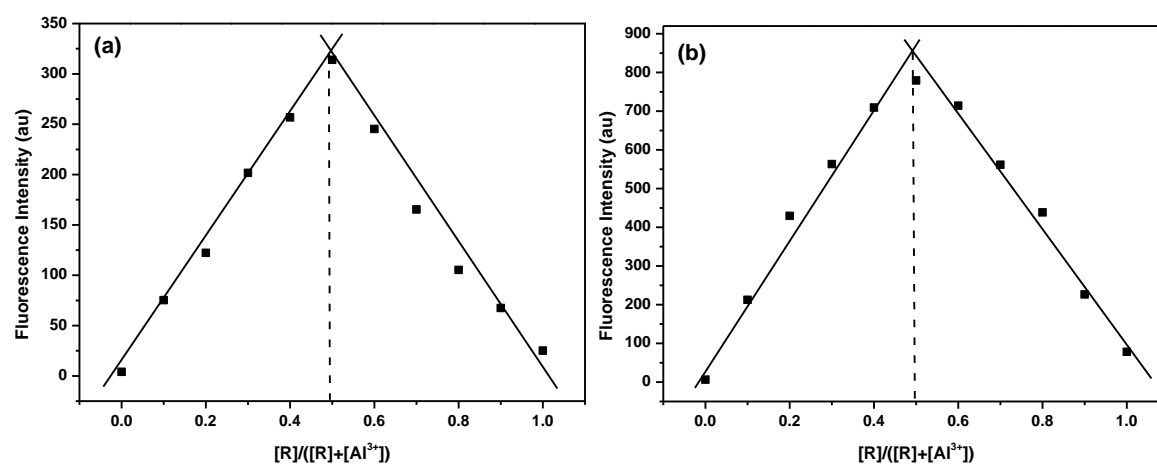
5.3.2.1.2.2. Proposed binding mode

Figure 5.22. Job's plot for the determination of stoichiometry of [R–Al^{3+}] system in methanol for receptors **R2** (a) and for **R3** (b).

Further, the stoichiometry of receptor **R2**–Al^{3+} and **R3**–Al^{3+}, complexes formed was calculated using the Job's plot method. The plot between fluorescence emission intensity versus molar fraction of [R]/([R]+[Al^{3+}]) was shown in Figure 5.22(a and b) which clearly depicts that formed metal ion complex posses 1:1 stoichiometry for the Al^{3+} and the receptors.

The receptor–Al^{3+} complexes were subjected to HRMS (ESI, *m/z*) analysis. The mass spectra of the complexes formed are presented in Figure 5.23(a and b). In order to
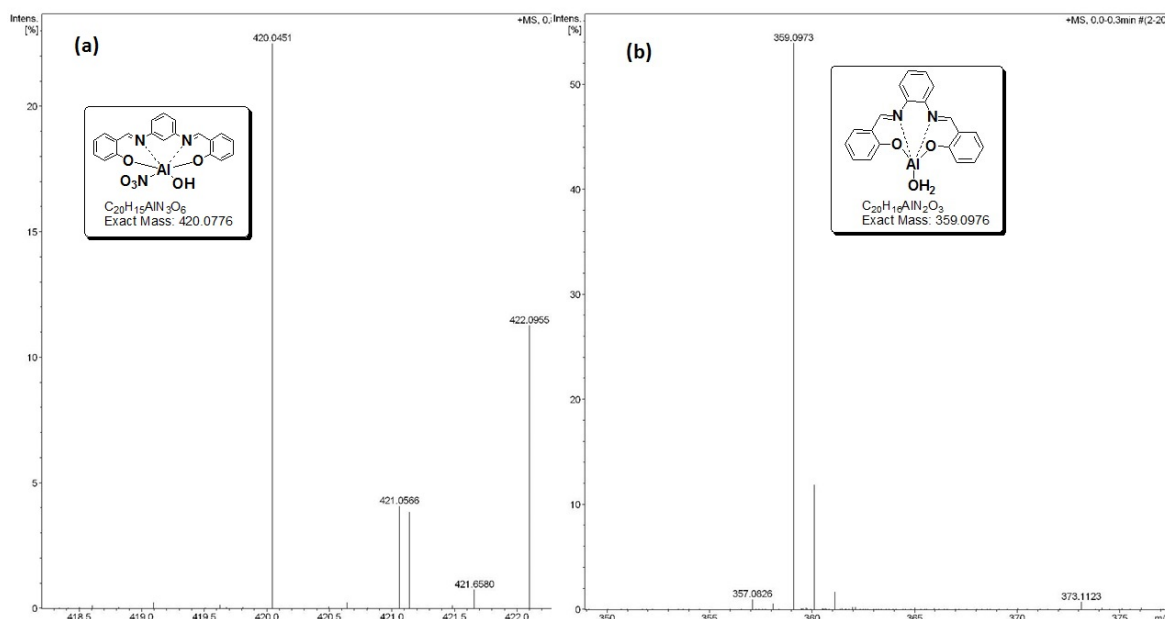
Figure 5.23. HRMS spectra showing complexation behavior with Al^{3+} for receptors **R2** (a) and for **R3** (b), respectively.

further confirm the stoichiometry of the receptor and Al^{3+} complexes, it is seen that the spectra shows well defined isotopic sharp peaks for both the complexes corresponding to $m/z = 420.0451$ and $m/z = 359.0973$ which fit well with molar mass of the receptor **R2** and **R3** complexes $[C_{20}H_{16}N_2O_2+Al(NO_3)-2H+OH]^+$ and $[C_{20}H_{16}N_2O_2+Al-2H+H_2O]^+$ respectively. The results also supports the 1:1 metal–to–ligand ratio of the R–Al^{3+} complex as concluded from the job's plot method.

To prove the chemical reversibility of the ligand to metal ion, EDTA titration method with receptor–Al^{3+} complex solution was used. Upon addition of EDTA (0.0–1.0
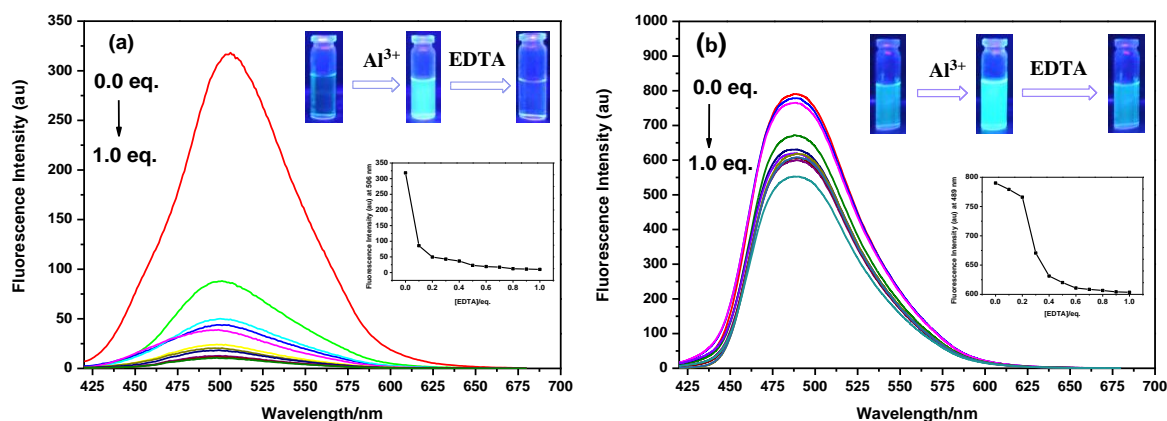

Figure 5.24. Fluorescence emission spectra of (a) receptor **R2** and (b) receptor **R3**; showing the changes of receptor–Al^{3+} complex upon addition of EDTA (0.0–1.0 equivalent). Inset: images showing the corresponding fluorescence color changes under UV lamp (top) and addition of EDTA equivalent as a function of fluorescence intensity (bottom).

equivalent), fluorescence emission intensity at 506 nm and 489 nm gradually declines due to chelation of Al^{3+} with EDTA releasing the free receptor **R2** and **R3** shown in Figure 5.24(a and b). This shows the reversible nature of the receptor and thus our synthesized receptors can be used again and again. Furthermore, the fluorescence response of the probe–Al^{3+} with added equivalent of EDTA is examined and was shown in inset of the same Figure. This quenching of fluorescence intensity upon the addition of EDTA reflects a powerful selective "ON–OFF" fluorescent signalling property of the studied receptors **R2** and **R3**.

5.3.2.1.2.3. Selectivity of the receptor for Al^{3+} over other cations
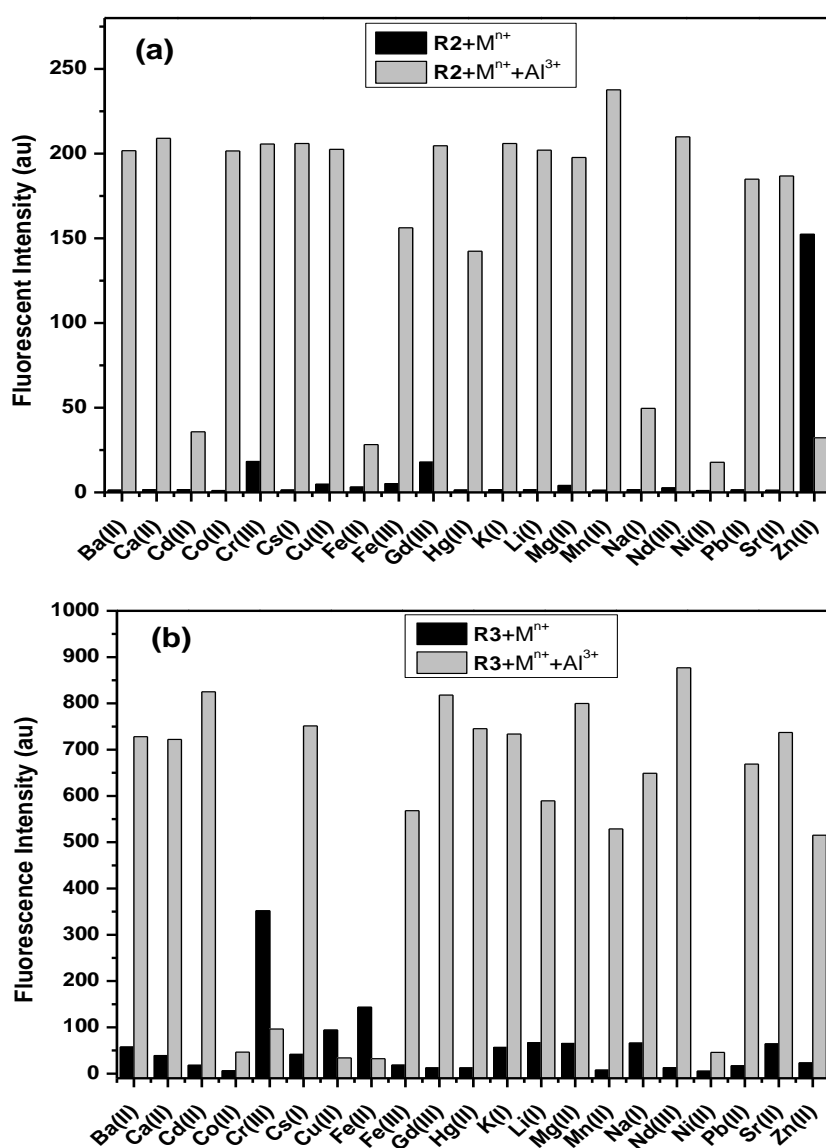

Figure 5.25. Fold of enhancement and % quenching for different cations upon binding with; (a) receptor **R2** and (b) receptor **R3** in methanol. Black bar: receptor (40 µM) and other competing metal ions (40 µM). Grey bar: (40 µM) of receptor with respective competing metal ions (40 µM) and Al^{3+} (1.0 equivalent) stated.

The selective response of the receptors towards aluminium has been further examined by determining the fluorescence of receptors (40 μM) with 40 μM aluminium metal ions and equivalent amount of other metal ions (including Ba^{2+}, Ca^{2+}, Cr^{3+}, Cs^{+}, Fe^{2+}, Fe^{3+}, Gd^{3+}, Hg^{2+}, K^{+}, Li^{+}, Na^{+}, Mg^{2+}, Mn^{2+}, Nd^{3+}, Pb^{2+}, Co^{2+}, Cd^{2+}, Cu^{2+}, Zn^{2+}, Ni^{2+} and Sr^{2+}). The fluorescence of the solutions was shown in Figure 5.25(a and b). From figures it can be easily concluded that the addition of Al^{3+} to the solution of competing metal ions and receptor lead to a remarkable enhancement of the fluorescence intensity. Metal ions such as Cd^{2+}, Ni^{2+}, Fe^{2+}, Zn^{2+}; and Co^{2+}, Cr^{3+}, Cu^{2+}, Fe^{2+} and Ni^{2+} for receptor **R2** and **R3** respectively induces the fluorescence emission intensity almost to negligible value and therefore these would interfere in the estimation of Al^{3+} by the receptors. Therefore, the synthesized receptors are highly selective in the recognition of Al^{3+} even in the bulk presence of other metal ions and thus it can be used for its estimation in biological or environmental samples where other metals usually co-exist with Al^{3+}.

5.3.2.1.2.4. Effect of pH
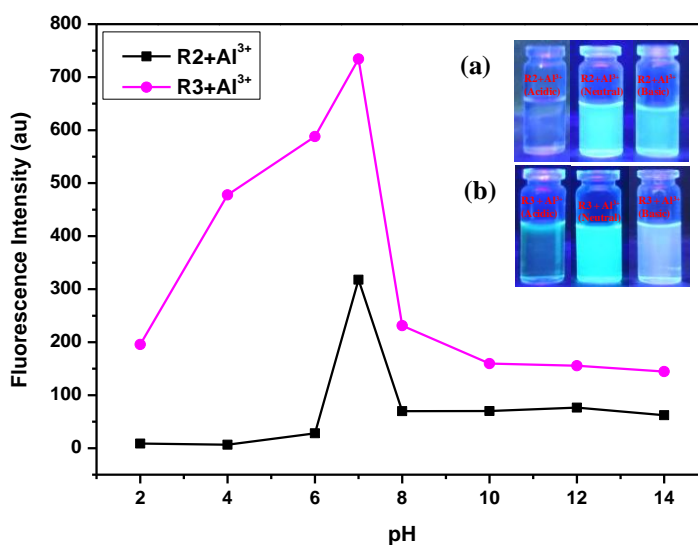
Figure 5.26. Fluorescence intensity recorded for Receptor–Al^{3+} complex in aqueous methanolic solution (80:20) at various pH values shown in the; black line: receptor **R2** and pink line: receptor **R3**. Inset: shows the fluorescence color changes under UV lamp in (a) and (b) for receptor **R2** and **R3**, respectively.

In addition to metal ion selectivity for some biological applications, it is exceptionally imperative to examine the pH span of the receptor–metal complex in which receptor can selectively detect Al^{3+} efficiently. However, on addition of Al^{3+} (methanol to water; 80:20) solution led to the fluorescence enhancement over a wide pH range of 5.5– 8.5 (Figure 5.26), and the color changes was also noticed under the UV light (inset in the

same figure). Therefore, the receptor may be suitable for measuring aluminium metal ions in the physiological pH range and was favourable for its application in environmental and biological samples.

5.3.2.1.2.5. Possible mechanism of the fluorescence detection of Al^{3+} using the receptors

Further, the interaction between the receptors (**R2** and **R3**) and Al^{3+} have been examined under the UV chamber and changes in color of the receptor before and after addition of Al^{3+} is viewed. It has established that when metal ions added to the receptor, it binds at the donating sites of the receptor and result in the blockage of electron transfer and enhancement of fluorescence intensity [48, 49]. Thus, the chelation enhanced fluorescence (CHEF) process was observed. It appears that the complexes may have tentative structures for receptors **R2** and **R3** with Al^{3+} depicted in Figure 5.27.
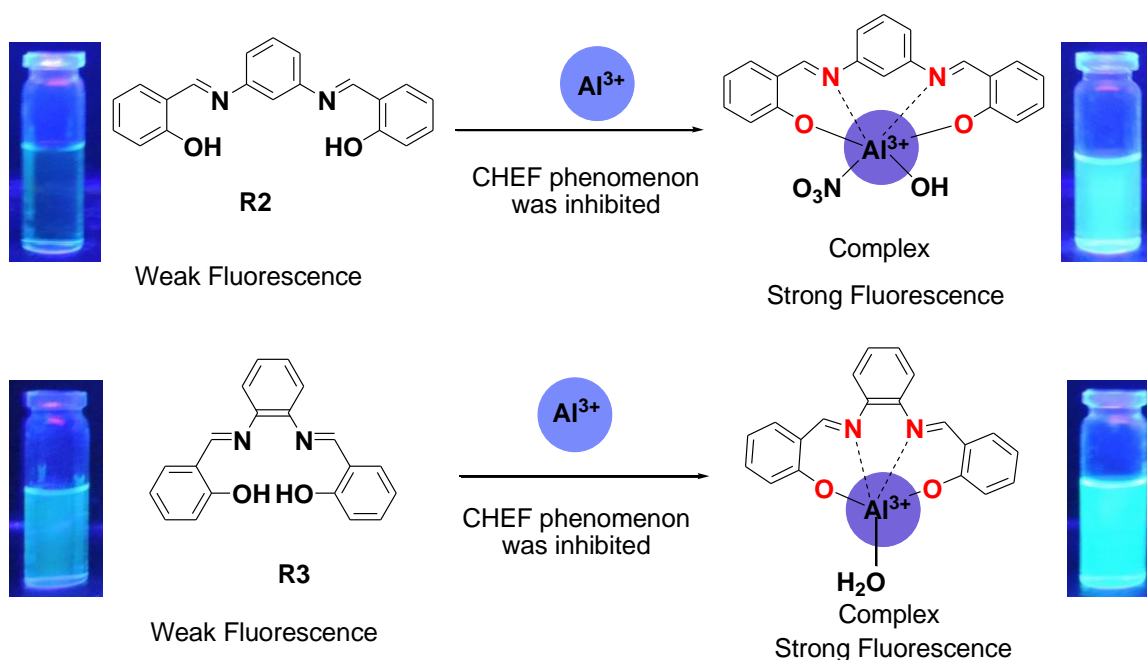
Figure 5.27. Possible mechanism of the complexation of receptors with Al^{3+} ions.

5.3.2.2. ^1H–NMR titration

To study the detailed complexation of Al^{3+} with the receptor **R2** and **R3**, ^1H–NMR spectra of both the receptors upon addition of different concentration of aluminium ions in CD_3OD was recorded. As depicted from Figure 5.28(a and b), the consecutive additions of Al^{3+} to the receptors induced significant changes in its ^1H–NMR spectral pattern. Upon addition of 1.0 equivalent of Al^{3+}, the imine proton signals around at 8.79 ppm (of **R2**) and at 8.70 ppm (of **R3**) was splitted and shifted to downfield at 8.92 ppm and at 8.75 ppm

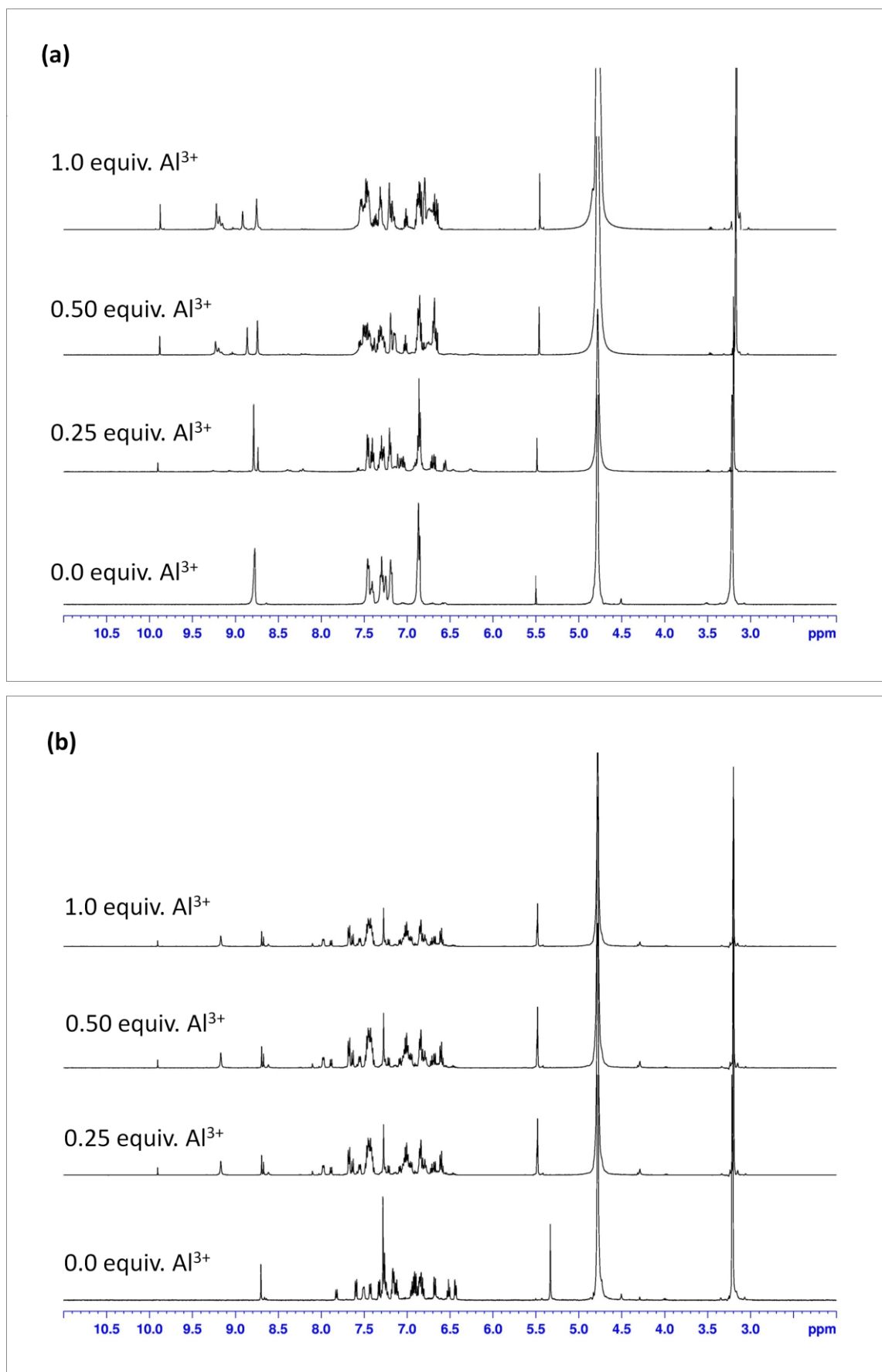**Figure 5.28.** ^{1}H–NMR titration spectra of receptor **R2** (a) and receptor **R3** (b) with 0.0, 0.25, 0.50, 1.0 equivalent of Al^{3+} in CD_3OD solvent.

respectively and new peaks were generated at 9.25 ppm and 9.95 ppm in both the receptors after addition of metal ions. In addition, the aromatic ring protons of the receptor **R2** (6.82–7.52 ppm) and receptor **R3** (6.41–7.83 ppm) also changes their multiplicity and more complicated as well as slightly downfield shifted around 0.22–0.45 ppm was observed. On the other hand, the peaks at about 5.32 ppm and 5.50 ppm for receptor **R2** and **R3** respectively show a slight downfield shift. Furthermore, addition of more than 1.0 equivalent of Al^{3+} does not cause an appreciable shift in the position of the signals suggests that the formation of a 1:1 complex between receptors and Al^{3+} [50]. Thus, it can be made-up that the Al^{3+} ion may be chelated by the counter anion or solvent in order to satisfy the need of six–coordination.

5.3.2.3. Electronic potential measurement and partial charge transfer

As a result, the corresponding wavelength for the calculation of band gap energy for both the receptors (**R2** and **R3**) and their complexes with Al^{3+} can be achieved by the cross point of absorption and emission onset lines shown in the Figure 5.29(a and b). The corresponding wavelength for receptors **R2** and **R3** are 391 and 408 nm; and 409 and 443 nm for their corresponding complexes with Al^{3+}, the band gap energy for the receptors **R2** and **R3** are 3.171 eV and 3.039 eV respectively and 3.032 eV and 2.799 eV for receptor **R2**–Al^{3+} complex and receptor **R3**–Al^{3+} complex respectively. However, for the calculation of electronic properties of the receptors (**R2** and **R3**) and their complexes with Al^{3+} have been achieved by the differential pulse voltammetric experiments based on the current voltage is illustrated in Figure 5.30(a and b). Thus, on the basis of this HOMO– LUMO were calculated for both the receptors and their corresponding complexes with Al^{3+}. It was concluded that after addition of Al^{3+} ion following changes were oberved i.e. decrease in the oxidation potential of complex; shows a stronger electron acceptor, easier
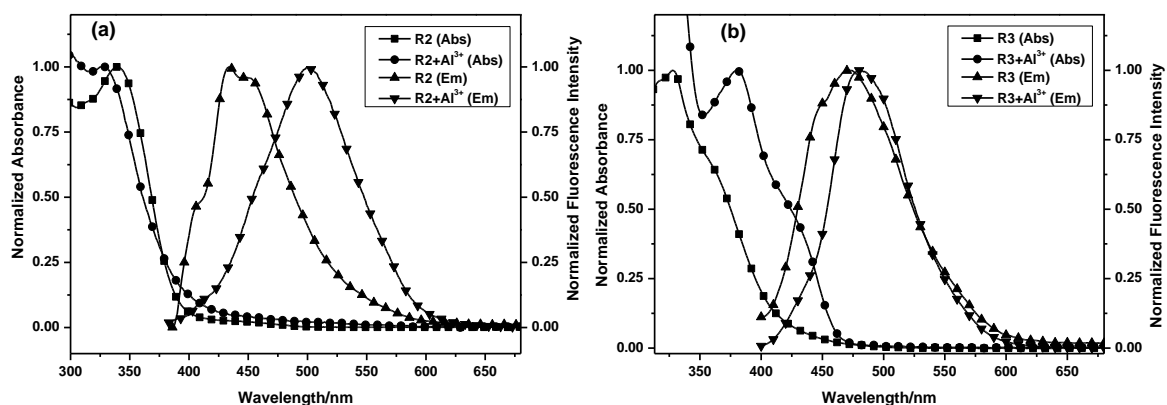

Figure 5.29. UV–vis absorption and fluorescence emission spectra of; (a) receptor **R2** and (b) receptor **R3**, and their corresponding complexes with Al^{3+}.

electron transfer, higher emission intensity in the fluorescence experiment than the receptors depicted in Figure 5.31. Thus, owing to the interaction between receptors and Al^{3+}, the experiment provides evidence to decrease in oxidation potential and decline in band gap energy.
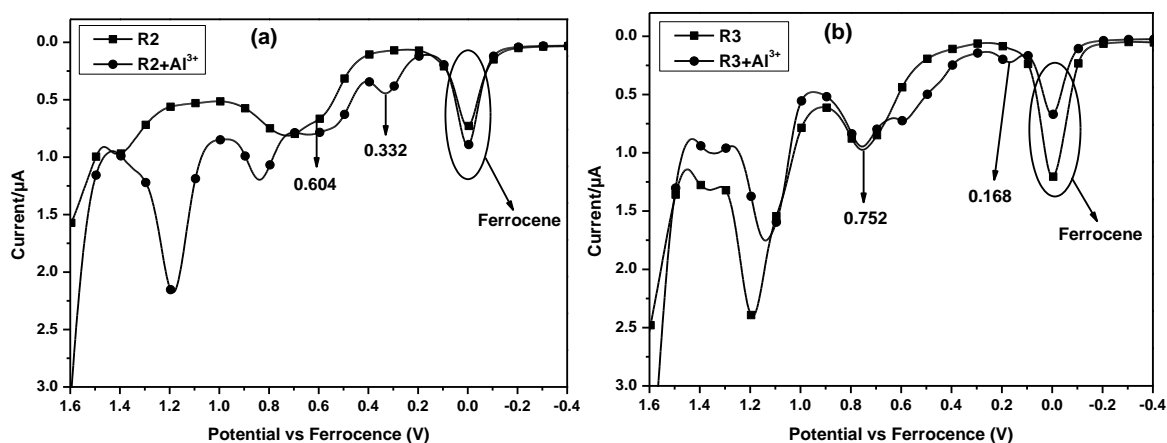

Figure 5.30. Differential pulse voltammograms recorded for both the receptors and their corresponding Al^{3+} addition product in methanol solvent.
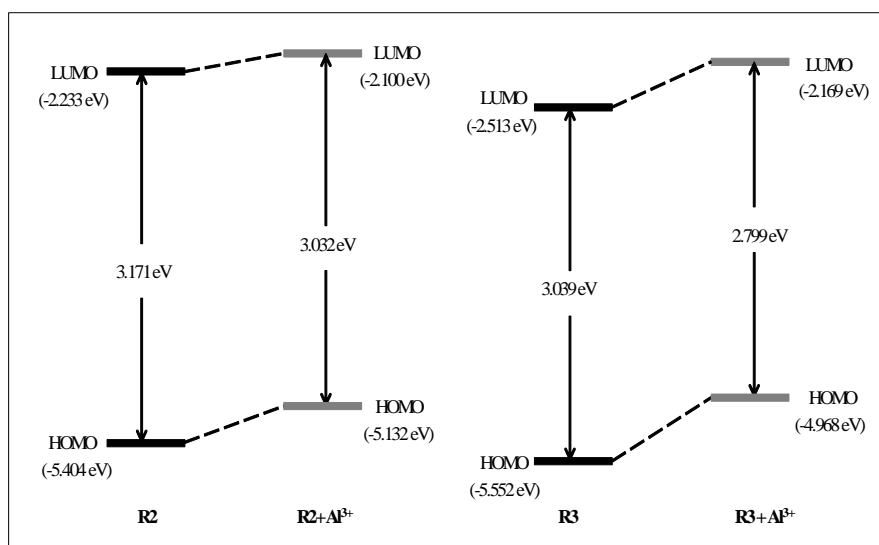
Figure 5.31. Energy level diagram of the receptors and their addition product with Al^{3+} metal ions.

5.3.3. Conclusion

The significant naked–eye "ON–OFF" type fluorescent probe (**R2** and **R3**) for detection of Al^{3+} was synthesized and characterized; the detection can be percept by the significant color changes from colorless to sharp bright blue in methanol media under UV light. It presents an outstanding selectivity to Al^{3+} qualitatively as well as quantitatively by the fluorescence spectrophotometry over other metal ions. Furthermore, the stability constants and the detection limits of the receptor–Al^{3+} complexes were found to be 1.41×10^4 M^{-1} and 1.59×10^4 M^{-1} and 4.79×10^{-8} M and 8.28×10^{-8} M for receptor **R2** and **R3**

respectively. The receptors can be successfully applied in the physiological pH range. On the other hand, the decrease in HOMO–LUMO band gap energy evidenced the more binding ability of receptors with Al^{3+}. Not only this, the ligand can also be used to detect Al^{3+} in various samples under the UV light even though naked eye. Consequently, it is of great utility for analysing large number of biological, analytical and environmental samples.

5.4. PART (C) Aluminium fluorescent sensor based on Schiff bases *N,N′*-bis(o-hydroxyacetophenone)-m-phenylenediamine and *N*-(o-hydroxyacetophenone)-o-phenylenediamine
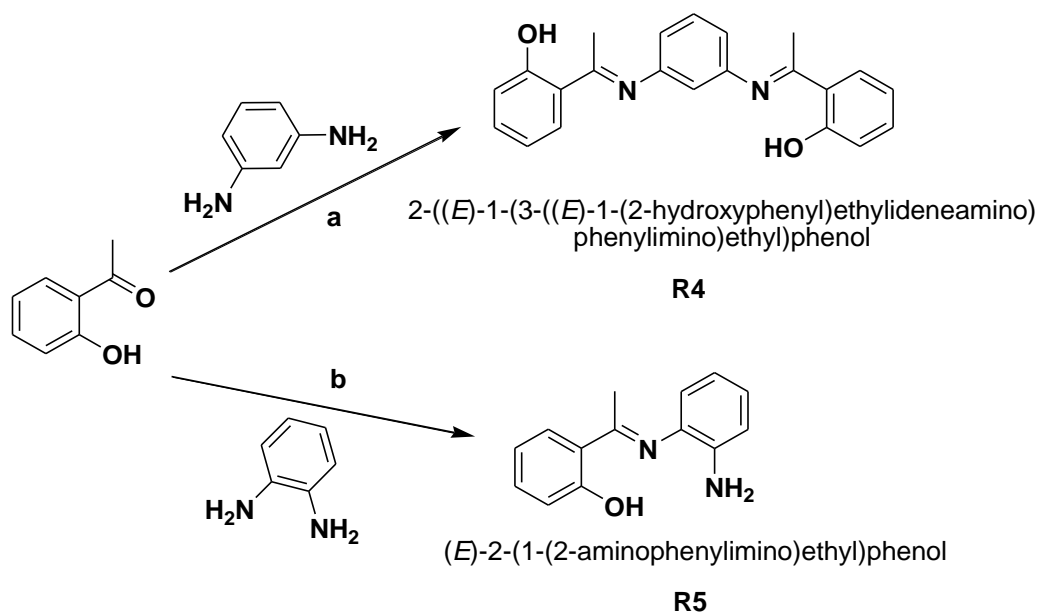
5.4.1. Experimental

5.4.1.1. Materials and measurements

2-Hydroxyacetophenone was obtained from Alfa Aesar and ortho-phenylenediamine from Loba Chemie (India). Meta-phenylenediamine and all the metal salts of analytical grade were procured from Merck, India and further used without purification. The IR spectra were recorded on a Thermo Scientific Nicolet 6700 FT–IR spectrometer in the range 4000–400 cm^{-1}. The ^1H–NMR and ^{13}C–NMR spectra were recorded on a Bruker 500 MHz (USA), using $CDCl_3$ and CD_3OD as solvent, TMS as an internal standard. The CHNS data were determined on a Vario MICRO Cube. The mass spectra were recorded on Bruker–MicrOTOF–Q II (USA). The differential pulse voltammetric experiments were performed using a CHI760E Electrochemical Workstation (USA) with a conventional three electrode cell system consisting of glassy carbon electrode as working electrode, calomel electrode as reference electrode and platinum wire as counter electrode. The UV–vis absorption spectra were recorded on a Shimadzu UV–2450 spectrophotometer and the fluorescence emission spectra were measured on a HORIBA Scientific, Fluoromax–4 spectrofluorometer using both the excitation and emission slit width value of at 0.5 nm. For all the measurements, excitation wavelength was 375 nm. The pH was determined through a Eutech CyberScan pH 510 (Singapore). All the metal solutions for the study were prepared in methanol. Stock solution (10 mM) of receptors (**R4** and **R5**), and of different metal chlorides and nitrates were prepared in methanol.

5.4.1.2. Synthesis of the Schiff base receptors

The receptors were prepared by condensation as per reported procedure [51] with a slight modification (Scheme 5.3). A typical procedure for the synthesis of schiff bases is as

2-((*E*)-1-(3-((*E*)-1-(2-hydroxyphenyl)ethylideneamino)
phenylimino)ethyl)phenol

R4

(*E*)-2-(1-(2-aminophenylimino)ethyl)phenol

R5

Scheme 5.3. Synthetic route for target compounds performing through; (a) for receptor **R4** and (b) for **R5**.

follows: a solution of 2-Hydroxyacetophenoene (10.0 mmol, 1.36 g) dissolved in 20 ml ethanol was slowly added to a solution of 1,2-phenylenediamine or 1,3-phenylenediamine (5.0 mmol, 0.54 g) in a 15 ml ethanol. The reaction mixture was magnetically stirred for about 30 min and then refluxed for 3 h at 70 °C. The resulting solution was concentrated by evaporation in vacuum and allowed to stand. The solid crystals were obtained and washed throughly with distilled water followed by rewashing with cold ethanol and recrystallized in ethanol. The pure schiff bases were isolated as a crystalline solid. The structures of receptors were characterized by FT–IR, ^{1}H–NMR, ^{13}C–NMR and HRMS spectroscopy.

***N,N′*-bis(o-hydroxyacetophenone)-m-phenylenediamine (R4):** Yield: 1.31 g (76%); color: brown-black solid; m.p. 147–149 °C, and Anal. calcd. for $C_{22}H_{20}N_2O_2$: C=76.72, H=5.85, N=8.13, found: C=76.62, H=5.82, N=8.28; FT–IR (KBr, v cm^{-1}): 3364 (O−H), 1602 (C=N), 1398 (C=C), 1301 (C−N), 1247, 1155 (C−O); ^{1}H–NMR (CDCl$_3$, 500 MHz, δ ppm): 2.337–2.382 (d, 6H), 3.732 (s, 1H), 6.240–6.297 (t, 1H), 6.469–6.515 (t, 1H), 6.731–6.746 (d, 1H), 6.863–6.914 (m, 2H), 6.998–7.031 (t, 2H), 7.137–7.168 (t, 1H), 7.341–7.419 (m, 2H), 7.603–7.646 (m, 2H), 14.413 (s, 1H); ^{13}C–NMR (CDCl$_3$, 500 MHz, δ ppm): 17.07, 17.27, 107.76, 111.39, 111.58, 113.97, 117.69, 118.06, 118.23, 118.28, 119.68, 128.88, 129.01, 129.83, 129.92, 132.94, 133.23, 147.22, 147.99, 161.89, 162.00, 171.52; HRMS (ESI, *m/z*): [M+Na]$^+$ calcd. for $C_{22}H_{20}N_2O_2$: 367.1422, found 367.1403.

149

***N*-(o-hydroxyacetophenone)-o-phenylenediamine (R5):** Yield: 0.78 g (69%); color: yellow solid; m.p. 108–110 °C; Anal. calcd. for $C_{14}H_{14}N_2O$: C=74.31, H=6.24, N=12.38, found: C=74.21, H=6.17, N=12.47; FT–IR (KBr, v cm^{-1}): 3449, 3341 (NH$_2$), 1613 (C=N), 1496 (C=C), 1416 (C–N), 1301, 1254 (C–O); ^{1}H–NMR (CDCl$_3$, 500 MHz, δ ppm): 2.382 (s, 3H), 3.656 (s, 2H), 6.722–6.737 (d, 1H), 6.789–6.817 (t, 2H), 6.897–6.927 (t, 1H), 7.032–7.063 (t, 2H), 7.376–7.407 (t, 1H), 7.652–7.667 (d, 1H), 14.815 (s, 1H); ^{13}C–NMR (CDCl$_3$, 500 MHz, δ ppm): 17.22, 115.79, 118.25, 118.32, 118.49, 119.78, 121.58, 126.20, 129.07, 133.24, 133.31, 138.21, 162.18, 173.69; HRMS (ESI, *m/z*): [M+H]$^+$ calcd. for $C_{14}H_{14}N_2O$: 227.1184, found 227.1188.

5.4.2. Results and discussion

The addition of a small amount of aluminium induced sharp intense blue fluorescence and the resultant solution were then subjected to UV–vis absorption, fluorescence emission, ESI–MS, electrochemical (DPV) and ^{1}H–NMR studies.

5.4.2.1. UV–vis spectral responses of the receptors

In preliminary study, the molecular interaction of the receptors (**R4** and **R5**) was explored by UV–vis absorption spectrum in methanolic solution (50 μM) in the presence of 50 μM of a variety of metal ions (Cr^{3+}, Ca^{2+}, Ba^{2+}, Fe^{2+}, Fe^{3+}, Co^{2+}, Cu^{2+}, Cd^{2+}, Cs^+, Hg^{2+}, Gd^{3+}, Li^+, K^+, Na^+, Mg^{2+}, Mn^{2+}, Nd^{3+}, Sr^{2+}, Zn^{2+}, Pb^{2+}, Ni^{2+} and Al^{3+}) and the spectra shown in Figure 5.32(a and b). Both the receptors show two absorption bands centered at 324 nm and 254 nm. These bands arise primarily due to n–π* and π–π* transitions. Upon addition of Al^{3+} ions, both the receptors (**R4** and **R5**) exhibit a weak absorption band in the range at about 380 nm and 324 nm, respectively. It has been found that, upon addition of metal ions such as mainly Cu^{2+} and Cr^{3+} with receptor **R4** and Cu^{2+}, Cr^{3+} and Ni^{2+} with receptor **R5**, shows a significant spectral changes in the absorption band in the region of 330–430 nm under identical conditions. On the other hand, the other metal ions did not cause any significant spectral changes under the identical conditions. Therefore, the results show that these metal ions (Al^{3+}, Cu^{2+}, Cr^{3+} and Ni^{2+}) could be distinguished easily over other ones, using UV–vis spectroscopy. To further explore the utility of both the receptors (**R4** and **R5**) as a metal ion-selective receptor for these metal ions, the fluorescence emission behavior of the receptors was investigated.
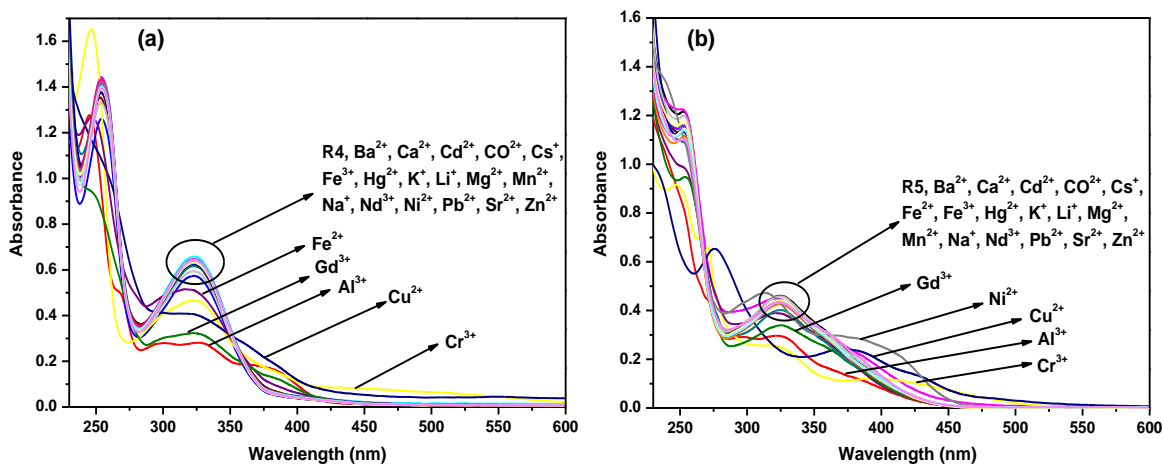
Figure 5.32. Absorption spectra of receptors **R4** and **R5** in methanol in the presence of 1.0 equivalent of various metal ions.

5.4.2.2. Fluorescence emission spectral responses of receptors
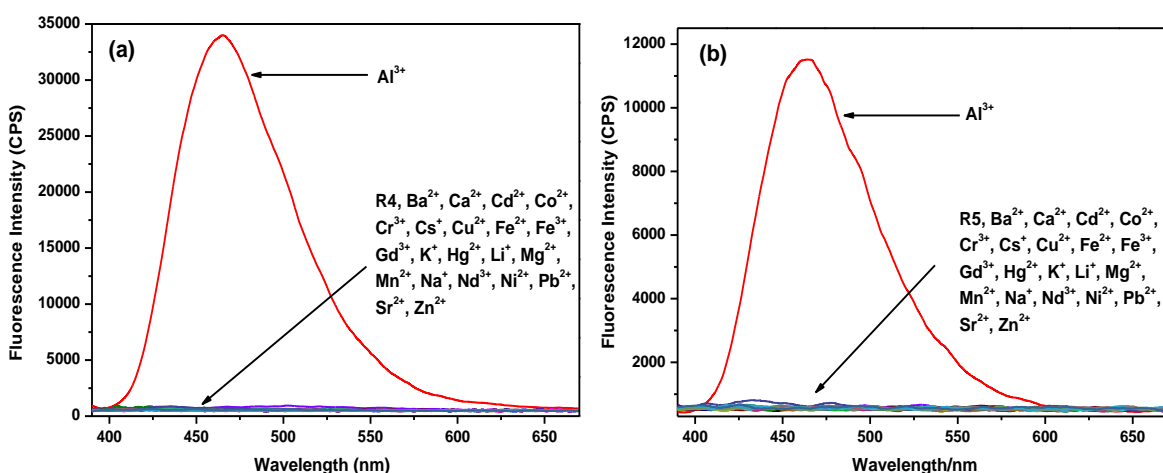

Figure 5.33. Fluorescence spectra of; (a) receptor **R4** and (b) receptor **R5** in the presence of 1.0 equivalent of a range of metal ions (40 µM) in methanol at λ_{ex} = 375 nm.

The fluorescence emission spectra of 40 µM solution of receptors **R4** and **R5** was examined in the presence of 40 µM of Al^{3+} and many other matal ions (Ba^{2+}, Ca^{2+}, Cr^{3+}, Fe^{2+}, Fe^{3+}, Co^{2+}, Cu^{2+}, Cd^{2+}, Cs^{+}, Hg^{2+}, Gd^{3+}, Li^{+}, K^{+}, Na^{+}, Mg^{2+}, Mn^{2+}, Nd^{3+}, Sr^{2+}, Zn^{2+}, Pb^{2+} and Ni^{2+}). It is seen from the fluorescence spectra Figure 5.33(a and b) that the addition of Al^{3+} generate high fluorescence emission peak with λ_{max} = 465 nm and 464 nm for receptors **R4** and **R5** respectively. Other metal ions do not generate any significant fluorescence under the identical conditions. Thus the response of the receptors to Al^{3+} is highly selective and can be used for its determination in the presence of these metals by means of calibration plot.
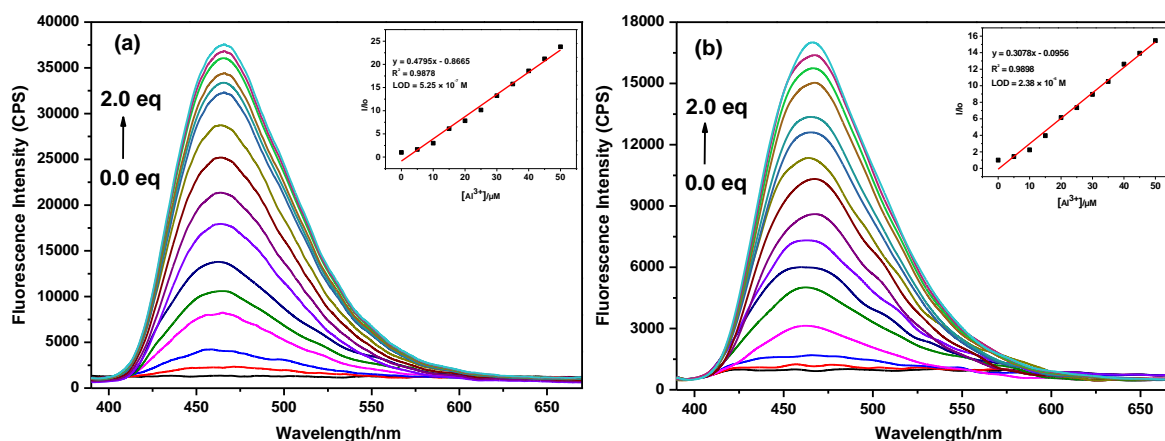
5.4.2.2.1. Quantitative fluorescence exposure of Al^{3+} ions

Figure 5.34. Fluorescence spectra of receptor **R4** and **R5** (40 µM) in methanol as a function of exterior gradual addition of Al^{3+} (from 0.0 to 100 µM); from bottom to top. Inset is the linear plot between amounts of metal ion (0.0–50 µM) added and intensity at; λ_{em} = 465 nm and 464 nm for receptor **R4** and **R5**, respectively.

Furthermore, the fluorogenic quantitative sensing ability of the probe for Al^{3+} was studied. It was noticed that upon addition of increasing concentration of Al^{3+} (0.0, 5, 10, 15, 20, 25, 30, 35, 40, 45, 50, 60, 70, 80, 90, 100 µM), the fluorescence intensity of the receptors **R4** and **R5** steadily increased up to 60 µM and after this no significant changes were noticed (Figure 5.34 a and b). On behalf of this, the quantitative response of the probe with Al^{3+} metal ions was examined, and working curve was obtained (inset in the same Figure). At the same time, a 1 nm and 3 nm red-shifts at the emission maxima were also observed for receptors **R4** and **R5**, respectively. The curve showed a good linear relationship between the fluorescence intensity of receptor and concentration of the Al^{3+} ions added (0–50 µM), which benefits for the establishment of working curves in practical
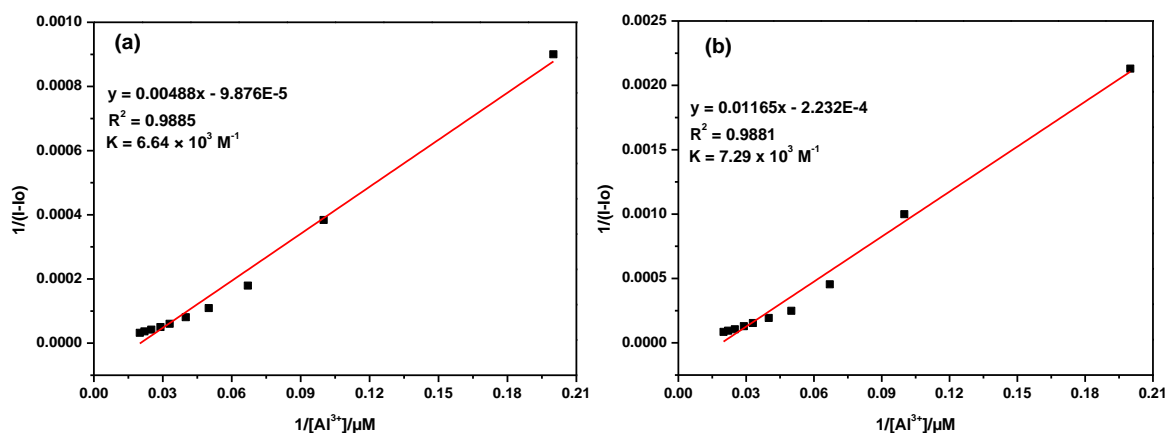

Figure 5.35. Benesi-Hildebrand plot (a and b) for the determination of stability constant of **R4** and **R5** for Al^{3+} in methanol at λ_{ex} = 375 nm.

Al^{3+} detection. Thus, the detection limit for Al^{3+} has been determined to be 5.25×10^{-7} M and 2.38×10^{-6} M for receptor **R4** and **R5**, respectively. The binding constants of the receptor–Al^{3+} complex for **R4** and **R5** was determined and found to be 6.64×10^{3} M^{-1} and 7.29×10^{3} M^{-1} respectively (Figure 5.35 a and b), as obtained by fitting the data to the Benesi–Hildebrand expression.

5.4.2.2.2. Selectivity of the receptor to Al^{3+} over other cations

To further explore the selectivity of Al^{3+} over other metal ions, competition experiments were carried out, where the receptors **R4** and **R5** were first treated with 1.0 equivalent of various metal ions (including Ba^{2+}, Ca^{2+}, Cs^{+}, Fe^{2+}, Fe^{3+}, Cr^{3+}, Gd^{3+}, K^{+}, Li^{+}, Na^{+}, Mg^{2+}, Mn^{2+}, Hg^{2+}, Nd^{3+}, Pb^{2+}, Co^{2+}, Cd^{2+}, Cu^{2+}, Zn^{2+}, Ni^{2+} and Sr^{2+}), followed by adding 1.0 equivalent of Al^{3+}. Figure 5.36(a and b), shows that the addition of Al^{3+} to the mixture of competing metal ions and receptor produces remarkable changes in the fluorescence intensity and no significant changes in fluorescent intensity was observed excluding Cd^{2+}, Fe^{2+}, Ni^{2+}, Zn^{2+}; and Cd^{2+}, Cs^{+}, Fe^{2+}, Zn^{2+} and Ni^{2+} for receptors **R4** and **R5**, respectively. Therefore, the synthesized receptors are adequate in the detection of Al^{3+} in the presence of competing metal ions and thus it can be used for its estimation in biological or environmental samples where other metals usually co-exist with Al^{3+}.
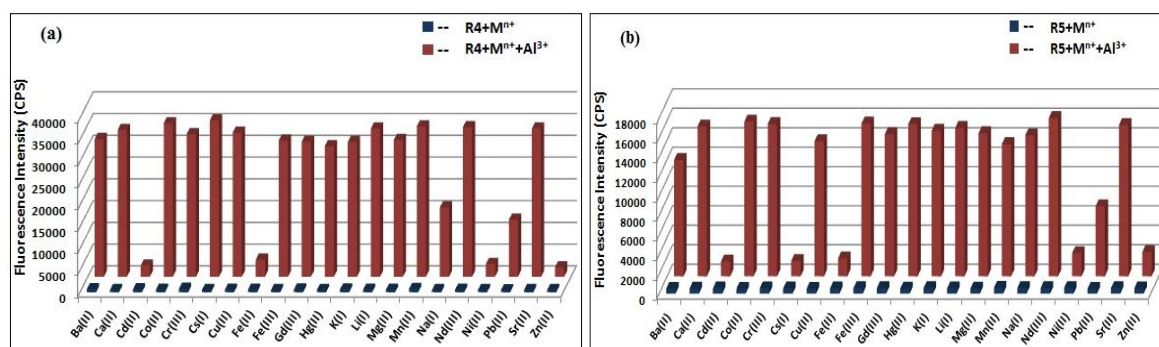

Figure 5.36. Bar diagram screening the fluorescence response of other diverse metal ions upon binding with; (a) receptor **R4** and (b) receptor **R5** in methanol (dark blue bar portion) and to the mixture of 1.0 equivalent of other competing metal ions with 40 μM of Al^{3+} (red bar portion).

5.4.2.2.3. Effect of pH

Further, to ensure the metal ion selectivity for some biological applications, it is exceptionally important to examine the pH effect. Therefore, the effect of pH on the fluorescence emission intensity of receptors **R4** and **R5**; and its complex with Al^{3+} ions were examined (methanol:water; 80:20) in the pH range of 2–10 and no significant

changes were observed in the fluorescence intensity of the receptors only. However, on the addition of Al^{3+} led to the fluorescence enhancement over a wide pH range of 6.0–8.0 (Figure 5.37). It was observed that, in the alkaline pH range i.e. pH > 7.0, fluorescence intensity declined due to formation of salt. On the other hand, the fluorescence emission intensity of receptor–Al^{3+} complex was quenched due to the protonation of receptors in acidic conditions. Therefore, the result shows that the receptors may be suitable for measuring Al^{3+} ions in the physiological pH range and favourable for its application in biological samples.
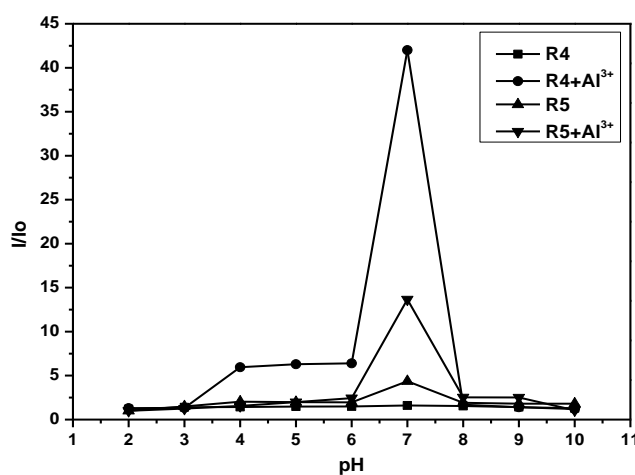

Figure 5.37. Fluorescence intensity recorded for receptor–Al^{3+} complex in aqueous methanolic solution (80:20) at various pH values shown at the slit width value of 0.5 nm.

5.4.2.2.4. Reversibility of the receptor towards metal ions

Reversibility is a necessity for developing a novel sensor for practical utility. Thus, the chemical reversibility of the receptors **R4** and **R5** were examined by adding chelating agent EDTA to Al^{3+}. The binding constant between Al^{3+} and EDTA is 1.30×10^{16} M^{-1} [52]; conversely the binding constants were found to be 6.64×10^3 M^{-1} and 7.29×10^3 M^{-1} for receptors (**R4** and **R5**) and Al^{3+}. Thus, the addition of increasing concentration of EDTA (0.0–1.0 equivalent) to a mixture of receptors (**R4** and **R5**) and Al^{3+} resulted in quenching of the fluorescence emission intensity at 465 nm and 464 nm gradually (Figure 5.38 a and b). It was observed that on adding of EDTA to the receptor–Al^{3+} solution, metal ions were displaced from the ligand-metal ion complex which point towards the chelation of Al^{3+} with EDTA releasing the free receptors **R4** and **R5** and receptor–Al^{3+} complex goes to turn–off. Additionally, the fluorescence response of the probe–Al^{3+} with added equivalent amount of EDTA was examined under UV light and the change in color demonstrated inset in the same figure. Such reversibility and regeneration are important for the production of devices for detection of the Al^{3+} ions.
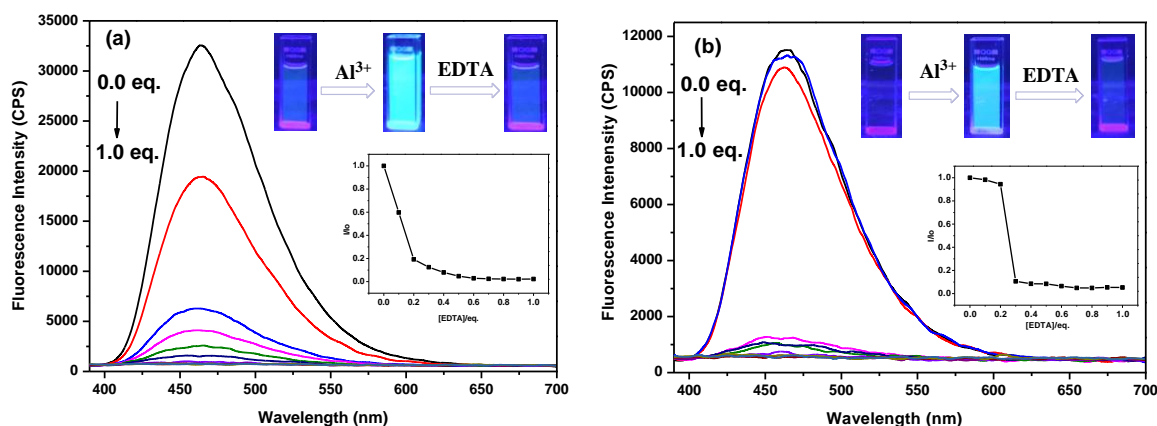
Figure 5.38. Reversibility experiment from fluorescence emission spectra of; (a) receptor **R4** and (b) receptor **R5** showing the changes of receptor–Al^{3+} complex upon addition of EDTA (0.0–1.0 equivalent). Inset: images showing the corresponding fluorescence color changes under a UV lamp (top) and addition of EDTA equivalent as a function of fluorescence intensity (bottom).

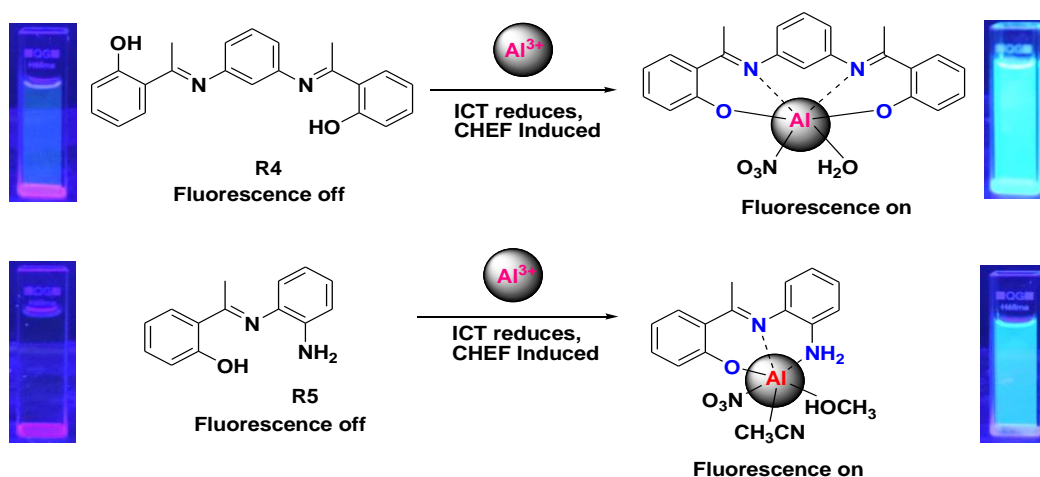### 5.4.2.2.5. Stoichiometries of receptor complexes

Figure 5.39. Proposed mechanism (CHEF) for the fluorescent sensing of receptor towards the Al^{3+} metal ions.

Further, a most probable coordination mode for receptors **R4** and **R5** with Al^{3+} was proposed and scrutinized. The changes in color of the receptors before and after addition of Al^{3+} were observed under UV radiation depicted in Figure 5.39. In the absence of Al^{3+} the quenching of fluorescence intensity might be sufficient owing to the extent of intramolecular charge transfer in the receptors [53]. On the other hand, the chelation of receptors with Al^{3+} restricts the free azomethine carbon with respect to the hydroxyl phenyl ring and consequences in a significant fluorescence intensity augmentation followed by a CHEF mechanism demonstrated in the same figure.

The stoichiometry of the receptor–Al^{3+} complex with **R4** and **R5** was determined by the job's method. Thus, the plot of fluorescence emission versus mole fraction [R]/([R]+[Al^{3+}]), was drawn in Figure 5.40(a and b). The maxima occur at 0.5 indicating 1:1 stoichiometry.
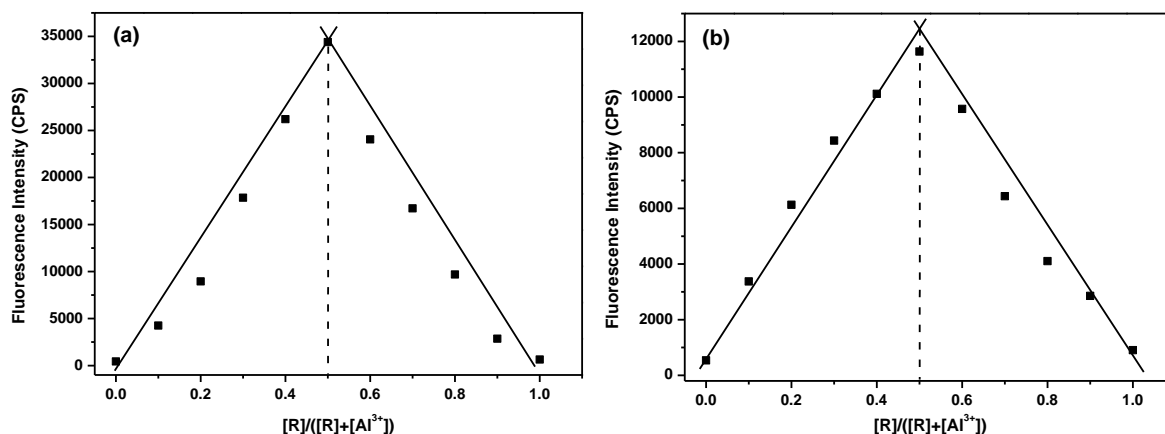

Figure 5.40. Job's plot for the interaction of receptor **R4** and **R5** with various mole fractions of Al^{3+}.
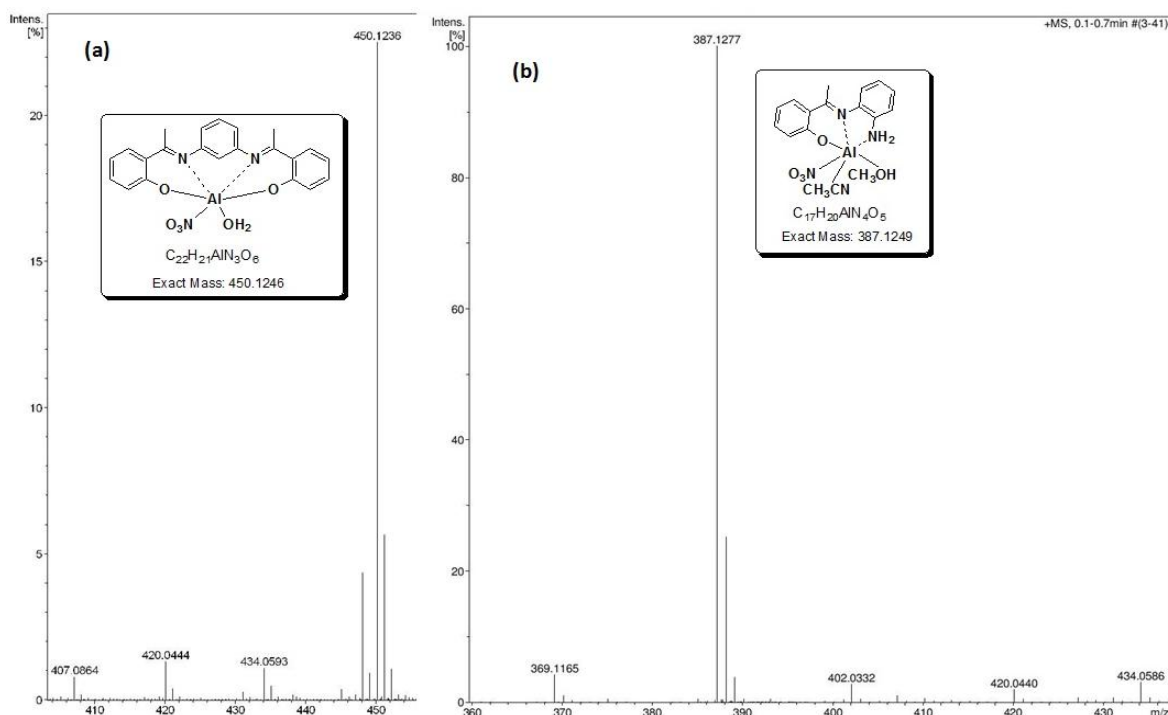
Figure 5.41. HRMS spectra of; (a) receptor **R4** and (b) receptor **R5** upon addition of $Al(NO_3)_3.9H_2O$ in methanol.

The stoichiometry was further confirmed by HRMS studies. HRMS plots are given in Figure 5.41(a and b), where peaks for m/z = 450.1236, 387.1277 are obtained for both the receptors **R4** and **R5**, respectively. The peak at m/z = 450.1236 was the isotopic peak of compound [**R4**–H+Al(NO_3)+H_2O]$^+$, the peak at m/z = 387.1277 corresponds to [**R5**–

$H+Al(NO_3)+CH_3OH+CH_3CN]^+$. As a little amount of moisture introduced with hydrated aluminium salts may hydrolyse it and so lead to the formation of hydroxylated aluminium compounds. Therefore, it can be assumed that the aluminium ions may be chelated by the counter anions or solvent in order to satisfy the need of six-coordination. Thus, HRMS studies further confirm the 1:1 stoichiometry of Al^{3+} complex with receptors.

5.4.2.2.6. Solvent effect

In order to confirm the consequence of the unlike solvents such as DMSO, THF, DMF, acetone and methanol; fluorescence spectrophotometry was explored for the receptors followed by addition of Al^{3+} and the results are depicted in Figure 5.42(a and b). Thus, the change in fluorescence intensity owing to the unlike binding mode of the receptors with Al^{3+} ions was observed in different solvents. Consequently, methanol was concluded as the best solvent for the spectrophotometric investigation of the receptors.
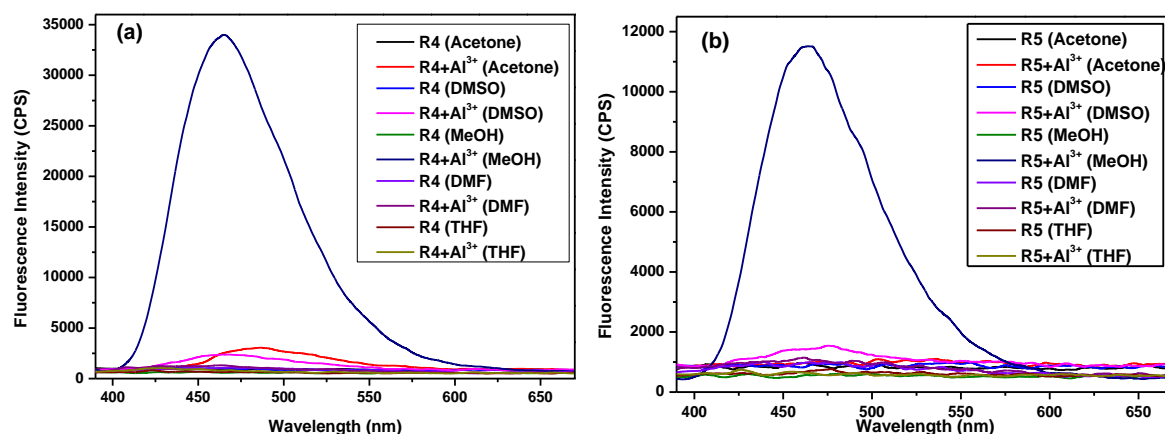

Figure 5.42. The effect of a range of solvents on the fluorescence intensity; (a) for receptor **R4** and (b) for **R5**.

5.4.2.3. ^{1}H–NMR titration

Stoichiometry was further confirmed by ^{1}H–NMR titration experiments and spectral changes are shown in Figure 5.43(a and b). The protons of aromatic ring (6.12–7.69 ppm and 6.58–7.67 ppm for receptor **R4** and **R5**, respectively) as well as the protons of aliphatic group shifted to downfield and became more complicated upon addition of 1.0 equivalent of the Al^{3+} metal ions which indicated that the structure of receptors became more rigid after coordination with Al^{3+}. Additionally, the peak at 2.26 ppm due to $-NH_2$ group (Figure 5.43b) disappeared after addition of 1.0 equivalent of Al^{3+}, clearly indicating the bonding between $-NH_2$ and Al^{3+} ions. These observations apparently designated that the original intramolecular
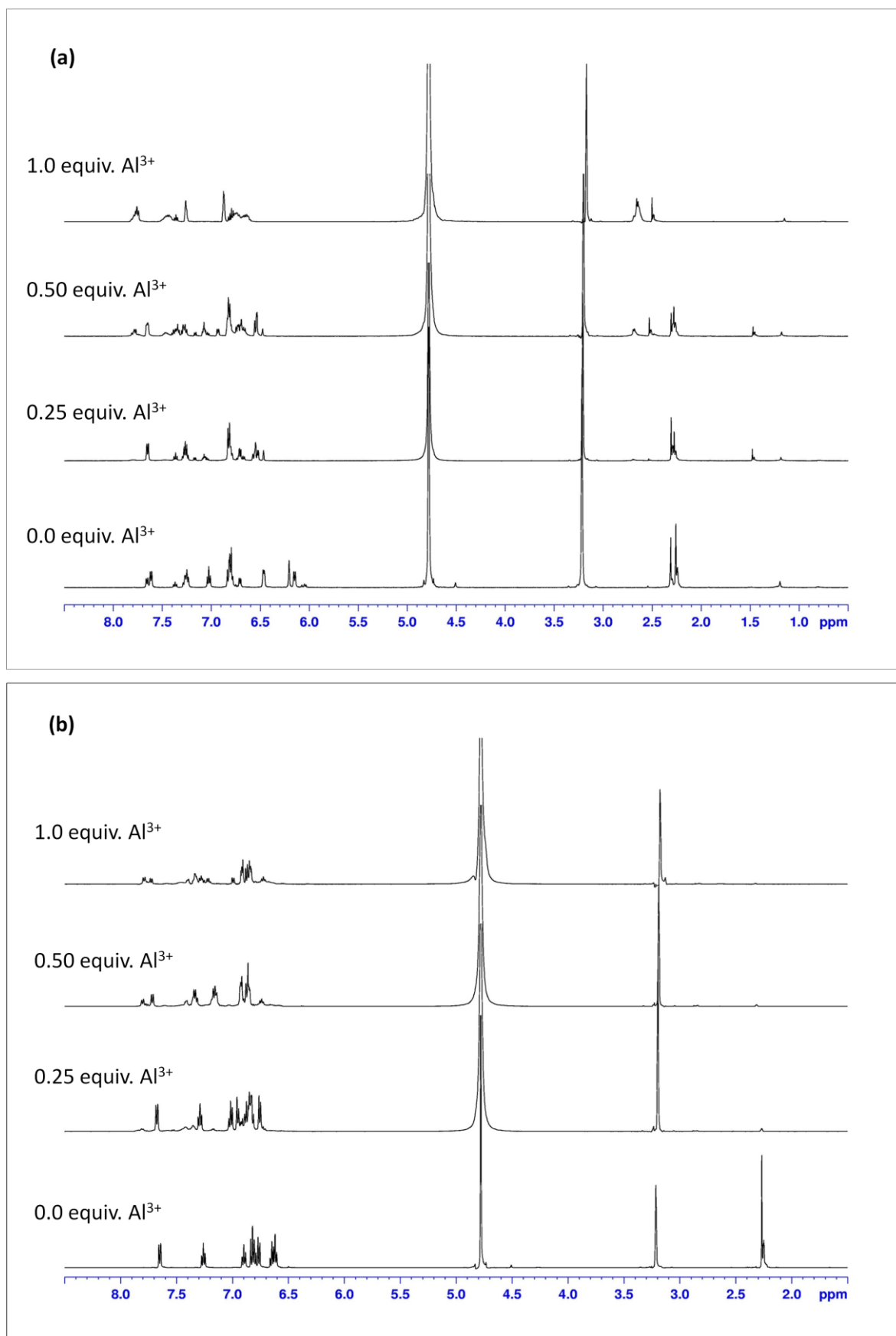
Figure 5.43. ^{1}H–NMR spectra of receptor **R4** (a) and receptor **R5** (b) with 0.0, 0.25, 0.5 and 1.0 equivalent Al^{3+} ions in CD_3OD.

hydrogen bonding interaction between the phenolic O–H and the nitrogen atom of the imine has been interrupted by the addition of Al^{3+} and a complicated ^1H–NMR spectrum is observed [54, 55].

5.4.2.4. Electrochemical measurements

Voltammetric studies were also carried out to support the view that Al^{3+} forms complexes with the receptors in methanol via ferrocene as a reference in DCM. Differential pulse voltammograms for applied potential as a function of current attained for both the receptors and their complex via Al^{3+} depicted in Figure 5.44(a and b). Owing to this the oxidation peaks were detected at 0.296, 0.624 and 1.128 V for receptor **R4** whereas all these peaks were shifted to 0.332, 0.636 and 1.108 V respectively and a new peak also observed at 1.244 V after addition of Al^{3+} to the receptor. On the other hand, the oxidation peaks were observed for receptor **R5** at 0.184, 0.628, 0.872 and 1.200 V while after addition of Al^{3+} all the peak potentials were shifted and found at 0.152, 0.680, 1.092 and 1.204 V. Thus, it can be concluded that the changes in redox potentials after addition of Al^{3+} ions confirm the formation of **R4**–Al^{3+} and **R5**–Al^{3+} complex.
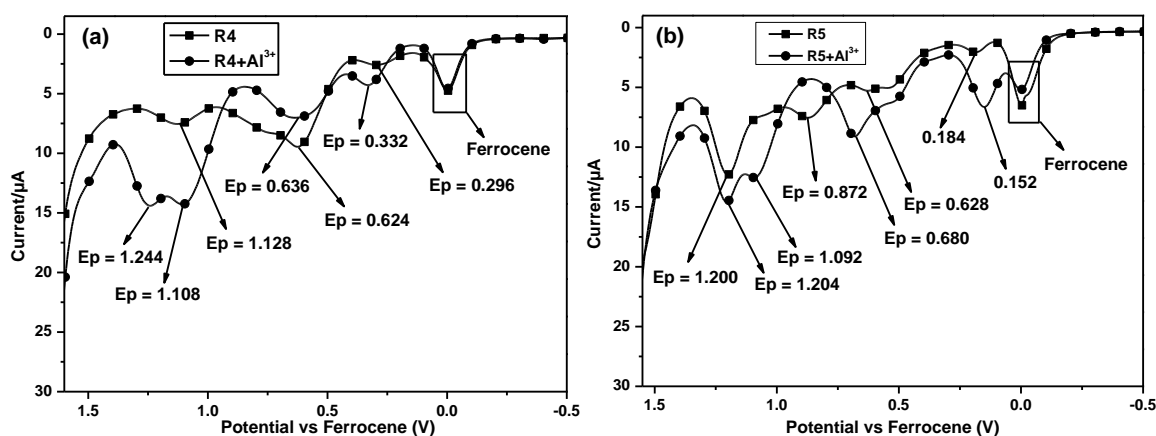
Figure 5.44. Differential pulse voltammograms; (a) for receptor **R4** and (b) for **R5** and its complex subsequent to addition of 1.0 equivalent of Al^{3+} in methanol.

5.4.2.5. Logic function

There are numerous reports in the literature on multifunctional molecular logic devices which engage multiple fluorescent output modes. Therefore, starting with two integrated inputs (Al^{3+} and EDTA) the fluorescence behavoir of both the receptors **R4** and **R5** have ability to exhibit the logic function via an emission output. The value of the emission can be obtained only when individual Al^{3+} is present with receptors **R4** and **R5** and the value of the all other actions are 0 (Figure

5.45). Furthermore, the logic function can be successfully developed when we observe the intensity of fluorescence emission at 465 and 464 nm. Thus, on the basis of these two input signals the ON–OFF mechanism of the developed sensor can be symbolized as a combination of NOT and AND gate whether one of the two input lines contains an inverter [56–58]. Consequently, the fluorescence intensity changes at 465 and 464 nm upon the inputs of Al^{3+} and EDTA which can be interpreted as a monomolecular circuit depicted in the same figure.
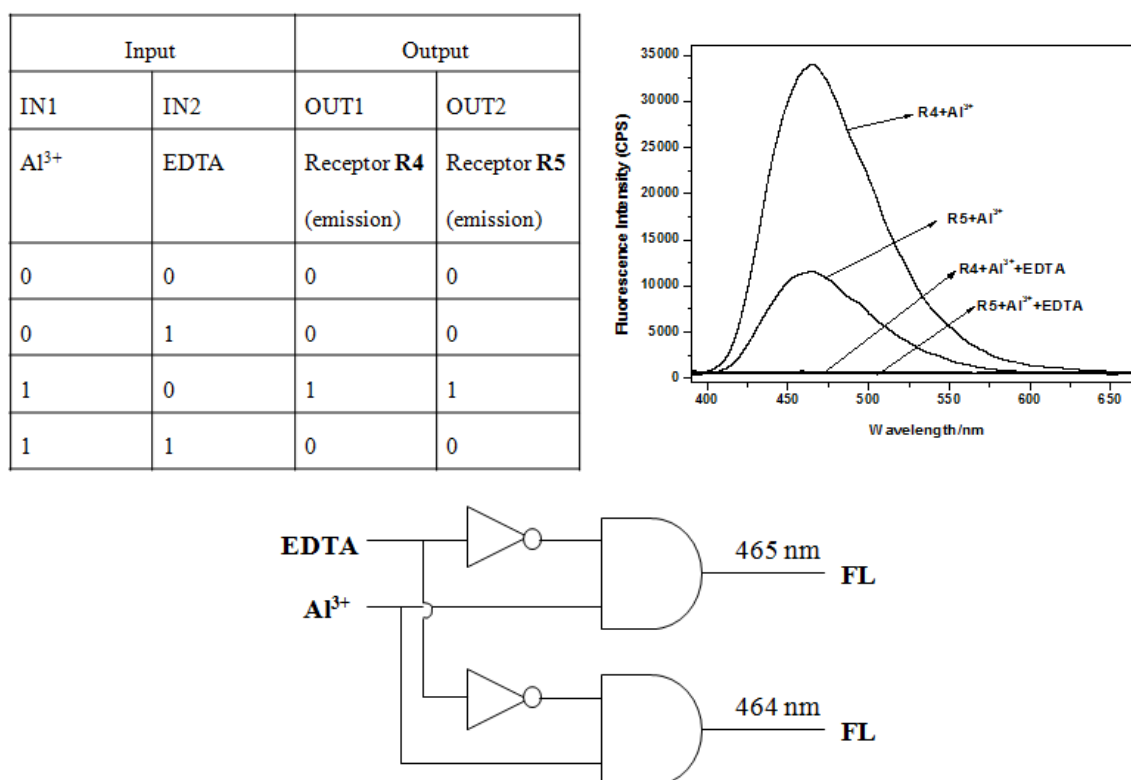
Input		Output	
IN1	IN2	OUT1	OUT2
Al^{3+}	EDTA	Receptor **R4** (emission)	Receptor **R5** (emission)
0	0	0	0
0	1	0	0
1	0	1	1
1	1	0	0

Figure 5.45. Truth table and the monomolecular circuit based on Al^{3+} and EDTA by means of fluorescence intensity. Spectral changes upon addition of EDTA to R–Al^{3+} complex (upper right side).

5.4.3. Conclusion

In summary, we have effectively developed an inexpensive and simple naked-eye fluorescent probe (receptors **R4** and **R5**) for Al^{3+} in methanol media. It shows high sensitivity and fluorescence selectivity towards Al^{3+} over other metal ions. Further, the reversibility of the receptors was also examined by quenching the fluorescence intensity via EDTA titration. The detection limit was sufficiently low to detect the micromolar concentration of Al^{3+}. More importantly, the receptors work efficiently in the physiological pH spectrum and shows higher selectivity towards Al^{3+} ions. Not only this, we can

illustrate the one set of integrated logic gates: a combination of NOT and AND logic gate approach under the actions of the receptor–Al^{3+} complex behavior by means of EDTA, through the fluorescence emission. Thus, we believe both the receptors (**R4** and **R5**) have the ability to serve as a practical sensor for Al^{3+} analyzing a large number of biological, analytical and environmental samples.

¹H-NMR Spectrum (500 MHz, CD₃OD) of R1

^{13}C-NMR Spectrum (500 MHz, CDCl$_3$) of R1

¹H-NMR Spectrum (500 MHz, CDCl₃) of R2

¹³C-NMR Spectrum (500 MHz, CDCl₃) of R2

ESI-MS Spectrum of R2

^{1}H-NMR Spectrum (500 MHz, CDCl$_3$) of R3

¹³C-NMR Spectrum (500 MHz, CDCl₃) of R3

ESI-MS Spectrum of R3

¹H-NMR Spectrum (500 MHz, CDCl₃) of R4

^{13}C-NMR Spectrum (500 MHz, CDCl$_3$) of R4

ESI-MS Spectrum of R4

Acquisition Parameter

Source Type	ESI	Ion Polarity	Positive	Set Nebulizer	0.4 Bar
Focus	Not active	Set Capillary	4500 V	Set Dry Heater	180 ℃
Scan Begin	50 m/z	Set End Plate Offset	-500 V	Set Dry Gas	4.0 l/min
Scan End	3000 m/z	Set Collision Cell RF	150.0 Vpp	Set Divert Valve	Source

¹H-NMR Spectrum (500 MHz, CDCl₃) of R5

^{13}C-NMR Spectrum (500 MHz, CDCl$_3$) of R5

173.69

162.18

138.21
133.31
133.24
129.07
126.20
121.58
119.78
118.49
118.32
118.25
115.79

17.22

BRUKER

ESI-MS Spectrum of R5

Acquisition Parameter

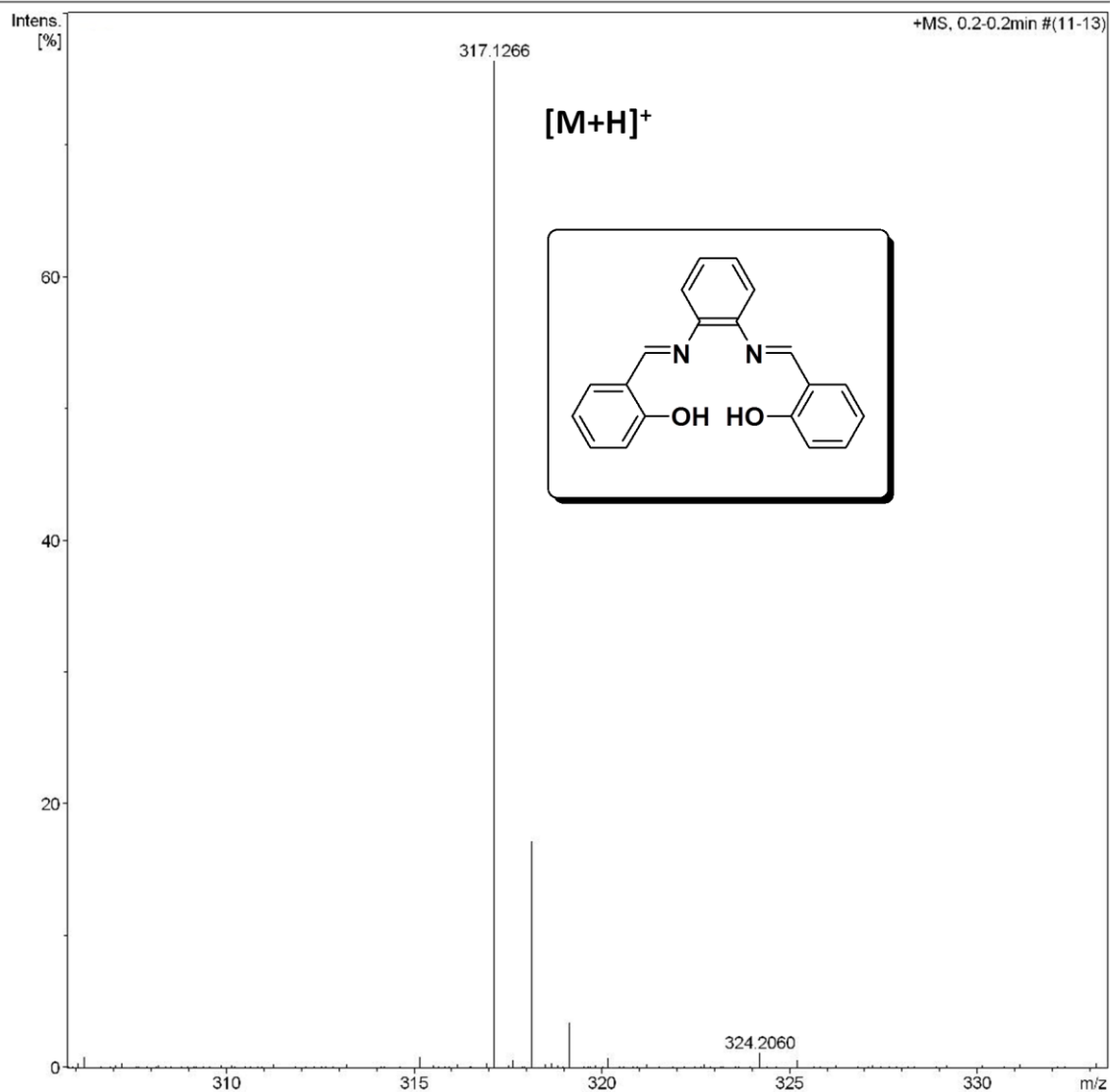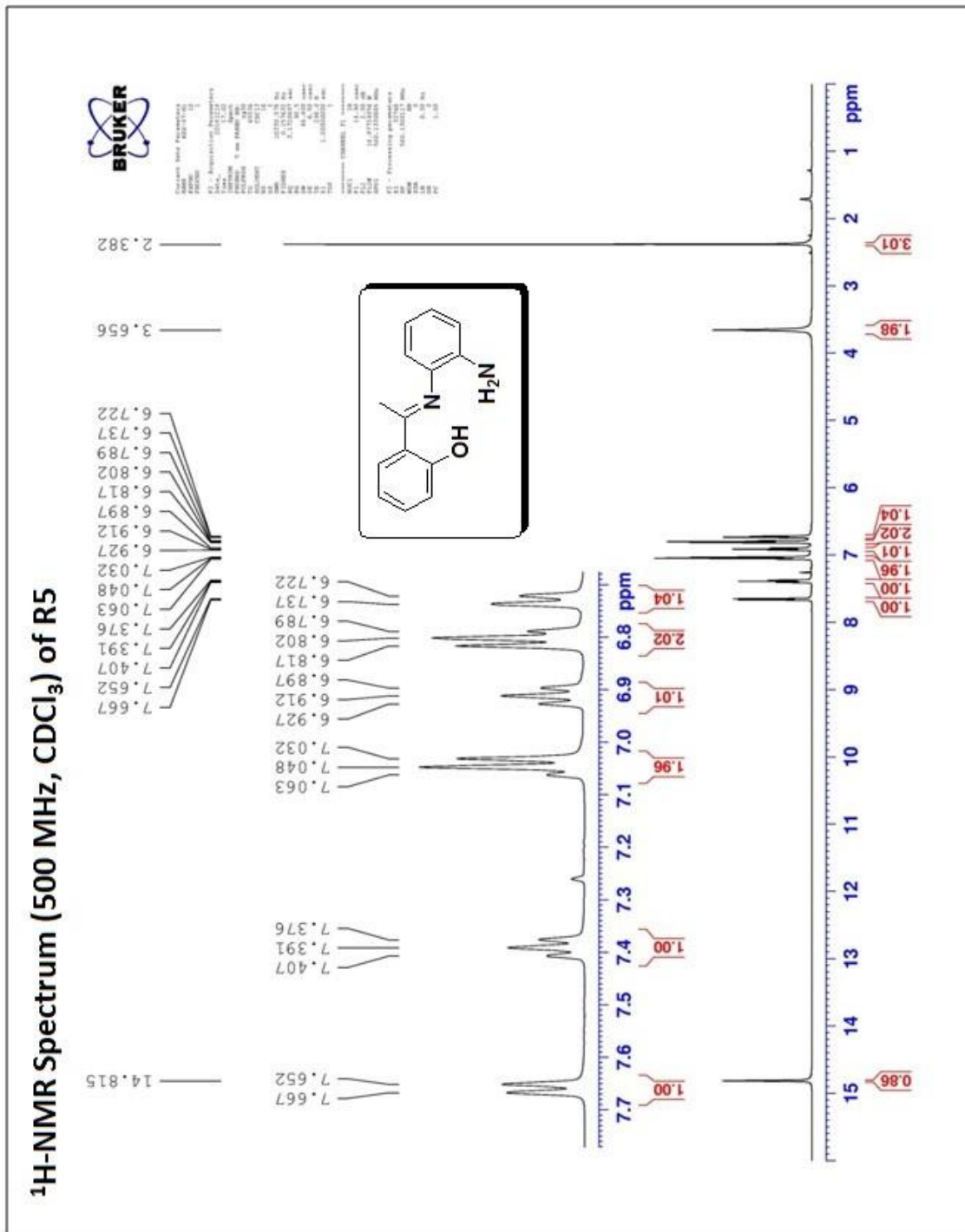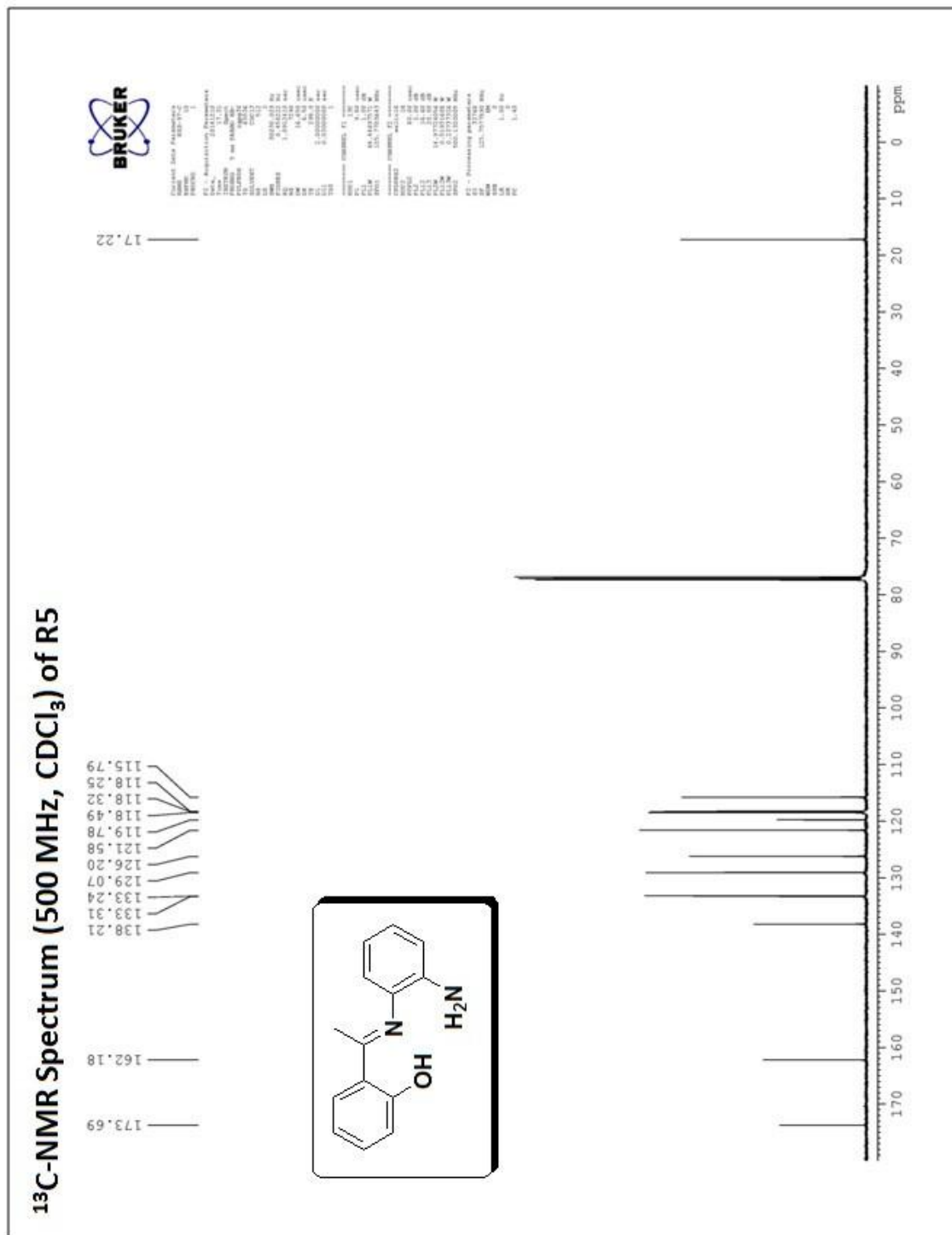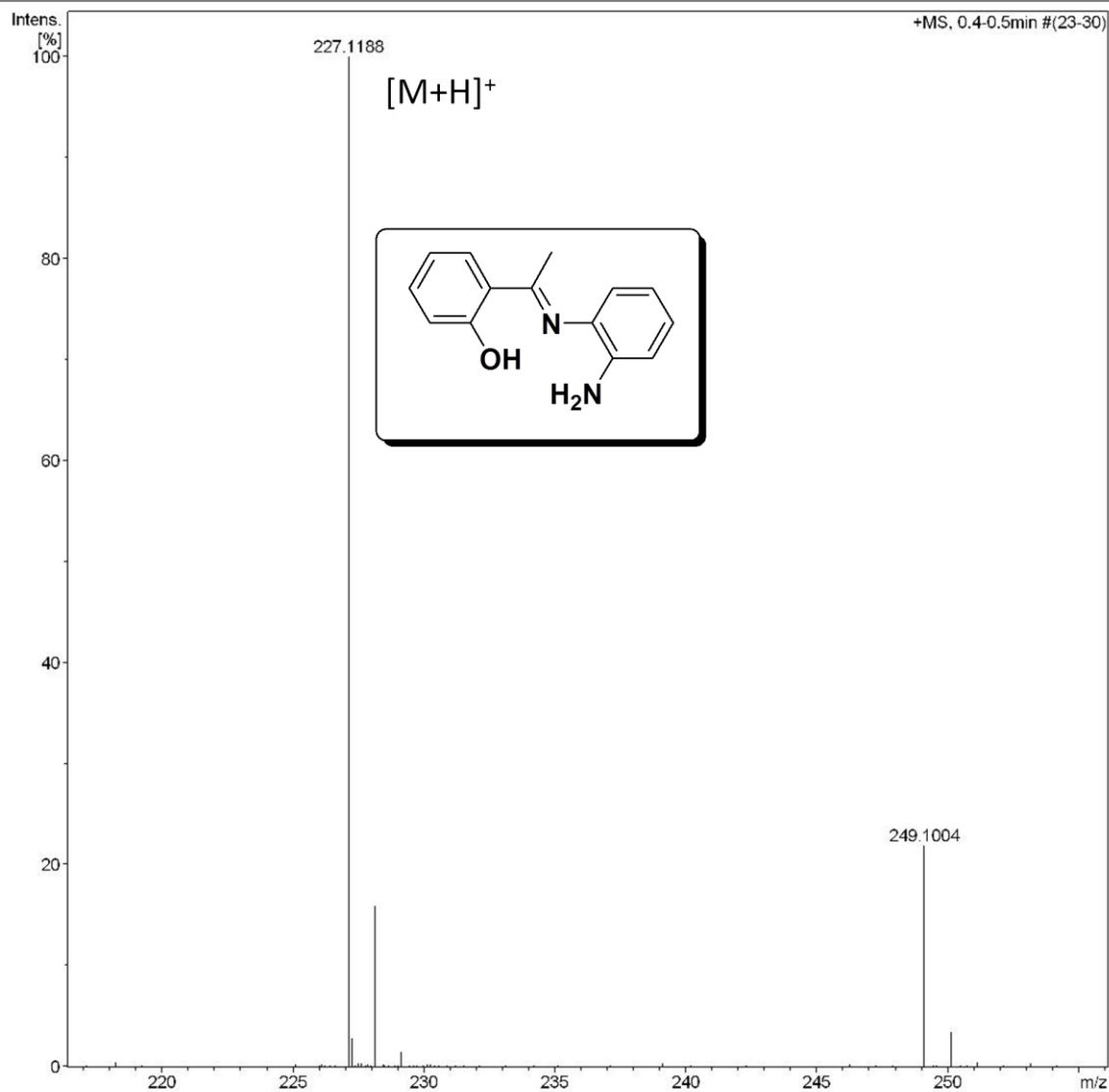|					
Source Type	ESI	Ion Polarity	Positive	Set Nebulizer	0.4 Bar
Focus	Not active	Set Capillary	4500 V	Set Dry Heater	180 °C
Scan Begin	50 m/z	Set End Plate Offset	-500 V	Set Dry Gas	4.0 l/min
Scan End	3000 m/z	Set Collision Cell RF	150.0 Vpp	Set Divert Valve	Source

References

1. K.B. Kim, D.M. You, J.H. Jeon, Y.H. Yeon, J.H. Kim, C. Kim, A fluorescent and colorimetric chemosensor for selective detection of aluminum in aqueous solution, *Tetrahedron Lett.* **55** (2014) 1347–1352.

2. L. Zhi, J. Liu, Y. Wang, W. Zhang, B. Wang, Z. Xu, Z. Yang, X. Huo, G. Li, Multifunctional Fe_3O_4 nanoparticles for highly sensitive detection and removal of Al(III) in aqueous solution, *Nanoscale* **5** (2013) 1552–1556.

3. A. Bencini, V. Lippolis, Probing biologically and environmentally important metal ions with fluorescent chemosensors: Thermodynamic versus optical response selectivity in some study cases, *Coordin. Chem. Rev.* **256** (2012) 149–169.

4. K. Alizadeh, R. Parooi, P. Hashemi, B. Rezaei, M.R. Ganjali, A new Schiff's base ligand immobilized agarose membrane optical sensor for selective monitoring of mercury ion, *J. Hazard. Mater.* **186** (2011) 1794–1800.

5. L. Wang, H. Li, D. Cao, A new photoresponsive coumarin-derived Schiff base: Chemosensor selectively for Al^{3+} and Fe^{3+} and fluorescence "turn-on" under room light, *Sens. Actuators B* **181** (2013) 749–755.

6. S. Goswami, K. Aich, S. Das, A.K. Das, D. Sarkar, S. Panja, T.K. Mondal, S. Mukhopadhyay, A red fluorescence 'off–on' molecular switch for selective detection of Al^{3+}, Fe^{3+} and Cr^{3+}: Experimental and theoretical studies along with living cell imaging, *Chem. Commun.* **49** (2013) 10739–10741.

7. Y.J. Jang, Y.H. Yeon, H.Y. Yang, J.Y. Noh, I.H. Hwang, C. Kim, A colorimetric and fluorescent chemosensor for selective detection of Cr^{3+} and Al^{3+}, *Inorg. Chem. Commun.* **33** (2013) 48–51.

8. Y.W. Choi, G.J. Park, Y.J. Na, H.Y. Jo, S.A. Lee, G.R. You, C. Kim, A single Schiff base molecule for recognizing multiple metal ions: A fluorescence sensor for Zn(II) and Al(III) and colorimetric sensor for Fe(II) and Fe(III), *Sens. Actuators B* **194** (2014) 343–352.

9. M. Yang, Y. Bai, W. Meng, Z. Cheng, N. Su, B. Yang, A novel selective fluorescent and colorimetric chemosensor for the visual detection of Pd^{2+} and application of imaging in living cells, *Inorg. Chem. Commun.* **46** (2014) 310–314.

10. V.V. Kumar, M.K. Thenmozhi, A. Ganesan, S.S. Ganesan, S.P. Anthony, Hyperbranched polyethylenimine-based sensor of multiple metal ions (Cu^{2+}, Co^{2+} and Fe^{2+}): colorimetric sensing via coordination or AgNP formation, *RSC Adv.* **5** (2015) 88125–88132.

11. H.M. Chawla, P. Munjal, P. Goel, Synthesis and evaluation of a new colorimetric and ratiometric fluorescence probe for copper ions, *J. Lumin.* **164** (2015) 138–145.

12. L. Liu, A. Wang, G. Wang, J. Li, Y. Zhou, A naphthopyran-rhodamine based fluorescent and colorimetric chemosensor for recognition of common trivalent metal ions and Cu^{2+} ions, *Sens. Actuators B* **215** (2015) 388–395.

13. S.H. Kim, H.S. Choi, J. Kim, S.J. Lee, D.T. Quang, J.S. Kim, Novel optical/electrochemical selective 1,2,3-triazole ring-appended chemosensor for the Al^{3+} ion, *Org. Lett.* **12** (2010) 560–563.

14. X. Sun, Y.W. Wang, Y. Peng, A selective and ratiometric bifunctional fluorescent probe for Al^{3+} ion and proton, *Org. Lett.* **14** (2012) 3420–3423.

15. N. Na, F. Wang, J. Huang, C. Niu, C. Yang, Z. Shang, F. Han, J. Ouyang, An aggregation-induced emission-based fluorescent chemosensor of aluminium ions, *RSC Adv.* **4** (2014) 35459–35462.

16. D. Jeyanthi, M. Iniya, K. Krishnaveni, D. Chellappa, A ratiometric fluorescent sensor for selective recognition of Al^{3+} ions based on a simple benzimidazole platform, *RSC Adv.* **3** (2013) 20984–20989.

17. B. Jisha, M.R. Resmi, R.J. Maya, R.L. Varma, Colorimetric detection of Al(III) ions based on triethylene glycol appended 8-propyloxy quinoline ester, *Tetrahedron Lett.* **54** (2013) 4232–4236.

18. J. Kumar, M.J. Sarma, P. Phukan, D.K. Das, A new simple Schiff base fluorescence "on" sensor for Al^{3+} and its living cell imaging, *Dalton Trans.* **44** (2015) 4576–4581.

19. R. Ali, S.S. Razi, P. Srivastava, M. Shahid, A. Misra, A polynuclear hetero atom containing molecular organic scaffold to detect Al^{3+} ion through a fluorescence turn-on response, *RSC Adv.* **5** (2015) 61513–61520.

20. P. Ding, J. Wang, J. Cheng, Y. Zhao, Y. Ye, Three N-stabilized rhodamine-based fluorescent probes for Al^{3+} via Al^{3+}-promoted hydrolysis of Schiff bases, *New J. Chem.* **39** (2015) 342–348.

21. S. Das, A. Sahana, A. Banerjee, S. Lohar, D.A. Safin, M.G. Babashkina, M. Bolte, Y. Garcia, I. Hauli, S.K. Mukhopadhyay, D. Das, Ratiometric fluorescence sensing and intracellular imaging of Al^{3+} ions driven by an intramolecular excimer formation of a pyrimidine–pyrene scaffold, *Dalton Trans.* **42** (2013) 4757–4763.

22. R. Azadbakht, T. Almasi, H. Keypour, M. Rezaeivala, A new asymmetric Schiff base system as fluorescent chemosensor for Al^{3+} ion, *Inorg. Chem. Commun.* **33** (2013) 63–67.

23. Y.W. Liu, C.H. Chen, A.T. Wu, A turn-on and reversible fluorescence sensor for Al^{3+} ion, *Analyst* **137** (2012) 5201–5203.

24. S. Malkondu, A highly selective and sensitive perylenebisimide-based fluorescent PET sensor for Al^{3+} determination in MeCN, *Tetrahedron* **70** (2014) 5580–5584.

25. Y.J. Chang, P.J. Hung, C.F. Wan, A.T. Wu, A highly selective fluorescence turn-on and reversible sensor for Al^{3+} ion, *Inorg. Chem. Commun.* **39** (2014) 122–125.

26. D.F. Wang, Y.C. Ke, H.X. Guo, J. Chen, W. Weng, A novel highly selective colorimetric sensor for aluminum(III) ion using Schiff base derivative, *Spectrochim. Acta A* **122** (2014) 268–272.

27. Z. Li, Q. Hu, C. Li, J. Dou, J. Cao, W. Chen, Q. Zhu, A 'turn-on' fluorescent chemosensor based on rhodamine-N-(3-aminopropyl)-imidazole for detection of Al^{3+} ions, *Tetrahedron Lett.* **55** (2014) 1258–1262.

28. L. Fan, T.R. Li, B.D. Wang, Z.Y. Yang, C.J. Liu, A colorimetric and turn-on fluorescent chemosensor for Al(III) based on a chromone Schiff-base, *Spectrochim. Acta A* **118** (2014) 760–764.

29. S. Liu, L. Zhang, W. Zan, X. Yao, Y. Yang, X. Liu, A novel HBT-based Schiff base for colorimetric detection of aluminum: Synthesis, characterization, spectral and DFT computational studies, *Sens. Actuators B* **192** (2014) 386–392.

30. H. Bataineh, M.H. Al-Hamood, A.M. Elbetieha, Assessment of aggression, sexual behavoir and fertility in adult male rat following long-term ingestion of four industrial metals salts, *Hum. Exp. Toxicol.* **17** (1998) 570–576.

31. M. Shellaiah, Y.H. Wu, H.C. Lin, Simple pyridyl-salicylimine-based fluorescence "turn-on" sensors for distinct detections of Zn^{2+}, Al^{3+} and OH$^-$ ions in mixed aqueous media, *Analyst* **138** (2013) 2931–2942.

32. X.H. Jiang, B.D. Wang, Z.Y. Yang, Y.C. Liu, T.R. Li, Z.C. Liu, 8-Hydroxyquinoline-5-carbaldehyde Schiff-base as a highly selective and sensitive Al^{3+} sensor in weak acid aqueous medium, *Inorg. Chem. Commun.* **14** (2011) 1224–1227.

33. S. Sinha, R.R. Koner, S. Kumar, J. Mathew, P.V. Monisha, I. Kazia, S. Ghosh, Imine containing benzophenone scaffold as an efficient chemical device to detect selectively Al^{3+}, *RSC Adv.* **3** (2013) 345–351.

34. S. Kim, J.Y. Noh, K.Y. Kim, J.H. Kim, H.K. Kang, S.W. Nam, S.H. Kim, S. Park, C. Kim, J. Kim, Salicylimine-based fluorescent chemosensor for aluminum ions and application to bioimaging, *Inorg. Chem.* **51** (2012) 3597−3602.

35. M. Dong, Y.M. Dong, T.H. Ma, Y.W. Wang, Y. Peng, A highly selective fluorescence-enhanced chemosensor for Al^{3+} in aqueous solution based on a hybrid ligand from BINOL scaffold and β-amino alcohol, *Inorg. Chim. Acta* **381** (2012) 137–142.

36. T.T. Wei, J. Zhang, G.J. Mao, X.B. Zhang, Z.J. Ran, W. Tana, R. Yu, An efficient fluorescence turn-on probe for Al^{3+} based on aggregation-induced emission, *Anal. Methods* **5** (2013) 3909–3914.

37. M. Echabaane, A. Rouis, I. Bonnamour, H.B. Ouada, Studies of aluminum(III) ion-selective optical sensor based on a chromogenic calix[4]arene derivative, *Spectrochim. Acta A* **115** (2013) 269–274.

38. M.I. Velasco, C.O. Kinen, R.H.D. Rossi, L.I. Rossi, A green alternative to synthetize azo compounds, *Dyes Pigm.* **90** (2011) 259–264.

39. K. Kaur, V.K. Bhardwaj, N. Kaur, N. Singh, Imine linked fluorescent chemosensor for Al^{3+} and resultant complex as a chemosensor for HSO_4^- anion, *Inorg. Chem. Commun.* **18** (2012) 79–82.

40. K. Tiwari, M. Mishra, V.P. Singh, A highly sensitive and selective fluorescent sensor for Al^{3+} ions based on thiophene-2-carboxylic acid hydrazide Schiff base, *RSC Adv.* **3** (2013) 12124–12132.

41. X. Zhou, B. Yu, Y. Guo, X. Tang, H. Zhang, W. Liu, Both visual and fluorescent sensor for Zn^{2+} based on quinoline platform, *Inorg. Chem.* **49** (2010) 4002–4007.

42. Y.Y. Guo, L.Z. Yang, J.X. Ru, X. Yao, J. Wu, W. Dou, W.W. Qin, G.L. Zhang, X.L. Tang, W.S. Liu, An "OFF-ON" fluorescent chemosensor for highly selective and sensitive detection of Al(III) in aqueous solution, *Dyes Pigm.* **99** (2013) 693–698.

43. T. Keawwangchai, N. Morakot, B. Wanno, Fluorescent sensors based on BODIPY derivatives for aluminium ion recognition: An experimental and theoretical study, *J. Mol. Model.* **19** (2013) 1435–1444.

44. W.H. Ding, W. Cao, X.J. Zheng, D.C. Fang, W.T. Wong, L.P. Jin, A highly selective fluorescent chemosensor for Al^{III} ion and fluorescent species formed in the solution, *Inorg. Chem.* **52** (2013) 7320–7322.

45. H.S. Kim, Y.K. Choi, K.H. Chjo, S.K. Kook, H.G. Woo, Effect of transition metal(II)-N,N-Bis(salicylaldehyde)phenylenediimines on the Electrochemical reduction of thionyl chloride, *Bull. Korean Chem. Soc.* **17** (1996) 223–227.

46. D.M. Boghaei, S. Mohebi, Non-symmetrical tetradentate vanadyl Schiff base complexes derived from 1,2-phenylene diamine and 1,3-naphthalene diamine as catalysts for the oxidation of cyclohexane, *Tetrahedron* **58** (2002) 5357–5366.

47. Y.K. Jang, U.C. Nam, H.L. Kwon, I.H. Hwang, C. Kim, A selective colorimetric and fluorescent chemosensor based-on naphthol for detection of Al^{3+} and Cu^{2+}, *Dyes Pigm.* **99** (2013) 6–13.

48. Q. Meng, H. Liu, S. Cheng, C. Cao, J. Ren, A novel molecular probe sensing polynuclear hydrolyzed aluminium by chelation-enhanced fluorescence, *Talanta* **99** (2012) 464–470.

49. R. Azadbakht, S. Rashidi, A new fluorescent chemosensor for Al^{3+} ion based on Schiff base naphthalene derivatives, *Spectrochim. Acta A* **127** (2014) 329–334.

50. G.J. Park, D.Y. Park, K.M. Park, Y. Kim, S.J. Kim, P.S. Chang, C. Kim, Solvent-dependent chromogenic sensing for Cu^{2+} and fluorogenic sensing for Zn^{2+} and Al^{3+}: A multifunctional chemosensor with dual-mode, *Tetrahedron* **70** (2014) 7429–7438.

51. D.M. Bhoghaei, S. Mohebi, Unsymmetrical tetradentate Schiff bases derived from 2-[(2-2-amino-phenylimino)-methyl]-phenol and 2-[1-(2-amino-phenylimino)-ethyl]-phenol, *J. Chem. Research (S)* 2002 72–75.

52. C.H. Chen, D.J. Liao, C.F. Wan, A.T. Wu, A turn-on and reversible Schiff base fluorescence sensor for Al^{3+} ion, *Analyst* **138** (2013) 2527–2530.

53. N. Dash, A. Malakar, M. Kumar, B.B. Mandal, G. Krishnamoorthy, Metal ion dependent "ON" intramolecular charge transfer (ICT) and "OFF" normal switching of the fluorescence: Sensing of Zn^{2+} by ICT emission in living cells, *Sens. Actuators B* **202** (2014) 1154–1163.

54. X.J. Jiang, H. Tang, X.Y. Li, S.Q. Zang, H.W. Hou, T.C.W. Mak, Two new isomerous fluorescent chemosensors for Al^{3+} based on photoinduced electron transfer, *Spectrochim. Acta A* **115** (2013) 26–32.

55. D. Zhou, C. Sun, C. Chen, X. Cui, W. Li, Research of a highly selective fluorescent chemosensor for aluminum(III) ions based on photoinduced electron transfer, *J. Mol. Struct.* **1079** (2015) 315–320.

56. O.A. Bozdemir, R. Guliyev, O. Buyukcakir, S. Selcuk, S. Kolemen, G. Gulseren, T. Nalbantoglu, H. Boyaci, E.U. Akkaya, Selective manipulation of ICT and PET processes in styryl-bodipy derivatives: Applications in molecular logic and fluorescence sensing of metal ions, *J. Am. Chem. Soc.* **132** (2010) 8029–8036.

57. J. Andreasson, U. Pischel, S.D. Straight, T.A. Moore, A.L. Moore, D. Gust, All-photonic multifunctional molecular logic device, *J. Am. Chem. Soc.* **133** (2011) 11641–11648.

58. L. Zhao, X. Chen, F. Guo, B. Gou, C. Yang, W. Xia, Luminescent properties and logic nature of a crown Schiff base responding to sodium ion and zinc ion, *J. Lumin.* **145** (2014) 486–491.